6-1-2018

Immobilized titanium dioxide for emerging contaminant removal in wastewater

Abdel-Maksoud Yasmine

THE AMERICAN UNIVERSITY IN CAIRO | SCHOOL OF SCIENCES AND ENGINEERING

Immobilized Titanium Dioxide for Emerging Contaminant Removal in Wastewater

Thesis submitted in partial fulfillment of the requirements of

PhD in Science & Engineering

With Concentration in Environmental Engineering

Submitted by

Yasmine Kamal Abdel-Maksoud

Under the supervision of

Dr Emad Imam

Professor of Hydraulics and Water Resources Engineering

Dr Adham Ramdan

Professor of Chemistry

January 2018

Acknowledgement

I believe the most precious thing anyone has is his time. The elapsed moment will never come again. I will always be grateful to my advisors Dr Emad Imam and Dr Adham Ramadan. I am grateful for their precious time and their guidance. I was honored being their student.

I am grateful to Dr Yousef Jameel. His program “Catalyst of Change” to support PhD students had enabled me to be enrolled in the AUC PhD program. This inspires me to endeavor to be myself a Catalyst of Change as well.

I would not gone so far without the support of my dear husband Eng. Maged Moustafa. Day after day, every day, Maged helps me and encourages me. I dedicate any and every success to my lovely girls Layal, Hya and Reemy.

Abstract

There have been rising concerns about emerging contaminants that are not efficiently removed by conventional wastewater treatment plants. TiO_2 photocatalysis is one of the promising routes for sustainable wastewater treatment. Research on the use of TiO_2 photocatalysis for water/wastewater treatment for the removal of persistent non-biodegradable emerging water pollutant is active worldwide. Since the mid-1970s the viability of photocatalytic degradation of organic compounds in water using TiO_2 was demonstrated. More than 1,000 substances have been degraded using TiO_2. Despite the extensive research on photocatalytic oxidation using TiO_2, pilot and demonstration plants through the last four decades are still countable. Widespread use of photocatalytic treatment of water and wastewater require the development of an innovative photocatalytic reactor that is efficient, reliable, simple to construct, easy to maintain, has low energy consumption, low capital and operating cost and provides easy separation of catalyst after treatment ends. In an attempt to develop this desired photo-reactor, three photo-reactors were designed and constructed: the slurry water-bell photo-reactor, the immobilized water-bell photo-reactor and the immobilized tray photo-reactor.

The slurry water-bell photo-reactor is based on generating a thin water film to allow for solar light penetration for photo-catalyst activation and continuous oxygenation. Recirculating the reaction solution at a high flow rate ensures good mixing and avoids dead zones in the photo-reactor. the reactor performance for degradation of phenol, as a model compound, was evaluated using commercial TiO_2. Factors affecting the degradation efficiency were studied including catalyst loading, light intensity, initial pollutant concentration, oxidant addition and exposure time. Dissolved oxygen levels, temperature and pH were monitored through all the conducted tests. The performance of the slurry water-bell was compared with other photo-reactors using two benchmarks: the degradation rate constant and the reactor throughput. The reactor throughput is a function of the treated volume, treatment duration and reactor area footprint, thus it is as a versatile indicator for comparison between reactors of different types and geometries as well as selection of reactor configurations suitable for scale-up and commercialization.

TiO_2 was immobilized on sand grains for use as dispersed photo-catalyst in the water-bell reactor. Immobilization of TiO_2 was conducted by two methods; direct immobilization using sol-gel synthesis and binding with epoxy coating. Photo-catalyst abrasion was encountered. The strong

mixing conditions and flow through the recirculating pump resulted in high abrasion of the photo-catalyst off the sand surface.

The tray photo-reactor was developed to avoid the high friction of the photo-catalyst particles in the recirculating pump while maintain fulfilling all the other photocatalytic process requirements of light penetration, continuous oxygen supply, and turbulent flow. The immobilized tray photocatalytic reactor uses a fixed-bed of TiO_2 supported on sand grains. The reactor maintains a thin water film over the supported TiO_2 catalytic bed. TiO_2 was immobilized on the sand grains using 3 different immobilization approaches: 1) direct immobilization using the sol gel technique, 2) coating with TiO_2/cement grout; and (3) binding with TiO_2-epoxy coating. Reactor performance for the degradation of phenol as a model compound was evaluated for the three photo-catalysts. Immobilization of TiO_2 on sand particles using epoxy was successful in achieving the highest phenol degradation and resistance to abrasion. The water turbidity remained unchanged indicating photo-catalyst resistance to abrasion even after multiple use of the catalytic bed. Successful operation of the tray photo-reactor in the continuous mode was also achieved.

The performance of the immobilized tray photo-reactor was compared with other photo-reactors using three benchmarks: the initial degradation rate, the reactor throughput and turbidity. The immobilized tray photo-reactor is suitable for scale-up and commercialization due to five distinctive features which are: modular design; integrated storage; passive oxygenation; absence of need for UV transmitting components that are susceptible to breakage and optical losses, and simple and cheap components.

Table of Contents

List of Figures

List of Tables

List of Symbols & Abbreviations

AOPs	advanced oxidation processes
atm	atmosphere
BET	Brunauer-Emmett-Teller
BJH	Barret-Joyner-Halender
BL	black light
BTEX	benzene, toluene, ethylbenzene, xylene
CAPMAS	Central Agency for Public Mobilization and Statistics
CB	conduction band
CdS	Cadmium sulphide
CFD	computational fluid dynamics
CO_2	Carbon dioxide
COD	chemical oxygen demand
Conc	concentration
CPC	compound parabolic concentrator
DCA	dichloroacetic acid
DO	Dissolved Oxygen
DOC	dissolved organic carbon
Dp	particle diameter
DSSR	double-skin sheet reactor
ECs	emerging contaminants
EDTA	Ethylene diamine tetra acetic acid
E_g	band gap energy
EOP	electrochemical oxidation potential
EPA	US Environmental Protection Agency
eV	electron-volts
GaP	Gallium phosphide
H_2O_2	Hydrogen peroxide
$HO_2^{\bullet}$	Perhydroxyl radicals
HCl	Hydrochloric acid
hp	horsepower
ID	inner diameter

ITP	Immobilized tray photo-reactor
IWBP	Immobilized water-bell photo-reactor
K_a	acid dissociation constant
K_{app}	apparent degradation rate constant
keV	Kilo electron-volts
mM	millimolar
NaOH	Sodium hydroxide
$OH^{\bullet}$	Hydroxyl radicals
O_3	Ozone
PCP	pentachlorophenol
PSA	Platforma Solar de Almeria
PTR	parabolic trough reactor
PZC	point of zero charge
ROP	relative oxidation power
ROS	reactive oxidizing species
SWBP	Slurry water-bell photo-reactor
t_{30W}	Normalized illumination time at 30 W/m^2
TTB	titanium tetra n-butoxide
TCE	trichloroethylene
TiO_2	Titanium dioxide
TFFBR	Thin-film fixed-bed reactor
TOC	total organic carbon
TTIP	titanium tetra isopropoxide
UV	ultra-violet
V	volt
VB	valence band
Vs	settling velocity
W	watt
WO_3	Tungesten trioxide
WW	wastewater
XRD	X-ray Diffraction
XRF	X-ray florescence

ZnO	Zinc oxide
ZnS	Zinc sulphide

Chapter I

Introduction

1.1 Unrestricted Wastewater Reuse: A Need not An Option

Areas having annual water resources less than 1700 m^3/capita/year are Water Stress areas. Areas having annual water resources less than 1000 m^3/capita/year suffer water scarcity according to worldwide freshwater availability data published by the FAO. Egypt is classified as a water scarce area [1] as shown in Figure 1. In 2017, with a population exceeding 96 million capita, the national water availability is 794 m^3/capita/year. The national water availability is expected to further decrease with the population increase, growing demand for industrial and agricultural uses [2] and the possible impact of dams constructed in upper Nile countries. In 2016, agriculture water use amounted to 62.15 billion m^3 out of the 76.25 billion m^3 available water resources [3] consuming almost 82 % of the available water resources. Reuse of treated sewage effluent in irrigation can be a sustainable water resource through providing a nutrient rich source for agricultural and landscape irrigation as well as stimulating economic growth by providing an additional supply of water [4].

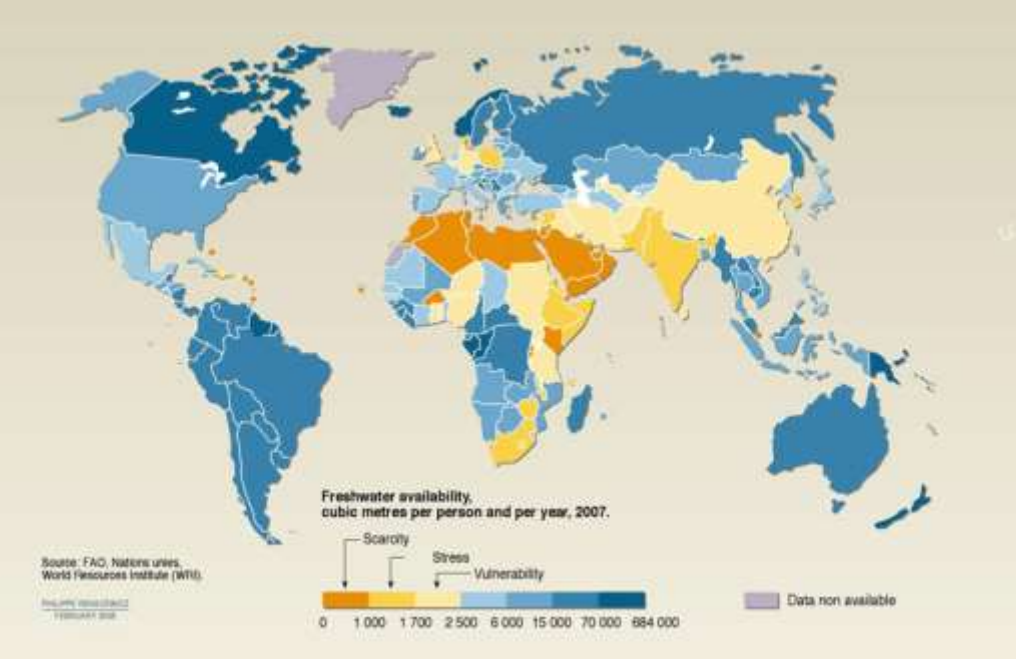

Figure 1: Worldwide fresh water availability, source [1]

Reuse of treated wastewater is considered a possible strategic solution to cope with the increasing water shortage especially in arid and semi-arid regions [5]. However in Egypt, the treated sewage is used for the irrigation of wooden forests and green belt around cities as a safe disposal method of treated wastewater in the context of the national program for using treated wastewater in wooden forests irrigation [6]. Despite the associated positive environmental impacts attributed to this safe disposal, enhanced ambient air quality and combating desertification, the reuse of treated wastewater need to be extended to other applications, for instance: agricultural uses for irrigation of food crops and non-food crops, environmental reuse that includes the use of reclaimed water to support wetlands and to supplement stream and river flows, industrial uses for cooling towers.

The end use of the treated wastewater and degree of human contact with the reclaimed water define the required water quality standards and treatment level [7]. According to the Egyptian code for treated wastewater reuse, there are restrictions on reuse of treated sewage effluent. These restrictions pertain to type of crop being irrigated (non-food crops, crops to be processed, crops eaten raw), area being irrigated (whether it is accessed by public or restricted access of workers), type of irrigation method (sprinklers or dripping), and health and safety standards to be followed by workers and exposed groups [8]. The choice of the appropriate wastewater treatment for treated sewage effluent does not only have cost implications, but also public health and social awareness implications.

In this context tertiary treatment of wastewater effluent for unrestricted use in irrigation is the most appropriate, since produced treated effluent can be safely used for any type of plantation, using any method of irrigation, regardless of soil type and nearness of the fields to residential areas, allowing free access of people as well as cattle to irrigated fields or landscaped areas. Almost no stringent precautions or measures are required for the safety and hygiene of workers.

A major problem in the tertiary treatment of industrial, agricultural, and possibly domestic wastewaters is the presence of emerging contaminants (ECs). ECs also known as trace organic pollutants or micro-pollutants, are a broad range of chemicals found in water at very low levels. ECs can be categorized by their end use (pharmaceuticals, metabolites and hormones; personal care products, food additives, artificial sweeteners and preservatives; pesticides, biocides, and herbicides; household cleaning chemicals, surfactants and disinfectants; flame-retardants and disinfection byproducts), chemical structure (aliphatic organics, halogenated hydrocarbons,

polycyclic aromatic compounds, and polychlorinated biphenyls) or ecological and health effects (hormonally active agents, and endocrine disrupting compounds, carcinogens) [7].

More than two thousands emerging contaminant have been identified in surface waters around the world [9]. Many endocrine-disrupting chemicals including pharmaceuticals, personal care products, and hormones were found in treated effluents in many locations around the world [10], [11], [12], [13], [14], [15], [16], [17], [18], [19], [20], [21]. Municipal water treatment plants are identified as the major source for emerging contaminants [22].

With an estimate of 38,000 chemicals and more currently being used worldwide and additional 300 new material synthesized annually [23], [24], the concerns about emerging contaminants are rising. ECs can pose hazards regardless of whether the treated wastewater effluent is disposed to surface water or reused in irrigation. Endocrine disrupting contaminants having estrogenic effects on living organisms, can mimic or oppose the hormonal effect, alter the pattern of hormonal metabolism and interfere with the normal endocrine functions of living organisms [25]. Arrival of residual antibiotics to surface water lead to increasing of antibiotic resistance in pathogenic as well as nonpathogenic micro-organisms [26].

Conventional secondary wastewater treatment is ineffective in degrading these persistent non-biodegradable compounds [27]. The use of advanced oxidation processes (AOPs) for water/wastewater treatment are rapidly growing worldwide for the removal of persistent non-biodegradable emerging water pollutants [28], [29]. AOPs depend on the generation of hydroxyl radicals that are strong non-selective oxidizing agents that oxidize and mineralize almost all organic water pollutants to ultimately yield CO_2 and inorganic ions [30], [31]. The electrochemical oxidation potential (EOP) of hydroxyl radicals is 2.8 V while chlorine EOP is 1.36 V [32] . Hydroxyl radicals have a relative oxidation power (ROP) to chlorine of 2.05.

AOPs conducted at near ambient temperature and pressure include chemical oxidation using O_3 and O_3/H_2O_2; fenton and photo-fenton processes; UV-based processes including UV/H_2O_2, UV/O_3 and $UV/H_2O_2/O_3$; photocatalytic redox processes using semiconductors [33]. Ozonation is an energy intensive process [29]. For synthesis of ozone using air, 22 – 33 kWh/kg O_3 is required, when using pure oxygen for ozone production, energy requirement is 12-18 kWh/kg O_3 [33]. Fenton and photo-fenton is carried out at an acidic pH from 2-4 [29] to avoid iron precipitation. Production of inorganic sludge and its safe disposal is one of the concerns associated with fenton

and photo-fenton processes [34]. UV-based processes have a disadvantage of high energy consumption specially when treating wastewater containing UV absorbing pollutants [34].

Various semiconductors were tested for use in photocatalytic redox processes including but not limited to TiO_2, ZnS, ZnO, WO_3, CdS, GaP, etc [35]. TiO_2 is one of the most promising semiconductors since it is highly reactive having a high oxidation power of 3.2 eV [36], capable of mineralizing a wide range of organic pollutants, non-toxic, relatively inexpensive, chemically and thermally stable [37]. TiO_2 is resistant to acids and alkalis [23], insoluble in water in all pH range [38]. Unlike CdS or GaP that degrade forming toxic products after repetitive use cycles, TiO_2 is resistant to photo-corrosion [35].

Table 1: Comparative operating costs for some AOPs, source [33]

Process	Cost of Oxidant	Cost of UV
UV/H_2O_2	Medium	High
UV/Ozone	High	Medium
$Ozone/H_2O_2$	High	0
UV/TiO_2	Very low	Medium to high

As seen from Table 1, TiO_2 photocatalysis is one of the most promising AOPs technologies especially if solar energy is used where the operating cost for the process can be substantially reduced [23]. Areas at which the UV flux is higher than $15W/cm^2$ lies between latitudes 35°N and 35°S [39] can use solar light for Photocatalytic activation. Equatorial and tropical countries, including Middle East countries, African countries, Australia, Indian subcontinent and South America, as shown in Figure 2 can use abundant solar radiation as an economic UV light source during daytime [40].

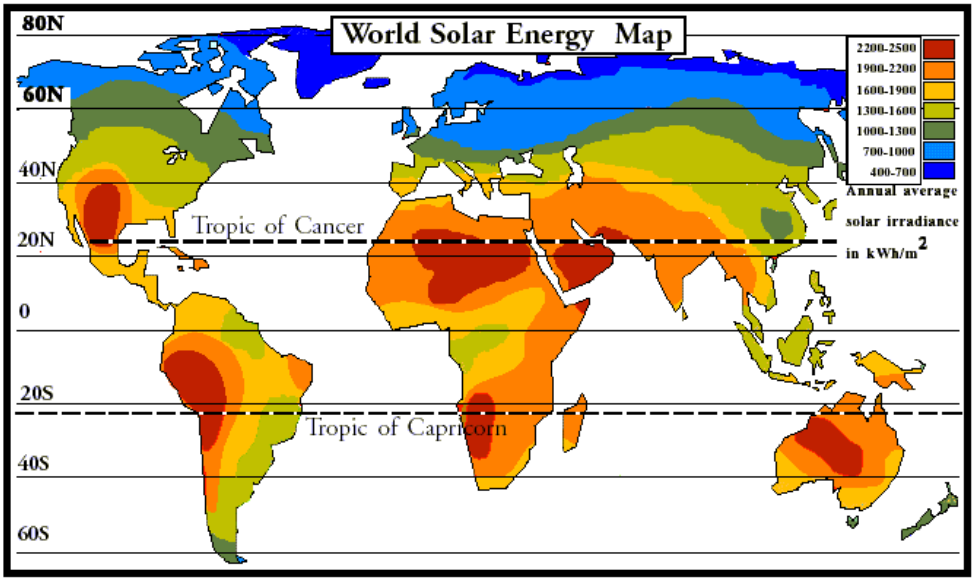

Figure 2: Global solar insolation map, [41]

TiO_2 photocatalysis has been studied for the treatment of secondary treated municipal wastewater [42], [43] , for removal of endocrine disrupting chemicals [25], [44], [30] and disinfection [45], [46] specially effluents containing pathogens resistant to chlorination [47], [48], [49], [50], [51], [52], [53]; treatment of hazardous effluents from hospitals [54], [55]; industrial effluents from pulp and paper [56], [57], [58], [59], dairy manufacturing [60], textile dyeing [61], [62], [63], [64], [65], [66], [67], [68], agricultural oil mills and distilleries [69], [70], and pharmaceutical industry [28], [29] , [71] , [72] ; wastewater effluents containing phenols [73], [74], [75], [76] and chlorophenols [77], [78], herbicides and pesticides [79], [80], [81] ammonia [82], [83] plasticizers [84] and surfactants [85]; drinking water disinfection [86] and purification from micro-pollutants [87], heavy metals [88], cyanide [89], [90] and arsenic [91], [92].

1.2 Problem Statement and Research Objective

TiO_2 photocatalysis is one of the promising routes for sustainable wastewater treatment due to five distinctive features: 1) it can be used at ambient temperature and atmospheric pressure, 2) pollutants are mineralized into CO_2, water and mineral acids, 3) TiO_2 is abundant, cheap and non-toxic, 4) oxygen required for the process can be obtained from the atmosphere, 5) sunlight can be used for catalyst activation.

In spite of the extensive academic research that has been conducted during the last four decades on the possibility of mineralization of a vast range of water pollutants using TiO_2 photocatalysis, commercial application of TiO_2 photocatalysis treatment systems is still very limited [93]. Using TiO_2 nanoparticles in suspension is hindering the wide application of TiO_2 photocatalysis in water treatment [94]: TiO_2 slurry systems require post separation of the catalyst from the effluent to avoid catalyst loss as well as water contamination with TiO_2 particles that may pose threats to aquatic life [95]. This additional post separation is expensive and renders the process economically unfeasible [35]. The design of photocatalytic reactor that is simple, energy efficient, less expensive to build and operate and can handle large volumes of wastewater is a key research area [96] for the development and widespread of TiO_2 photocatalysis.

This research aims at developing a photocatalytic reactor using immobilized TiO_2 activated by sunlight to be used for the removal of emerging contaminants. The objective of this research is to develop a pilot TiO_2 photocatalytic reactor that can be easily scaled up for commercial application.

1.3 General Approach

To avoid the need for a post separation system, TiO_2 will be immobilized. The reactor will be hydraulically designed to control the residence time in the reactor, based on continuous flow mode. The development of the target photo-reactor using immobilized TiO_2 was planned to be performed through the following tasks:

i. Identify the attributes of the target photo-reactor to ensure the efficiency of degradation of organic pollutants using TiO_2 photocatalysis.

ii. Review of the designs of the published reactors to assess how well they meet the desired attributes of the target photo-reactor

iii. Develop the conceptual design of supported TiO_2 continuous large-scale solar photocatalytic reactor and the governing sizing relationships as well as determining suitable support material to be used for TiO_2 immobilization.

iv. Design and manufacturing of pilot-scale photo-reactor, and hydrodynamic testing of the photo-reactor system.

v. Photo-reactor testing for photodegradation of a model contaminant using slurry commercial TiO_2 to evaluate the photodegradation efficiency and investigate the effect of different process parameters on the effluent quality.

vi. Investigate different techniques for immobilization of TiO_2 on the chosen support, and identify a suitable one.

vii. Fabrication of the immobilized TiO_2 photo-catalyst and characterization of the synthesized photo-catalyst.

viii. Prototype testing using the immobilized TiO_2 to evaluate the photodegradation efficiency of the model contaminant, stability of supported TiO_2 and its resistance to abrasion.

ix. Evaluation of the system performance using benchmarks.

Chapter II

Background and Literature Review

2.1 Mechanism of TiO_2 Photocatalysis

TiO_2 has wide applications in protective anti-reflection coatings, solar cells and lithium batteries antibacterial paints and pigments, cosmetics and food stuff, self-cleaning windows, stain resistant textiles, gas sensors and electrochromic devices including smart windows to achieve buildings energy efficiency, and self-darkening car rear view mirrors, catalytic oxidation of carbon monoxide and fine chemicals production, photodegradation of pollutants for air and water treatment, sterilization and disinfection [36], [97], [98].

TiO_2 has three crystalline phases: anatase, rutile and brookite. Brookite is orthorhombic, anatase and rutile are tetragonal. Rutile differs than from anatase in that the octahedral share 4 edges instead of 4 corners [98] as shown in Figure 3. Rutile is the stable crystalline form of TiO_2 where anatase transforms to rutile at temperatures higher than 600 ^oC [99] and brookite transforms into rutile at a temperature of 750 ^oC. Anatase has high photocatalytic activity while rutile is used as a whitening agent [98].

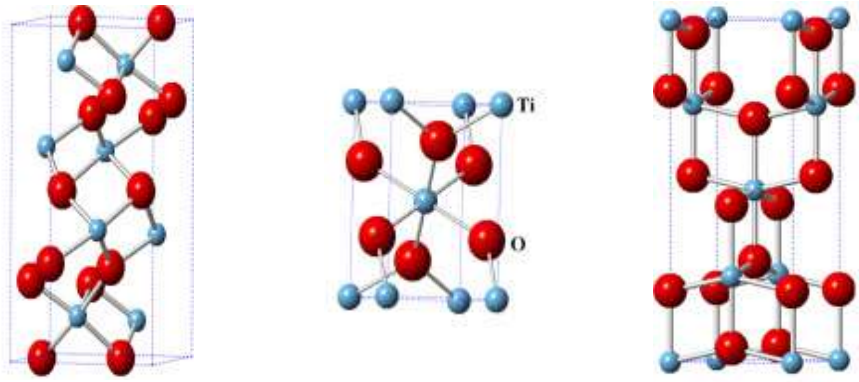

Brookite Rutile Anatase

Figure 3: TiO_2 crystal structure, source: [100]

TiO_2 is characterized by having a completely filled valance band and an empty conduction band. When TiO_2 surface is illuminated with photon energy equal to or greater than its band gap energy (E_g), the lone electron in its outer orbital- valance band is photoexcited to the empty conduction

band leaving an unfilled valence band thus leading to the electron – hole pair formation as shown by Equation 1 [38]. In the absence of electron scavengers, the electron - hole will recombine again dissipating heat. In the presence of oxygen, the electron is scavenged forming superoxide radicals as shown by Equation 2 and preventing the electron-hole recombination [39].

Photoexcitation	$TiO_2 \xrightarrow{h\gamma \geq E_g} h^+ + e^-$	*Equation 1*
Electron scavenging	$e^- + O_2 \rightarrow O_2^{\bullet -}$	*Equation 2*

The positively charged hole on TiO_2 has an ROP of 2.35 [33]. The positive holes bound to the TiO_2 surface can directly oxidize the pollutants adsorbed on the TiO_2 surface as shown by Equation 3, or oxidize water molecules forming hydroxyl radicals as shown by Equation 4. The powerful oxidizing hydroxyl radicals attack the water pollutants as shown by Equation 5 [38].

Direct holes oxidation	$h^+ + R \rightarrow R^{+\bullet}$	*Equation 3*
Hydroxyl radical formation	$h^+ + H_2O \rightarrow OH^\bullet + H^+$	*Equation 4*
Hydroxyl radicals oxidation	$OH^\bullet + R - H \rightarrow R'^\bullet + H_2O$	*Equation 5*

Superoxide radicals are protonated forming hydroperoxyl radicals according to the equilibrium equation shown by Equation 6 where the acid dissociation constant k_a equals $10^{-4.8}$ [80]. The hydroperoxyl radicals are reactive oxidizing intermediates having an EOP of 1.7 V and ROP of 1.25 [23]. Hydrogen peroxide is formed [101] as shown by Equation 7 and Equation 8. On scavenging an electron, hydrogen peroxide generates hydroxyl radicals [59] as shown by Equation 9.

Superoxide protonation	$O_2^{\bullet -} + H^+ \leftrightharpoons HO_2^\bullet$	*Equation 6*
H_2O_2 formation	$2\, HO_2^\bullet \rightarrow H_2O_2$	*Equation 7*
	$O_2^{\bullet -} + 2H^+ \rightarrow H_2O_2$	*Equation 8*
Hydroxyl radical formation	$H_2O_2 + e^- \rightarrow OH^\bullet + OH^-$	*Equation 9*

All the generated reactive oxidizing species (ROS), $OH^{\bullet}$, $HO_2^{\bullet}$, $O_2^{\bullet -}$, take part in successive oxidative reductive reactions degrading organic pollutants until complete mineralization is achieved yielding carbon dioxide, water and mineral acids [95] as shown by Equation 10. The mechanism of photocatalysis using TiO_2 is illustrated in Figure 4.

$$Organic\ pollutant \xrightarrow[O_2]{TiO_2,\ h\gamma \geq E_g} intermediates \xrightarrow[O_2]{TiO_2,\ h\gamma \geq E_g} CO_2 + H_2O + mineral\ acids \qquad \textit{Equation 10}$$

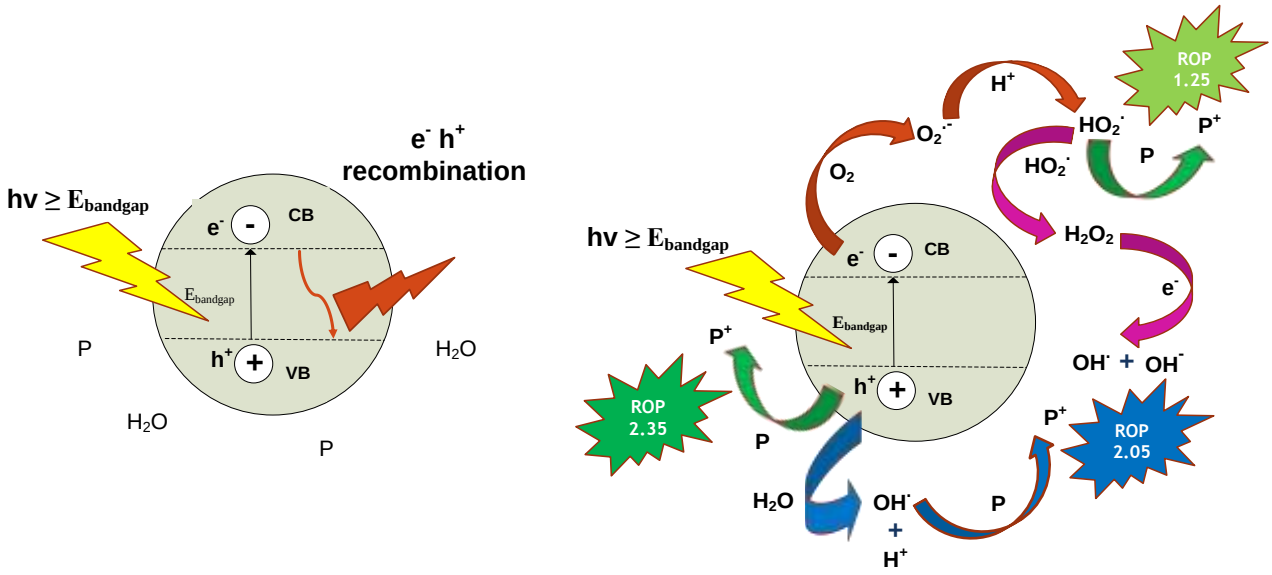

In absence of O_2 / electron scavengers *In presence of O_2 / electron scavengers*

Figure 4: Mechanism of photocatalysis, adapted from [102], [96]

From the aforementioned mechanism, it is obvious that a photocatalytic reactor should have the following attributes [37];

1- A high photo-catalyst surface area to reaction solution volume ratio
2- Adequate irradiation throughout the whole reaction volume
3- Continuous purging of the reaction solution with air or oxygen/continuous supply of oxygen to the reaction solution
4- A high rate of mass transfer of oxygen/substrate to catalyst surface

2.2 Previous Work on Development of TiO_2 Photocatalytic Reactors

2.2.1 Preamble

Since the mid-1970s the viability of photocatalytic degradation of organic compounds in water using TiO2 was demonstrated by several research groups [103]. Since that time, there was an increase on research conducted using TiO2 for photo-oxidation of organic compounds, inorganic compounds, metal-containing ions as well as disinfection. More than 1,000 substances have been tested [104]. The first field demonstration for solar heterogeneous photocatalytic water treatment tests was conducted in the late-1980s using parabolic trough concentrator [105]. Despite the extensive research on photocatalytic oxidation using TiO2, pilot and demonstration plants through the last four decades are still countable [103], [105], [36], [96], [106], [39], [35], [107], [102], [108], [109] as shown in Table 2.

Different reactor configurations have been used to degrade various types of pollutants using solar or artificial light simulating sunlight. In order to select the reactor configuration that is most suitable for the photocatalytic process and is optimum for scale-up and commercialization, a comparison criteria will be used to ease performance assessment for the different reactor configurations.

Table 2: Solar TiO_2 pilot and demonstration plants

Reactor Type	**Treated water**	**Pollutant**	**Treated Volume**	**Applied TiO_2**	**Operation Mode**	**Erection Year**	**Location, Country**	**Ref**
PTR	Deionized water	Salycilic acid	1100 L	Slurry	Recirculating batch	1989	Albuquerque, New Mexico, USA	[110]
PTR	Contaminated groundwater	TCE	15 L/min	Slurry	Recirculating batch	1990	Lawrence Livermore National Laboratories (LLNL), California, USA	[111]
PTR	Industrial wastewater	PCP	837 L	Slurry	Recirculating batch	1991	Platforma Solar de Almeria (PSA), Spain	[112]
Tubular	Pretreated groundwater	BTEX	530 L	Slurry	Recirculating batch	1993	Tyndall Air Force Base, Florida, USA	[113]
CPC	Deionized water	Cyanide	247 L	Slurry	Recirculating batch	1996	Platforma Solar de Almeria (PSA), Spain	[90]
TFFBR	Textile wastewater	TOC	1 m^3	immobilized	Recirculating batch	1998	Menzel Temimi,Tunsia	[114]
DSSR	Biologically pretreated industrial WW	TOC	0.5 m^3	Slurry	Recirculating batch	1998	Volkswagen factory, Wolfsburg, Germany	[115]
CPC	Raw water	Cyanide	1 m^3	Slurry	Recirculating batch	1999	Hidrocen, Madrid, Spain	[116]
Packed Tubular	City water	aromatic organics	1 m^3/day	Immobilized on silica beads	Continuous	2004	Kitakyushu City, Japan	[87]
Shallow tank	Tap water	phenol	1.35 m^3	immobilized	Recirculating batch	2011	Poland	[117]
Open tank	Oil and gas wastewater	oil, phenol & ammonia	4 m^3/day	Slurry	Continuous	2011	Indonesia	[118]

2.2.2 Assessment Criteria of Reactors

The quantum yield which is the ratio of rate of reaction to rate of light absorption was used by some researchers to demonstrate photo-reactor energy efficiency [119]. The quantum yield was further modified into photochemical thermodynamic efficiency factor [120], which is:

$$\eta = \frac{Q_{used}}{Q_{absorbed}} = \frac{r_{OH} * \Delta H_{OH} * W}{Q_{absorbed}} \qquad \textit{Equation 11}$$

where r_{OH} is the rate of OH radicals formation (mol/g of catalyst) Δ_{OH} is the enthalpy of OH radicals formation (J/mol) and W is mass of catalyst (g). In addition to the difficulty of determining these energy efficiency factors [95], they cannot be used for the intended reactor configuration comparison. They do not include other two parameters of extreme importance for scale-up and commercialization of photocatalytic wastewater treatment: the treated volume and the reactor foot print.

Figures of merit in terms of collector area per mass (A_{CM}) and collector area per order (A_{CO}) were proposed for comparison of photo-reactors of different configurations based on the collector area. Collector area per mass (A_{CM}) is the collector area required to degrade one kg of pollutant in one hour after receiving solar radiation of intensity 1000 W/m^2 while collector area per order (A_{CO}) is the collector area required to decrease the pollutant concentration of 1m^3 by one order of magnitude [121].

$$A_{CM} = \frac{A_r \,.\, \bar{E}_s \,.\, t \,.\, 1000}{M \,.\, V_t \;.\, E_s^o \,.\, t_o \,(c_i - c_f)} \qquad \textit{Equation 12}$$

$$A_{CO} = \frac{A_r \,.\, \bar{E}_s \,.\, t}{V_t \;.\, E_s^o \,.\, t_o \,.\, log\frac{c_i}{c_f}} \qquad \textit{Equation 13}$$

where A_{CM} and A_{CO} are in m^2/kg and m^2/m^3-order respectively; A_r is the actual reactor area (m^2); t and t_o are irradiance and reference time (hr); $\bar{E}_s$ and E_s^o are average solar irradiance and reference solar irradiance (W/m^2); V_t treated volume (L); M molar mass g/mol; and c_i and c_f are initial and final pollutant molar concentrations. Collector area per mass has been used by researchers to compare performances of reactors of different configurations based on estimate of area required for scale-up [122], [123] . For the cases in which the treated volumes/degraded pollutants are much lower than the proposed $1m^3$ treated volume and 1 kg of pollutant identified by the proposed figures of merit, A_{CM} and A_{CO} figures of merit will represent extrapolated indicators [36] not a real reflection of the system performance. Another issue is that A_{CM} and A_{CO} assume a linear dependence on the light intensity. This contradicts other researchers' findings that at light intensities higher than a threshold value, the reaction rate is independent of the light intensity [124]. Hence, figures of merit will not be used for reactor performance comparison.

For a given degradation efficiency, reactor throughput ($L/min/m^2$) will be used as an actual indicator on the treatment unit production rate based on the area it occupies. In case of batch operations, reactor throughput is the volume treated/total treatment time/reactor area, while in case of continuous operations it is the flow rate/reactor area. For solar reactors, aperture area is the area in which solar radiation enters the reactor while gross area is the area based on reactor outer dimensions. Throughput calculation is based on the area having the bigger footprint.

Another aspect of evaluation is ease of catalyst removal from treated effluent. One of the major financial obstacles hindering the widespread of TiO_2 photocatalysis is the need to use of TiO_2 nanoparticles in suspension [94]. Costly post separation of the catalyst from the effluent is required to avoid catalyst loss [37]. Another ecological concern is effluent contamination with TiO_2 particles. Several studies have shown that long exposure to TiO_2 nanoparticles adversely affect aquatic organisms [125]. Not only effluent contamination with TiO_2 nanoparticles is encountered when using slurry TiO_2 but also when using immobilized TiO_2 and where the immobilization technique is not robust enough to avoid photo-catalyst spalling and attrition.

Comparison between different types of TiO_2 photo-reactors is conducted by reviewing treatment trials for each reactor type to illustrate system components and calculate throughput. Photocatalytic reactors whose reaction solution volume is less than 1L are classified as lab-scale reactors [96].

This review focuses on pilot scale demonstrations using solar or external artificial lighting simulating solar radiation.

2.2.3 Parabolic Trough Reactors

Parabolic Trough Reactor (PTR) consists of a transparent pipe through which contaminated water flows. The pipe is located at the focal line of a collector that is a parabolic light-reflecting surface. The collector is mounted on a mobile platform equipped with solar tracking system [107]. Figure 5 shows a typical slurry PTR system operating in a recirculating batch mode.

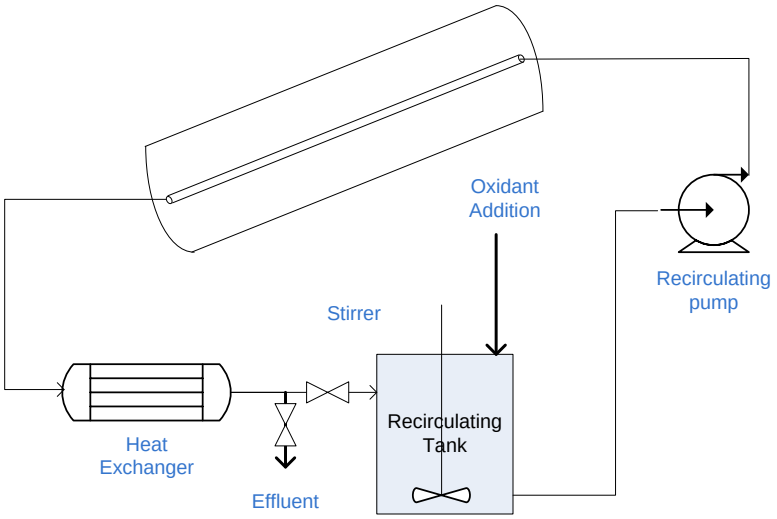

Figure 5: Schematic drawing of PTR system, adapted from [110], [111]

PTRs have a concentrating ratio of 10-50 [102]. The concentrating ratio is determined using the collector width and half the circumference of the glass pipe, taking into consideration reflective and transmissive losses [110]. PTRs are operated at high flow rates, and turbulent flow ensures high mass transfer rates between the pollutants and photo-catalyst [108].

PTR was used in Sandia National Laboratory, New Mexico for treating water contaminated with salicylic acid. The reactor was 218 m in length and 2.1 m in width, having a borosilicate glass pipe of 38 mm diameter. The system had a total aperture area of 465 m^2 and a concentrating ratio of 50. The reactor worked in a recirculating batch mode using slurry TiO_2. An air radiator was used for cooling water. However the radiator cooling capacity or extent of temperature rise during treatment were not specified. 1100 liters of water contaminated with salicylic acid were treated using 1 g/L

slurry TiO_2. 96% destruction was achieved in 40 min at a recirculation rate of 100 L/min, corresponding to a residence time of 2.5 min, and UV intensity of 1600 W/m^2. The same system was used in treating trichloroethylene, tetrachloroethylene, chloroform, trichloroethane, carbon tetrachloride, and methylene chloride. Chlorinated ethylenes were easily destroyed [126].

PTRs were used in treating groundwater contaminated with trichloroethylene in LLNL, California. The solar detoxification system consisted of 2 PTR strings. Each string had a length of 36.6 m and a width of 2.1 m, and a borosilicate glass pipe of 51 mm diameter. The used PTRs had a concentrating ratio of 20 and a total aperture area of 154 m^2. A heat exchanger was used for cooling water [111]. However, the researchers did not specify the heat exchanger cooling capacity nor the extent of temperature rise during treatment. An important outcome of this work was a performance comparison for concentrating PTRs and one-sun configurations. In the one-sun configuration, the PTRs were aligned horizontally such that the PTRs are not concentrating any sunlight. While concentrating PTR had an aperture area of 465 m^2 (PTR width * length), one- sun system had an aperture area of is 3.73 m^2 (pipe diameter * length). The system throughput in case of the one-sun PTR was 8 times higher than the concentrating PTR suggesting that photo-catalyst efficiency is increased at low UV light intensities [111]. This finding has been confirmed by many other researchers [35].

Recently a pilot scale PTR was used for the treatment of diluted paper mill effluent. The increase of BOD/COD ratio proved the viability of using solar photocatalytic as a pretreatment to increase paper mill effluents biodegradability [56].

PTRs receive large amount of energy per unit volume. Thus the reactor tube is small, enabling the use of high quality UV transmission material. Despite the fact that the tube area is small, the area equipped by the parabolic collector for light harvesting is very large. Moreover, the installation of PTRs require an additional large area to avoid PTR modules projecting shadows on each other [127]. Another limitation of PTRs is the use of direct radiation only [128]. For thermal applications, this is not a problem since diffuse radiation accounts for only 10-15% of total solar radiation [105]. For photocatalytic applications, this is a disadvantage. TiO_2 Photocatalysis uses only solar UV radiation, which accounts for 4-6% of total solar radiation [25]. 50 % or more of UV radiation is in the diffuse radiation especially in humid locations and during cloudy days [108]. Thus, PTRs do not operate efficiently during cloudy and overcast days.

A major demerit of the PTR is the reaction solution overheating [109]. Not only does overheating of the reaction solution leads to leaks and corrosion [108], but also affect treatment efficiency. As temperature increases, the solubility of oxygen in water decreases leading to bubble formation. Since oxygen is needed for reaction completion [126], a continuous supply of oxygen to the reaction solution is essential. To avoid bubble formation, electron scavengers such as hydrogen peroxide / sodium persulfate can be used [112]. However, the use of additional reagents complicate water purification process and render it less practical [39].

2.2.4 Concentrating Falling Film Reactors

Another type of concentrating reactors, though based on a falling film configuration, consists of heliostats (large rotating mirrors) that are used to concentrate solar radiation on a vertical falling film of water. Large tracking heliostats were used to concentrate solar radiation on a vertical aluminium panel (3.5 m * 1 m). The aluminum panel was mounted on a tower 37 m above the ground. The heliostats had a total aperture area of 750 m^2. Commercial TiO_2 powder was suspended in the wastewater in the holding tanks using mixers. 300 mg/L of TiO_2 were used for the treatment of the water containing 30 mg/L salicylic acid. 380 liters of water were treated at a flow rate of 17 L/min resulting in a thin film thickness of 3 mm. A cooler was required to remove excess heat energy before recirculation [110]. The use of concentrating thin films for photocatalytic treatment of water was not reported by any other researchers. This may be attributed to the complexity of system set-up. Concentrating falling film reactors, similar to PTRs, have the demerits of requiring huge area for light harvesting, reaction solution overheating, high capital cost for solar tracking devices and high operational cost for water cooling.

2.2.5 Compound Parabolic Concentrator

Compound Parabolic Concentrators (CPC) are static reactors that consist of transparent pipes mounted on a reflector. The reflector has the shape of two half parabolas intersecting beneath each tube, this shape allows any incident light to be concentrated on transparent pipe without need for sun tracking systems. CPCs use direct as well as diffuse solar radiation while exhibiting a small concentration factor (<1.2) [129]. A typical slurry CPC system operating in a recirculating batch mode is illustrated in Figure 6.

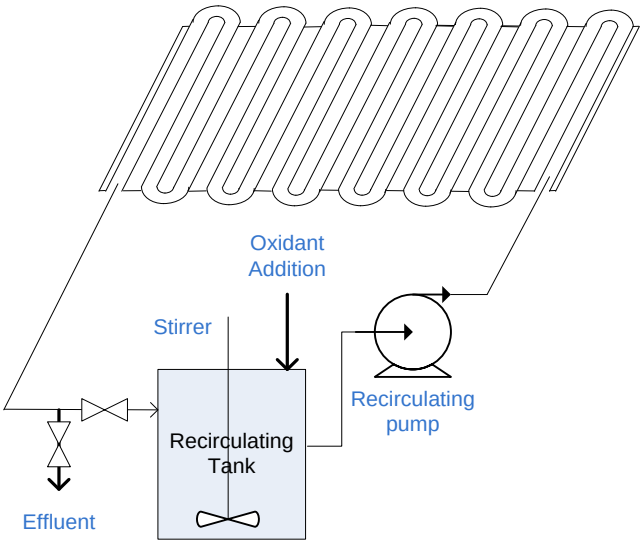

Figure 6: Schematic drawing of slurry CPC system, adapted from [72], [90]

A demonstration plant using CPC reactors was erected in HIDROCEN, Madrid. The plant is fully automated for the treatment of 1 m^3 of water. The plant consists of two rows of 21 CPC collectors connected in series having a total aperture area of 100 m^2. Each collector is 1.5 m * 1.5 m encompassing 16 parallel glass tubes of 29.2 mm ID. The collector reflector is made of anodized aluminum. The plant was operated in a recirculating batch mode. After treatment, pH was adjusted in the sedimentation tank to enhance TiO_2 agglomeration into bigger particles for quick settling. The supernatant water from the sedimentation tank containing <7 mg/L TiO_2 was passed through a microfiltration system for the final removal of the photo-catalyst [116].

The treatment performance of the demonstration plant and the large pilot plant (LPP) in PSA, Spain, were compared using cyanide. LPP has a total plant volume of 247 liters, and an aperture area of 8.9 m^2. 200 mg/L slurry TiO_2 was used to degrade aqueous cyanide solutions having an initial concentration of 50 mg/L. Complete degradation of cyanide could be achieved in the LPP after a normalized illumination time (t_{30W}) of 89 min. Only 76% degradation could be achieved in the demonstration plant after t_{30W} of 115.5 min. [90]. This lower treatment efficiency achieved by the demonstration plant was partially attributed to the difference of the used water matrix. LPP used distilled water while the demonstration plant used tap water. The presence of carbonates that are hydroxyl radical scavengers, leads to tapering off photocatalytic degradation rates [37]. The authors postulated another reason for the lower treatment efficiency which was the low O_2 concentration and uneven O_2 distribution in the demonstration plant. O_2 injection was carried

directly in reactor pipes of the demonstration plant using an injection system, while for the LPP, oxygenation was carried out in the recirculation tank [90] through contact with ambient air during stirring [130]. However DO profiles during treatment in both of the demonstration plants and LPP were not included.

Experiments investigating the treatment of synthetic sewage water were conducted in the small pilot plant in PSA. For an accumulation energy of 50 KJ/L, corresponding to 6 hours of illumination, DOC was decreased by only 18% when using 0.2 g/L TiO_2 alone. For the same accumulated energy and experimental conditions, degradation increased to 51% when adding 2 g/L H_2O_2. When using 4.3 g/L sodium persulfate, degradation increased to 75% [131]. CPCs are closed reactors that require continuous supply of oxygen to the reaction solution by purging the reaction solution with oxygen/air or the use of oxidants.

Several test trials have been conducted with packed CPCs. Packed CPCs in which TiO_2 is immobilized on a support eliminates the need for expensive post-separation processes. A packed CPC composed of 5 Pyrex tubes (1.9 m length and 22.2 mm OD) connected in series was used for treating 21 liters of aqueous triclosan solution. The tubes were packed with TiO_2 immobilized on volcanic porous stones. Stones, having an average size of 1 cm, were TiO_2 coated using the sol-gel method followed by sintering for 3 hours at 605^{o}C. Locally available porous stones served as a cheap catalyst support [97].

SOLWATER reactor is another packed CPC reactor. The reactor is composed of four tubes mounted on a CPC collector. The first two tubes contain TiO_2 immobilized on Ahlstrom paper. The other two tubes contain supported photosensitizer. The water to be treated runs in series through the four pipes. Field tests were carried in Los Pereyra, Argentina to disinfect groundwater from a shallow aquifer for the use as drinking water. Groundwater was contaminated by fecal coliforms, Enterococcus Faecalis and Pseudomonas Aeruginosa that is a chlorine resistant pathogen. The reactor was operated in a recirculating batch mode and treated 20 liters. A 20 cm free fall of water returning to the feed tank was allowed for water oxygenation. The reactor efficiently removed fecal coliforms and Enterococcus Faecalis while removal of Pseudomonas Aeruginosa was not achieved. For fecal coliforms, the total disinfection of groundwater contaminated with $6.6*10^5$ CFU/100 ml fecal coliforms could be achieved in 6 hours on cloudy days with a maximum UV-A intensity of 30 W/m^2. After 3 month of operation, the removal

efficiency decreased. 1-3% of bacteria were still cultivable at the end of the tests. This loss of efficiency was attributed to calcium carbonate deposition on the photo-catalyst and the photosensitizer [132].

A similar finding regarding loss of TiO_2 effectiveness with prolonged use was obtained when CPC packed with TiO_2 immobilized on glass spheres was used for the degradation of emerging contaminants spiked in secondary treated wastewater effluent. Researchers found that hydroxybiphenyl, triclosan, progesterone, ibuprofen, diclofenac, ofloxacin, acetaminophen and caffeine could be degraded within t_{30W} of 60 min. After five cycles of treatment, a prolonged treatment duration was required. Contaminants were then degraded in t_{30W} of 90 min [133].

Loss of efficiency due to clogging of packed CPC and catalyst fouling is an operational concern. Platinized TiO_2 immobilized on silica gel was packed in M-7 plastic tube of ID 0.5″ and length of 2 m. The reactor was used to treat groundwater spiked with BTEX in a continuous mode. Reactor efficiency decreased significantly after 2 days of operation when treating extracted groundwater. A filter (0.35 micron) and an anionic/cationic ion exchange resin were used as a pretreatment for well water. The reactor receiving the pretreated water worked efficiently continuously during daytime for 25 days [134]. Catalyst fouling was also encountered when using a tubular reactor packed with TiO_2 immobilized on silica beads for city water treatment. After one month of operation red iron deposits fouled the catalyst impairing the treatment efficiency [87].

CPC has the merits of maintaining a turbulent flow that guarantees good mixing and negligible mass transfer. They use both direct and diffuse radiations [35]. However, CPC suffers from optical losses due to UV absorbance by the tube and the reflector material [128]. Another challenge typically faced is glass tubes aging, known as UV-solarization. Long exposure to solar radiation lead to the reduction of tubes UV transmittance [127] impairing treatment efficiency and incurring additional costs for tubes regular replacement. One of the CPC limitations is the need for oxygen injection, or alternatively adding oxidants to act as electron scavengers. In case of using supported catalysts, reactor clogging and catalyst fouling are operational concerns. The demonstration plant in PSA using slurry TiO_2 for treating just $1m^3$ of water was composed of 672 pipes, each having a length of 1.5 m. If a supported catalyst was to be used, the ease of operation regarding regular inspection and replacement of the supported catalyst is questionable. The support size should be

optimized to avoid high pressure drop across the reactor and the associated excessive pumping cost.

2.2.6 Tubular Reactor

Tubular reactor is a non-concentrating reactor in which water flows through transparent pipes. The pipes can be connected between an inlet and outlet header [135] or directly folded in a coil shaped pattern [136]. Tubular reactors are a variation of CPCs. The difference is the absence of a reflector. This reflector lows CPC to have a small concentrating factor. A field-test facility based on tubular photo-reactors was used to treat groundwater spiked with BTEX at Tyndall Air Force Base, Florida. Experiments were conducted in a recirculating batch mode using 5 photo-reactors connected in series. Each photo-reactor contained 132 tubes (6.4 mm ID). The tubes were made of a UV transparent material and had a length of 2.4 m. The reactors had an aperture area of 10 m^2 and gross area of 37.2 m^2. Groundwater was filtered through 0.5 micron filter. 530 liters of filtered groundwater were recirculated with TiO_2 slurry with a high flow rate maintaining a turbulent flow. BTEX destruction using TiO_2 only with no oxidant was limited [135]. Adding 100 mg/L H_2O_2, 75% destruction of BTEX was achieved in 3 hours [113]. Recently a tubular pilot plant was used to treat 15 liters of water contaminated with nitrophenol, naphthalene, and dibenzothiophene, which are typical oil industry pollutants, using slurry TiO_2 [136]. Tubular reactors share the operational merits and demerits of compound parabolic concentrators.

2.2.7 Shallow Pond Reactor

Shallow pond reactor is a non-concentrating reactor utilizing both direct and diffuse radiations, thus operating in sunny as well as cloudy and overcast days. A solar pond fabricated from plywood and lined with polyethylene sheets was used for degradation of chlorophenol in tap water. Solar pond (106.5 cm * 53.3 cm) had a surface area of 0.57 m^2, and depth of 2". The pond worked in a recirculating batch mode using slurry TiO_2. Strong mixing was achieved using a recirculating pump and a submerged spray bar. After treatment, the mixing facility was stopped and TiO_2 settled to the pond's bottom. Treated effluent was decanted from the pond surface [137]. However, the researchers did not evaluate the TiO_2 content of treated effluent.

Chlorophenol solution was treated using 3 g/L TiO_2. 88% degradation was achieved in 2 hours, under an average UV intensity of 31.4 W/m^2. A test was conducted using two identical ponds of 2 inch depth, one of which was equipped with bubbler wands for air sparging. Pollutant concentration variation with time in the two ponds was almost identical indicating that dissolved oxygen in the 2 inch ponds was sufficient. When the pond depth was increased to 4 and 6 inches, degradation efficiency decreased to 60 and 48% respectively. [137]. This can be attributed to limited solar radiation penetration or insufficient dissolved oxygen.

A fluidized bed photo-reactor using TiO_2 coated on floating ceramic spheres was used for treating distilled water spiked with bisphenol A. The photo-reactor was rectangular (15 cm * 25 cm). When treating one liter, the reactor had a depth of 2.66 cm, and can be viewed as a shallow pond reactor using TiO_2 immobilized on floating spheres. The reactor was aerated using air diffusers and illuminated using black light lamps. Light intensity at water surface was 30 W/m^2. The ceramic spheres had a density of 1 gm/cm^3 so that they are easily suspended in water. The spheres were 0.7 mm in diameter so that they can be easily removed after treatment. Sol gel was used for TiO_2 immobilization on the spheres by dip coating followed by drying and sintering at 600 ^oc for 5 hours. However, the researchers did not specify TiO_2 loading on the spheres. Although the researchers did not quantitatively evaluate the stability of immobilized TiO_2 on spheres, they noted that water remained transparent during treatment. The reactor operated in a batch mode. Using a catalyst loading of 8%, 10 mg/L of bisphenol A were degraded in 13 hours while degradation byproducts were mineralized in 20 hours [138].

Another photocatalytic reactor for treating of 1.5 m^3 was mounted in a mobile container to be easily transferred to sources of polluted water. The reactor tank had an operating volume of 0.06 m^3 and an area of 1.8 m^2. The water depth in the reactor was 3.3 cm and can be viewed as a shallow tank reactor. The system was equipped with an impeller pump for water recirculation. The 1.5 m^3 recirculation tank was aerated through an air diffuser using an air compressor. The reactor was illuminated by a 6 kW mercury lamp giving a UV intensity of 330 W/m^2, which is a very high UV flux. Most researchers agree that, at high UV fluxes, the reaction rate becomes constant with respect to the radiant flux [35]. High UV flux lead to the loss of photonic efficiency. as the rate of electron/hole recombination becomes higher. The photo-reactor worked in a recirculating batch mode for treatment of phenol solution with a concentration of 25 mg/L. Commercial

photospheres-40 were used as photo-catalyst. Photospheres-40 are hollow microspheres of silica coated with TiO_2, having an average particle size of 45 microns, and a low density ($0.22 g/cm^3$) that makes them float on water surface. Photospheres were completely destroyed after 3 cycles of treatment as the fragile floating spheres did not withstand vigorous mixing and flow through the pump impeller [117]. The researchers also tested degradation efficiency using TiO_2 immobilized on a steel mesh. A mixture of TiO_2 and a white titanium photocatalytic paint was applied twice onto a steel mesh. The reactor bottom was also painted using the same procedure. The researchers tested degradation efficiency using TiO_2 immobilized on commercial fiberglass cloth as well. TiO_2 was immobilized by the immersion of the fiberglass cloth in TiO_2 ethanol suspension and then drying at 80^oC [117]. The researchers did not report TiO_2 stability on the fiberglass cloth. Although slurry deposition is simple, produced TiO_2 coatings lack sufficient mechanical integrity and are prone to rapid attrition [139].

Shallow ponds have potential for the treatment of industrial wastewater especially in industries that already use holding ponds including pulp and paper, pharmaceuticals and textiles [105]. Sparging the pond/tank with air might not be needed given that pond/tank depth does not limit a continuous oxygen supply from atmosphere and light penetration. However, finding an efficient immobilized catalyst is still needed. Immobilized shallow pond systems working in a batch mode are illustrated in Figure 7.

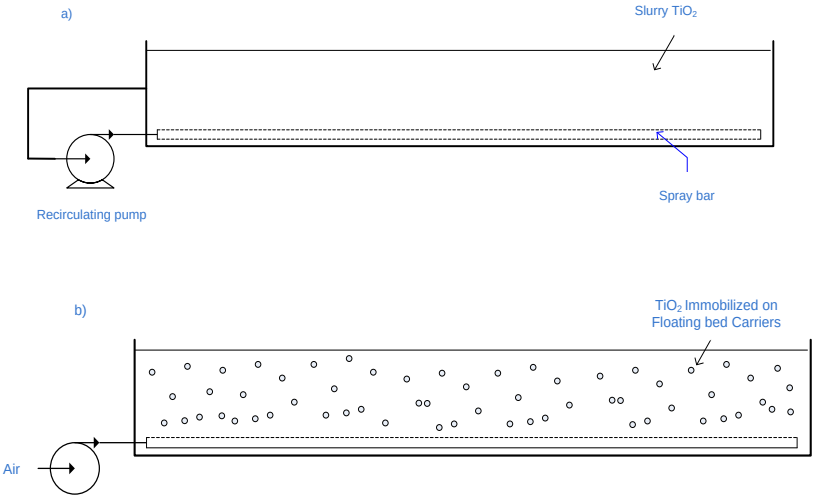

Figure 7: Schematic drawing of photocatalytic shallow pond: a) employing slurry TiO_2, b) fluidized bed shallow pond reactor, adapted from [140], [105]

2.2.8 Double-Skin Sheet Reactor

Double-skin sheet reactor (DSSR) is a non-concentrating reactor made of commercially available Plexiglas double skin sheet that is modified by milling the connecting straps at alternating ends and sealing the sheets sides by Plexiglas [141]. Plexiglass transmits all light above 320 nm. DSSR uses slurry TiO_2. High flow rates guarantee a turbulent flow that overcomes mass transfer limitations between TiO_2 and pollutants and avoid photo-catalyst deposition in the reactor during recirculation. Since DSSR is a closed reactor, purging reaction solution with air is required.

A pilot plant consisting of 12 DSSRs (2.45 m * 0.94 m) having a total surface area of 27.6 m^2 was constructed at the Volkswagen plant in Wolfsburg to treat 0.5 m^3/day biologically pretreated wastewater using 5 g/L TiO_2 [115]. Pretreated wastewater was passed over a filter, then to reservoir that contained the TiO_2 suspension. The pilot plant worked in a recirculating batch mode. When treatment ended, TiO_2 was allowed to settle down in the reservoir, then the supernatant liquid was filtered. 40% reduction of TOC could be achieved under an average UV solar intensity of 13.3 W/m^2 in 330 min [142].

DSSRs have the merits of using direct and diffuse radiation, maintaining a turbulent flow regime. However they can only be operated in a slurry mode. They suffer from low optical efficiency and bubble entrapment [128]. They need purging of reaction solution with oxygen or addition of oxidants [129].

2.2.9 Flat Plate Reactor

Flat plate reactor is an inclined rectangular flat plate covered with a thin UV transmissive glazing. The reactor is closed preventing contact between water to be treated and ambient air [128].

An outdoor flat plate reactor made of a stainless steel flat back plate (243.8 cm * 111.8 cm, 2.73 m^2 aperture area) was used for treating 57 liters of aqueous solution of 4-Chlorophenol. The back plate was covered by a woven fiberglass mesh to damp out surface waves and even out flow. The reactor had a thin film glazing made of fluoropolymer that is 90% UV transmissive. Water to be treated was evenly distributed from a spray bar at the reactor top. Water was drained from the reactor by gravity through two drain holes. The reactor worked in a recirculating batch mode.

About 60% degradation of chlorophenol was achieved after 150 minutes under sunny conditions using slurry TiO_2 having a concentration of 1 g/L. When TiO_2 was immobilized on fiberglass mesh, degradation efficiency was lower. Although fiberglass mesh is not an expensive support for TiO_2, catalyst loading on the mesh and the immobilization technique efficiency in terms of TiO_2 content of treated effluent need to be evaluated. Recently a flat plate reactor using slurry TiO_2 was used for the degradation of pyrimethanil which is the active compound found in fungicides used in agriculture [143].

Flat plate reactors are characterized by a laminar flow [144]. At higher flow rates, water film thickness is increased, limiting solar radiation penetration required to activate the photo-catalyst thus decreasing degradation efficiency [145]. Enclosing the flat plate reactor with a UV transparent material is a limitation against scale-up and commercialization. For covering large-scale flat surfaces, the cost of UV transmissive glazing will significantly add to the reactor cost. Glazing needs to be thick to withstand pressures, and increasing the thickness will decrease UV transmissivity. Additional support may be required [105] increasing construction complexity and reactor cost. Filming of the glazing from inside and outside will decrease UV transmissivity into the reactor thus decreasing its optical efficiency. Regular cleaning of the glazing from inside and outside is an operational concern.

2.2.10 Falling Film Photo-reactor

Falling film reactor is a variation of the flat plate collector where the surface of reactor is left open to the atmosphere [106]. Falling film reactor is a non-concentrating reactor employing both direct and diffuse solar radiations. Laminar flow conditions prevail resulting in film thickness of 1mm [107]. Eliminating the reactor cover has two advantages: (1) purging the reaction solution with air/oxygen is unnecessary since oxygen is exchanged rapidly between air and water [39], (2) Falling film reactors have higher optical efficiency, elimination of transmissive losses due to cover material and thickness [106]. Thin-film fixed-bed reactors (TFFBRs) are falling film reactors having TiO_2 immobilized on the reactor surface.

Diluted pretreated leachate of Goslar landfill, Germany, was treated using TFFBR. TFFBR was made of glass plate having an area of 0.7 m^2 (60 cm*118 cm). TiO_2 was immobilized on the glass plate. The glass plate was etched with NaOH then dipped in TiO_2 slurry. The coated plates were

left to dry overnight in room temperature. Multiple coating cycles were conducted. UV-A lamps having a maximum intensity of 100 W/m^2 were used for illumination. Wastewater was dispersed over the top of the coated plate using a multichannel peristaltic pump. In a single pass experiment, 52% reduction of TOC and 56% reduction of COD were achieved at a flow rate of 1.5 L/hr [146].

A TFFBR solar pilot plant was constructed in a textile factory in Menzel Temime, Tunisia. The pilot plant had two concrete reactors, each having a width of 2.5 m and a length of 10 m, resulting in a total illuminated area of 50 m^2. Each reactor was connected to a 1 m^3 tank from which water is pumped to a distributor at the top of the reactor [114]. One of the pilot plant reactors was used for the destruction of two commercial textile azo dyes in well water using immobilized TiO_2. A painting roll was used to apply a TiO_2 suspension in water as a coat onto the reactor surface. The researchers reported that some of the photo-catalyst was stripped off under the experimental conditions used [145]. Coating resistance to abrasion and attrition is highly questionable using this primitive immobilization technique. The reactor was operated in a recirculating batch mode to treat 730 liters having a TOC of 44.8 mg/L. 47% degradation of TOC was achieved in 8 hours during sunny day of July and August [145]. A falling film reactor with immobilized TiO_2 working in a recirculating batch mode is illustrated in Figure 8.

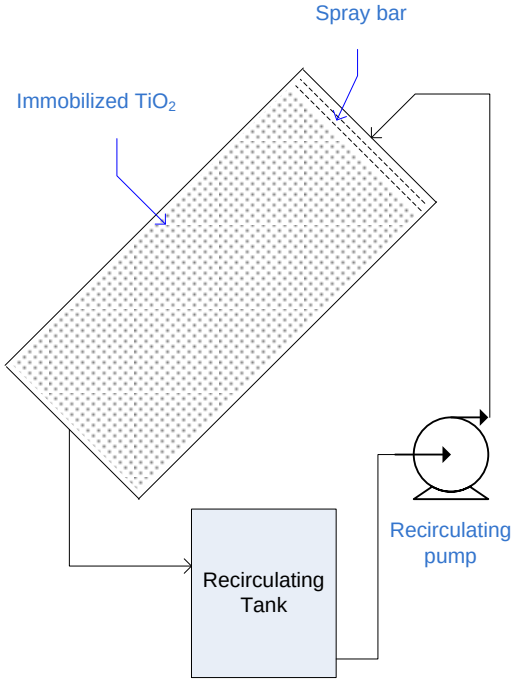

Figure 8: Schematic drawing of TFFBR system, adapted from [114], [146]

Falling film reactors suffer during strong winds from losing the homogeneity of the falling film [69]. The photo-catalytic film on TFFBR is exposed to pollution agents [128]. During cross winds, parts of the photo-catalyst is dry, thus impairing the treatment efficiency [147]. Another profound limitation is the difficulty of immobilizing TiO_2 on large flat surfaces without the risk of the water flow stripping off the photo-catalyst.

2.2.11 Thin Film Cascade Photo-reactor

Laminar flow conditions associated with thin film flow pattern result in mass transfer limitations between the pollutants and photo-catalyst resulting in a limited treatment efficiency [128]. Waterfall effects of the cascade photo-reactor offer turbulence that reduces mass transfer limitations and enhances oxygen transfer [148].

When a three plate thin film cascade reactor was used for the degradation of an aqueous solution of benzoic acid, degradation was slightly higher than that achieved when using a flat plate reactor. Final dissolved oxygen concentration was also higher, suggesting that better degradation results could be achieved with a cascade reactor having an increased number of steps [149]. A pilot scale thin film cascade reactor consisting of nine stainless steel plates (17.5cm * 28 cm each) was developed. The plates were coated with TiO_2 using an electrophoretic method resulting in a catalyst loading of 0.89 mg/cm^2 [148]. Electrophoretic deposition requires plates degreasing, then etching with nitric acid. An electrolytic cell equipped with a magnetic stirrer is used for TiO_2 deposition. Plates are then dried and annealed in an oven at 200^{o}C for 90 min [149]. The reactor worked in a recirculating batch mode to treat benzoic acid in deionized water using sunlight. Similar to the falling film reactor, the thickness of the thin film is approximately 1 mm. Seven liters of water having 100 mg/L benzoic acid were treated at an average UV-A intensity of 17.4 W/m^2. 30% reduction of benzoic acid concentration was achieved after 180 min [148].

Although immobilization of TiO_2 on plates eliminated the necessity of a post-separation step of TiO_2 out of the treated effluent, the cost of electrophoretic deposition is high especially for large surfaces. Plates encountering filming and deposition problems might be an operational concern.

2.2.12 Step Photo-reactor

Step photo-reactor is based on a cascading thin-film principal. It is a stainless steel staircase (2m*0.5m) having 21 steps, covered with a Pyrex glass sheet. TiO_2 is deposited on a flexible support of Ahlstrom paper using a silica-based inorganic binder. The coating method is patented. It is based on the impregnation of Ahlstrom paper with a mixture of TiO_2 and silica binder, then the pressing of the paper by cylindrical rolls under constant speed and pressure [150]. However, the researchers did not report the TiO_2 loading on the Ahlstrom paper nor the coating stability. The step reactor with immobilized TiO_2 working in a recirculating batch mode is illustrated in Figure 9.

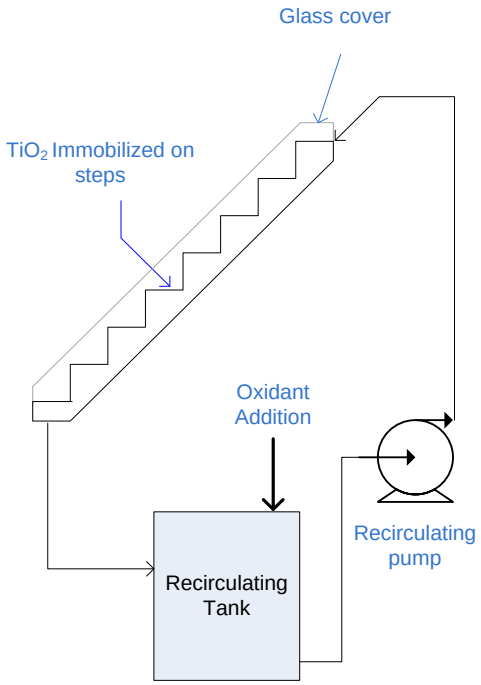

Figure 9: Schematic drawing of Step photo-reactor system, adapted from [150]

The reactor was operated in a recirculating batch mode, treating 25 Liters. The photo-reactor was used for treating an aqueous mixture of pesticides having an initial TOC concentration of 8 mg/L. 80% degradation was achieved in 4.5 hours under an average UV-A intensity of 30 W/m^2 [150]. The researchers did not report dissolved oxygen levels throughout their experiment. Since the step reactor is a closed reactor, the initial dissolved oxygen in water might not be sufficient to complete the reaction and additional air sparging would be required. Another concern is that the silica binder

surface is negatively charged as silica has a point of zero charge (PZC) close to 2 in contrast to TiO_2 which has a neutral PZC. This hinders the adsorption of anionic pollutants leading to a decrease in their photo-degradation efficiency [150]. Although using this supported TiO_2 eliminates post-separation processes, it deprives TiO_2 photocatalysis from the merit of being non-selective, degrading various organic contaminants.

Similar to flat plate reactors, enclosing a large scale reactor with a UV transparent material is a limitation against scale-up and commercialization due to increased capital cost associated with cover material, filming problems that would decrease reactor efficiency and have regular cleaning requirements, and increased operational costs associated with the need for reaction solution purging with oxygen or oxidants.

2.2.13 Fountain Photocatalytic Reactor

A thin film photocatalytic reactor was developed in which water passes through a nozzle forming a water-bell that flows around a vertical UV- lamp [151]. Unsupported water thin film offers two advantages: (1) a high oxygen exchange rate between air and water thus eliminating the need for additional aeration systems, (2) light penetration for the excitation of the photo-catalyst, thus allowing the use of higher catalyst loading [152]. The water-bell reactor was modified to use an external UV light source or sunlight. The resulting fountain photocatalytic reactor is a slurry type reactor in which a thin film of polluted water containing dispersed TiO_2 is continuously generated by pumping water through a specially designed nozzle [153]. The use of a reflecting surface mounted beneath the lower side of the fountain allow the water thin film to be irradiated from both sides. A schematic drawing of the fountain reactor is shown in Figure 10.

A fountain photo-reactor was operated in a continuous mode with very high recycle ratios. Almost all the water was recirculated through the nozzle with a minimum effluent flow rate. The photo-reactor was used for the degradation of 20 mg/L salicylic acid in deionized water using UV-A intensity of 68.5 W/m^2. Using 1 g/L of TiO_2, conversions attained were 21% when the feed flow rate was 0.2 L/min while the recirculation flow rate through the nozzle was 40 L/min, with a recycle ratio of 200. The irradiated diameter was 0.9 m corresponding to an aperture area of 0.64 m^2 [154]. Treated effluent was directed to a settling tank for TiO_2 recovery.

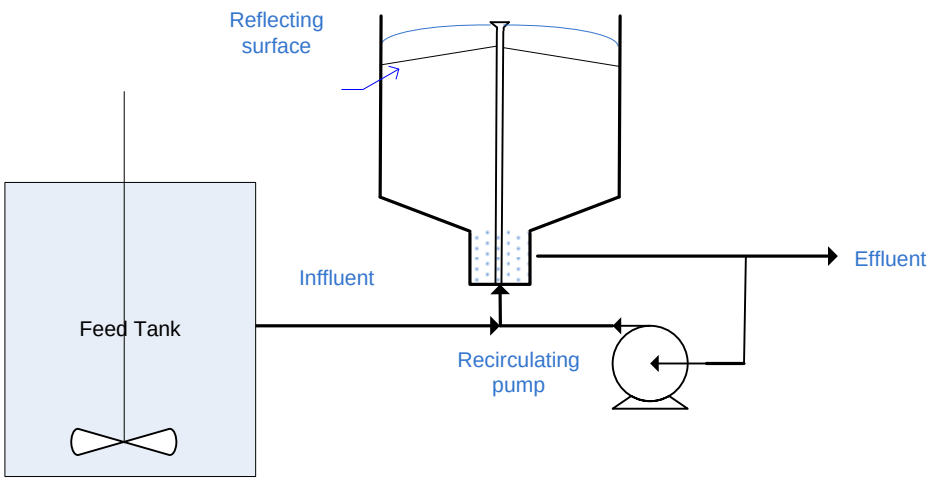

Figure 10: Schematic drawing of fountain photo-reactor, adapted from [153]

A thin film configuration allows light penetration to activate the photo-catalyst and provide a continuous oxygen supply. The recirculation of the reaction solution allows for good mixing and efficient mass transfer while avoiding treatment dead zones. Although the fountain reactor works on a continuous mode, using TiO_2 in the slurry form is still an operational concern.

2.2.14 Slurry Bubble Column Reactor

A slurry bubble column reactor was composed of a borosilicate glass column of 100 mm ID and 3 m length. Water to be treated entered the column at the top while air was supplied to the reaction medium from the column bottom using a diaphragm air compressor. Sieve plates were used to reduce backmixing throughout the column. A schematic drawing of the slurry bubble column reactor is shown in Figure 11. A parabolic reflector of a total surface area of 6 m^2 was used to concentrate solar radiation on the reactor. The collector position was changed every 15 min to continuously track the sun. TiO_2 was separated from treated water by a candle filter placed before the effluent outlet. The photo-reactor worked in a recirculating batch mode treating 19.5 liters. Aqueous solutions of nitrobenzene, chlorobenzene and phenol were treated using slurry TiO_2 with concentrations of 3, 0.15 and 2 g/L respectively. In each case, the pollutant initial concentration was 100 mg/L. After 4 hours, degradation achieved for nitrobenzene and chlorobenzene were 70 and 96 % respectively. Only 25 % degradation of phenol was achieved in 6 hours [40]. The photo-reactor performance was higher when using a low TiO_2 concentration. When using 1 g/L TiO_2 in

a parabolic trough collector, transmittance drops to zero over a 10 mm path length [90]. In this 100 mm column, increased suspension opacity caused a screening effect that reduced the system efficiency.

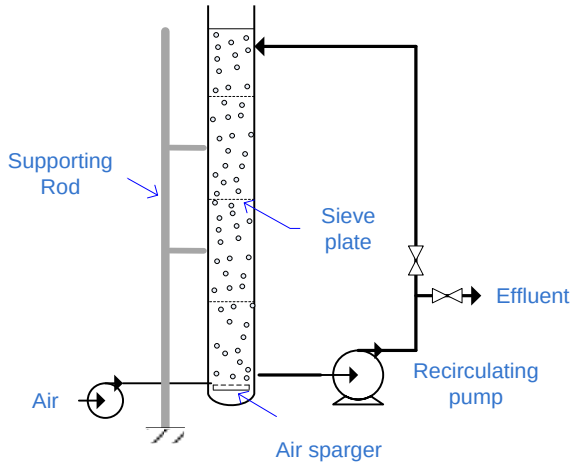

Figure 11: Schematic drawing of non-concentrating slurry bubble column photo-reactor, adapted from [40]

The concept of a concentrating slurry bubble column reactor is not attractive for scale-up and commercialization for the following reasons: (1) the presence of moving solar tracking parts adds to the investment and operation costs, (2) reactors with transparent walls for radiation transmittance experience problems of filming and are prone to breakage risks.

2.2.15 Flat Plate Column Reactor

Designing a photo-reactor takes into account the hydrodynamic field, radiation source and field, mass balance and reaction kinetics [155]. CFD model was used in conjunction with Helmholtz equation for predicting the light distribution to design a reactor having a flat plate geometry. The resultant reactor had a width of 5 cm, thickness of 2.5 cm and height of 30 cm. The reactor walls along the width are transparent. A schematic diagram for a flat plate column reactor is illustrated in Figure 12. The reactor was packed with N-doped TiO_2 immobilized on glass spheres. The influent was aerated then pumped to the column bottom by a liquid distributor for a homogeneous liquid flow through the packing material. The reactor was tested for degrading an aqueous solution

of methylene blue (10 mg/L). 65% degradation was achieved after 6.5 hours using visible light, while degradation reached 90% when using UV light [156].

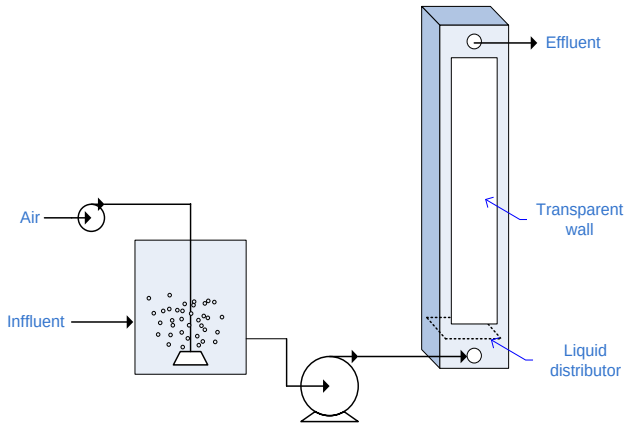

Figure 12: *Schematic drawing of flat plate column reactor, adapted from [156]*

Since the reactor is closed, aeration or the addition of oxidants is a must. For scaling up purposes, channeling need to be avoided through the use of multiple liquid distributors throughout the column. Similar to the slurry bubble column reactor, flat plate column reactor are not promising for scale-up reactors. The reactor transparent walls for radiation transmittance are prone to breakage risks and filming problems.

2.2.16 Pebble Photo-reactor

The pebble photocatalytic reactor was used for the treatment of water containing dyes simulating a textiles dye house effluent. The reactor was composed of a trough (52 cm * 45 cm) made of Perspex transparent sheet. White pebbles having a mean diameter of 9 mm were fixed on the trough surface using two epoxy adhesives [123].

TiO_2 was immobilized on the pretreated pebbles surface by spraying a 2% TiO_2 ethanol suspension followed by drying at 70^{o}C. Five coating cycles were conducted to obtain an adequate TiO_2 coating. The coated pebbles were dried at 150 ^{o}C for 8 hours [157]. However, the researchers did not evaluate the stability of the immobilized TiO_2 specially that calcination of the coated pebbles at high temperatures is normally practiced to enhance TiO_2 coat adherence to the support [74],

[76], [77], [158]. The photo-reactor worked in a recirculating batch mode treating 10 liters of water having an initial TOC concentration of 83 mg/L. 15% TOC reduction was achieved in 5 h [123]. Similar to all reactors characterized by a laminar flow, the pebble bed reactor experiences limited degradation efficiency.

2.2.17 Flat Packed Bed Reactor

TiO_2 immobilized on sand was used in the photo-reactor. The photo-reactor had a packed bed of 40 gm sand, of 35 cm length and 2 cm width. Using naturally occurring sand as a support enables the preparation of a cheaply immobilized photo-catalyst. TiO_2 was immobilized on quartz sand with average grain size of 250 microns using the sol gel method, followed by calcination at 850^{o}C. Although unsupported anatase generally transforms to rutile at temperatures around 600^{o}C [99], the researchers attributed the stabilization of the anatase phase in the coatings to the possible diffusion of Si, Zr and Al from the sand into the TiO_2 coatings, inhibiting the atomic rearrangement to the rutile phase.

The photo-reactor operated in a recirculating batch mode. One liter of deionized water inoculated with E-Coli, was recirculated through the photo-reactor. At a UV intensity 3.7 W/m^2, complete sterilization was not achieved after 100 min. Poor performance was attributed to the limited catalyst exposure to light since only the top layer of grains were exposed to light [159]. A packed bed reactor working in a recirculating batch mode is illustrated in Figure 13.

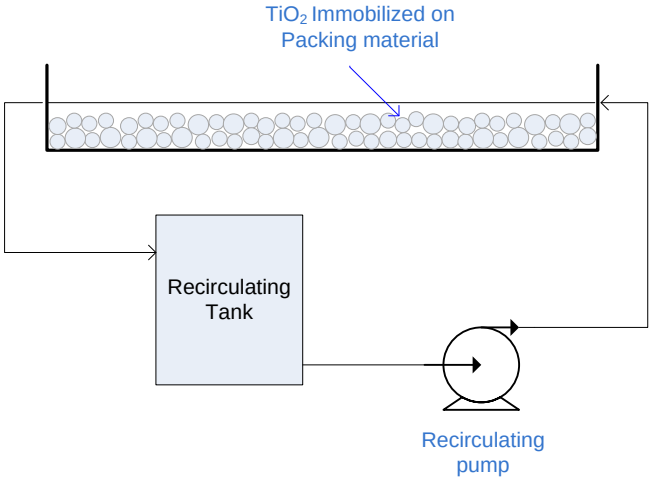

Figure 13: Schematic drawing of packed bed photo-reactor system, adapted from [159]

2.3 Comparison of Different Reactors Throughput

Table 3 presents throughputs of different slurry reactors and their degradation efficiencies achieved during selected treatment trials. Throughputs of reactors using immobilized TiO_2, and their degradation efficiencies are presented in Table 4. All the selected treatment trials were conducted using solar light or UV-A light simulating solar light at neutral pH, without the addition of chemical oxidants, unless otherwise stated. An exact comparison between all reactor configurations is not possible since the treatment trials have different target pollutants with different concentrations, and different water matrices. However an insight on the throughput and efficiency that can be achieved by each reactor configuration is given.

Although PTRs could achieve high degradation efficiency for wastewater streams having a low organic content, throughput is low due to large light harvesting areas. Lower throughput is achieved when PTR was used for treating wastewater of relatively high COD (2 g/L). This demonstrates that advanced oxidation is considered optimal for the treatment of water containing a low organic load – having a TOC lower than 100 mg/L, and a COD lower than 250 mg/L [103].

Throughputs achieved by CPC vary greatly according to the water matrix and pollutant concentration. Throughputs for CPC is calculated based on the reflector area. However these throughputs would further decrease when taking into account the areas left between CPC modules to prevent CPC shadowing on each other [36].

All reactors using immobilized TiO_2 and characterized by a laminar flow (thin-film fixed-bed, pebble bed, thin film cascade reactors) experience limited degradation efficiency as well as limited throughput.

Solar pond photo-reactor operating in a slurry mode achieved high throughput and an acceptable degradation efficiency. The fountain reactor has shown a relatively high throughput for a limited degradation efficiency of 20%. Allowing for a higher residence time will increase degradation efficiency and lower the throughput. Similarly a shallow tank reactor using immobilized TiO_2 achieved high throughput for a degradation efficiency of 50%. A lower throughput is expected when allowing longer treatment to attain a higher degradation efficiency.

Table 3: Slurry Reactors throughput and degradation efficiencies

Reactor type	Pollutant & conc	Treated volume / flow rate	Water matrix	TiO_2 conc	UV-A W/m^2	Removal %	Reactor footprint m^2	duration	Throughput $L/hr/m^2$	Ref
PTR	Salicylic Acid 30 mg/L	1100 L	Deionized water	1 g/L	1600	96	465	40 min	3.54	[110]
PTR	TCE 107 µg/L	15 L/min	Filtered groundwater	1 g/L	NA	90	154	Single-pass mode	5.82	[111]
PTR	PCP 10 mg/L	838 L	Deionized water	1 g/L	24-30	100	384	20 min	6.55	[112]
PTR	COD 2.075 g/L	3.5 L	Diluted paper mill effluent	0.75 mg/L	35-45	70.5	3.7	180	0.32	[56]
CPC	• Cyanide – 50 mg/L • DCA – 50 mg/L	1 m^3	Tap water	200 mg/L	30	• 76 • 100	100	• 115 min • 56.7 min	• 5.16 • 10.58	[90]
CPC	Cyanide 50 mg/L	247 L	Deionized water	200 mg/L	30	100	8.9	89 min	18.72	[90]
CPC	• Dichlorophenoxyacetic acid - 58 mg/L • Bentazon - 32 mg/L	5 L	water containing herbicides	1 g/L	30	• 80 • 100	0.248	1.34 hr [b]	15.05	[79]
CPC	DCA 50 mg/L	39 L	Deionized water	200 mg/L	30	100[c]	3	35.3 min	21.97	[90]

Reactor type	Pollutant & conc	Treated volume / flow rate	Water matrix	TiO_2 conc	UV-A W/m^2	Removal %	Reactor footprint m^2	duration	Throughput $L/hr/m^2$	Ref
CPC	DOC 200 mg/L	35 L	Synthetic wastewater	200 mg/L	30	18[c]	3.08	5.5 hr	2.06	[131]
CPC	COD 11 g/L	24 L	Real cardboard industry effluent	2 g/L	NA	38	2.15	7 hr	1.59	[58]
CPC	COD 89 g/L	30 L	Olive oil mill effluent	1 g/L	NA	12[a]	3.08	32 hr	0.3	[69]
Tubular	BTEX 2 mg/L	530 L	Filtered groundwater	1 g/L + 100 mg/L H_2O_2	45.3	75	37.2	3 hr	4.74	[113]
Tubular	Mixture of Naphthalene and Dibenzothiophene	15 L	Deionized water	1.5 g/L	30	92	NA	21 min	Could not be calculated	[136]
Shallow pond reactor	Chlorophenol 8.5 mg/L	28.8 L	Tap water	3 g/L	31.4	88	0.57	2 hr	25.3	[137]
DSSR	DCA 50 mg/L	25 L	Deionized water	7.5 g/L	NA	100	1.37	3.5 hr	5.21	[141]
DSSR	TOC 16.7 mg/L	0.5 m^3	Biologically treated wastewater	5 g/L	13.3	40	27.6	5.5 hr	3.36	[142]
Flat plate reactor	Chlorophenol 12.85 mg/L	56.8 L	Deionized water	1 g/L	37.5	60	2.73	2.5 hr	11.1	[144]

Reactor type	Pollutant & conc	Treated volume / flow rate	Water matrix	TiO_2 conc	UV-A W/m^2	Removal %	Reactor footprint m^2	duration	Throughput $L/hr/m^2$	Ref
Flat plate reactor	Pyrimethanil 23 mg/L	15 L	Deionized water	1.5 g/L	30[a]	100	0.3	10.37 hr [b]	4.82	[143]
Fountain reactor	Salicylic acid 20 mg/L	0.2 L/min	Deionized water	1 g/L	68.5	20	0.64	Continuous flow	18.75	[153]
Slurry bubble column reactor	• nitrobenzene • chlorobenzene • phenol 100 mg/L	19.5 L	Deionized water	• 3 g/L • 0.15 g/L • 2 g/L	NA	• 70 • 96 • 25	NA	• 4 hr • 4 hr • 6 hr	Could not be calculated [d]	[40]

NA: not available

[a] pH adjusted to 2.8

[b] Degradation efficiency was reported as a function of accumulated energy, assuming UV-A intensity of 30 W/m^2, a normalized treatment duration is calculated

[c] Conducted at pH 3.8, 3.3

[d] Calculating throughput for this reactor based on its aperture area is not valid since the parabolic trough is vertical. Calculating the throughput should be based on the reactor's footprint area, which is the area bounded by the path of the revolving parabolic trough. Since the radius of the revolving path is not specified, the throughput could not be calculated.

Table 4: Immobilized TiO_2 Reactors throughput and degradation efficiencies

Reactor type	Pollutant & Conc	Treated volume/flow rate	Water matrix	Support	UV-A W/m^2	removal %	Reactor footprint m^2	duration	Throughput L/hr/m^2	Ref
One packed tube	BTEX 2 mg/L	2.4 L/hr	pretreated groundwater	Silica gel	3.2	100	0.375 [a]	Single-pass mode	6.4	[134]
Packed CPC	Triclosan 12 mg/L	21 L	Water-ethanol solution	porous stones	30	50.5	1.71	2 hr	6.14	[133]
Packed CPC	Humic acids 5 mg/L	50 L	Deionized water	Ahlstrom paper	NA	100	1	12 hr	4.16	[160]
Packed CPC	Amazil Acetamiprid thiabendazole 100 µg/L each	8 L	Secondary treated municipal WW	Glass spheres	30	• 70 • 10 • 10	0.25	13.3 hr [d]	2.41	[80]
Packed CPC	15 emerging contaminant 100 µg/L each	10 L	Secondary treated municipal WW	Glass spheres	30	90[e]	0.3	136 min	14.7	[133]
Packed CPC (Solwater)	Fecal coliforms $6.6*10^5$ CFU/100 ml Enterococcus Faccalis $5.4*10^4$ CFU/100 ml	20 L	Ground water	Ahlstrom paper	30	100	1 [b]	6 hr	4.98	[132]

Reactor type	Pollutant & Conc	Treated volume/flow rate	Water matrix	Support	UV-A W/m^2	removal %	Reactor footprint m^2	duration	Throughput L/hr/m^2	Ref
Packed Tubular	TOC	1 m^3/day	City water	Silica beads	NA	Variable through 3 month	NA	Single-pass mode	Could not be calculated	[87]
Fluidized bed shallow tank	Bisphenol A 10 mg/L	1 L	Deionized water	ceramic carriers	30	100	0.0375	13 hr	2.05	[138]
Floating bed shallow tank	Ammonia 975 mg/L	5 L	Petrochemical plant effluent	Light expanded clay aggregate	35-45	59	0.071	21 hr [c]	3.35	[82]
Shallow tank reactor	Phenol 25 mg/L	1.35 m^3	Tap water	• Photospheres • Steel mesh • Filtercloth	330	• 50 • 47 • 80	1.8	15 hr	50	[117]
TFFBR	TOC 66 mg/L	1.5 L/hr	pretreated landfill leachate	reactor surface	100	52	0.7	Single-pass mode	2.16	[146]
TFFBR pilot plant	Azo dye 44.8 mg/L	730 L	Well water	reactor surface	NA	47	25	8 hr	3.65	[145]
Thin film Cascade reactor	Benzoic acid 100 mg/L	7 L	Deionized water	reactor plates	17.4	30	1.68	3 hr	1.39	[148]
Step reactor	Pesticides mixture 8 mg/L	25 L	Tap water	Ahlstrom paper	30	80	1	4.5 hr	5.56	[150]

Reactor type	Pollutant & Conc	Treated volume/flow rate	Water matrix	Support	UV-A W/m^2	removal %	Reactor footprint m^2	duration	Throughput $L/hr/m^2$	Ref
Pebble bed	dyes 83 mg/L	10 L	Simulated dyehouse effluent	pebbles	18.9	15	0.234	5 hr	8.52	[123]
Flat packed bed	E-coli	1 L	Deionized water	quartz sand	3.7	No complete sterilization	0.07	100 min	8.57	[159]

NA: not available

[a] The reactor having 4 pipes has a gross area of 1.5 m^2, 0.375 m^2 corresponds to operating only one reactor pipe

[b] The reactor aperture area is estimated to be 1m^2 (length of pipe 0.97m, taking into consideration spacing between the 4 pipes, 1 m width is assumed

[c] Equivalent to treatment on 3 successive days, 7 hours/day, pH adjusted to 9

[d] Degradation efficiency was reported as a function of accumulated energy, assuming UV-A intensity of 30 W/m^2, a normalized treatment duration is calculated

[e] Only 11 emerging contaminants were 90% degraded with in this time, atrazine, antiyirine, flumequine and carbamazepine needed longer time

2.4 Analysis of Previously Used Reactors

It is postulated that using TiO_2 nanoparticles in suspension is hindering the wide application of TiO_2 photocatalysis in water treatment. However, a thorough review of the literature revealed that commonly tested reactor configurations for TiO_2 photocatalysis suffer from other limitations that hamper their scale-up and commercialization.

PTRs have a low throughput. PTRs are expensive due to the presence of moving parts and solar tracking devices. They have high operational costs associated with water cooling. PTRs are not competent for scale-up and commercialization. For the same reasons and complexity of set-up, concentrating falling film reactors are also not competent for scale-up.

Flat plate reactors, step photo-reactor and DSSR are enclosed reactors having a UV transmissive glazing. For enclosing large reactors, the glazing thickness should be sufficient to withstand the operating pressures. Increasing the glazing thickness reduces the UV transmissivity as well as add to the reactor capital cost. Also, there is a need for the continuous purging of the reaction solution with oxygen or adding oxidants. The UV glazing encounters filming problems, known as window fouling where photo-catalyst and/or water contaminants stick on the reactor surface leading to further decrease in UV transmissivity and lowering treatment efficiency.

Falling film reactors operate in a laminar flow regime, thus experiencing limited treatment efficiency due to mass transfer limitations between the contaminants and the photo-catalyst. A large reactor area is required to attain acceptable treatment efficiencies. In addition, falling film reactors suffer from operation disturbances during windy weather where parts of the reactor surface would be dry thereby reducing the reactor effective surface area. A cost effective technique for immobilizing TiO_2 on large flat surfaces that is resistant to photo-catalyst stripping off is still needed.

CPCs are the most commonly used reactor configuration for use in experimental testing and demonstration plants. This can be partially attributed to the ease of experimental set-up. CPCs need purging with oxygen or the addition of oxidants, thus increasing the operational cost as well as the need for a thorough process control to avoid an uneven O_2/oxidants distribution throughout the reactor. They suffer from optical losses and tubes aging due to long exposure to solar radiation.

Therefore regular tube replacement is necessary, incurring additional operational costs. Another issue with CPCs is the difficulty of using supported TiO_2 since they frequently encounter problems of reactor clogging, catalyst fouling, and high pumping energy requirement to compensate for the pressure drop across the reactor. CPCs are not competent for scale-up and commercialization.

For shallow pond or shallow tank reactors either using slurry TiO_2, TiO_2 immobilized on fluidized supports, TiO_2 immobilized on fixed support or packed bed, water depth cannot exceed a few centimeters to maintain sufficient light penetration to activate the catalyst and attain high treatment efficiency.

This analytical review reveals that there is a need to design a TiO_2 photocatalytic reactor that meets all the process requirements - light penetration to activate the photo-catalyst, uniform reactor irradiation to avoid treatment dead zones, turbulence for efficient mass transfer, immobilized TiO_2, continuous oxygen supply, and a reasonable reactor throughput and simple catalyst separation after treatment.

Chapter III

Design and Development of the Photocatalytic Reactor

3.1 Conceptual Design

A heterogeneous photocatalytic reactor for an efficient water treatment, suitable for scale-up and commercialization, should fulfil the following requirement: (1) high turbulence to ensure good mixing and high mass transfer rates between the pollutants and photo-catalyst [108], (2) sufficient light penetration to activate the photo-catalyst taking into consideration that light transmittance in a glass tube drops to zero over a 10 mm path length when using TiO_2 concentration of 1 g/L [90], (3) a continuous supply of oxygen to the reaction solution since oxygen is essential for electron scavenging and treatment completion [126], and (4) the easy separation of photo-catalyst after treatment ends, and (5) operates on either a batch or continuous inflow mode.

The proposed photo-reactor is based on exposing a thin water film containing TiO_2 supported on high density grains to sunlight or artificial light. The thin water film is generated by recirculating polluted water and supported TiO_2 through a water-bell nozzle, as shown in Figure 14. The thin water film has two advantages: (1) it allows for continuous oxygenation of the water film due to a high exchange rate of oxygen between air and the water film [107] thus not needing any additional aeration systems for purging the reaction solution with air [112], (2) it allows the use of high catalyst loading since complete light penetration through the thin film guarantees activation of the photo-catalyst [152]. In the proposed photo-reactor, TiO_2 immobilized on supports dispersed in the polluted water is used. This enhances the system efficiency as it eliminates mass transfer limitations related to diffusion of contaminant to the catalyst surface [114]. Recirculating the reaction solution at a high flow rate ensures long exposure times, provides good mixing and avoids treatment dead zones in the photo-reactor. The photo-reactor has a sufficient depth to allow for gravitational separation of the photo-catalyst from the treated effluent, where the clarified effluent is discharged from an outlet in the clarifying zone.

As shown in Figure 14, the reactor is a circular tank with open top and a sloping bottom towards a central hoper. The bottom slope is steep enough to direct the photo-catalyst to the center hopper of the reactor tank. Water and photo-catalyst are withdrawn from the central hoper by a pump and

re-injected into the vertical feeders that terminate at their top with the water-bell nozzles. The recirculating flow exiting the nozzle is in the form a thin radial water film exposed to air from above and below, where the thin film is set higher than the water level in the reactor. The thin film is uniformly illuminated by solar radiations or UV light located above the reactor. The thickness of the radial sheet jet is small enough to ensure light penetration for efficient catalyst activation and water oxygenation. Wastewater is continuously discharged into the reactor through the inlet. The reactor outlet is located just below the water level in the reactor in the form of a weir to ensure that the outflow is always equal to the inflow, thereby keeping the reactor effective volume (V) constant.

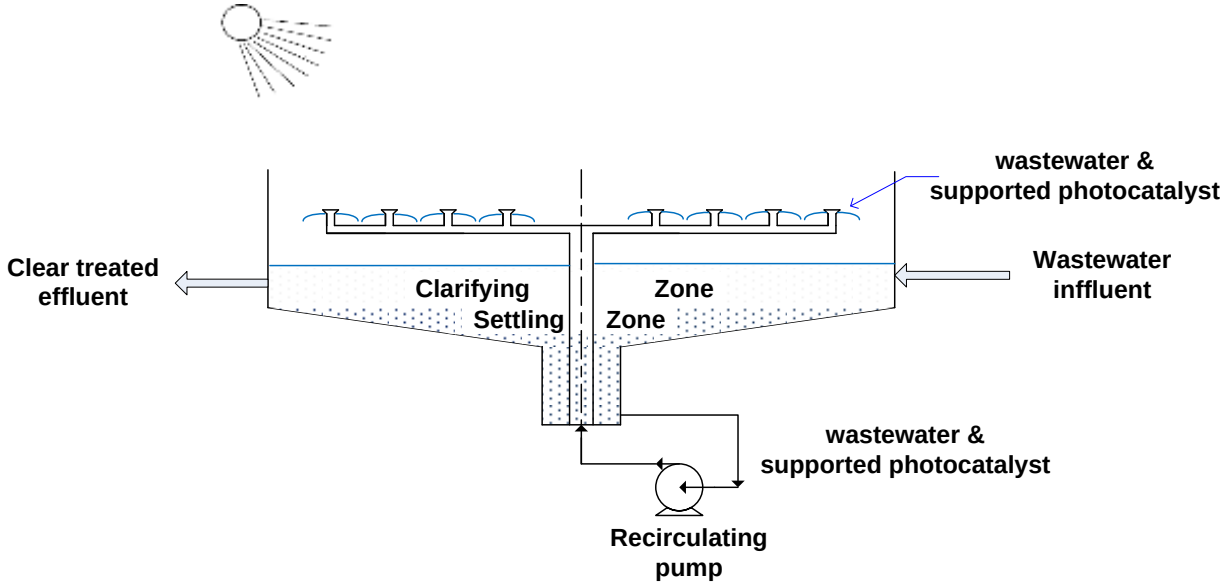

Figure 14: Schematic section of supported TiO_2 water- bell photo-reactor

The proposed conceptual design is suitable for scale-up and commercialization due to five distinctive features that are: (1) the modular design, increasing the number of nozzles for treating a larger volume, (2) an integrated storage to cope with treatment disturbances; no external recirculating tank is needed, (3) the photo-reactor does not include any UV transmitting components that would suffer from optical losses [128] and would be prone to UV-solarization from long exposure to solar radiation [127], (4) the photo-reactor does not include any UV transmitting walls that pose limitations on reactor size due to risk of breakage as well as having sealing and filming problems, and includes a section for the settling of the immobilized catalyst.

3.2 Support Selection

Suitable support material to be used for TiO_2 immobilization should be chemically inert, with good resistance to UV degradation, of low cost, and high density for easy separation by gravity. Sand was selected as a TiO_2 support for its high density (specific gravity 2.65). Additionally, it is locally available and cheap, chemically inert, mechanically resistant and abundant in various particle sizes.

The important issue here was determining the sand particle size and sand loading that meet the process hydrodynamic requirements. Two aspects were considered: the smaller the particle size, the larger is the surface area available for TiO_2 immobilization and the less susceptibility that the sand particles would cause pump wear. The larger the particle size, the faster the sand particles to settle by gravity and easier to separate from the treated effluent after treatment completion.

An analogy can be used from the commercial ACTIFLO process. ACTIFLO is a ballasted clarification process developed by Veolia Water Solutions where micro-sand is used to enhance floc formation and act as a ballast to aid in rapid settling of the coagulated material [161]. Micro-sand used in ballasted flocculation can vary in size from 40 to 300 microns, typical sand loading is in the range of 1 to 12 g/L [162]

Table 5 shows settling velocities for sand particles of different sizes calculated using stokes law [163] for discrete particle settling [164] of spherical particles under laminar flow conditions as shown by *Equation 14*.

$$v_S = \frac{g\,(\rho_p - \rho)\,Dp^2}{18\,\mu} \qquad \textit{Equation 14}$$

where v_S is settling velocity in m/s, g is the gravitational acceleration m^2/s, ρ_p and ρ are the density of sand and water respectively in kg/m^3, Dp is the solid particle diameter and μ is the water dynamic viscosity in kg/m.s .

Table 5: Settling velocities for sand particles of different sizes

Dp	micron	40	75	150	180	240	300
v_S	m/s	0.001	0.005	0.020	0.029	0.052	0.081
v_S	cm/min	8.62	30.32	121.28	174.64	310.46	485.10

Commercial non-technical grade sand used in construction activities was sieved using mechanical sieve shaker shown in Figure 15. Fraction having particle size ranging from 150-180 microns (passing sieve 80 and retained on sieve 100) was used for the photo-reactor hydrodynamic testing.

Figure 15: Mechanical Shaker

3.3 Light Source Selection

Rutile has a bandgap of 3.00 eV while anatase has a bandgap of 3.23 eV [98]. UV radiation is classified as UV-A which has its wavelength spans from 400 to 315 nm having photon energy of 3.10 to 3.94 eV, UV-B whose wavelength spans from 315 to 280 nm having photon energy of 3.94 to 4.43 eV and UV-C whose wavelength spans from 280 to 100 nm having photon energy of 4.43 to 12.4 eV [37]. The photon energy is calculated using Equation 15 [165]:

$$E = \frac{h.c}{\lambda} = \frac{1.2398}{\lambda} \qquad \textit{Equation 15}$$

where E is the photon energy in keV, h is the Planck's constant ($6.62 * 10^{-34}$ j/s), c is the speed of electromagnetic radiation in vacuum ($3 * 10^{8}$ m/s) and λ is the wavelength in nm. From Equation 15, anatase, can be activated using light having wavelength < 384 nm.

Among the commercially available artificial UV light sources are Xenon arc lamps, low pressure germicidal lamps and black light (BL) lamps. Xenon arc lamps are high intensity discharge lamps in which Xenon gas is kept at high pressure of several atmospheres. Xenon lamps are available from 5 to 32,000 W [166]. They have a broadband emission spectra that extends from the UV range to the infrared (185 – 2000 nm) [167]. Most of the input electrical energy is converted to heat and visible light, while about 10% is emitted in the UV range [168]. Although Xenon arc

lamps can be used as sun simulators, they are expensive [169]. They also have a short operational life time of about 1000 hours [39].

Low pressure germicidal lamps are discharge lamps containing mercury at low pressure of 0.01 atm [170]. They emit UV-C light having a wavelength of 254 nm. BL are fluorescent lamps that emit UV-A light having a wavelength of 350±20 nm. Fluorescent lamps are low pressure mercury discharge lamps whose bulbs are internally coated with a phosphor. Germicidal lamps and fluorescent lamps have an operational life time of 4000 to 14000 hours [39]. Their power is limited to < 215 watt [166]. Germicidal lamps are made of quartz to allow the transmission of UV-C light, where quartz has cut off at 200 nm [39] while fluorescent lamps are made of the cheap low-iron borosilicate glass that transmits radiations higher than 285 nm [127].

UV-C light which is dangerous and may cause skin cancer and blindness. Atmospheric ozone absorbs all UV-C and prevent them from reaching earth surface [171]. Although UV-A light photocatalytic systems are less efficient than UV-C light photocatalytic systems in terms of photon energy, BL lamps were selected as an artificial UV-A light source since UV-A light poses less risk to biological systems. BL lamps are used insect traps [172], thus no special safety precautions are needed to be incorporated in the photo-reactor design.

In order to select the appropriate BL lamps in terms of wattage and number, it is necessary to determine the light intensity range at which the photocatalytic degradation experiments are to be conducted. The ultimate objective of the photocatalytic reactor design is to use solar radiation for catalyst activation. The UV light intensity reaching a particular location depends on solar elevation, scattering by clouds, absorption by ozone, aerosols and atmospheric gases, altitude, surface albedo and the elliptical orbit of the earth about the sun [171]. The average amount of UV solar radiation received by the earth's atmosphere per unit area is given by UV solar constants. UV-A solar constant is 70.64 W/m^2 for $320 \leq \lambda \leq 390$ and while UV-B solar constant is 19.02 W/m^2 for $290 \leq \lambda \leq 320$ [173]. 90 W/m^2 is the upper limit for UV intensity to be used for conducting the photocatalytic tests.

3.4 Model Contaminant Selection

Phenol is chosen as a model contaminant in this study since:

1- It is one of the pollutants included in the EPA priority pollutants list [174]
2- It is a precursor for various emerging contaminants in the environment [44]
3- It is an intermediate product in the oxidation pathway of high molecular weight aromatic compounds [175].
4- Phenols and phenol derivatives easily donate a free electron forming phenoxy radicals that can penetrate living cells, damaging their mitochondria, endoplasmic reticulum membranes, nucleus, nuclic acids and enzymes [101].

Heterogeneous TiO_2 catalysis has been successfully used in the degradation of numerous phenolic compounds including chlorophenol [60], [176], [144], [78], [140], dinitrophenol [40], [136], pentachlorophenol [112], trimethylphenol [73], bisphenol A [42], the antimicrobial triclosan [97], the fungicides pyrimethanil [143] and Imazlil [80], the herbicide 2,4-D [79], the analgesic salicylic acid [177], [153] and paracetamol [178], the anti-inflammatory Dichlofenac [133], the surfactant Triton-X 100 [85], the dyes methyl orange [179], [180], direct yellow 12 [68] and congo red [150], the food colorants fast green and patent blue [62]. The chemical structures of some these phenolic compounds are shown in Figure 16.

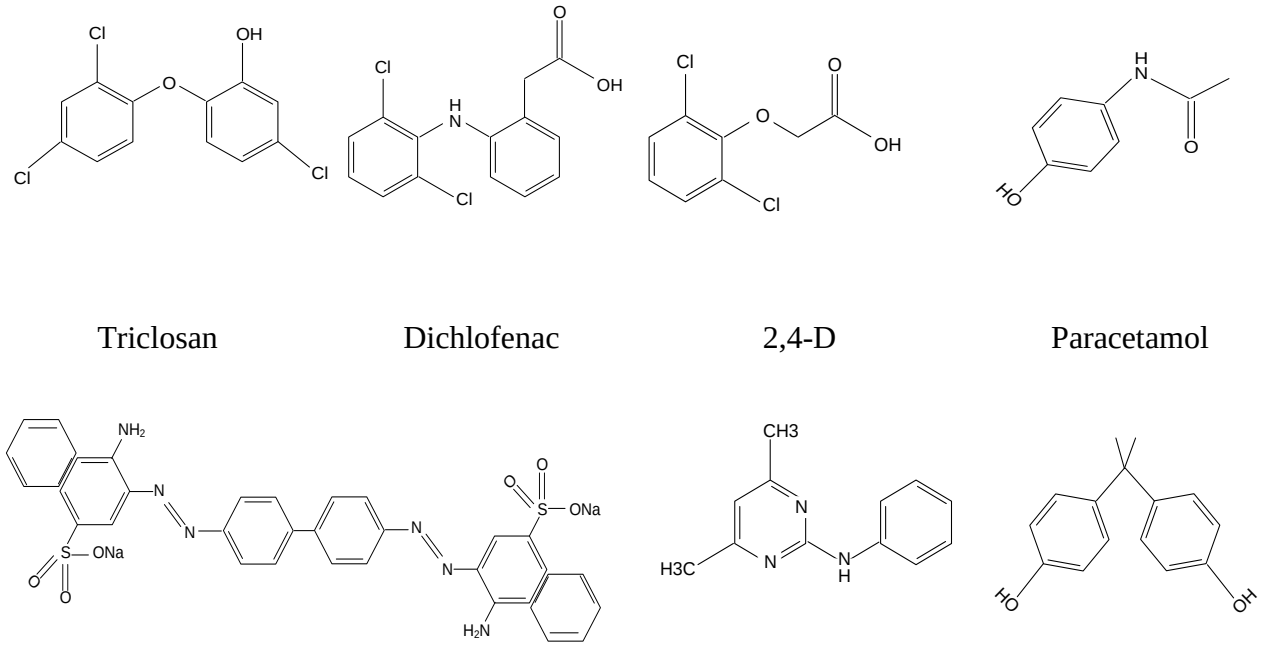

Figure 16: Chemical structure of some popular phenolic compounds, adapted from [133], [150]

3.5 Development of Pilot-scale Reactor

Sizing of the physical model including reactor dimensions and determination of recirculation components specifications, was accomplished after the determination of sand particle size and catalyst loading range. The proposed design is shown in Figure 17.

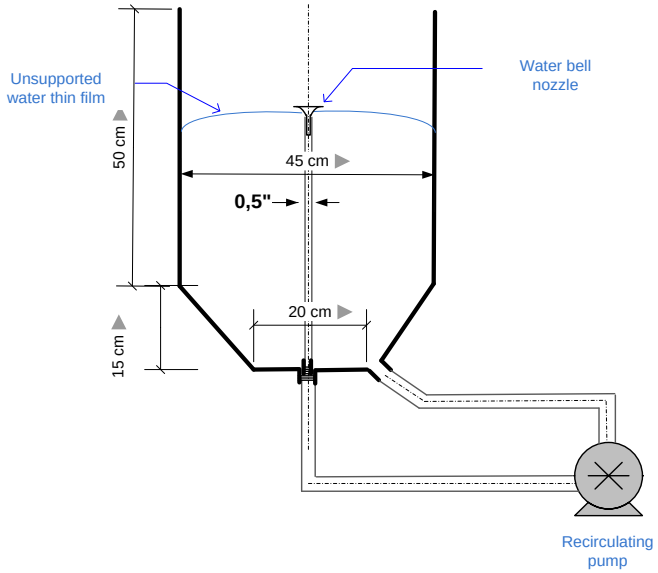

Figure 17: Schematic drawing of preliminary photo-reactor

A preliminary cheap plastic reactor with the suggested dimensions was fabricated. The preliminary plastic reactor is shown in Figure 18.a and Figure 18.b. The reactor was assembled with a commercial water-bell nozzle, recirculation pump, piping and fittings. Thin film generation as well as recirculation of the sand were successfully achieved through the reactor model, however, an issue of sand settling in the reactor bottom was encountered as shown in Figure 18.c.

Figure 18: Preliminary plastic reactor

These results were used for modifying the reactor model. In order to facilitate sand suction with the flow, the pump suction line was connected to a narrow sump at the tank bottom while the pump discharge line was connected to the vertical feeder and the nozzle from the tank side as shown in Figure 19.

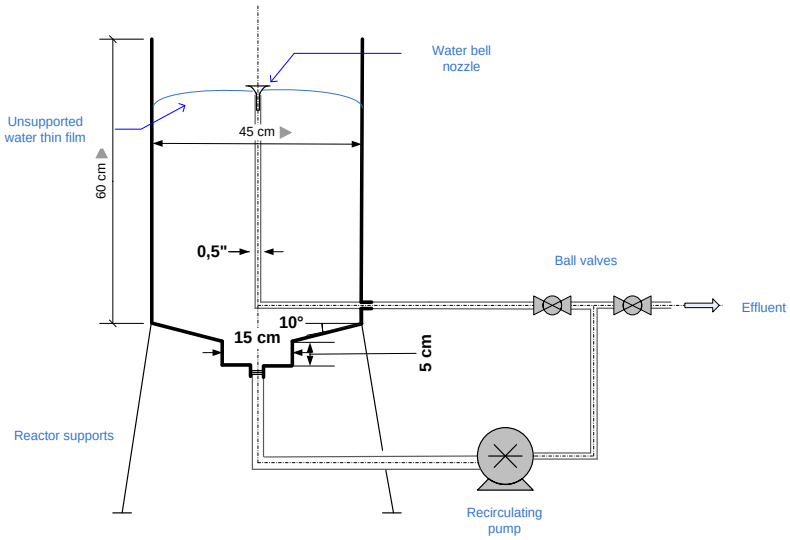

Figure 19:Schematic drawing of modified photo-reactor

The new prototype was fabricated from stainless steel, an inert material that would not interfere with the treatment outcomes. The new prototype is shown in Figure 20.a and Figure 20.b. Despite the modifications, the settled sand was not directed to the central hoper, as seen in Figure 20.c, which indicates that the internal circulation was missing the catalyst.

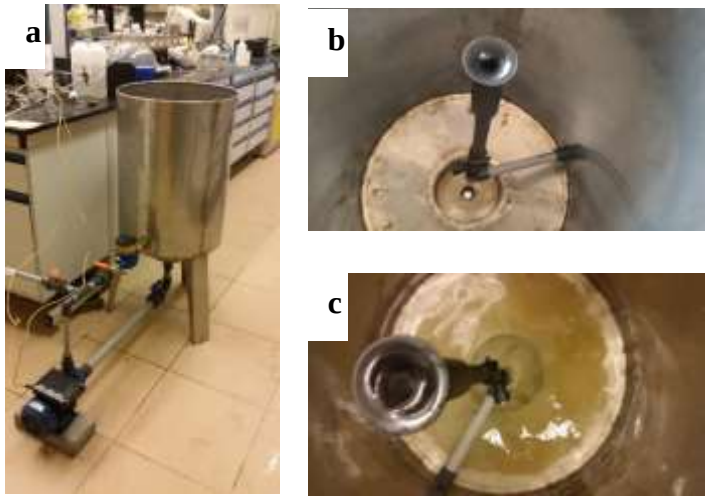

Figure 20: Stainless steel photo-reactor

These results were used for finalizing the physical model. The photo-reactor was modified to have a conical bottom to avoid sand settling outside the central hoper.

3.6 Pilot-scale Photocatalytic Reactor

The final photocatalytic reactor is a stainless cylindrical steel tank, 45 cm in diameter, having a conical bottom, equipped with a commercial water-bell nozzle and a commercial peripheral pump (Matra, CM6/1, 0.5 hp). The pilot-scale photo-reactor is operated in a recirculating mode after being filled as a batch reactor. The flow rate through the water-bell nozzle is measured by a commercial flow meter (½" multi-jet water meter, magnetic drive dry-dial). Four UV-A lamps (Sylvania, blacklight 350 nm, 15 W each) are used for illuminating the reactor. These lamps are emitting UV radiation between 315 nm and 400 nm with a peak at 352 nm. The lamps are installed equidistantly in a 45 cm*45 cm lamp casing that is hung over the reactor using a chain block to guarantee a uniform light distribution over the water film. The light intensity on the thin water film is controlled by varying the distance between the water film and the light source. Figure 21 shows a schematic section of the pilot-scale photo-reactor.

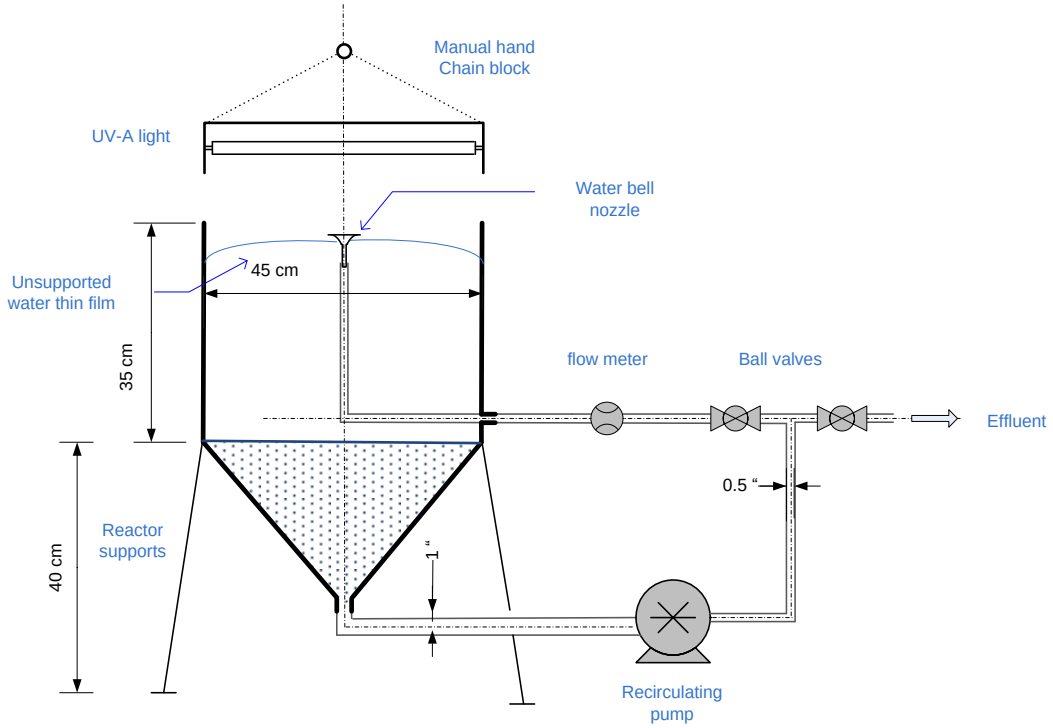

Figure 21: Schematic section of the pilot scale water-bell photocatalytic reactor

The pilot water-bell photoreactor is shown in Figure 22.a .As seen from Figure 22.b and Figure 22.c, a water fountain that extended along the tank diameter was generated, and sand recirculation was achieved.

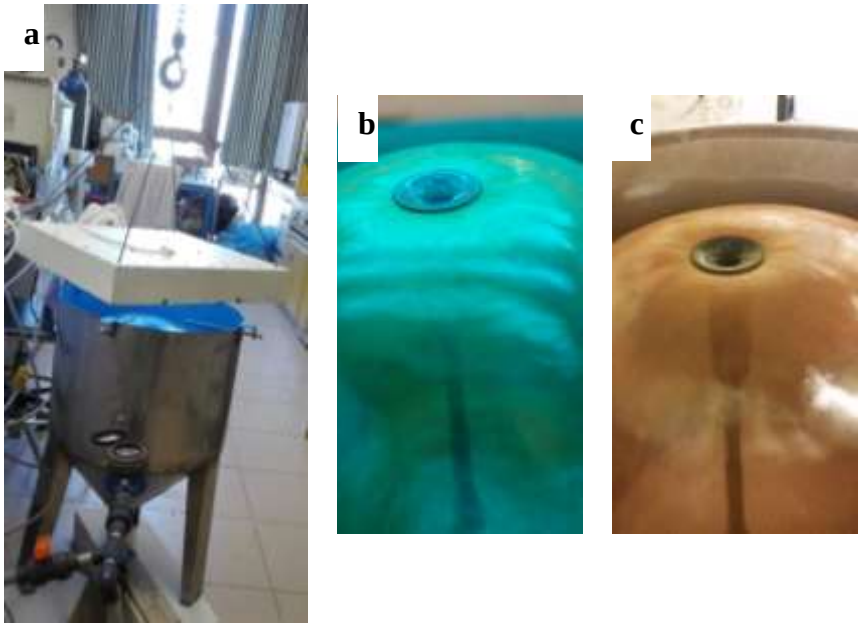

Figure 22: Pilot scale water-bell photocatalytic reactor

After the successful hydrodynamic testing of the prototype, evaluation of the photocatalytic reactor performance in phenol degradation using slurry TiO_2 started.

Chapter IV

Slurry Water-bell Photo-reactor

A set of tests using slurry TiO_2 were carried out to assess the photocatalysis function of the slurry water-bell photo-reactor (SWBP), referred to as slurry mode tests. The tests were planned to investigate the effect of catalyst loading, light intensity, initial concentration, addition of hydrogen peroxide and exposure time on treatment efficiency. Dissolved oxygen (DO) concentration, temperature and pH were monitored throughout all the runs. Photocatalytic degradation tests were carried in a recirculating batch mode using commercial TiO_2 (aeroxide P25). All treatment tests were conducted at natural tap water pH with no pH adjustment. All treatment tests were restricted to 4 hours. A longer treatment period would result in a low throughput that will render the photo-reactor inappropriate to scale-up and commercialization.

4.1 Experimental Procedure

The aeroxide P25 (purity 99.5%, Aldrich, with an average particle size of 21 nm, approximate BET surface area 35-65 m^2/g, anatase to rutile ratio is 80:20) was used as received. Phenol (purity 99.5 %, Riedel-deHaen) used as received was added to tap water. No pH adjustment was conducted. A 25mL sample was withdrawn hourly for analysis. DO concentration, temperature and pH were monitored throughout all runs. An oxygen probe and oximeter (Hach, Lange LDO101) were used for measuring DO and temperature. A probe and pH meter (Thermofischer, Orionstar A211 pH meter) were used for measuring pH.

The samples were filtered using 0.45 micron Whatmann syringe, then phenol analysis was conducted. The 4-Aminoantipyrine method adapted from EPA method #420.1 [181] and Hach method #8047 [182] was used for phenol determination. The direct photometric method without solvent extraction is adequate for measuring phenolic concentrations higher than 50 µg/L. At an alkaline pH of 10, phenols react with 4-aminoantipyrine in the presence of potassium ferricyanide producing antipyrine dye that has a stable reddish-brown color. A direct-reading spectrophotometer (Hach, DR/2000) was used to read absorbance at 510 nm after 15 min for samples as well for the standards needed for constructing the concentration – absorbance calibration curve.

Light intensity was measured hourly using a digital UV light meter (General UV513AB) and adjusted if necessary. The digital UV light meter measures UV radiation in the range of 280 nm to 400 nm. Flow through the system was measured hourly using the commercial flow meter. All standards were prepared using deionized water. Hydrogen peroxide solution (50% W/W) was used. The detailed operational parameters and degradation results for some of the experimental runs are included in **Annex I**.

4.2 Catalyst Loading and Light Intensity

A factorial design of experiments was adopted, testing two levels of light intensity (60 and 90 W/m^2) and four levels of catalyst loading (0.35, 0.7, 1.4 and 3 g/L). Tests were conducted for treating 7 liters with a phenol initial concentration of 20 mg/L and recirculating flow rate of 19 L/min. Variation of phenol concentration (C) as treatment proceeded is shown in Figure 23.

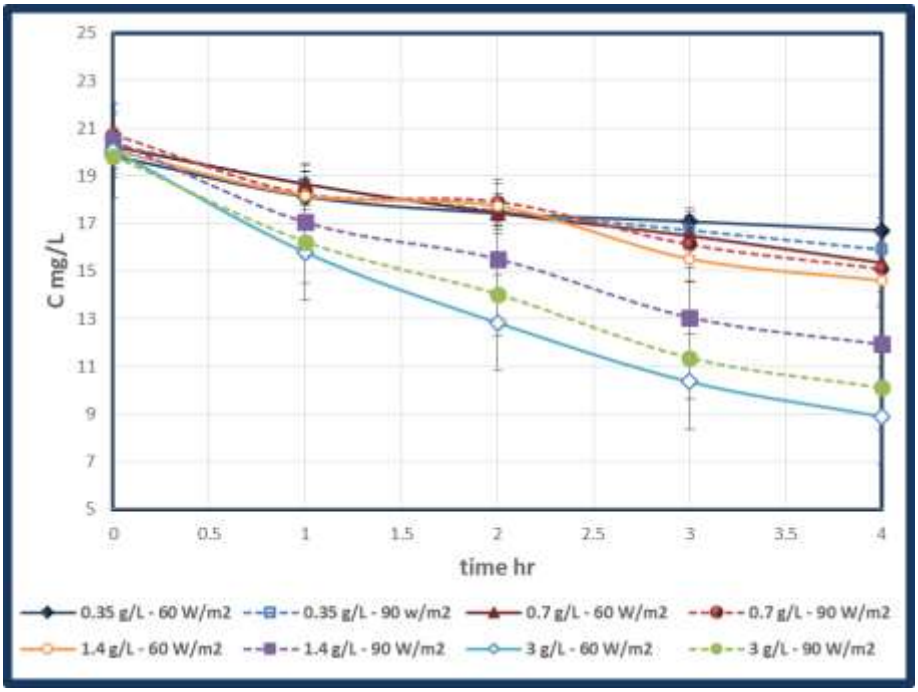

Figure 23: Effect of catalyst loading and light intensity on phenol treatment

To ensure that the achieved degradation was attributed to photocatalytic degradation not air stripping nor photolysis, wastewater was recirculated for 4 hours at similar flow rate: 1) in absence of light and TiO_2, 2) under UV-A light in absence of TiO_2. There was no phenol removal by

aeration only. This is in agreement with other researchers' finding that phenol is not lost by stripping even while air bubbling of the reaction solution is conducted [183]. This is expected owing to the phenol low henry's constant ($3.97*10^{-7}$ at 20°c). Additionally, there was no phenol removal when recirculation was carried under UV-A irradiation in absence of TiO_2. This is in accordance with other researchers finding that photolysis of phenol with UV-A light does not occur [138], [184].

The residual phenol concentration decreased from 16.7 to 8.9 mg/L as the catalyst loading increased from 0.35 to 3 g/L at a light intensity of 60 W/m^2. At light intensity of 90 W/m^2, the residual phenol concentration decreased from 15.9 to 10.1 mg/L as the catalyst loading increased from 0.35 to 3 g/L. Table 6 presents phenol percent reduction achieved for different catalyst loadings at the two levels of light intensity.

Table 6: Phenol percent reduction as a function of catalyst loading at different light intensities

catalyst g/L	Light Intensity	
	60 W/m^2	90 W/m^2
0.35	15.8	21.7
0.7	24.2	27.3
1.4	27.3	41.8
2.9	55.7	49.0

At low and moderate catalyst loadings up to 1.4 g/L, phenol degradations at 90 W/m^2 were higher than those at 60 W/m^2. When using a high catalyst loading of 3 g/L, phenol reductions at 60 and 90 W/m^2 were comparable as demonstrated in Figure 24.

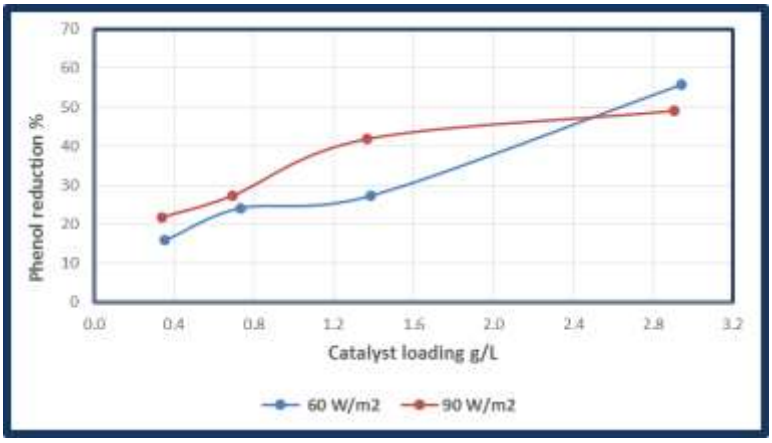

Figure 24: Phenol reduction as a function of catalyst loading at different light intensities

A two-way analysis of variances (ANOVA) was conducted to investigate the effect of catalyst loading and light intensity and to determine which of the two parameters has a significant effect on the treatment efficiency. At a level of significance (1- alpha) of 95, the catalyst loading had $F_{Catalyst\ loading}$ (13.7) which was higher than $F_{Critical}$ (9.2), indicating that catalyst loading significantly affects the treatment efficiency. The P-value (0.03) was smaller than the used alpha (0.05). As for light intensity, the $F_{Light\ intensity}$ (0.6) was smaller than $F_{Critical}$ (10.1), indicating that variation of light intensity from 60 to 90 W/m^2 does not enhance the treatment efficiency.

To confirm this finding, Tukey's test was conducted to compare the treatment means at the two light intensity levels for different catalyst loadings. Tukey's difference (Tα) is calculated by Equation 16 [185].

$$T\alpha = q\alpha(a, f)\sqrt{MSE/n} \qquad \textit{Equation 16}$$

At a significance level of 99.5, for every catalyst loading, the difference between the treatments averages at the two light intensity levels where smaller than Tα confirming that variation of light intensity from 60 to 90 W/m^2 did not affect the treatment efficiency. The detailed two-factor ANOVA analysis and Tukey's test are included in **Annex II** and **Annex III**.

A similar finding was encountered on treating diluted landfill effluent in a TFFBR using light intensity of 50 and 100 W/m^2. TOC removal of 36 % and 43% were achieved respectively. A 6% increase in TOC removal, achieved when light intensity was increased from 50 to 100 W/m^2, reflected a loss of photonic efficiency as light intensity was increased [146]. On treating ammonia in a shallow pond reactor using light intensities of 45 and 171 W/m^2, degradation achieved was 42.2 % and 58.1% respectively. An additional degradation of 16% was attained while using the 171 W/m^2 light intensity taking into consideration that a cooling water system was needed to keep the reactor temperature at ambient temperature [83].

It is well known from the literature that at low levels of light intensity, the photocatalytic reaction rate increases as the light intensity increases until a threshold value is reached where the reaction rate is independent of the light intensity [124]. At low light intensities, the rate of electron-hole formation increases as the light intensity increases, where the hole formation is the rate-limiting step. At high light intensities, with the abundance of the photogenerated oxidative species, the

reaction rate becomes mass transfer controlled [35]. This light intensity threshold value varies according to the reactor design and target pollutant [130].

To avoid loss of photonic efficiency and unnecessary heating of the reaction solution, high light intensities were not further applied for photocatalytic degradation tests in the water-bell photo-reactor.

4.3 Appropriate Catalyst Loading

Since the rate of photo-degradation has increased with increasing the catalyst loading, additional tests were conducted using 2, 4 and 6 g/L to determine the maximum catalyst loading. Tests were conducted treating 3 liters with phenol initial concentration of 25 mg/L, recirculating flow rate 19 L/min, at a light intensity of 60 W/m^2. Using 4 g/L led to the highest degradation efficiency of 64% as shown in Figure 25.a. At catalyst loadings higher than 4 g/L the degradation efficiency decreased. This can be attributed to the screening effect induced by the highly turbid suspension and the associated light scattering [37]. As shown in Figure 25.b, the increase in catalyst loading from 2 to 4 g/L lead to an incremental increase in the degradation efficiency of only 7%. From an operational cost point of view, this relatively small enhancement does not justify doubling the catalyst loading. Therefore a catalyst loading of 2 g/L may be considered as more appropriate.

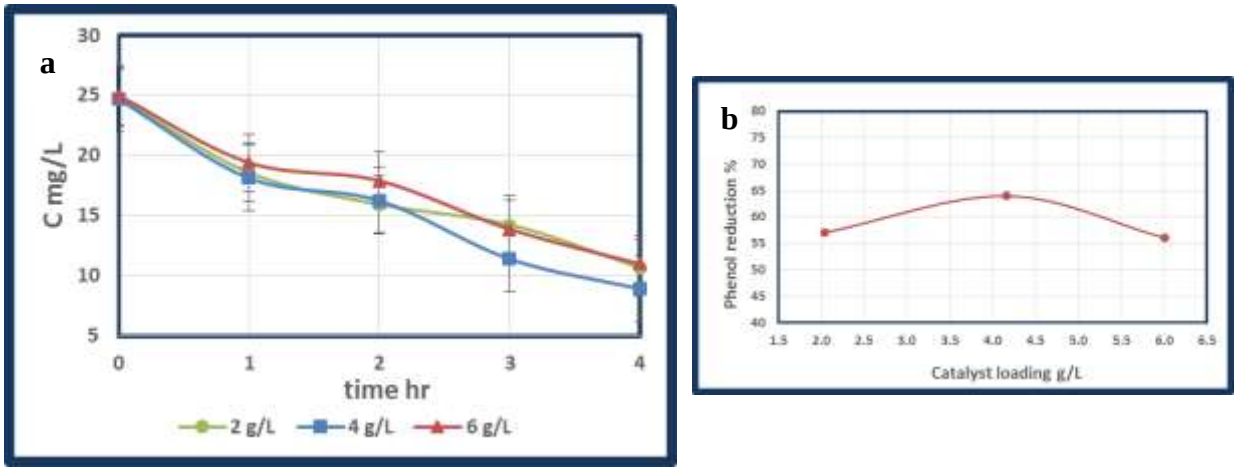

Figure 25: Effect of catalyst loading on phenol reduction: a) concentration profile, and b) reduction %

4.4 Degradation Kinetics

Photocatalytic degradation kinetics can be widely explained using Langmuir-Hinshelwood (L-H) kinetic model - Equation 17 - for solid-liquid reactions [186], where C is the pollutant initial concentration, k_r is the reaction rate constant and K_{ads} is the adsorption coefficient of the pollutant on the TiO_2 surface. When the pollutant concentration is high (C> 5 mM), the term $K_{ads}C$ will be much higher than 1, thus the L-H model is simplified into the zero-order reaction model [124]. The degradation rate is maximum as described by Equation 18, where K is the degradation rate constant. When the pollutant initial concentration is low (C<<1 mM), the term $K_{ads}C$ will be negligible thus the L-H model is simplified into the pseudo first-order reaction model [95], as described by Equation 19, where K_{app} is the apparent degradation rate constant.

$$r = -\frac{dC}{dt} = \frac{k_r \,.\, K_{ads}.\, C}{1 + K_{ads}.\, C} \qquad \textit{Equation 17}$$

$$r = -\frac{dC}{dt} = K \qquad \textit{Equation 18}$$

$$r = -\frac{dC}{dt} = K_{app}.\, C \qquad \textit{Equation 19}$$

$$C = C_0\, e^{-K_{app} t} \qquad \textit{Equation 20}$$

For different catalyst loadings at the two light intensities, a plot of -ln C/Co against t was constructed, where C, Co and t are the pollutant concentration, initial concentration and time, respectively. The plot was linear with a slope of K_{app} as shown in Figure 26. The values of K_{app} and their corresponding coefficient of determination (R^2 value) are shown in the figure as well. Phenol photocatalytic degradation fitted the pseudo-first order reaction kinetic model expressed by Equation 20.

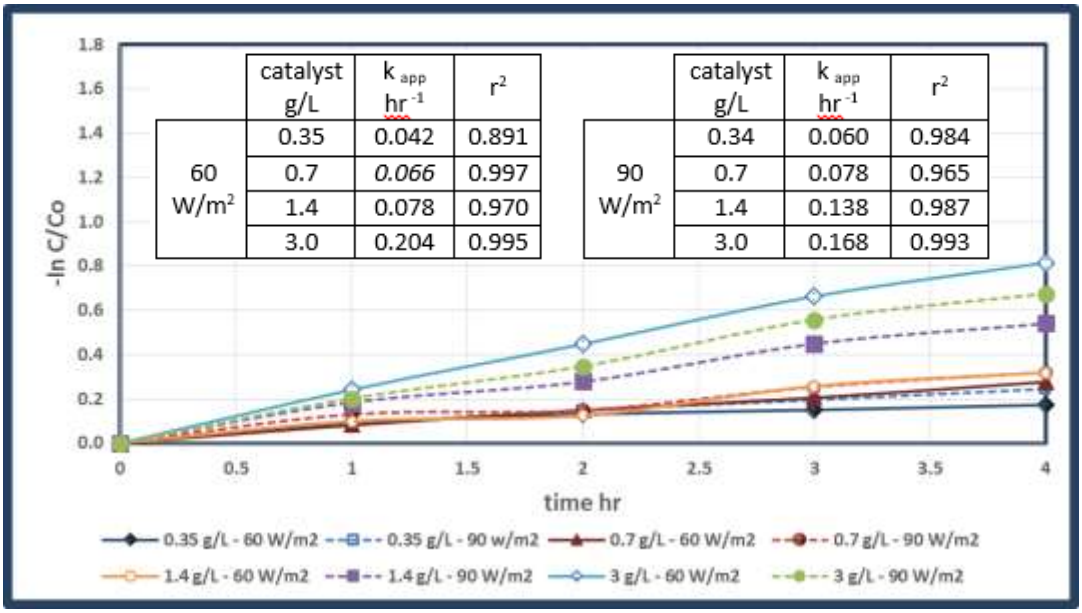

	catalyst g/L	k_{app} hr^{-1}	r^2
60 W/m²	0.35	0.042	0.891
	0.7	*0.066*	0.997
	1.4	0.078	0.970
	3.0	0.204	0.995

	catalyst g/L	k_{app} hr^{-1}	r^2
90 W/m²	0.34	0.060	0.984
	0.7	0.078	0.965
	1.4	0.138	0.987
	3.0	0.168	0.993

Figure 26: Effect of catalyst loading and light intensity on degradation rate

In order to confirm that phenol photocatalytic degradation in the SWBP fitted the pseudo-first order reaction kinetic model, the effect of initial concentration of phenol on the apparent degradation rate constant was investigated using an initial concentration of 13 and 25 mg/L (0.14 and 0.26 mM). Tests were conducted for treating 3 liters under UV-A light intensity of 60 W/m^2, at a recirculating flow rate of 18.6 L/min. K_{app} was almost equal for the two initial concentrations, 0.192 and 0.198 hr^{-1} as shown in Figure 27.

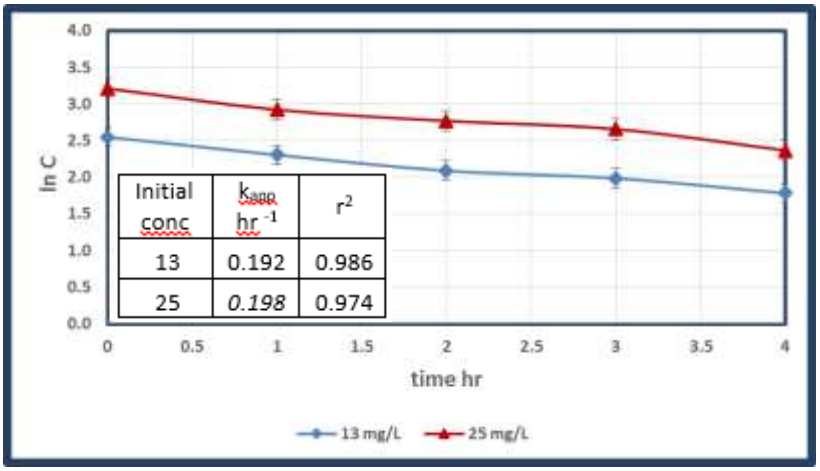

Initial conc	k_{app} hr^{-1}	r^2
13	0.192	0.986
25	*0.198*	0.974

Figure 27: Effect of initial concentration on apparent degradation rate

This finding is further confirmed when explained in the context of reaction pH. Researchers have reported that TiO_2 photocatalytic degradation of phenol increases as pH increases from 2 to 6.5, and decreases at higher pH up to 11 [33]. In another study, it was demonstrated that at pH 4, 68% phenol degradation was achieved. Phenol degradation was decreased to 51% at pH 7 and 39% at pH 9 [34]. This was attributed to the catalyst surface charge that affects the contaminants adsorption-desorption on the catalyst surface. The PZC of P25 is around 6.5 [61]. At lower pH values, the TiO_2 surface is positively charged. At PZC, the surface is neutral while at higher pH values, the TiO_2 surface is positively charged according to the equilibrium equations (Equation 21 & Equation 22) [37];

$$\text{At pH} < \text{PZC} : TiOH + H^+ \leftrightarrow TiOH_2^+ \qquad \textit{Equation 21}$$

$$\text{At pH} > \text{PZC} : TiOH + OH^- \leftrightarrow TiO^- \qquad \textit{Equation 22}$$

Phenol is a weak acid, having an acid dissociation constant k_a of 10^{-10}. Phenol dissociates in water according to Equation 23, where PHOH and PHO^- are phenol and phenolate ion concentrations. At pH < pKa, phenol exists in the non-ionic form, while at pH > pKa, phenol exists as the phenolate ion.

$$PHOH \rightleftharpoons PHO^- + H^+ \quad , \quad pKa = 10 \qquad \textit{Equation 23}$$

In acidic pH, phenol exists in the nonionic form, and adsorption on the positively charged TiO_2 enhances the degradation rate. In alkaline pH, phenol exists as the negatively charged phenolate ions, and the coulombic repulsion between phenolates and the negatively charged TiO_2 surface slows the degradation process [36]. Through all the runs, tap water spiked with phenol is used. Tap water pH is alkaline in the range of 8. At this pH, phenol adsorption on the negatively charged TiO_2 surface is disfavored as concluded from the pC-pH diagram shown in Figure 28, where pC equals –log(C), C being the concentration of the species at hand. However all the tests were conducted at this pH that is more likely to resemble municipal wastewater pH.

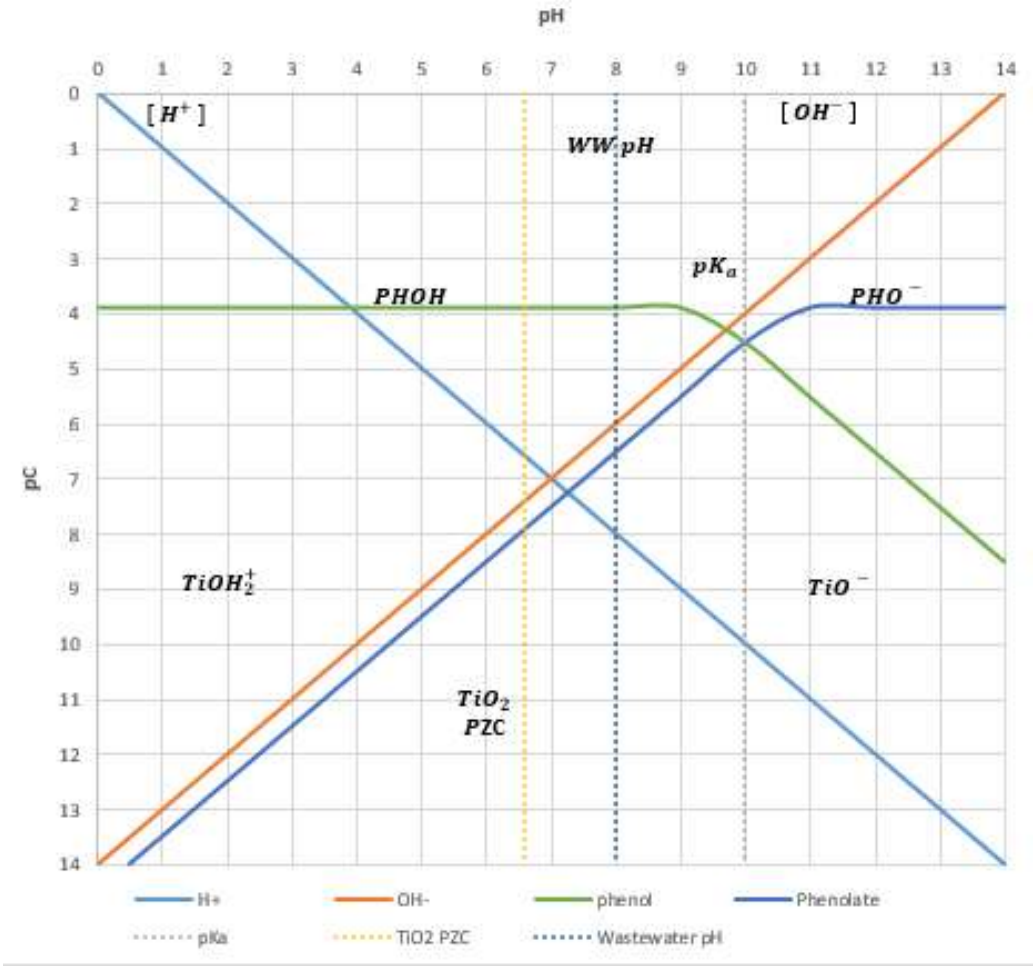

Figure 28: pC - pH diagram for a total phenol concentration of 0.14 mM, at 25°C, adapted from [32].

4.5 Temperature and DO Levels

DO levels are expected to decrease as the treatment proceeds due to: (1) consumption in the degradation process, (2) stripping off due to the rise in water temperature. The increase of the reaction temperature without aeration has an adverse effect on the degradation efficiency. In photocatalytic degradation tests of water contaminated with benzoic acid, using thin film cascade reactors without solution aeration, as the temperature increased from 18 to 28 °C, TOC removal decreased by 8%. Researchers attributed reduced removal efficiency to the decrease in DO levels [149].

Throughout all the runs in the SWBP, despite the rise in temperature, aeration was sufficient to keep DO levels constant around saturation. The maximum rise in temperature during the experimental runs had an average of 3.2°C. Figure 29 shows the results achieved during the trial that recorded the highest maximum rise in temperature while treating 3 L of wastewater containing 25 mg/L phenol. The test was conducted using a catalyst loading of 4 g/L, at a recirculating flow rate 19 L/min and light intensity of 60 W/m^2. DO concentration remained constant during the treatment although 64% reduction in phenol concentration was achieved while an increase of 4.7°C in water temperature was encountered.

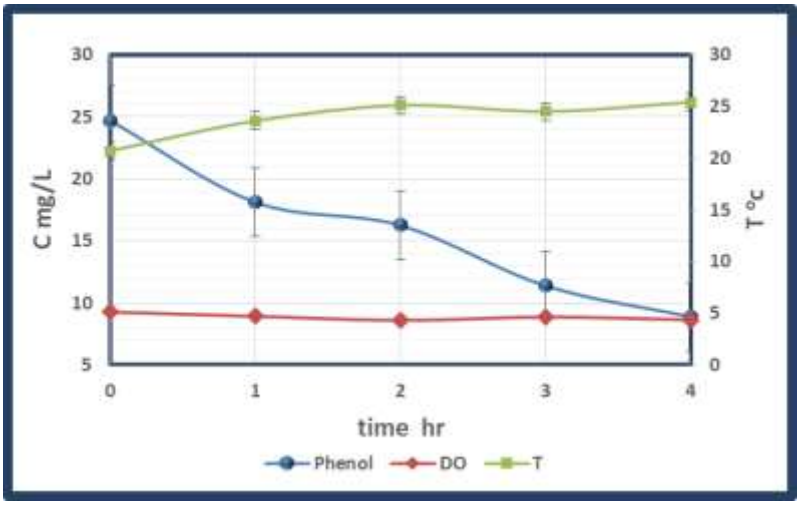

Figure 29: Variation of phenol concentration, reaction temperature & DO with treatment time

During several tests conducted using CPCs under sunny conditions in PSA, Spain, with UV-A intensity in the range of 20-30 W/m^2, the temperature of the effluent in these experiments was 40°C [150] and higher [69], [131]. One of the merits of the passive aeration of the water-bell photo-reactor is the limited temperature rise rendering temperature control and additional cooling unnecessary. This is obvious from the results of the test conducted on a sunny day in February 2017. The test was conducted on the roof of the School of Sciences and Engineering building on the AUC campus in New Cairo. The maximum and minimum wind speed reported in Cairo during that day were 34.5 and 9.61 mph respectively. The average UV light intensity (UV-A & UV-B) during the test was 45 W/m^2. Photocatalytic degradation of 56% of phenol was achieved during treating 7 L of wastewater having a phenolic concentration of 20 mg/L. The maximum rise in

temperature was 0.5 °C, in fact as treatment proceeded temperature decreased. The UV light intensity, temperature, phenol and DO concentration are shown in Figure 30.

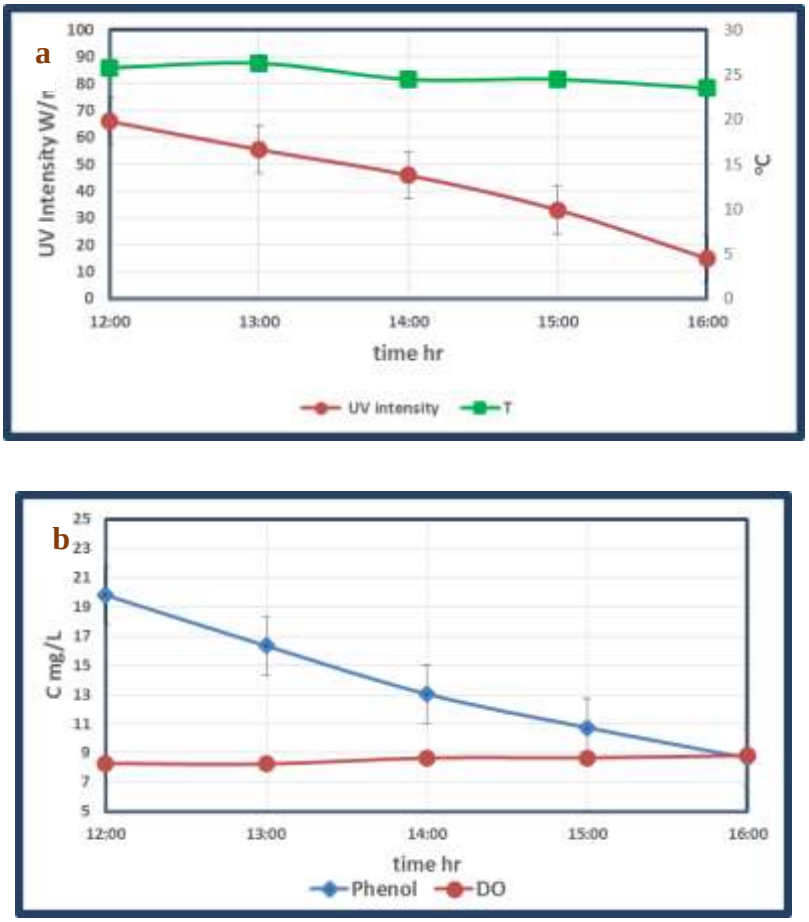

Figure 30: Variation of : a) UV intensity and temperature, b) phenol & DO concentration, during sun condition test

4.6 Oxidants Addition

Dissolved oxygen desorption from TiO_2 surface is favored with an increase in temperature. The absence of electron scavengers on the catalyst surface promotes hole/electron recombination thus impairs the degradation process [95]. One strategy to enhance the degradation efficiency is to add chemical oxidants to act as electron scavengers. Hydrogen peroxide and persulfates are the commonly used oxidants in photocatalytic treatment tests. Persulfate, having an EOP of 2.01 V [35] is a more powerful oxidant than hydrogen peroxide. However, hydrogen peroxide was used

in this study, because with an increased dose of persulfate, it can become a secondary pollutant itself increasing sulfate levels in the treated water. Sulfates in treated water for reuse are being regulated recently at a maximum limit of 500 mg/L in many countries [4].

The tests treated 7 L of wastewater having a phenol initial concentration of 20 mg/L, recirculating at a flow rate of 19 L/min, and using light intensity of 60 W/m^2. Figure 31 shows phenol reductions achieved when using: (i) 250 mg/L H_2O_2 only, (ii) TiO_2 only, (iii) TiO_2 and 50 mg/L H_2O_2, (iv) TiO_2 and 150 mg/L H_2O_2. The maximum temperature rise during the four tests were 3.3, 3.4, 3.5 and 2.8 °C respectively. Analysis of variances for H_2O_2 addition was conducted. At a level of significance of 95, H_2O_2 addition had the P-value (0.026) smaller than alpha (0.05), $F_{H_2O_2\ addition}$ (5.92) was higher than $F_{Critical}$ (4.46), indicating that H_2O_2 addition significantly affects the treatment efficiency. The detailed two-factor ANOVA analysis is included in **Annex IV.**

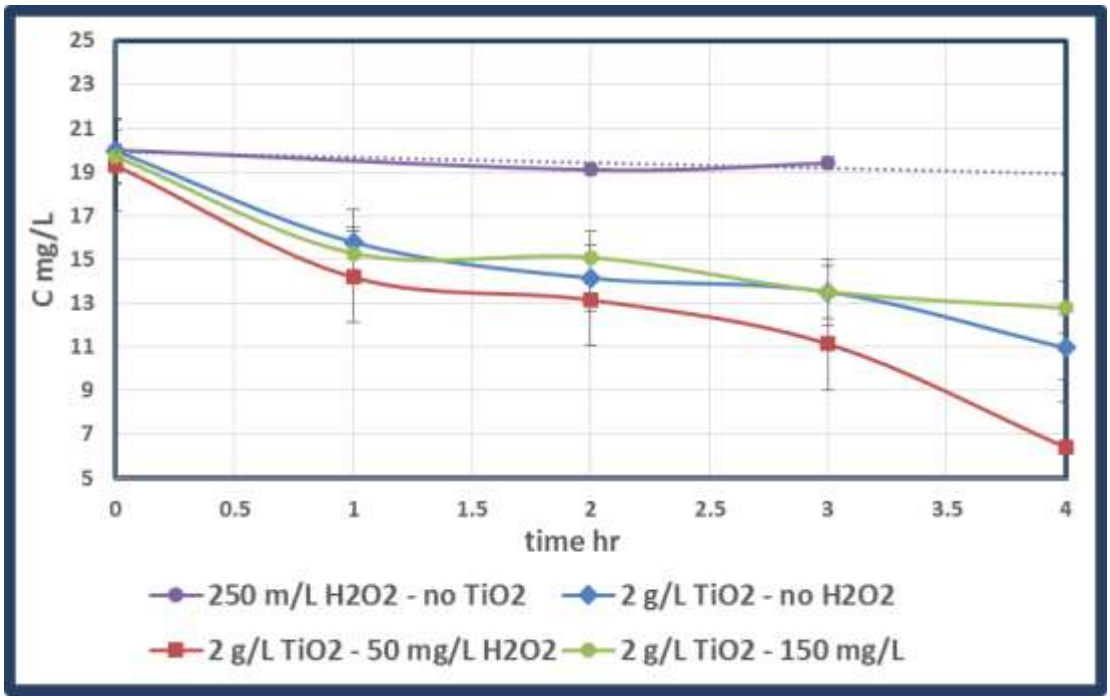

Figure 31: Effect of H_2O_2 addition on phenol reduction

Using of 250 mg/L H_2O_2 alone under UV-A light did not lead to any phenol degradation. This was expected since cleavage of the peroxide bond to produce highly reactive $OH^{\bullet}$ requires UV-B light having wavelength shorter than 300 nm [70]. H_2O_2 is stable at room temperature, and its

decomposition into reactive hydroxyl radicals requires activation. Activation can be achieved either by UV, ozone, or catalysis by transition metals such as Fe^{2+}/Fe^{3+} (Fenton process) [187].

$$H_2O_2 \xrightarrow{\lambda \leq 300\ nm} 2\ OH^{\bullet} \qquad \textit{Equation 24}$$

On treating 7L of water, phenol reduction increased from 41% when using TiO_2 solely to 67% when using TiO_2 and 50 mg/L H_2O_2. When the concentration of H_2O_2 was increased to 150 mg/L, there was no degradation improvement. This is in agreement with other researchers' findings about the optimum concentration for H_2O_2 when it acts as an electron scavenger that produces additional hydroxyl radicals as previously illustrated by Equation 9. At higher concentrations, H_2O_2 impairs the degradation efficiency where excess H_2O_2 scavenges $OH^{\bullet}$ producing the less reactive $HO_2^{\bullet}$ which can further scavenge more $OH^{\bullet}$ according to Equation 25 and Equation 26 [71].

$$H_2O_2 + OH^{\bullet} \rightarrow HO_2^{\bullet} + H_2O \qquad \textit{Equation 25}$$

$$HO_2^{\bullet} + OH^{\bullet} \rightarrow O_2 + H_2O \qquad \textit{Equation 26}$$

4.7 Exposure Time

The water-bell photo-reactor has two distinctive times: residence time and direct exposure time ($t_{exposure}$). For the recirculating batch mode, residence time is the total treatment duration ($t_{treatment}$). The exposure time $t_{exposure}$ is the time of exposure of the water thin film to the light which is the sum of exposure cycles. The exposure time of a cycle ($t_{exposure/cycle}$) is the time duration during which the water particle is exposed to light as it exits the nozzle until it hits the tank boundary and falls downward. The total exposure time is calculated using Equation 27 to Equation 29.

$$t_{exposure} = t_{exposure/cycle} * N_{cycle} \qquad \textit{Equation 27}$$

$$N_{cycle} = \frac{t_{treatment}}{t_{cycle}} \qquad \textit{Equation 28}$$

$$t_{cycle} = \frac{V}{Q} \qquad \textit{Equation 29}$$

Where $t_{exposure}$, $t_{exposure/cycle}$, $t_{treatment}$, t_{cycle} are exposure time, exposure time per cycle, treatment time and time of one cycle respectively, all times are in min, V is the treated volume in L, Q is the flow rate through the recirculating nozzle in L/min.

The direct exposure time per cycle is calculated using the projectile motion equation, Equation 30, where v_{nozzle} is the initial velocity exiting the water-bell nozzle in m/s; x is the horizontal distance from the nozzle to the tank side in m, and θ is the initial launch angle in radians; h is the nozzle opening, the vertical spacing between the nozzle outlet and the capping disc; r_n is the radius of the nozzle; $and\ r_D$ is the radius of the capping disc as illustrated in Figure 32.

$$t_{exposure/cycle} = \frac{x}{v_{nozzle} * cos\theta} \qquad \textit{Equation 30}$$

$$v_{nozzle} = \frac{Q}{A_{nozzle}} = \frac{Q}{\Pi\,(r_D + r_n)\sqrt{(r_D - r_n)^2 + h^2}} \qquad \textit{Equation 31}$$

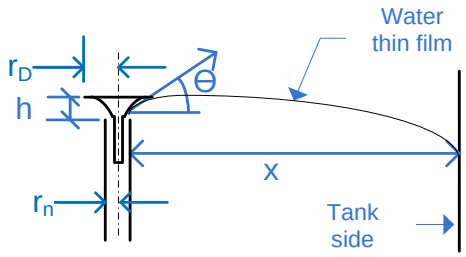

Figure 32: Water trajectory pathline

From equations 27 – 31, it is clear that the exposure time is a function of number of exposure cycles and nozzle design. For a given recirculating flow rate, different nozzle openings (h) were tested until the generated water film extended across the whole tank with an elongated water trajectory pathline before hitting the tank sides.

The direct exposure time was evaluated for different volumes of treated water (3, 7 and 18 L) while the nozzle parameters were kept constant. The nozzle r_D and r_n were 55 and 30 mm respectively. During the 3 tests, h was 4 mm and θ was 12°. Phenol reduction for different treated volumes is shown in Figure 33 . The flow rate, total number of cycles, exposure time/cycle and exposure time are shown along with the achieved phenol reduction in Table 7.

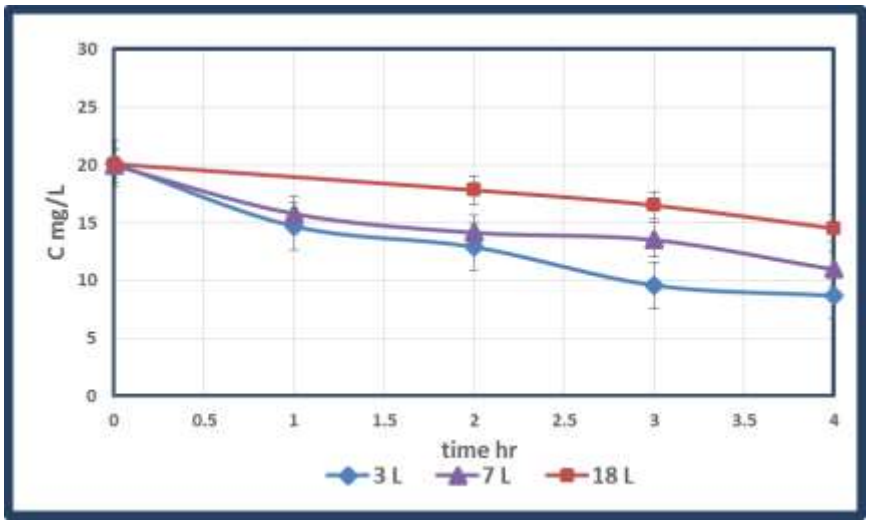

Figure 33: Phenol reduction as a function of treated volume

Table 7: Exposure time for different treated volumes

treated volume	L	3	7	18
flow rate	L/min	18.4	18.2	20.2
time of 1 cycle	s	9.8	23.1	53.4
number of cycles/min		6.1	2.6	1.1
total number of cycles		1471	623	270
v nozzle	m/s	0.17	0.17	0.19
exposure time/ cycle	s	1.315	1.330	1.195
exposure time	min	32.2	13.8	5.4
exposure/treatment	%	13.4	5.8	2.2
Phenol reduction	%	57	45	28
Phenol degraded	mg	34.4	63.1	100.4
	mg/L	11.4	9.1	5.6

Phenol reduction increased with the direct exposure time as shown in Figure 34. Increasing exposure time is crucial for enhancing the photo-reactor performance.

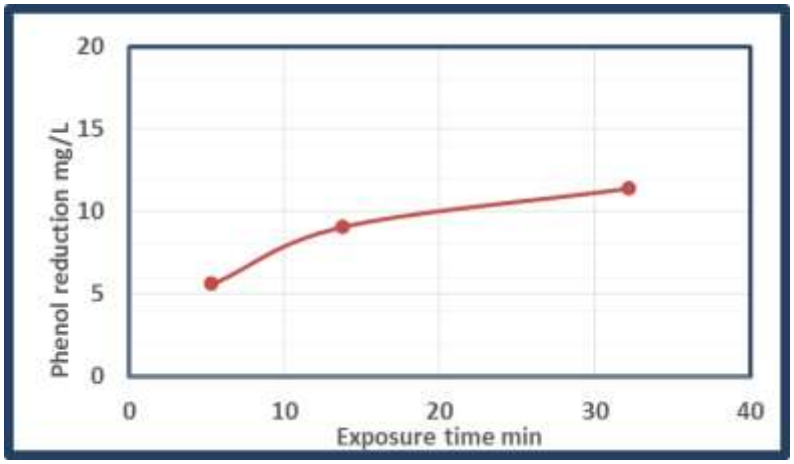

Figure 34: Effect of exposure time on phenol reduction

In an attempt to determine whether the degradation occurs in the thin film only or inside the tank as well, the degradation rate constant was calculated based on treatment time and direct exposure time. Degradation rate constants deducted from Figure 35 and Figure 36 are given in Table 8.

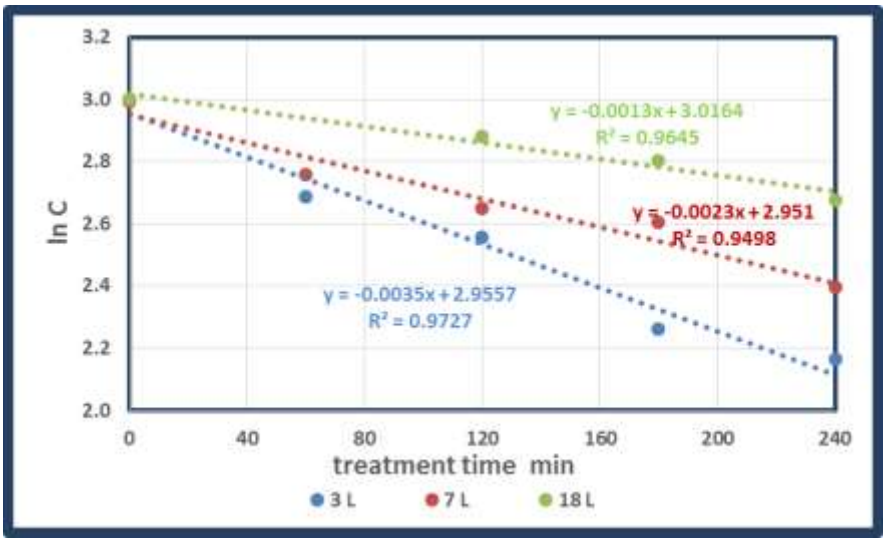

Figure 35: Degradation rate constant based on treatment time

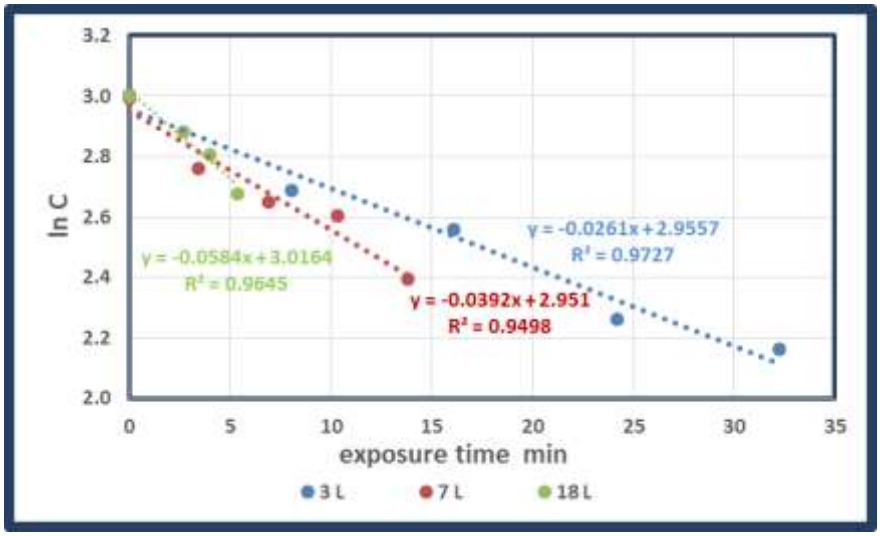

Figure 36: Degradation rate constant based on exposure time

Table 8: Degradation rate constants based on treatment and exposure times

Treated batch	Direct exposure time min	Area of Illuminated water surface m^2	K_{app} hr^{-1}	$K_{exposure}$ hr^{-1}
3L	32.2	0.034	0.21	1.566
7L	13.8	0.068	0.138	2.352
18 L	5.4	0.159	0.078	3.504

K_{app} based on treatment time increased as the direct exposure time increased, while $K_{exposure}$ increased with decreasing direct exposure time. During these degradation tests, the average light intensity on the water thin film was 60 W/m^2 while the average light intensity on the water surface on the tank was 20 W/m^2. The area of the illuminated water surface in the tank increased as the water depth in the tank conical bottom increased. It can be deducted that degradation not only occurred due to illumination of the thin film but also inside the tank due to illumination of the water surface in the tank.

The intensity of light on an illuminated surface (I) is a function of the power of the illumination source (P), and the distance between the power source and the illuminated surface (d) as given by Equation 32 [166].

$$I = \frac{P}{d^2}$$ *Equation 32*

The reactor performance is expected to be better under real sun conditions, since the light intensities on the surface of the water film and the water surface in the tank would be the same. The distance between the surface of the water film and the water surface in the tank is about 50 cm. Unlike the used low power artificial light source whose light intensity significantly changes over this small distance, the solar light intensity does not change over this small distance.

4.8 SWBP Performance Comparison with Other Slurry TiO_2 Systems

In order to evaluate the SWBP performance in degrading phenol, the reactor performance was compared against other photo-reactors employing slurry TiO_2. Since water pH significantly impacts phenol degradation efficiency [188], [189]. Tests were conducted in the SWBP using tap water. The average pH was 8. Tests from the literature conducted at close pH values were included in the comparison.

In order to quantitatively compare the performance of test trials from the literature with SWBP performance, two benchmarks are used: the apparent degradation rate constant and the reactor throughput. Table 9 presents the degradation rate and throughput for test trials found in the literature as well as for the water-bell photo-reactor.

Table 9: Degradation rate constant and reactor throughput for slurry TiO_2 photo-reactors

Reactor	UV source	Treated volume L	Initial Conc mg/L	pH	Treatment duration hours	Reactor area m^2	T Control	O_2 Supply	Removal %	K_{app} hr^{-1}	Throughput $L/m^2.hr$	Ref
Pyrex glass cell [a]	external 15 W	0.2	34	8	10	0.006 [b]	Cooling bath	Air pump	36	0.048	3.15	[190]
Annular reactor	internal 400 W	0.85	34	8	2	NA	Cooling bath	micro-air compressor	51	NA	could not be calculated	[191]
Shallow tank	external 125 W	0.9	50	6.5	2.5	0.484	Cooling fan	Air pump	26	0.078	0.74	[183]
Helical reactor	internal 400 W	3	25	7	6	NA	External cooling system	air compressor	56	0.168 [c]	could not be calculated	[192]
CPC	sun	4	100	8.8	2.5[d]	0.360 [e]	-	Mechanical stirring of the water in recirculating tank	65	0.378 [c]	4.44	[193]
Water-bell	external 60 W	3	25	8.3	4	0.159	-	Passive oxygenation	64	0.252	4.72	current study
	sun	7	20	8.3	4	0.159			56	0.21	11.01	

NA not avaialble
[a] magnetically stirred
[b] estimated based on Pyrex cells commercial dimensions
[c] calculated from concentration profiles
[d] t_{30W}
[e] not including area of recirculating tank

An insight on the design merits of the SWBP and efficiency could be clearly demonstrated. The water-bell reactor had the highest throughput. No external recirculation tank was needed. The water-bell has a relatively high degradation rate constant. Meanwhile, all the aforementioned reactors needed purging the reaction solution with air, the water-bell has the merit of passive oxygenation. No temperature control was needed for the water-bell reactor. The system complexity and operating cost associated with supplying air to the reaction solution and cooling are totally eliminated in the water-bell reactor.

Photo-reactors employing an internal UV illumination source cannot be applied to benefit from solar radiation. Using solar light renders the treatment more economic [194]. In addition to high energy consumption, UV lamps have limited life [23], their replacement incurs a high maintenance and operation cost. The water-bell photo-reactor is designed to use sunlight aiming to decrease the treatment energy footprint as well as the operating cost. SWBP does not include any transparent walls or parts for radiation transmittance that: experience problems of filming; are prone to breakage risks and UV solarization; and pose limit on the reactor size. All these design merits render the water-bell reactor the most promising reactor configuration for scale-up and commercialization.

4.9 Inferences from SWBP Testing

Testing the SWBP aimed to understand the factors affecting the treatment efficiency and find possible ways for enhancing the reactor performance. The photo-reactor has the merit of using high catalyst loading to allow for faster degradation rates while maintaining high DO near saturation levels. The photo-reactor is capable of treating relatively large volumes of wastewater, as the size of the pilot reactor can be increased while maintaining the favorable hydraulic conditions for enhanced photocatalysis.

The extent of phenol degradation achieved depends on the used process parameters. In spite of conducting the treatment tests at alkaline pH which is unfavorable for photocatalytic degradation of phenol, high phenol degradation rates were achieved by optimizing the process parameters. Increasing the exposure time is crucial for enhancing the reactor performance. **The results from the SWBP testing were satisfactory to proceed with the next step of the photo-reactor development by incorporating immobilized TiO_2 on high density grains.**

Chapter V

Immobilized TiO_2 Water-bell Photo-reactor

5.1 Selection of TiO_2 Immobilization method

Many techniques have been investigated for the immobilization of TiO_2 nanoparticles on various supports. Slurry deposition was used to coat coastal sand dunes [158] and quartz sand of 300 micron particle diameter [77] and silica gel of 250-500 micron particle diameter [134]. TiO_2 was added to an aqueous or alcoholic suspension of sand, and after mixing for few minutes the sand was filtered, dried and calcined. Although slurry deposition is simple, the produced TiO_2 coatings lacked sufficient mechanical integrity and were prone to rapid attrition [139], [195].

Dip coating in prepared sols was used to coat : micro-ceramic balloons of 700 microns particle diameter [138], 6 mm glass spheres [133], [196], and volcanic porous stones having an average diameter of 1 cm [97]. The prepared sol was poured in a beaker containing the substrates, the sol was then drained. Coated substrates were dried and heat-treated. This simple procedure is suitable for coating various types and shapes of supports [197]. However, there is a need to ensure that points of contact between support particles are well coated in order to avoid the presence of uncoated regions [196].

Direct immobilization of TiO_2 using sol-gel on quartz, zircon and rutile sand particles having an average particle size of 250, 120 and 100 micron, was conducted by gradual addition of sand to a rapidly stirred titanium alkoxide/alcohol solution. Sol was formed upon the dropwise addition of water. The coated sand was then dried and fired [159].

Sand having an average particle size of 165 microns (fraction having particle size ranging from 150-180 microns) was selected as a support for TiO_2 in the proposed water-bell photo-reactor. Direct immobilization of TiO_2 using sol-gel on sand was selected to ensure a uniform coating on all the sand particles. Sol-gel method has the advantages of producing homogeneous films, easy control of factors determining the film properties including porosity, surface area and composition (multicomponent, multiple layers). In addition to low processing and low sintering temperatures [139], [97].

5.2 Immobilization Procedure

A solution of titanium tetra isopropoxide (TTIP) and isopropanol was stirred for 5 min. Sand was added gradually to the solution and rapidly stirred for 5 min. Dropwise addition of water was conducted over 10 min. Stirring was maintained for another 5 min. Coated sand was dried in a muffle furnace temperature at 120°C, and the temperature was then increased to 500°C and held at 500°C for 1 hour. The furnace was naturally cooled down to room temperature.

5.3 Photo-catalyst Characterization

Scanning electron microscope (SEM) and energy dispersive X-ray (EDX) (Inca X-sight, Oxford Instruments) were used to confirm the presence of TiO_2 on the coated sand. X-ray fluorescence (XRF) spectrometer (Pananlytical Axiom max) was used for the elemental analysis. The sequential XRF was operated at a voltage of 60 V and current of 66 mA, θ from 13° to 147° using a step of 0.01 per min. Crystallite phase and crystal size of TiO_2 nanoparticles were determined from X-ray diffraction (XRD) patterns. X-ray powder diffractometer (Bruker D8) was operated using CuKα radiation (0.15418nm) at voltage of 40 V and current 30 mA, 2θ from 10° to 80° using a step of 0.03 and step time of 1s.

N_2 sorption analysis at -196°C using ASAP 2020 analyzer (Micromeritics Instrument Corporation) was used to determine specific surface area, average pore size and pore size distribution. The samples were pretreated by applying vacuum at 40°C for 4 hours. The adsorption and desorption isotherms were recorded using 53-point pressure tables with 20-s equilibrium intervals.

5.4 Selection of Parameters for Sol-gel Synthesis

When using TiO_2 anchored on supports as a photo-catalyst, the synthesis process aim at achieving good photocatalytic activity and mechanical stability. Parameters affecting film properties include precursor type and concentration, water/precursor molar ratio, solvent type and molar ratio, sol pH, drying and sintering temperature, presence and size of solid particles dispersed in the sol. Film hardness and adhesion are a function of the heat treatment [197].

5.4.1 Pretreatment of Support

Different pretreatment procedures were reported in the literature. Some had the purpose of cleaning the support, others were done for enhancing TiO_2 adhesion to the support surface. Cleaning procedures were as simple as washing sand particles three times with acetone [77] or ultrasonically cleaning sand particles in acetone and ethanol successively then drying at 110°C [159]. In another study, white pebbles were washed then leached in EDTA solution for 12 hours using a mechanical shaker followed by rinsing and drying at 80°C [123]. For adhesion enhancement, volcanic porous stones [97] and black sand [63] were washed, dried and coated with a rough silica layer. In another study, silica gel was immersed in a diluted ammonia solution for 2 hours then dried at 100°C [73]. The concentration of hydroxyl groups bonded to the support surface enhance the catalyst dispersion on it [198]. Immersion in diluted ammonia solution was the chosen pretreatment for the sand.

5.4.2 Titanium Alkoxide Type

Nanoparticles synthesized from TTIP were more photoactive than nanoparticles synthesized from titanium tetra butoxide (TTB) for degradation of C.I. Acid Red 27 dye. Nanoparticles synthesized from TTIP contained 95% anatase and 5% rutile. Nanoparticles synthesized from TBT were 100% anatase [98]. The presence of 5% rutile acted as a structural defect or impurity that delayed electron hole recombination thus enhanced TiO_2 photoactivity. TTIP was selected as the titanium precursor for the sol-gel synthesis process.

5.4.3 Alcohol Type

It is desirable to control the hydrolysis and condensation rates to favor the production of small colloidal clusters and prevent particle growth. The use of branched alkoxides as isopropoxide reduces the hydrolysis and condensation rates and promotes the formation of small colloidal clusters with a narrow particle size distribution [99]. Methanol has high polarity and reactivity leading to the occurrence of accelerated hydrolysis and condensation reactions [98]. Isopropanol was the chosen alcohol to be used in the sol-gel synthesis process.

5.4.4 Titanium Alkoxide Amount

A set of experiments was conducted to determine the optimum alkoxide amount. TTIP equivalent to 20, 35, 50 and 75 weight % of the sand was used. Molar ratios of TTIP: water: isopropanol were 1:4:30. Coated sand after drying and firing at 500°C for 1 hour is shown in Figure 37. As the weight of TTIP used in the sol preparation increased, TiO_2 agglomerates were formed. These TiO_2 agglomerates pose two problems: 1) they are a loss of raw material, decreasing the efficiency of the immobilization process, 2) they should be removed from the catalyst before being applied in water treatment, since agglomerates will not be easily recovered after treatment ends.

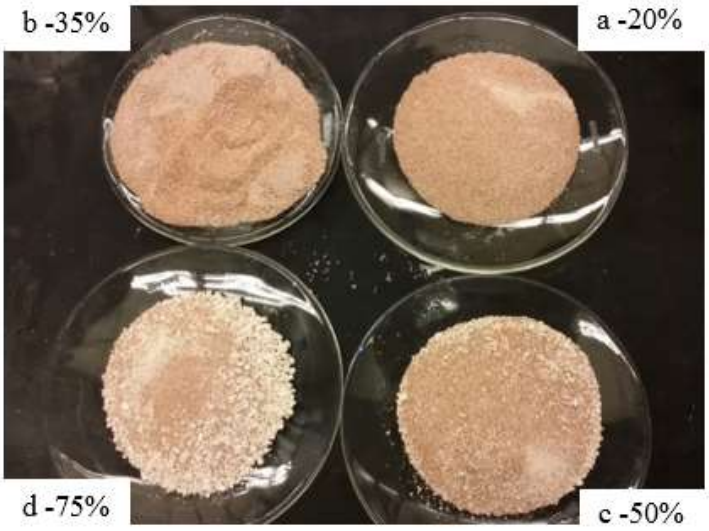

Figure 37: Weight of TTIP as a percentage of sand weight

The coated sand was washed and dried before analyzing its elemental composition. XRF analysis showed that TiO_2 weight % on the coated sand was 3.04 and 3.45 when using TTIP weight of 20 and 50%. Titanium recovery in the two cases was found to be 34 and 16% respectively. Calculations for titanium recovery are included in **Annex V**. The marginal increase of TiO_2 immobilized on the sand particles when increasing the TTIP amount does not justify the great loss in titanium recovery. A limited amount of alkoxide equivalent to 10% of the sand weight was used to avoid the formation of TiO_2 agglomerates.

5.4.5 Water Alkoxide Molar Ratio

A sol is a suspension of particles less than 50 nm. A sol turns on a gel when the sol particles aggregate forming long chains of particles. Sol-gel synthesis pass through three stages: 1- hydrolysis, 2- condensation and polymerization, 3- particles growth [99]. The overall reaction is described by Equation 33.

$$M(OR)_n + \frac{n}{2} H_2O \rightarrow MO_{\frac{n}{2}} + n\,ROH \qquad \textit{Equation 33}$$

Using TTIP, the stoichiometric molar ratio of water is 2 as shown by Equation 34

$$Ti(OC_2H_6)_4 + 2\,H_2O \rightarrow TiO_2 + 4\,C_2H_6OH \qquad \textit{Equation 34}$$

The crystal size can be controlled by adjusting the amount of water available for hydrolysis [196]. Increasing the molar ratio of water to titanium alkoxide reduces the titania crystal size. In a study using a water alkoxide molar ratio of 3.3, 10 and 165, the produced nanoparticles had a diameter of 82, 57 and 20 nm respectively. A high water alkoxide molar ratio favors nucleation over particle growth thus a uniform particle size with a narrow particle size distribution can be obtained [99]. It is desirable to have a small crystallite size since the rate of generation of the electron hole pair is a function of the TiO_2 radius [77].

Experiments were conducted using a water molar ratio of 4 and 10, TTIP : isopropanol ratio was 1:30. XRD spectra shown in Figure 38 were used to calculate the nanoparticles crystallite size. The crystal size was calculated using the Scherrer equation [199], based on half-peak width as illustrated by Equation 35.

$$L = \frac{k\,\lambda}{\beta\,\cos\theta} \qquad \textit{Equation 35}$$

where k equals 0.9, β is the full width at half the maximum peak in radians, θ is the Bragg angle and λ is the radiation wavelength (Cu kα = 0.15418 nm). Using a water alkoxide molar ratio of 4 and 10 led to the production of titania crystallites having a size of 14.6 nm and 13.4 nm respectively after drying and calcination at 500°c for one hour. Detailed crystallite size calculation is included in **Annex VI**.

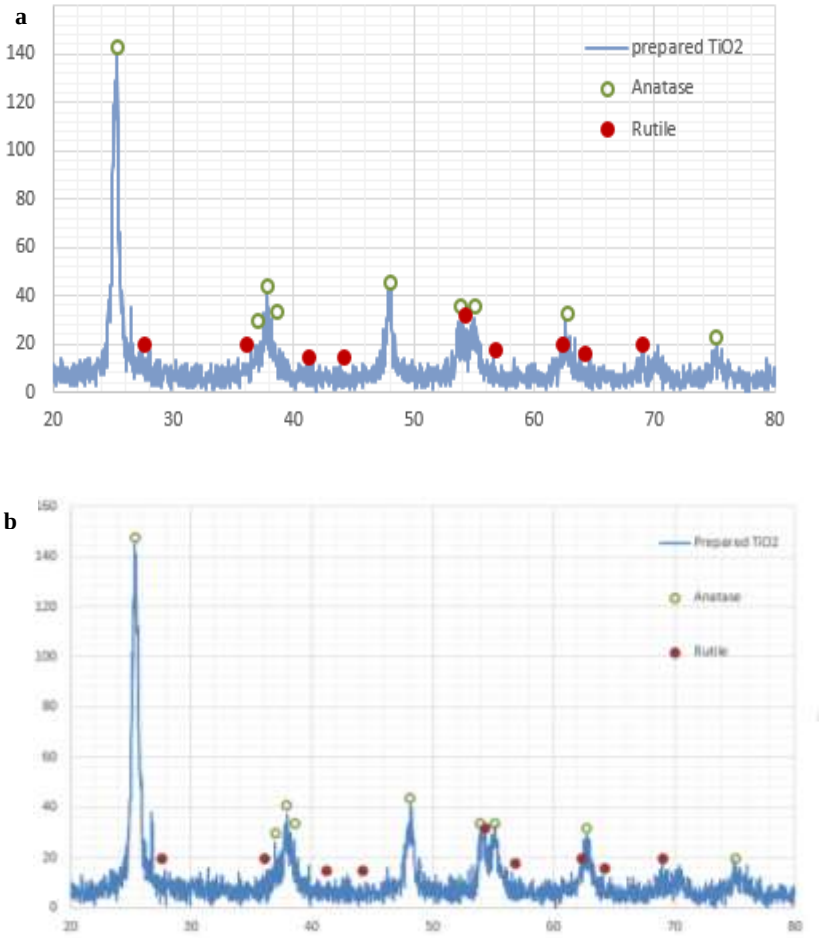

Figure 38: XRD spectra for nanoparticles synthesized with water molar ratio a) 4, and b) 10, using TTIP : isopropanol 1:30 and calcined at 500°c for 1 hour

The obtained crystallite size for the 4 and 10 hydrolysis ratios are comparable as reflected by their XRD spectra. The hydrolysis ratio of 10 was used. When using a moderate hydrolysis ratio, the hydrolysis rate is high, the excess water do not favor the development of closely packed Ti – O – Ti chains that lead to gel formation in the contrary excess water favors the formation of Ti-OH species that are loosely packed [200].

5.4.6 Alcohol Alkoxide Molar Ratio

There is a large variation of the alcohol alkoxide molar ratio used in the synthesis process. For preparation of sols used in dip coating/spin coating, or direct immobilization of TiO_2 on supports, alcohol alkoxide molar ratio vary widely from 5 up to 62.5 [97], [139], [196], [76], [177], [201].

The Alcohol alkoxide molar ratio effects the properties of the film. Films synthesized with a high alcohol molar ratio have higher porosity due to the evaporation of alcohol during the drying process.

For coating sand particles, TTIP equivalent to 10% of the sand weight and a hydrolysis ratio of 10 were used. The volume of the reaction solution needed to be at least twice the volume of sand to allow for efficient stirring of the sand dispersion. Three alcohol alkoxide molar ratio were used: 25, 30 & 35. For an alcohol alkoxide molar ratio of 25, sand gel matrix was formed as shown in Figure 39a. For a molar ratio of 30, a gel layer was formed on top of the sand after the mixing ended as shown in Figure 39b. At molar ratios above 35, a sol was easily separated from the coated sand as shown in Figure 39c.

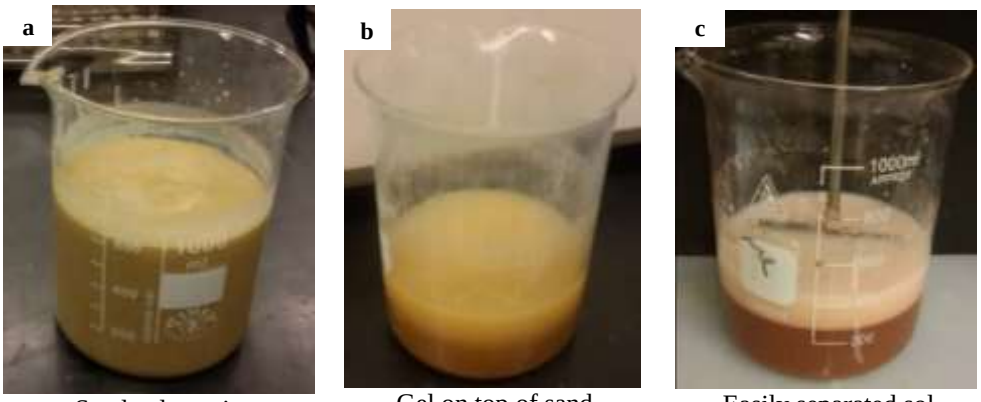

Sand gel matrix | Gel on top of sand | Easily separated sol

Figure 39: Alcohol alkoxide molar ratio of 25, 30 and 35

Sand gel matrix formation was avoided. If sand gel matrix was formed, longer heat requirement for drying the coated sand was needed, and the used alcohol was lost by evaporation. Minimizing the process energy requirements and associated air emissions would result in a more sustainable immobilization technique.

5.4.7 Aging and Drying

Thermal drying is mostly adopted for sol drying [98]. Aging is a slow process that causes macroscopic or microscopic changes in the formed solid due to modifications in the crystal type and size. In a study, it was found that aging at a temperature below 70°C for six hours lead to rutile formation while aging at a temperature higher than 70°C lead to anatase formation [99].

In order to evaluate the effect of aging, experiments were conducted using a water alkoxide molar ratio of 10, TTIP : isopropanol ratio was 1:25. Sol was either aged at 80°C for 24 hours prior to drying or directly dried for 2 hours. The dried nanoparticles were then calcined at 450°C for 1 hour. Nanoparticles aged for 24 hours had a crystallite size of 12.4 nm and phase composition of 75.7% anatase and 24.3% rutile. Nanoparticles synthesized at similar conditions without aging had comparable crystallite size and phase composition (crystallite size of 11.5 nm, 77% anatase and 23% rutile). Detailed crystallite size calculation is included in **Annex VII**. No aging was conducted for the synthesis process.

5.4.8 Calcination Time and Temperature

Amorphous TiO_2 transforms to anatase at a temperature of 400°C. Anatase transforms to rutile at a temperature of 600°C. in a study, on calcining sol-gel synthesized nanoparticles at 350, 450 and 750 °C for 3 hours, nanoparticles calcined at 350°C were amorphous, nanoparticles calcined at 450°C had 95% anatase while those calcined at 750°C were 100% rutile [98].

Increasing calcination temperature impairs the photocatalytic activity not only due to transforming the metastable anatase into the stable rutile phase [159], but also due to increasing of particle size and reduction of surface area, shrinking of agglomerates and reducing of fine pores size [139]. Calcination time varies widely in literature from half an hour up to 10 hours [158], [196], [77], [139], [97], [138], [133], [176], [97]. Heating up rate also varies from 35°C /hr [138], up to 360 °C /hr [139].

XRD patterns for synthesized nanoparticles shown in Figure 38a, were used for determining the phase content. The phase content was calculated using the Spurr-Myers equation [202]:

$$Rutile\ phase\ \% = \frac{100}{1 + 0.8\ (\frac{I_A}{I_R})} \qquad \textit{Equation 36}$$

where I_A and I_R are the intensity of the strongest diffraction peaks of anatase (101) and rutile (110) respectively. The strongest peaks of TiO_2 corresponding to anatase (101), $2\theta = 25.28°$ and rutile (110), $2\theta = 54.23°$ were used. The TiO_2 nanoparticles composed of 78% anatase and 22% rutile.

The N_2 Adsorption and desorption isotherms for the immobilized TiO_2 on the sand grains shown in Figure 40 reveals a type IV isotherm characteristic to mesoporous solids [203]. The isotherm shows Type H4 hysteresis loop indicating the presence of narrow slit-like pores [204]. BET specific surface area was 3.38 m^2/g.

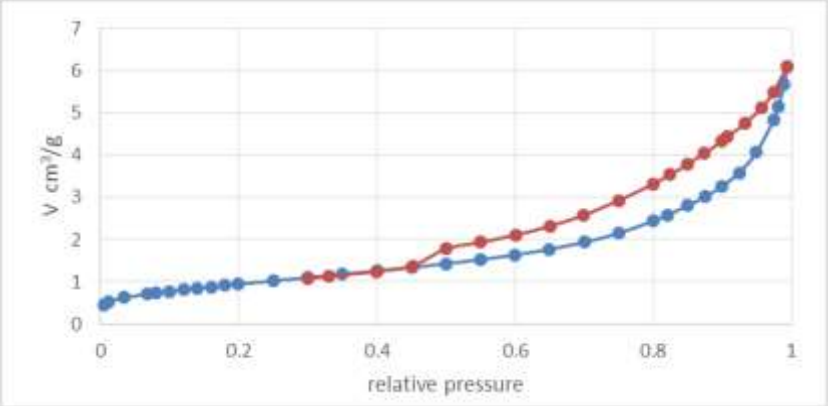

Figure 40: Adsorption/ desorption isotherm

The pore size distribution shown in Figure 41 was determined by BJH method using the adsorption isotherm. The pore size distribution shows a bimodal pore size distribution of micropores (smaller than 2 nm) and mesopores (ranging from 2 nm to 50 nm). Almost no macropores (larger than 50 nm) were found. The average pore size determined by BJH adsorption was 10.7 nm. Formation of macropores and large mesopores increase the mass transfer of the contaminants in the large pore channels [197].

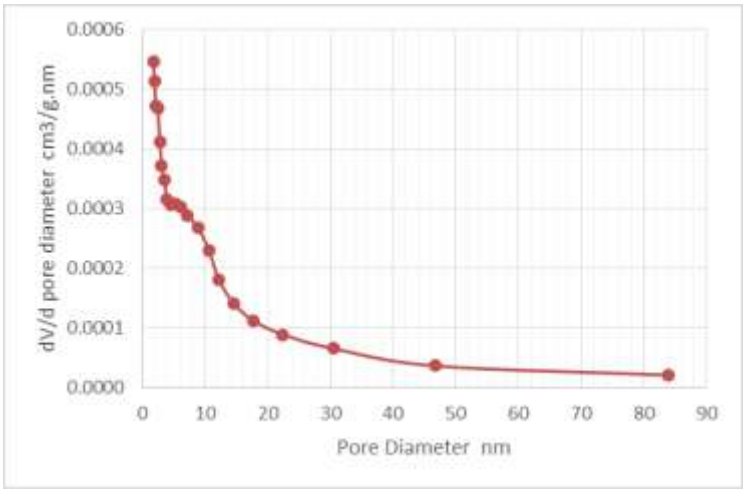

Figure 41: Pore size distribution

The adsorption/desorption isotherms and the pore size distribution confirms that the immobilized TiO_2 film on the sand support is porous however the low surface area was attributed to the non-porous nature of the sand particles where TiO_2 was only deposited as a thin film on the sand surface.

5.4.9 Sol pH

In a study investigating the effect of TiO_2 particle size on phenol degradation, 50 mL of water containing 100 mg/L phenol were degraded at an apparent degradation rate constants of 0.48 and 0.138 hr^{-1} when using TiO_2 of particles sizes 10 and 32 nm respectively [205]. A higher degradation rate was achieved with smaller particles. Lowering the sol pH can lead to the production of titania particles with reduced sizes. The presence of acid increases the hydrolysis rate and prevents particle growth. It also prevents particles agglomeration. TiO_2 isoelectronic point lies between pH of 5 -7. In an acidic medium, the surface charges keep particles in dispersion by electrostatic repulsion [99].

In a study, the effect of HCl addition was investigated using a water : alkoxide molar ratio of 165 and a TTIP: HCl molar ratio of 0.54. Titania crystals of 14 and 20 nm after sintering at 450°C were produced with and without acid addition respectively [99]. HCl was not incorporated in the immobilization procedure since the produced nanoparticles without acid addition are sufficiently small for the intended catalytic use.

5.5 TiO_2 Nanoparticles Preparation

TiO_2 nanoparticles were prepared using a sol-gel technique where water is added drop by drop to a rapidly stirred mixture of TTIP and isopropanol. The molar ratio of TTIP: isopropanol: water was 1:25:10. After 15 min of rapid stirring, the resulting sol was filtered using Whatmann filter papers (Grade 1, pore size 11 micron). The nanoparticles were rinsed with deionized water. Rinsing was conducted to avoid nanoparticles blackening during subsequent calcination step. The nanoparticles were dried in a muffle furnace. Drying was conducted first at 80°C for 1 hour to avoid bloating, then drying was continued at 120°C for another 1 hour. The muffle furnace temperature was gradually raised at a rate of 2°C /min from 120°C to 450°C. The dried TiO_2

powder was calcined at 450°C for 1 hour. The furnace was naturally cooled down to room temperature. The TiO_2 aggregates formed during drying were then manually crushed using a porcelain pestle and mortar.

5.5.1 TiO_2 Nanoparticles Characterization

XRD diffraction pattern for the lab-synthesized TiO_2 nanoparticles, shown in Figure 42, was used for calculating the crystallite size as well as the phase content. The crystal size was calculated using the Scherrer equation (Equation 35). The crystal size was found to be 11.5 nm. The phase content was calculated using the Spurr-Myers equation (Equation 36). The TiO_2 nanoparticles composed of 77% anatase and 23% rutile after sintering at 450°C for 1 hour.

SEM analysis was conducted at a voltage of 6 kV and a working distance of 3.1 mm and a magnification of 24 kX. The SEM revealed the presence of agglomerates that vary widely in shape and size. N_2 sorption analysis revealed that BET specific surface area was 142.5 m^2/g.

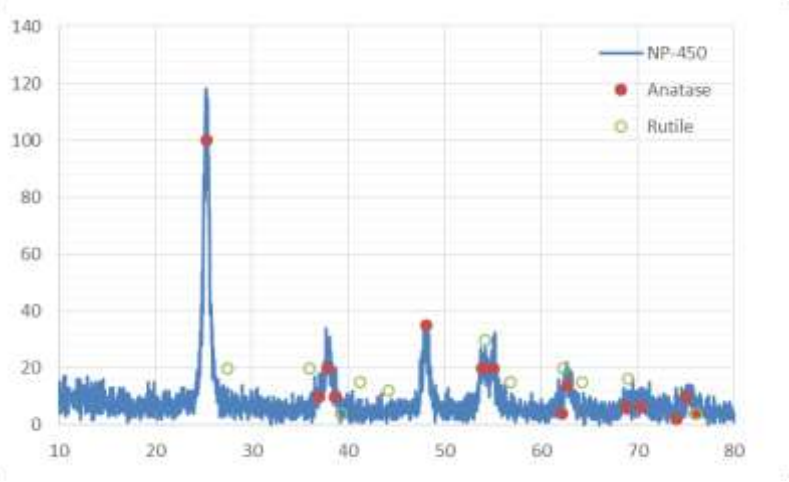

Figure 42: XRD spectra for lab-synthesized nanoparticles, calcined at 450°c for 1 hour

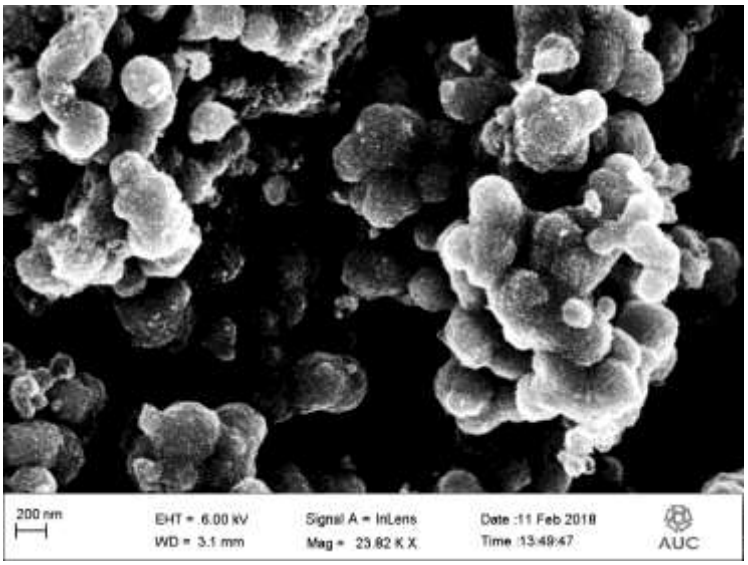

Figure 43: SEM for lab-synthesized nanoparticles, calcined at 450°c for 1 hour

5.6 Adopted Immobilization Technique

The following procedure was used to prepare batches of 350 gm of coated sand. The immobilization technique is illustrated in Figure 44. Sand was pretreated by ammonia solution. Sand was rinsed with water then agitated in an aqueous ammonia solution for 2 hours. The sand was dried at 120°C for 2 hours. TTIP equivalent to 10% of the sand weight was used.

A solution of TTIP and isopropanol is stirred using a mechanical stirrer for 5 min. Molar ratio of TTIP : isopropanol was 1:35. An alcohol alkoxide molar ratio of 35 used to avoid local excess of precursor and associated gel formation thus ensuring reduced drying time and allow for sol recovery.

Sand was gradually added to the solution and rapidly stirred for 5 min at 300 rpm. A water alkoxide molar ratio of 10 was used. Dropwise addition of water was conducted. Due to the large reaction solution, no water dilution with alcohol was needed. Stirring was maintained for another 5 min. The sol was filtered. The coated sand was dried, then sintered in a furnace on a wide tray to avoid entrapment of alcohol that would ignite during the sintering processes. The furnace temperature was held at 120°C for 2 hours then temperature was increased to 500°C and held at 500°C for 1 hour. The furnace was naturally cooled down to room temperature.

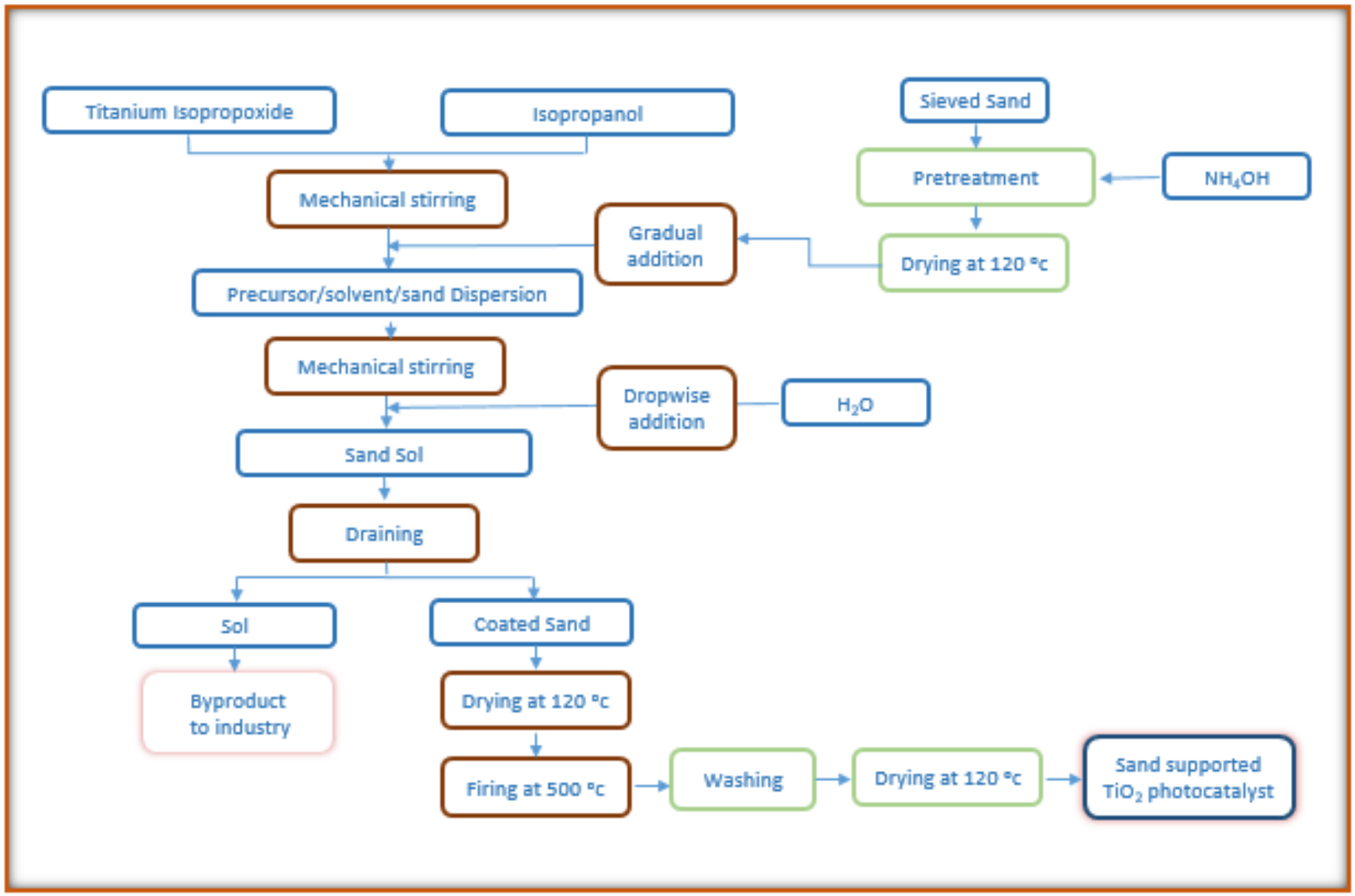

Figure 44: Schematic flow chart for immobilization technique

During the synthesis process, three forms of TiO_2 could be produced: 1) TiO_2 agglomerates, 2) loosely adsorbed TiO_2 on the support surface, 3) well attached TiO_2 to the sand surface. [63]. Formation of TiO_2 agglomerates was avoided by using a limited amount of alkoxide. The high alcohol alkoxide molar ratio and the high water alkoxide molar ratio avoided local excess of alkoxide thus favoring nucleation over particle growth. Washing under vigorous stirring was conducted to remove loosely bound TiO_2. The coated sand was then dried yielding the desired photo-catalyst. The coating/heating cycle was repeated two times to produce the desired photo-catalyst.

5.7 Immobilized TiO_2 Preparation

TiO_2 was immobilized on sand grains for use in the immobilized water-bell photo-reactor (IWBP) attempting two different methods: (1) direct immobilization on sand grains using the sol-gel technique as detailed in section 0, the resulting TiO_2-sand composite is referred to as TSC; (2) coating the sand grains with TiO_2/epoxy mixture, the resulting epoxy TiO_2 sand particles are referred to as E-TSP.

5.7.1 Immobilization Using Epoxy Coating

EUXIT 50 is a solvent free, non-pigmented, commercial epoxy coating. It is a trademark of SwissChem (Egyptian Swiss Chemical Industries Company). It is prepared by mixing two components: EUXIT-I, an epoxy resin, and EUXIT-II, a formulated amine hardener. The mix ratio of the resin and hardener is 3:1 by weight. To allow for a higher TiO_2 loading on the sand, sand fraction having particle size ranging from 63-88 microns (passing sieve 170 and retained on sieve 230) was selected as a support for TiO_2 immobilization.

Lab-synthesized TiO_2 was added to EUXIT-I and thoroughly mixed using a magnetic stirrer for 15 min. EUXIT-II was added to the TiO_2 epoxy resin mixture, and quickly mixed with a spatula. The mixture was immediately added to the sand and thoroughly mixed by hand to have a homogeneous mixture. The weight of the epoxy coating was 15% of the sand weight. TiO_2 was added as 25 weight % of the epoxy coating. The TiO_2-epoxy sand particles had TiO_2 weight percent of 3%. The coated sand particles were left to dry at room temperature for 24 hours. For

this sand fraction having an average particle size of 75 microns, this small amount of epoxy is just enough to wet the sand particles. After drying the formed agglomerates are easy to break into free flowing particles using a porcelain pestle and mortar. The particles were then sieved again. The resulting TiO_2-epoxy sand particles are referred to as E-TSP

5.7.2 E-TSP Characterization

E-TSP was gold sputtered for 120 seconds at a current of 10 mA using Hummer 8 sputtering system prior to SEM analysis. Film microstructure was investigated by SEM at a voltage of 6 kV and a working distance of 3 mm and a magnification of 356X.Figure 45.a shows discrete sand particles. The TiO_2/epoxy coating was free of any cracks. EDX spectrum shown in Figure 45.b confirms the presence of TiO_2 in the epoxy matrix.

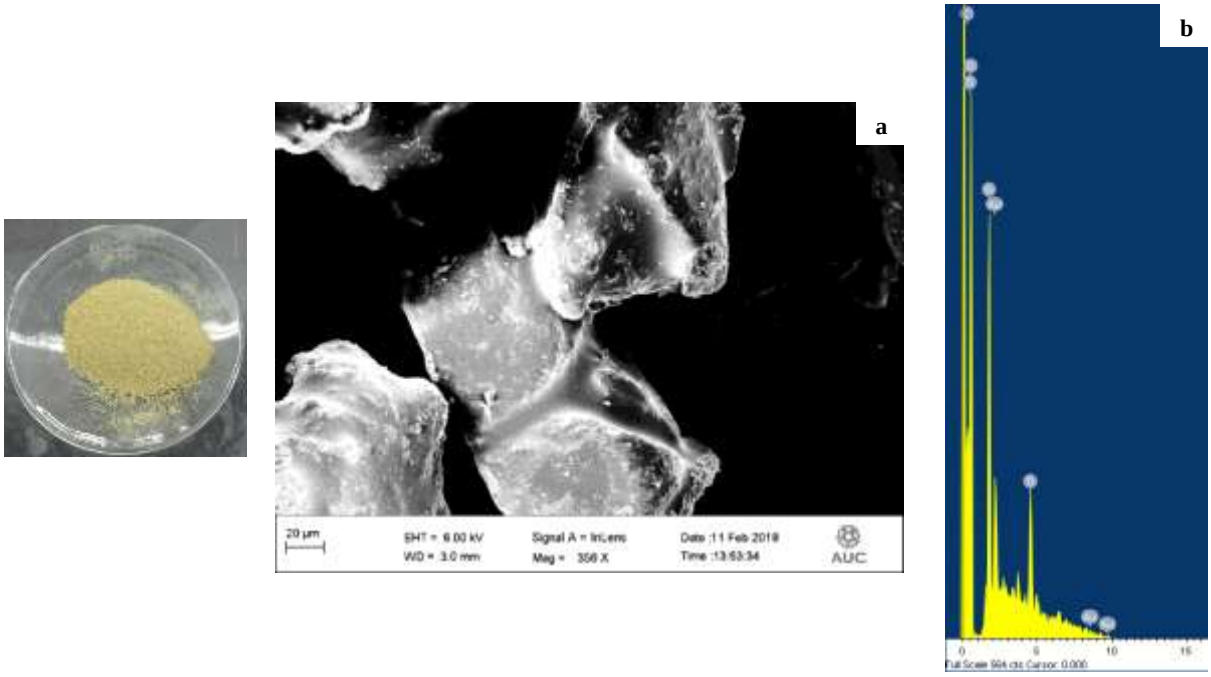

Figure 45: E-TSP: a) SEM , b) EDX

5.8 IWBP Photocatalytic Degradation Tests

5.8.1 Experimental Procedure

Photocatalytic degradation tests were carried in the immobilized water-bell photo-reactor (IWBP) in a recirculating batch mode. Photocatalytic tests were planned to assess the phenol degradation achieved and immobilized TiO_2 resistance to abrasion. Same experimental procedure as detailed in section 4.1 was used. Additionally, turbidity was measured using a direct-reading spectrophotometer (Hach, DR/2000). For the degradation tests carried using E-TSP, the commercial peripheral pump was replaced with a commercial centrifugal pump with a single open-impeller. Open-impeller centrifugal pumps are suitable for liquids having high content of solids. The used peripheral and centrifugal pumps are shown in Figure 46.

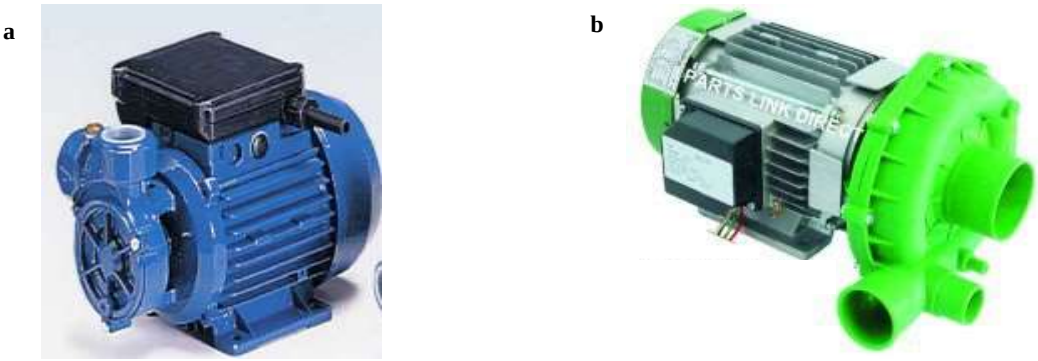

Figure 46: a) Peripheral pump, b) open-impeller centrifugal pump

5.8.2 IWBP Degradation Test Results

On using TSC loading of 10 g/L and 20 g/L, resulting in 140 and 275 mg/L of TiO_2 in the system respectively, limited phenol reduction was achieved due to the low concentration of TiO_2 in the system. However, the profound problem was the drastic increase in water turbidity. Abrasion of the catalyst was observed as shown in Figure 47a. After a while, TiO_2 settled as shown in Figure 47b.

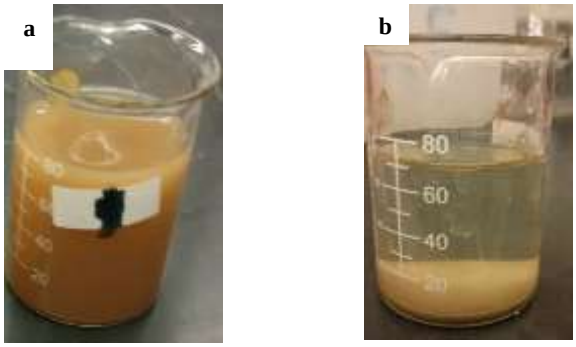

Figure 47: Treated water after: a) taking the sample, b) settling

TiO_2 immobilized by sol-gel has mostly been used for water treatment in tubular packed bed reactors [134] , [97], [133], flat packed bed [159] and pebble bed [123] where low laminar flow conditions prevailed. Few supported TiO_2 were used as fluidized bed [138]. Flow of photo-catalyst through the recirculating pump was only tested in a recirculating shallow tank reactor. The used photospheres 40 were completely damaged after 3 treatment cycles. The damage of the photospheres 40 was attributed to their fragile nature [117].

On using E-TSP loading of 20 g/L, resulting in 750 mg/L of TiO_2 in the system, 19% phenol degradation was achieved. However, the drastic increase in water turbidity was still encountered as shown in Figure 48. Replacing the peripheral pump with the centrifugal pump did not prevent the photo-catalyst abrasion and turbidity increase.

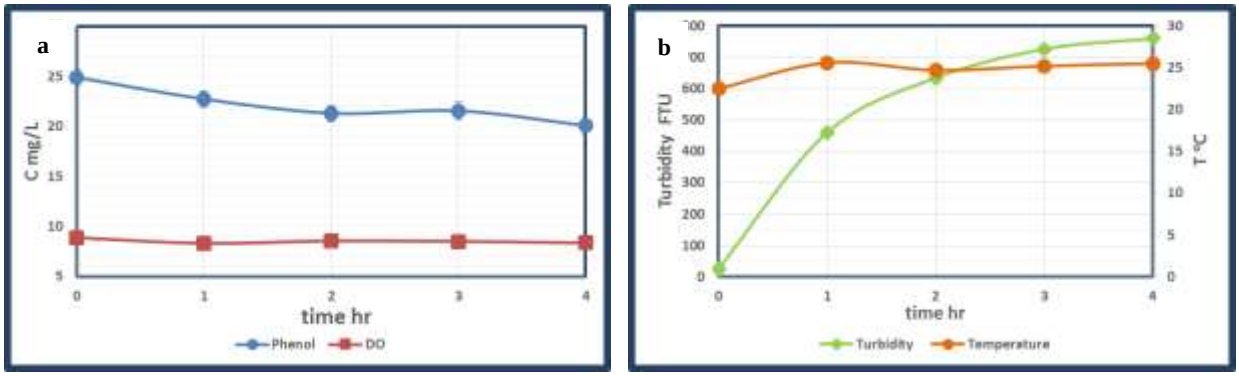

Figure 48: E-TSP Photocatalytic activity tests: a) phenol & DO concentration, b) turbidity & temperature

5.9 Inferences from IWBP Testing

Robust bonding between the support and TiO_2 is crucial for long-term application to avoid TiO_2 loss as well as water secondary contamination with TiO_2 nanoparticles. The proposed reactor configuration using sand as a support for TiO_2 immobilization did not meet the process requirement of having a stable photo-catalyst resistant to abrasion. Two routes for modifications were proposed:

Route 1: Formulation of a new TiO_2 composite resistant to abrasion at high friction forces induced by the pump high-speed rotating impeller.

Route 2: Use of positive displacement pumps with no internal moving parts that can handle liquids with fragile solids such that abrasion of the photo-catalyst does not occur.

However, both of those two routes would incur cost implications that might render the developed treatment unit not cost-effective. **In an attempt to fulfil the objective of developing a simple cheap treatment unit, the design of a new reactor configuration was attempted.**

Chapter VI

TiO_2 Immobilized Tray Photo-reactor

6.1 TiO_2 immobilized Pilot-Scale Photocatalytic Reactor

The strong mixing conditions and flow through the recirculating pump resulted in high abrasion of the photo-catalyst. A new reactor configuration was needed to avoid the high friction of the photo-catalyst particles in the recirculating pump. The new reactor configuration should maintain fulfilling the photocatalytic process requirements of light penetration to activate the photo-catalyst, continuous oxygen supply by passive oxygenation, turbulent flow for efficient mass transfer and recirculation to avoid treatment dead zones.

The basic revision in this 3rd photo-reactor is to retain the TiO_2 immobilized on sand particles onto a tray that replaces the free projectile water-sheet subject to UV light. A revised pilot-scale TiO_2 Immobilized Tray pilot-scale photo-reactor (ITP) is illustrated in Figure 49.

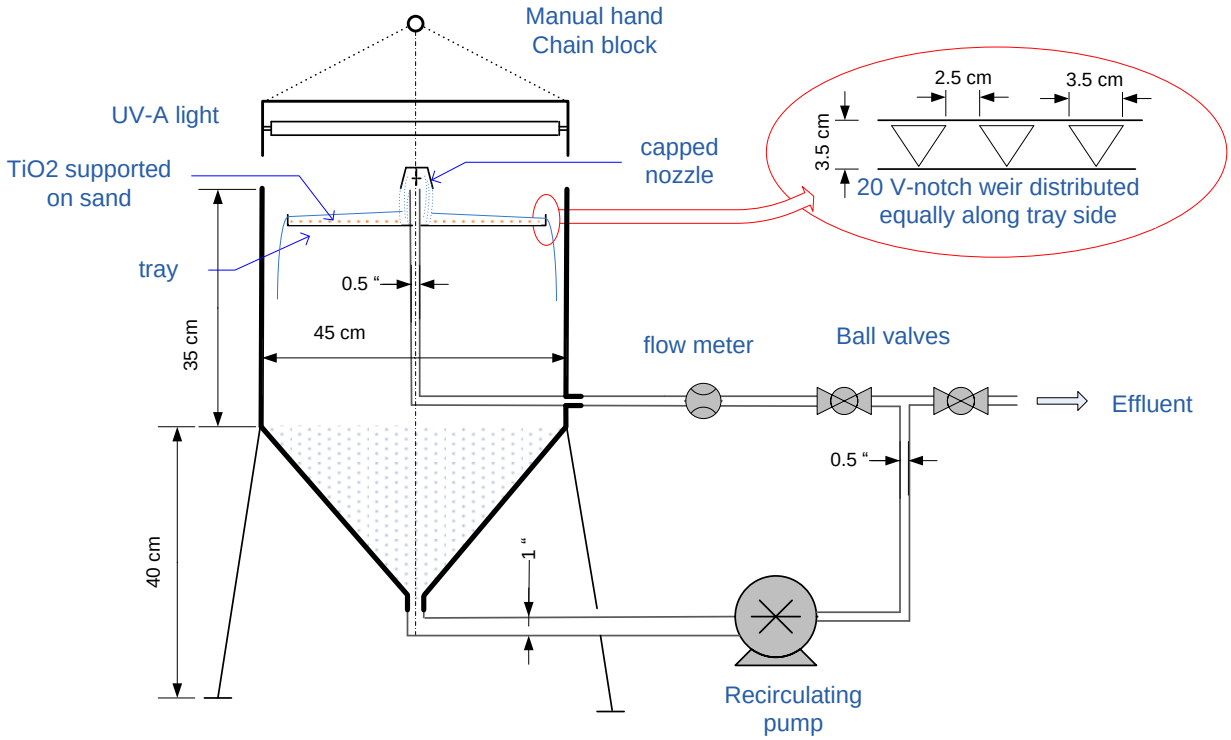

Figure 49: Pilot-scale immobilized TiO_2 tray photocatalytic reactor

The reactor is equipped with a tray having a diameter of 36 cm for supporting the immobilized TiO_2. The tray is mounted on the tank edges. The reactor is operated in a recirculating mode. The water is withdrawn from the tank conical bottom, and pumped via the recirculation pump into the central vertical feeder that passes through the tray center. The vertical feeder terminates at its top with a capped nozzle. The capped nozzle concentrates the exiting water in a ring-shaped impact area around the vertical feeder. This spray pattern is intended to allow a radial flow of water along the tray.

The tray side has 20 v-notch weirs, each weir with a width of 3.5 cm, and depth of 3 cm. Weirs are 2.5 cm apart from each other. The v-notch weirs maintain a controlled depth of water above the tray. The recirculating flow rate is controlled such that the thickness of the water film over the supported catalyst does not hinder light penetration for efficient catalyst activation. Water falls off the tray into the water surface in the tank bottom, thus ensuring water oxygenation. The arrangement for UV-A radiation, components for water recirculation and flow measurement are the same as that described in section 3.6.

6.2 Supported photo-catalyst preparation

TiO_2 was immobilized on sand grains attempting three different methods: (1) direct immobilization on sand grains using a sol-gel technique, the resulting TiO_2-sand composite is referred to as TSC; (2) coating the sand grains with TiO_2/cement grout, the resulting cement TiO_2-sand composite is referred to as C-TSC; and (3) binding TiO_2 on sand surface with TiO_2-epoxy coating, the resulting epoxy TiO_2-sand composite is referred to as E-TSC. The Sand particles used were passing sieve 40 and retained on sieve 50, i.e having particle size of 300 to 420 micron. For both of C-TSC and E-TSC, lab-synthesized TiO_2 was used. The preparation procedure of these nanoparticles followed is detailed in section 5.5. The nanoparticles phase composition and particle size are included in section 5.5.1.

6.2.1 Direct Immobilization of TiO_2 Using Sol-Gel

The sand layer used to cover the tray was coated with TiO_2 using direct immobilization sol-gel as detailed in section 5.5 to ensure a uniform coating on all the sand particles. A second coating cycle

was conducted to increase the thickness of the immobilized TiO_2 film on the already coated sand grains.

6.2.2 Coating with TiO_2-Cement Grout

Coating concrete surface with TiO_2 or incorporating TiO_2 in the concrete mix is receiving interest for reduction of NO_x and air pollutants [206], [207]. Coating concrete surfaces with TiO_2 is also investigated for the decomposition of phenolic wastewater [208], [209]. In this research, TiO_2 was mixed with cement to form a grout to cover the sand particles.

Lab-synthesized TiO_2 was mixed with cement with a weight ratio (TiO_2 to cement) of 1:3. Water was added to the TiO_2/cement mixture with a weight ratio of 1:1. The TiO_2-cement grout was added to the sand and mixed thoroughly by hand to obtain homogeneous mixture. The weight ratio of TiO_2/cement grout to sand was 1:10. For coating of 300 gm of sand, 7.5 gm of TiO_2 and 22.5 gm of cement were mixed with 30 gm water.

The coated sand was left to dry at room temperature for 24 hours. C-TSC was washed with water to remove unattached TiO_2 /cement particles. For covering the 0.1 m^2 tray, 300 g of sand was used for preparing the C-TSC composite, resulting in an approximate TiO_2 loading of 75 gm/m^2 of tray area.

6.2.3 Binding with TiO_2/Epoxy Coating

In the third method of immobilizing TiO_2 immobilized on the sand, epoxy EUXIT 50 was used. The same procedure as detailed in section 5.7.1 was used. The weight of the epoxy coating was 20% of the sand weight. TiO_2 was added as 2.5, 5, 10 and 20 weight % of the epoxy mixture. The TiO_2-epoxy sand composite had TiO_2 weight percent of 0.38, 0.75, 1.5 and 3% respectively. For covering the 0.1 m^2 tray, 350 gm of sand was used for preparing the E-TSC composite, resulting in a TiO_2 loading of 17.5, 35, 70 and 140 gm/m^2 of tray area respectively.

The coated sand was left to dry at room temperature for 24 hours. For this sand fraction having an average particle size of 360 microns, this amount of epoxy lead to the formation of an agglomerated epoxy sand composite. The resulting epoxy TiO_2 sand composite is be referred to as E-TSC-X, where X indicates the TiO_2 weight % in the epoxy coating.

6.3 Photo-catalysts Characterization

All methods used for photo-catalysts characterization are detailed in section 5.3.

6.4 ITP Photocatalytic Degradation Tests

The performance of the ITP was assessed by conducting photocatalytic degradation tests similar to the testing of the slurry mode reactor in a recirculating batch mode. Photocatalytic tests were planned to assess the phenol degradation achieved and TiO_2-sand composites resistance to abrasion. The same experimental procedure as detailed in section 4.1 was used.

For tests conducted using TSC and C-TSC, sample filtration was conducted using 0.45 micron Whatmann syringe filters. For E-TSC samples, no filtration prior to phenol analysis was required. Additionally, turbidity was measured using a direct-reading spectrophotometer (Hach, DR/2000). TOC was measured using Phoenix 8000 UV-persulfate TOC analyzer following the EPA method #415.2 [181]. The detailed operational parameters and degradation results for some of the experimental runs are included in **Annex VIII**.

6.5 Photo-catalysts Characterization Results

6.5.1 TSC

Films microstructure was investigated by scanning electron microscope (SEM) to confirm the presence of TiO_2 on the sand surface. The analysis was conducted at a voltage of 6 kV and a working distance of 9.7 mm and a magnification of 17 kX. Figure 50 shows that the sand surface coated with TiO_2 film. The coated surface was continuous with TiO_2 agglomerates and visible cracks in the TiO_2 film.

TSC

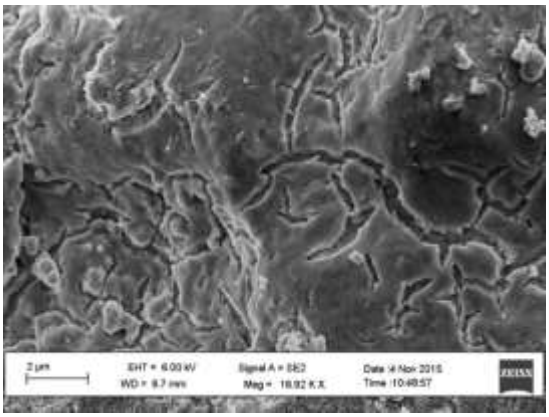

Figure 50: SEM of TSC

6.5.2 C-TSC

Films microstructure was investigated by SEM at a voltage of 8 kV and a working distance of 3.5 mm and a magnification of 939X. Figure 51.a shows that the surface is rough and continuous with agglomerates. EDX spectrum illustrated in Figure 51.b confirms the presence of TiO_2 on the sand surface.

C-TSC

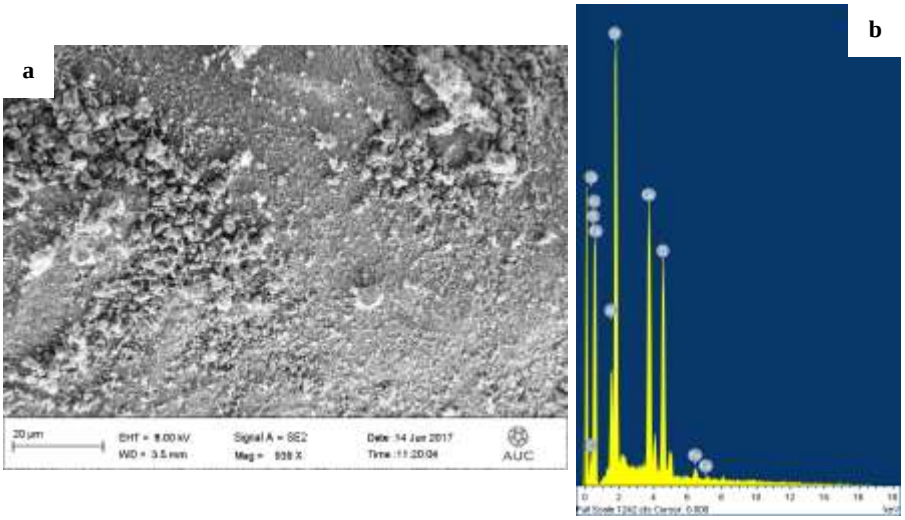

Figure 51: C-TSC : a) SEM , b) EDX

6.5.3 E-TSC

Film microstructure was investigated by SEM at a voltage of 8 kV and a working distance of 3.5 mm and a magnification of 939X. Figure 52.a shows that TiO_2/epoxy coating was continuous and free of any cracks. Tiny droplets indicates that better mixing conditions were needed to attain

complete dispersion of TiO_2 nanoparticles in the epoxy matrix. EDX spectrum shown in Figure 52.b confirms the presence of TiO_2 in the epoxy matrix.

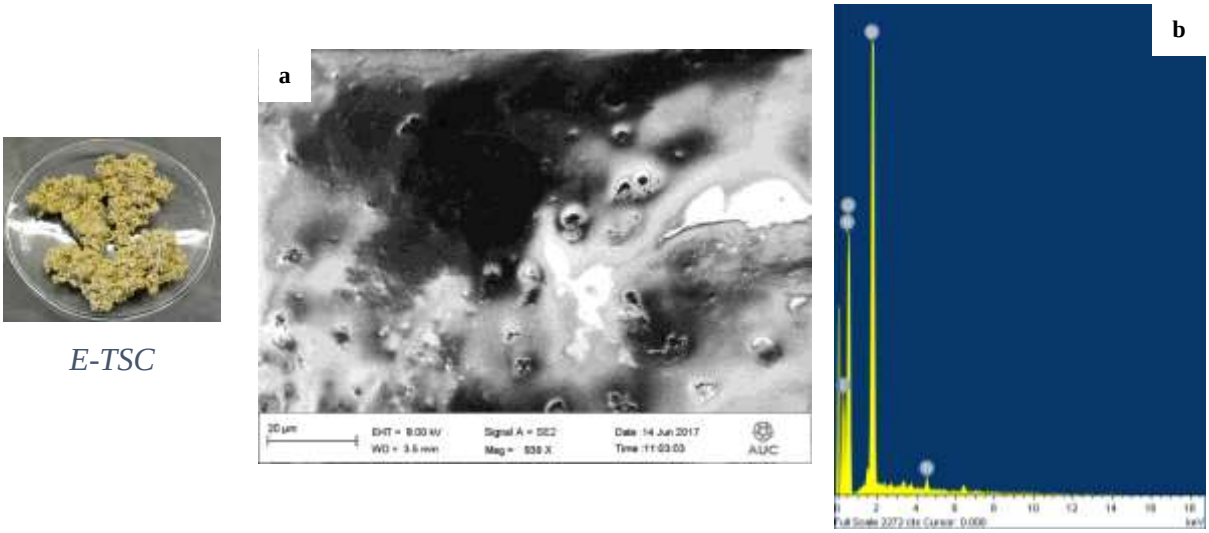

E-TSC

Figure 52: E-TSC-5: a) SEM , b) EDX

6.6 ITP Photocatalytic Degradation Tests Results

The efficiency of the tray reactor for phenol degradation for the *three-immobilization* approaches was investigated by treating wastewater containing 25 mg/L phenol. The treated batch wastewater had a volume of 3 liter, and it was recirculated at an average rate of 18 L/min, under a UV-A intensity of 60 W/m^2. Figure 53.a shows the phenol degradation curves for TSC, C-TSC, and E-TSC-10. Figure 53.b shows levels of turbidity during the 4 hour treatment for the three-immobilization methods.

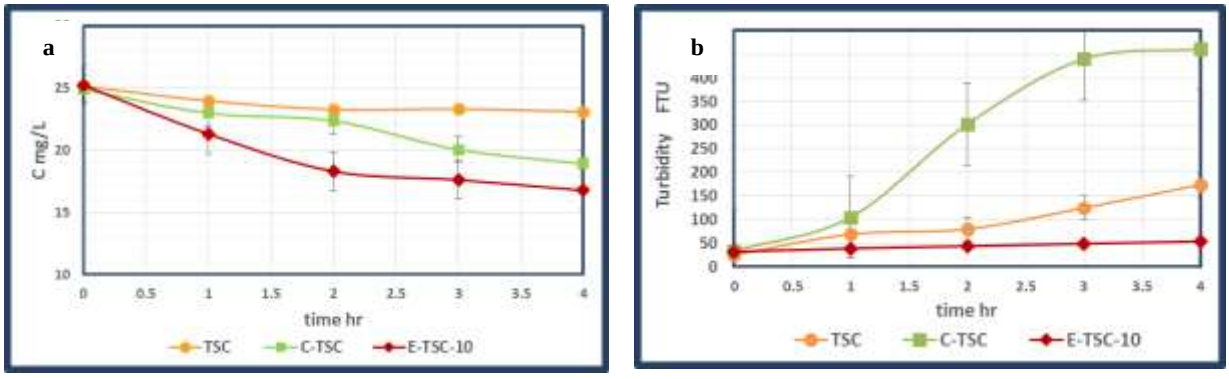

Figure 53: Photocatalytic activity tests: a) phenol concentration, b) turbidity

Analysis of variances (ANOVA) was conducted to test the hypothesis that the treatment means are equal. At a significant level of 95%, the P-value (0.008) was smaller than alpha (0.05), and $F_{treatment}$ (9.35) > $F_{0.05,2,8}$ (4.46) indicating that the treatment means by the three immobilization approaches are not equal. The detailed two-factor ANOVA analysis is included in **Annex IX.**

As shown in Figure 53.a, when using TSC, limited phenol reduction of 9 % was achieved after 4 hours of treatment. This can be attributed to the low TiO_2 concentration in the system. The low TiO_2 concentration on TSC could not be detected either by the EDX or from the XRD patterns. Multiple coating cycles were needed to increase the film thickness which is time consuming and an energy intensive process However, the major challenge is the catalyst abrasion. As seen in Figure 53.b, water turbidity increased from 25 FTU to 174 FTU after 4 hours of treatment indicating the TiO_2 loss from the TSC surface.

Sol-gel is widely adopted for TiO_2 immobilization as it has the advantages of producing homogeneous films, ease of control of factors determining the film properties including porosity and surface area, purity and low sintering temperature [139]. Although TiO_2 immobilization using sol-gel has been reported to successfully degrade organic pollutants in several studies [97], [40], [30], [133], [80], [176], yet all of these studies focused on the catalyst photocatalytic activity not the increased turbidity and the immobilization robustness [210]. The decreased photoactivity was noticed with repeated use and was attributed to loss of Photoactivity.

The stability of the photo-catalyst and its resistance to abrasion is crucial for real large-scale application for water/wastewater treatment. Physical adhesion of TiO_2 to sand provided by sol-gel method is not sufficient to prevent TiO_2 abrasion.

As shown in Figure 53.a, phenol degradation using C-TSC was 24%, higher than that achieved with the TSC. This can be attributed to the higher weight percent of TiO_2 in the coating. TiO_2 in the coating layer amounted to 12.5 % and 2 % of the total photo-catalyst weight. However, water turbidity drastically increased from 34 FTU to 461 FTU, as shown in Figure 53.b, as a result of the spalling of the TiO_2 cement coat. The concrete abrasion resistance is proportional to its mechanical strength [211] . Inclusion of TiO_2 nanoparticles into concrete enhance the mechanical properties up to a maximum limit. Further addition of higher TiO_2 content deteriorates the mechanical strength [212]. This maximum limit differs according to the water to concrete ratio, TiO_2 particle size, curing condition and curing age pozzolans type and content [213].

Phenol degradation attained while using E-TSC-10 was the highest reaching 34% while the turbidity increase from 32 FTU to 54 FTU was insignificant as shown in Figure 53. TiO_2 immobilization using epoxy has another advantage. In case of using TiO_2 immobilized on sand either by sol-gel or cement grout, the water flow lead to the scour of sand from the center of the tray to the outer side, as shown in Figure 54 leading to a decreased exposure area. However, in case of epoxy bound TiO_2, the photo-catalytic bed was not disturbed.

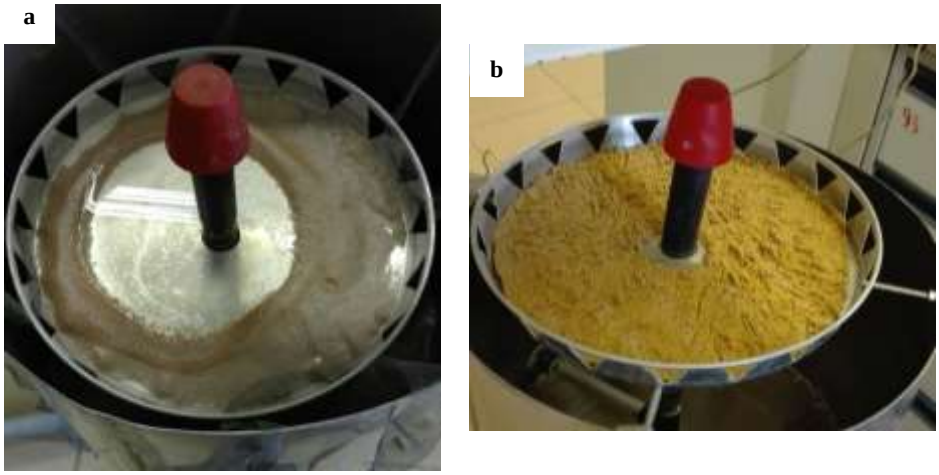

Figure 54: Photo-catalyst bed after treatment: a) TSC, b) E-TSC

The hydraulic residence time over the tray per cycle can be calculated using Equation 37. The total exposure time - the total hydraulic residence time over the tray - is calculated using Equation 40.

$$t_{tray} = \frac{V_{w-tray}}{Q_R} \qquad \textit{Equation 37}$$

$$t_{cycle} = \frac{V_{w-tank}}{Q_R} \qquad \textit{Equation 38}$$

$$\%_{exposure} = \frac{t_{tray}}{t_{cycle}} \qquad \textit{Equation 39}$$

$$t_{exposure} = \%_{exposure} * t_{treatment} \qquad \textit{Equation 40}$$

where $V_{w\text{-}tank}$ and $V_{w\text{-}tray}$ are the volume of water in tank and tray respectively in liters, Q_R is the recirculation rate in L/min, t_{tray}, is the hydraulic residence time on the tray per cycle, t_{cycle} is the time of one recirculation cycle, $t_{exposure}$ is the total hydraulic residence time and $t_{treatment}$ is the treatment time or reactor residence time.

For the treatment of a 3-liter batch at a recirculation rate of 18 L/min with a water depth of 10 mm over the 0.1 m^2 tray, the residence time on tray per recirculation cycle was 3 s. For this case, the total time of one recirculation of the reactor content was 10 seconds which corresponds to 30% of the total treatment time.

6.7 Optimization of TiO_2 Loading on E-TSC

Before optimizing the catalyst load, an adsorption study was conducted to test the phenol removal by adsorption on the E-TSC surface. Wastewater containing phenol was recirculated at similar flow rate in absence of light, and it was observed that the removal of phenol due to adsorption after 4 hours was insignificant.

To optimize the catalyst loading, 4 different TiO_2 loadings in the epoxy coating were used: 2.5, 5, 10 and 20%. The phenol degradation as a function of TiO_2 loading in the epoxy coating is shown in Figure 55.

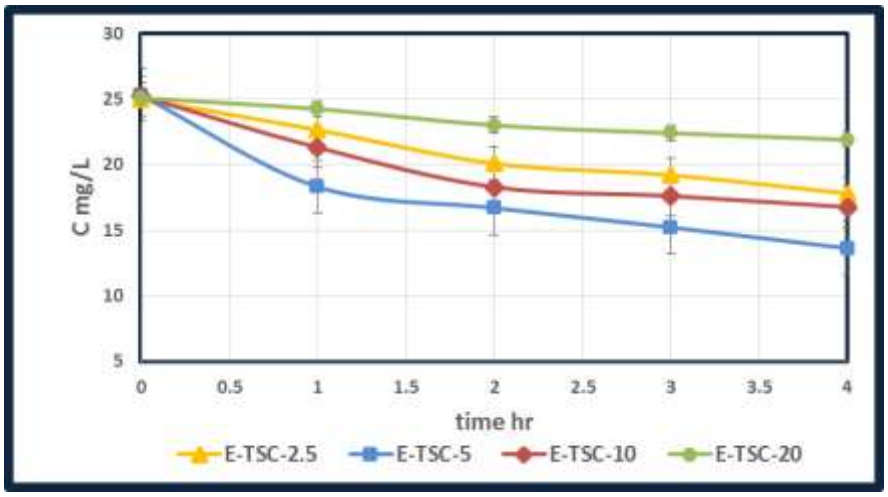

Figure 55: Phenol degradation at different catalysis loading

Analysis of variances (ANOVA) was conducted to test the hypotheses that the treatment means are equal. At a significant level of 95%, the P-value (0.0004) was smaller than alpha (0.05), and $F_{treatment}$ (13.3) > $F_{0.05,3,12}$ (3.49) indicating that the treatment means due to TiO_2 percentage in the epoxy coating are different. The detailed two-factor ANOVA analysis is included in **Annex X**.

Maximum removal occurred for 5% of TiO_2 in the epoxy coating. As the TiO_2 concentration in the epoxy coating increased higher than 5%, the degradation efficiency decreased. Similar patterns were encountered [75], [67], [87] where the photocatalytic activity increased as the loading of TiO_2 on the support increased until a maximum is achieved. Further increase of the TiO_2 loading on the support decreased the photocatalytic activity. This might be attributed to agglomeration of TiO_2 particles on the support surface. Agglomeration of TiO_2 particles lead to a decrease of the surface area.

Figure 56 shows the variation of phenol, TOC and DO concentrations, pH, and temperature over treatment time while using E-STC-5. Although DO levels were expected to decrease as the treatment proceeded due to its consumption during the degradation process, throughout all the runs, aeration was sufficient to keep DO levels around saturation level. TOC reduction proceeded at a lower rate than phenol degradation. This is in agreement with other researchers' findings that phenol degradation byproducts need longer treatment times for complete mineralization [214], [138], [117] and [40].

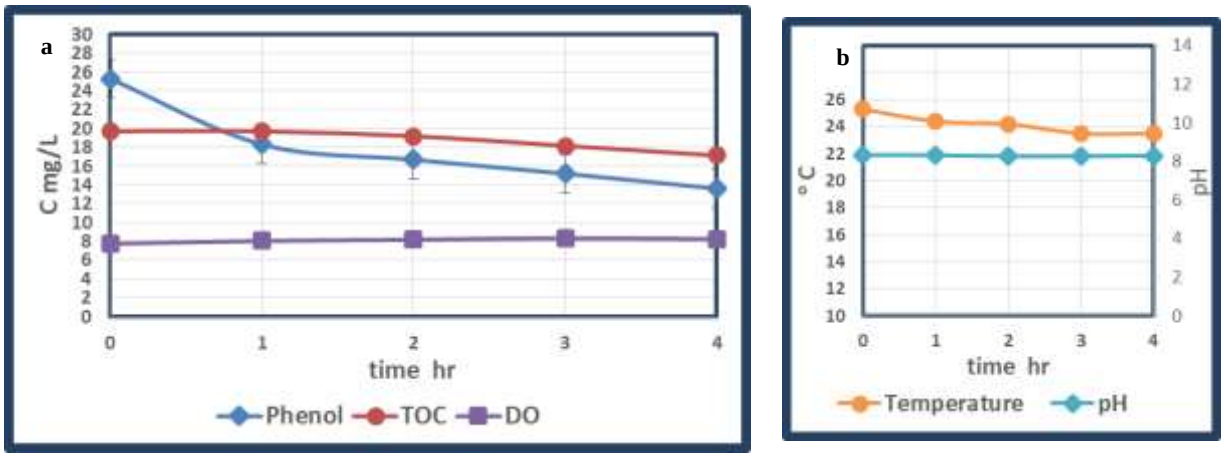

Figure 56: Variation over treatment time of: a) Phenol , TOC & DO , b) pH & temperature

6.8 TiO_2 Epoxy Film

After the success of the E-TSC in degrading phenol without TiO_2 abrasion, another technique of immobilization was tested where TiO_2 was dispersed in the epoxy matrix. The epoxy was used as the TiO_2 support.

6.8.1 TiO_2 - Epoxy Film Preparation

Lab-synthesized TiO_2 was added to EUXIT-I and thoroughly mixed using a magnetic stirrer for 15 min. EUXIT-II was added to the TiO_2 epoxy resin mixture and quickly mixed by a spatula and distributed on the tray. TiO_2 was added as 5 weight % of the epoxy coating. 150 gm of epoxy were used to cover the tray resulting in a TiO_2 loading of 75 gm/m^2 of tray area.

6.8.2 TiO_2 - Epoxy Film Degradation Tests

The efficiency of the TiO_2-epoxy film for phenol degradation was investigated by treating wastewater containing 25 mg/L phenol. The treated batch wastewater had a volume of 3 liter, and it was recirculated at a rate of 17.5 L/min, under a UV-A intensity of 60 W/m^2. The phenol degradation achieved using the TiO_2-epoxy film was only 15% as compared to 45% achieved by E-TSC-5 under the same treatment conditions. The phenol degradation achieved using the TiO_2-epoxy film and E-TSC-5 is shown in Figure 57. The lower phenol degradation achieved by the TiO_2-epoxy film was attributed to the loss of surface area. The epoxy film and E-TSC had BET specific surface area of 0.0027 and 0.0885 m^2/g, respectively. The smooth TiO_2-epoxy film had a lower surface area than the rough E-TSC.

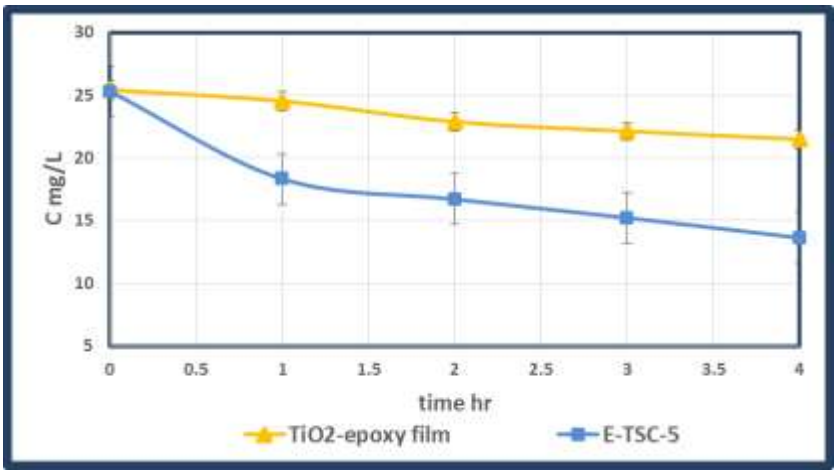

Figure 57: Phenol concentration achieved using TiO_2-epoxy film & E-TSC-5

6.9 Degradation Kinetics

The analysis of the degradation test results conducted using the E-TSC with different TiO_2 loadings showed that the degradation followed a second order degradation rate as illustrated by Equation 41 and Equation 42. A plot of 1/C against t was carried out, where C, C_o and t are the pollutant concentration, initial concentration, and time respectively. The plot was linear with a slope of K_{imm} as shown in Figure 58. The values of K_{imm} and their corresponding coefficient of determination (R^2 value) are shown in the figure as well.

$$r = -\frac{dC}{dt} = K_{imm}\, C^2 \qquad \textit{Equation 41}$$

$$\frac{1}{C} = \frac{1}{C_o} - K_{imm}t \qquad \textit{Equation 42}$$

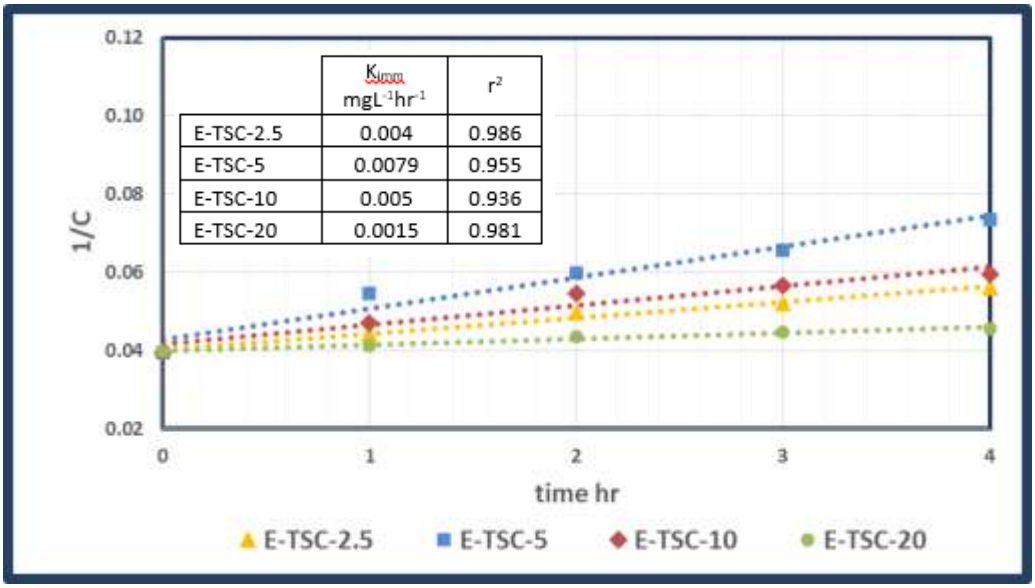

	K_{imm} mgL^{-1}hr^{-1}	r^2
E-TSC-2.5	0.004	0.986
E-TSC-5	0.0079	0.955
E-TSC-10	0.005	0.936
E-TSC-20	0.0015	0.981

Figure 58:Degradation rate constants of phenol on E-TSC composites

Degradation tests were carried for 8 hours with initial phenol concentrations of 25 and 50 mg/L using E-TSC-5. During long batch degradation tests, an average evaporation rate of 2.4 mL/min was encountered. Phenol concentration profile are shown in Figure 59. Phenol degradation followed second order rate as shown in Figure 60.a. The values of K_{imm} and their corresponding coefficient of determination (R^2 value) are shown in the figure as well. Degradation rate constants were also calculated based on exposure time as shown in Figure 60.b. The values of K_{exp} and their corresponding coefficient of determination (R^2 value) are shown in the figure as well.

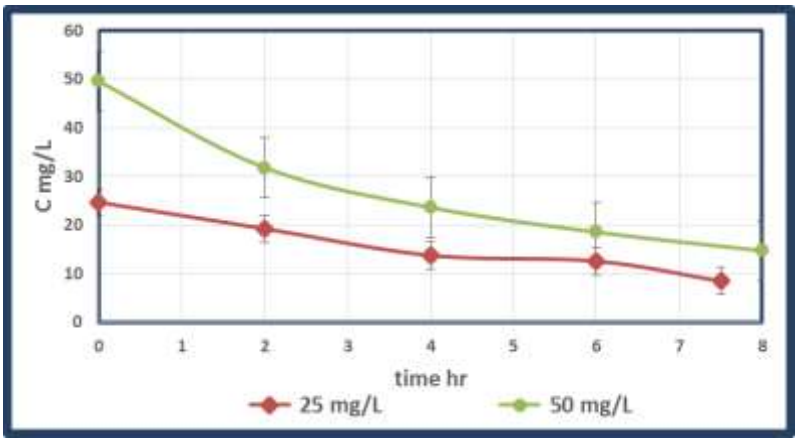

Figure 59: Phenol reduction using E-TSC-5

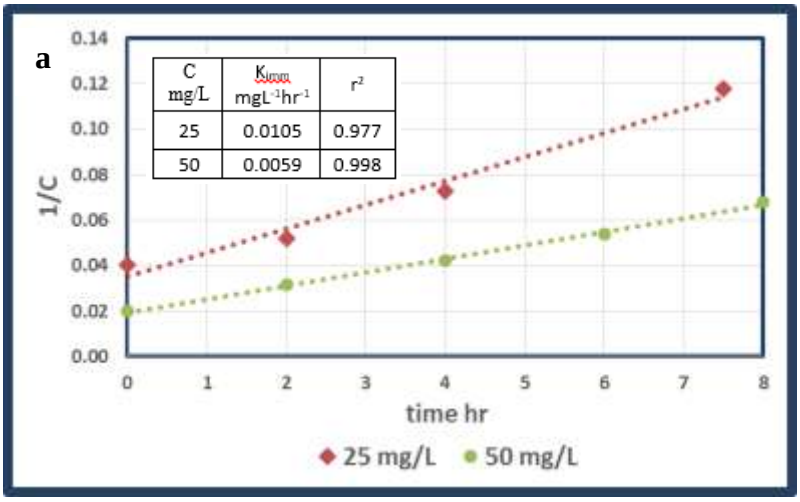

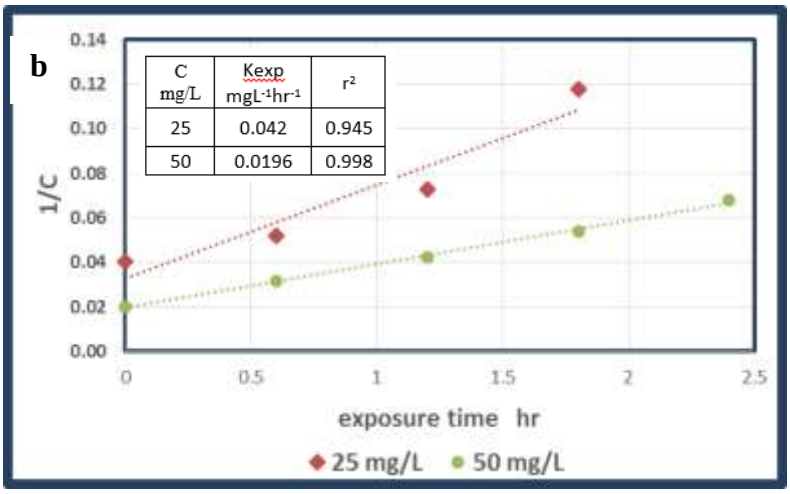

Figure 60: Phenol degradation rate constants using E-TSC-5

6.10 Continuous Flow Immobilized Tray photo-reactor

The experimental set-up for the continuous flow ITP is shown in Figure 61. The tray photo-reactor was equipped with two peristaltic pumps (FH 15, Thermo Scientific) to work in a continuous mode. The wastewater was continuously discharged into the reactor by the inlet pump. The water was withdrawn from the reactor just below the water level in the reactor on the opposite side of the inlet to avoid any short circuiting. The outflow was always equal to the inflow, thereby keeping the reactor effective volume (V) constant.

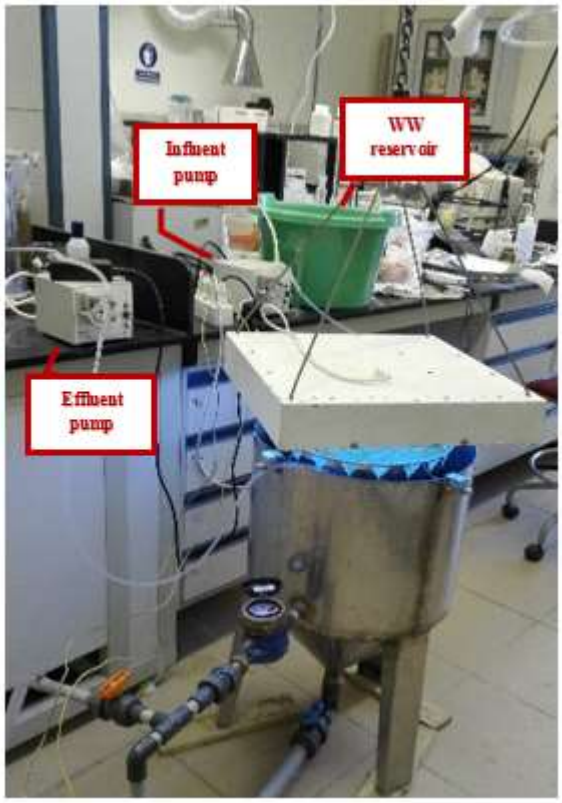

Figure 61: Experimental set-up for continuous flow tray photo-reactor

6.10.1 Continuous Flow Degradation Tests

The tank was filled with 3 liters of wastewater containing 25 mg/L phenol, the influent and effluent flowrates were adjusted to 500 mL/hr. The treatment proceeded at a recirculation flow rate 20.7 L/min under UV-A light intensity of 60 W/m^2 using E-STC-5. An average evaporation rate of 1.5 mL/min was encountered. Variation of phenol, DO and turbidity for the continuous operation

mode are shown in Figure 62. After 4 hours, phenol degradation exceeded 50%. Throughout the whole treatment duration, turbidity was insignificantly changed and Do levels remained constant.

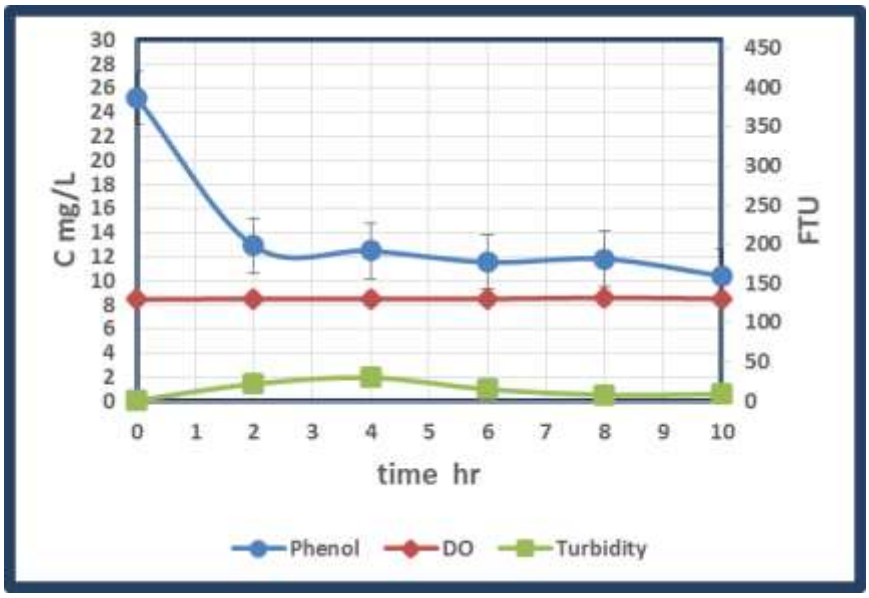

Figure 62: Variation of Phenol, DO & turbidity for continuous mode operation

Euler's method was used to model the concentration profile for the continuous operation mode. Concentration is calculated using Equation 43, where C_t is the concentration at time t in mg/L, while $\left(\frac{dC}{dt}\right)_t$ is the rate of degradation at time t. $\left(\frac{dC}{dt}\right)_t$ is calculated from the mass balance equation demonstrated by Equation 44, where Q_{in} and Q_o are the influent and effluent flow rates respectively in L/hr, V is the water volume in the tank in L, K_{imm} is the degradation rate constant obtained from the batch degradation tests in $mgL^{-1}hr^{-1}$.

$$C_{t+\Delta t} = \left(\frac{dC}{dt}\right)_t * \Delta t + C_t \qquad \textit{Equation 43}$$

$$\left(\frac{dC}{dt}\right)_t = \frac{Q_{in}C_{in}}{V} - \frac{Q_o C_t}{V} - K_{imm}C_t^2 \qquad \textit{Equation 44}$$

Figure 63.a illustrates the actual and theoretical phenol concentration profiles for the continuous mode operation. Figure 63.b illustrates the actual phenol concentration profile for the continuous mode operation and theoretical phenol concentration profile for the batch mode operation. Numerical values for theoretical concentration profiles are included in Annex XII.

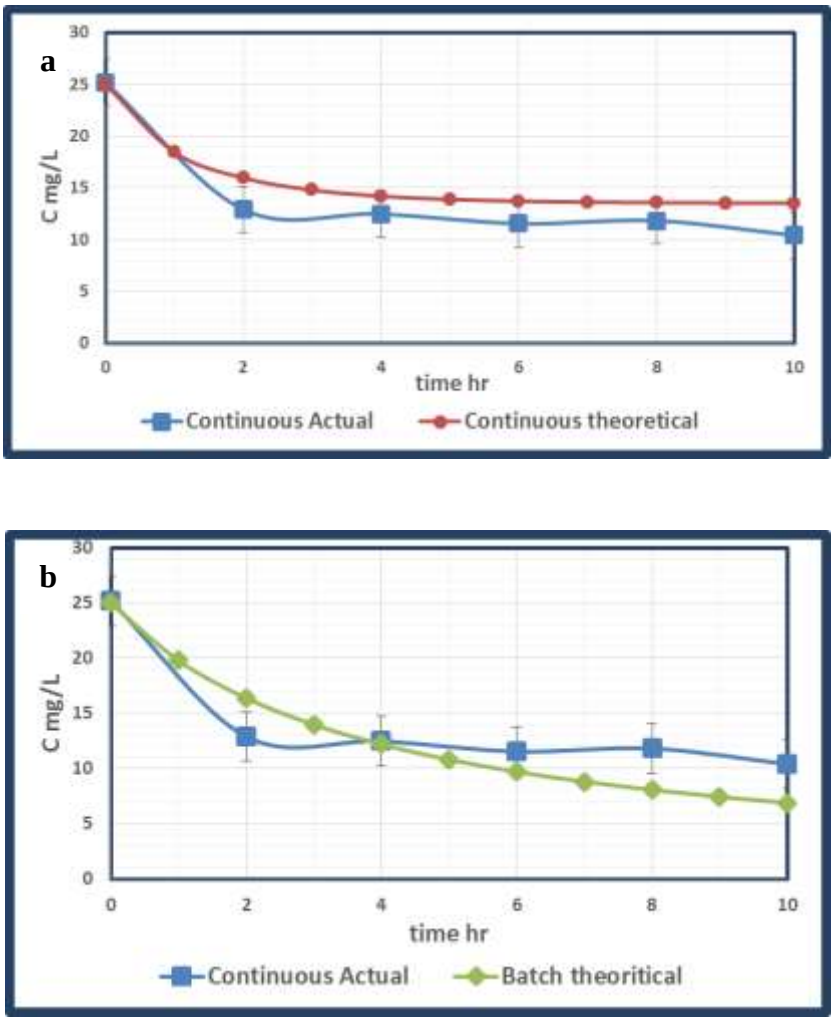

Figure 63: Phenol concentration profiles a) actual & theoretical for continuous operation, and b) actual for continuous operation & theoretical for batch operation

The theoretical concentration profile showed that steady state was reached after 6 hours of operation. Fluctuations around the steady state in the actual concentration profile could be attributed to the disturbances in the influent and effluent flow rates. Replacing the peristaltic pumps with dosing pumps would result in an efficient control of the influent and effluent flow rates.

Figure 64 shows phenol and TOC reduction achieved during continuous flow using E-STC-5 for an influent/effluent of 550 mL/hr and water volume of 3.4 L. The treatment proceeded at a recirculation flow rate of 23.6 L/min under UV-A light intensity of 45 W/m^2. An average evaporation rate of 2.4 mL/min was encountered. Steady state concentration of phenol was reached after 6 hours, where 65% degradation was achieved. Longer time for mineralization of phenol byproducts was needed. TOC reached steady state after 10 hours.

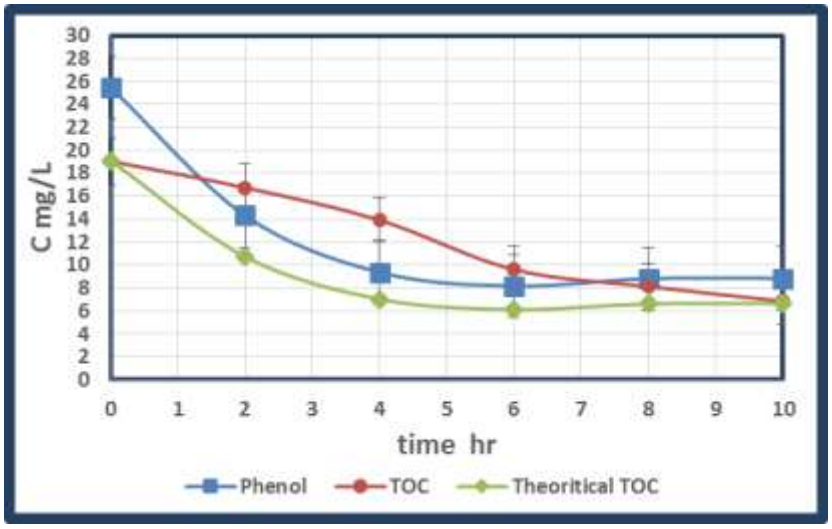

Figure 64: Reduction in Phenol & TOC during continuous operation using E-TSC-5

During long batch and continuous experiments, evaporation was noticed. During continuous operation under UV-A intensity of 60 W/m^2 and recirculating flow rate of 20.7 L/min, evaporation rate was 1.5 mL/min. During continuous operation under UV-A intensity of 45 W/m^2 and recirculating flow rate of 20.7 L/min, evaporation rate was 2.4 mL/min. This postulates that the evaporation rate is dependent on the recirculating flow rate not the UV intensity. In order to confirm this finding, a set of experiments were conducted using different recirculating flow rates under with no illumination was conducted as shown in Table 10. Figure 65 shows that evaporation increase with the recirculating flow rate. High recirculating flow rates need to be avoided in order to water loses by evaporation.

Table 10: Effect of recirculating flow rate & UV intensity on evaporation rate

Recirculating Flow rate L/min	**UV-A intensity** W/m^2	**Evaporation rate** mL/min
20.7	58.7	1.5
23.6	45	2.4
25.5	60	3.3
29.8	0	3.7
33.5	0	5.0

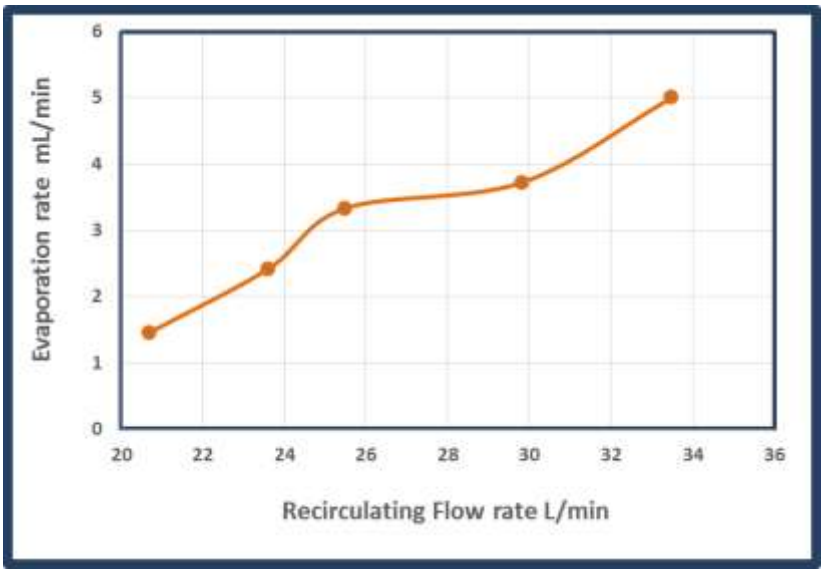

Figure 65: Effect of recirculating flow rate on evaporation rate

6.11 Photo-catalyst Multiple Use

E-TSC-5 was used for the batch and continuous degradation tests for a total of 50 hours of operation as detailed in Annex XIII. At an average flow rate of 23 L/min, 1142 L of water were passed over the catalytic bed. No deactivation of catalyst, loss of efficiency or increase of turbidity were encountered.

6.12 ITP Performance Comparison with Other immobilized TiO_2 Systems

The performance of the tray photo-reactor was compared with the performance of other photo-reactors using immobilized TiO_2. For the comparison of photo-reactors using immobilized TiO_2, 3 benchmarks are used: 1) the initial degradation rate, 2) the reactor throughput, and 3) the treated water turbidity. Initial degradation rate was used for this comparison since degradation on some of the supported catalysts followed first-order degradation model while others followed a second-order degradation model. Comparison of the degradation rate constants would not be possible in this case. Water turbidity was used as an indicator of the immobilized photo-catalyst stability and resistance to abrasion. Table 11 presents the initial degradation rate and reactor throughput for test trials using immobilized TiO_2 from the literature as well as for the tray photo-reactor.

Table 11: Degradation rate constant and reactor throughput for immobilized TiO_2 photo-reactors

Reactor	UV source	Support & immobilization technique	Treated volume L	Initial Conc mg/L	Treat. duration hours	Reactor area m^2	O_2 Supply	Removal %	K	$\left(\frac{dC}{dt}\right)_i$ mg/L.hr	Throughput $L/m^2.hr$	Ref
Cascade reactor [a]	external 60 W	concrete steps dispersion on epoxy layer	NA	25	6	0.375	air pump	95	0.426 1st [b]	10.65	Could not be calculated	[215] [216]
Cylindrical batch [c]	Internal 125W	porcelain photoactive tiles binding with silica-based compound,heat treatment at 680°c	1	25	6	na	Mechanical stirring	73	0.0177 2nd [b]	11.06	Could not be calculated	[217] [218]
Baffled shallow tank [d]	sun	glass sheet spraying and heat treatment at 450°c	138 mL/hr	0.94	continuous	0.0312	-	100	na	na	4.42	[219]
Fluidized bed shallow tank	external 30 W	floating ceramic spheres	1	10	12	0.0375	-	100	0.318 1st [b]	7.95 [e]	2.22	[138]
Shallow tank	external 250 W	inner/outer surface of quartz tubes dip coating	3.5	40	5	0.075	-	38	0.0907 1st [b]	2.27 [e]	9.33	[220]
Tray photo-reactor	external 60 W	Sand Epoxy binder	500 mL/hr	25	continuous	0.159	Passive aeration	65	0.011[f] 0.042[g] 2nd	6.56 26.25	3.46	current study

NA not available
[a] water depth was limited to 4 mm, pH 7
[b] calculated from concentration profiles
[c] reactor temperature was controlled using a cooling jacket
[d] glass strips were glued on the glass sheet to act as alternating vertical baffles to elongate the water path and residence time in the reactor. The size of allowable immobilization sheet was limited by the available firing oven
[e] initial degradation rate was calculated for an initial concentration of 25 mg/L
[f] based on total treatment time
[g] based on exposure time

Although the ITP did not achieve the highest throughput or the highest initial degradation rate, the tray photo-reactor fulfil the very important requirement of photo-catalyst stability and resistance to abrasion. In all the other aforementioned photo-reactor test trials, turbidity variation as the treatment proceeded was not evaluated nor the stability of TiO_2 on the support. Initial degradation rate for ITP based on the exposure time was the highest. Allowing a higher depth of water over the tray would result in a higher residence time on the tray and a higher exposure time. Maximizing the exposure time is crucial for enhancing the ITP performance.

6.13 Inferences from ITP Testing

Immobilization of TiO_2 on sand particles using epoxy was successful in achieving the highest phenol degradation and resistance to abrasion in the ITP. This immobilization method is simple carried in room temperature. The ITP was successfully operated in a continuous flow mode. No deactivation or loss of photoactivity were noticed after successive degradation treatment cycles. The ITP was successful in meeting the desired process requirements.

Chapter VII

Conclusions and Future Prospects

7.1. Summary

The design of TiO_2 photocatalytic reactor is not a trivial process, since it involves the reaction solution, solid photo-catalyst, supply of oxygen and ultra-bandgap light. The photocatalytic degradation process requirements include: uniform light penetration to activate the photo-catalyst, a high recirculation rate to avoid dead zones in the reactor, a turbulent flow that enhances mass transfer between the pollutants and the photo-catalyst, high catalyst loading to allow for faster degradation rates, a constant supply of oxygen and simple catalyst separation after treatment.

A thorough review of the literature revealed that commonly tested reactor configurations for TiO_2 photocatalysis suffer from limitations that hamper their scale-up and commercialization. These limitations might be attributed to high capital cost of use of UV transmissive walls or pipes. Use of UV transmissive components also pose a limitation on photo-reactor size and the associated risk of breakage. Other limitations might be related to high operating cost related to continuous supply of oxygen to reaction solution or consumption of oxidants that act as electron scavengers. There are also technical limitations associated with the use of immobilized catalysts. These technical limitations are either due to prevalence of laminar flow conditions resulting in slow degradation rates or due to difficulty of immobilization of photocatalyst on large surfaces efficiently and at a low cost.

The research objective was to develop a tertiary wastewater treatment unit using TiO_2 photocatalysis that can be scaled-up for commercial use. The development started with the conceptual design for a continuous large scale treatment unit taking into account all the attributes for an efficient TiO_2 photocatalytic process. The photo-reactor is based on generating a thin water film having dispersed photo-catalyst for efficient light penetration and passive aeration. Sand was selected as support for TiO_2 immobilization as it cheap and abundant. A pilot model was developed for testing the reactor configuration adequacy. The prototype was modified until successful photo-catalyst support recirculation in the reactor was achieved.

Testing of the prototype for phenol degradation in the slurry water-bell photoreactor (SWBP) was conducted using commercial TiO_2 nanoparticles. The SWBP achieved satisfactory results, consequently the photo-reactor development process proceeded to incorporate the immobilized TiO_2 on sand grains in the treatment process.

Immobilizing TiO_2 on sand grains for testing in the immobilized water-bell photoreactor (IWBP) was conducted by two methods; direct immobilization using sol gel, and binding with epoxy coating. Testing the IWBP was unsatisfactory. The proposed reactor configuration using recirculating sand as a support for TiO_2 immobilization did not meet the process requirement of having a stable catalyst resistant to abrasion. In an attempt to fulfil the objective of developing a simple cheap treatment unit, the design of a new reactor configuration was attempted.

The design of the immobilized tray photoreactor (ITP) was based on keeping the immobilized TiO_2 on a stationary mode while maintain fulfilling the photocatalytic process requirements of light penetration, continuous oxygen supply, turbulent flow and high recirculation rate. Three immobilization techniques were adopted for immobilizing TiO_2 on sand grains for use in the ITP; 1) direct immobilization using sol gel, 2) binding with cement grout, and 3) binding with epoxy coating. The ITP using epoxy-TiO_2 sand composite was successful in meeting the desired process requirements of high degradation rates and photo-catalyst resistance to abrasion and stability over consecutive treatment cycles.

7.2. Conclusion and Future Prospects

7.2.1. Slurry Water-bell Photo-reactor

- Phenol degradation achieved in the SWBP was not attributed to air stripping nor photolysis. Phenol degradation was attributed to photocatalytic degradation only.
- The degradation rate was affected by the catalyst loading.
    - Rate of photo-degradation increased with increasing the catalyst loading until a maximum of 4 g/L was reached.
    - At higher catalyst loadings, the degradation rate decreased due to screening effects induced by the highly turbid suspension and the associated light scattering.

- The use of 4 gm/L catalyst loading has induced only small enhancement in the degradation rate over the 2 gm/L loading which makes it not cost-effective.
- The SWBP was operated using an appropriate catalyst of 2 g/L.

- Variation of light intensity from 60 to 90 W/m^2 does not enhance the treatment efficiency.
  - High light intensity was not applied to avoid loss of photonic efficiency and unnecessary heating of the reaction solution.
- Phenol photocatalytic degradation in the water-bell photoreactor fitted the first order reaction kinetic model.
- Experiments were conducted at pH 8 which is more likely to resemble municipal wastewater pH. Although this pH is the least favorable pH for the TiO_2 photocatalytic degradation of phenol, 64% phenol degradation was achieved in 4 hours.
- The degradation efficiency of the reactor increased by 20% on the addition of 50 mg/L H_2O_2.
- Throughout all the runs, aeration was sufficient to keep DO levels constant around saturation.
- The maximum rise in temperature had an average of 3.2°C which was much lower than temperature rise in other reactor configurations.
  - The small temperature rise associated with the passive aeration renders temperature control and additional cooling unnecessary for the SWBP.
- Photo-reactor showed better degradation rate under sun conditions.
  - The rise in temperature was limited to 0.5°C due to the natural air and prevailing wind conditions.
  - The water temperature started to decrease as the treatment continued towards the sunset.
- The water-bell photoreactor has two distinctive times: residence time and direct exposure time of the thin water film to UV light. Phenol reduction increased with the direct exposure time.
- Analysis of degradation rate constants based on residence time and exposure time showed that phenol degradation occurred due to both of direct exposure of the water thin film to radiation as well as exposure of the water surface inside the tank.
- The performance of the SWBP was compared with other slurry photoreactors using two benchmarks: the degradation rate constant and the reactor throughput.
  - The water-bell reactor had the highest throughput and a relatively high degradation rate constant.

- Under sun conditions, the throughput was 11 L/m^2.hr and the degradation rate constant was 0.21 hr^{-1}.

- An insight on the design merits of the TiO_2 water-bell reactor and efficiency could be clearly demonstrated. However, for the newly developed photo-reactor increasing the exposure time is crucial for enhancing the photoreactor performance.
- The exposure time depends on the recirculation flow rate and the nozzle design.
- An optimum recirculation flow rate is needed to maximize the exposure time, since:
  - Increasing the recirculation rate will increase the number of exposure cycles thus increasing the exposure time.
  - However, increasing the recirculation rate will increase the velocity of water existing the nozzle. The exposure time is inversely proportional to the velocity of the jet flow thus decreasing the exposure time.
- Increasing the exposure time can be achieved by using a nozzle with a high initial launch angle will lead to a longer trajectory path-line.
- Another possibility of increasing exposure time is using a double nozzle. Although the total flow exiting the 2 nozzles is the same, the exposed area will increase.

7.2.2. Immobilized Water-bell Photo-reactor

- Parameters for synthesis and immobilization of TiO_2 using sol-gel has been adapted for a sustainable immobilization technique aiming to minimize the process energy requirements and associated air emissions.
- TiO_2 nanoparticles produced were adequate for the intended photocatalytic use. The TiO_2 nanoparticles had a particle size of 11 nm and 77% anatase phase content and a specific surface area of 142.5 m^2/g.
- The adopted sol-gel method has the advantages of proceeding at low processing and sintering temperatures using simple equipment.
- Abrasion of the TiO_2 immobilized by sol gel in the IWBP was encountered. The high friction forces induced by the peripheral pump lead to the photo-catalyst abrasion.

- Abrasion of TiO_2 immobilized by epoxy on the sand particles was also encountered. The high friction forces induced by the rotating impeller of the centrifugal pump also lead to the photo-catalyst abrasion.
- A new photoreactor configuration was needed to avoid the high friction of the catalyst particles in the recirculating pump.
- The IWBP has two additional distinctive advantages as a photo-reactor employing supporeted photo-catalyst:
    - The supported photo-catalyst is dispersed in the wastewater eliminating mass transfer limitations.
    - The IWBP has its settling compartment below the riser with a central hopper connected to the recirculating pump for easy separation of the photo-catalyst after treatment ends.
- For developing the IWBP, there are two routes for research to avoid the TiO_2 abrasion:
    - Using a recirculating pump with no internal moving parts. Positive displacement pumps can handle liquids with fragile solids such that abrasion of the photo-catalyst does not occur.
    - Developing a new TiO_2 composite which is highly resistant to abrasion. Research might be conducted using Teflon as TiO_2 support. Teflon has a high density (specific gravity of 2.2), yet a higher cost than sand.

7.2.3. Immobilized Tray Photo-reactor

- The design of the tray photoreactor was based on keeping the immobilized TiO_2 in a stationary mode while maintain fulfilling the photocatalytic process requirements of light penetration, passive oxygenation, turbulent flow for efficient mass transfer and recirculation to avoid treatment dead zones.
- The direct immobilization of TiO_2 on sand (TSC) using sol-gel was not successful. Physical adhesion of TiO_2 on the sand surface was not resistant to abrasion.
- Immobilization of TiO_2 using sol-gel requires multiple coating cycles to have an adequate TiO_2 loading on the sand rendering the process energy and time consuming without ensuring the prevention of abrasion.

- The abrasion resistance of the cement is adversely affected by the inclusion of TiO_2 nanoparticles which lead to a drastic increase of the treated water turbidity.
- The immobilization of TiO_2 on sand particles (E-TSC) using epoxy was successful in achieving the highest phenol degradation and resistance to abrasion. This immobilization method is simple carried in room temperature.
- E-TSC had another operational advantage over TSC and C-TSC. The photo-catalyst bed was not disturbed by the flowing water.
- Phenol degradation over E-TSC was due to photocatalytic degradation not adsorption.
- E-TSC-5 had achieved the highest degradation efficiency where 45% of phenol was degraded in 4 hours.
- TiO_2 directly dispersed in the epoxy matrix achieved a lower phenol degradation. The smooth TiO_2-epoxy film had a lower surface area of 0.0027 m^2/g, while the rough E-TSC had a surface area of 0.0885 m^2/g.
- The degradation using the E-TSC with different TiO_2 loadings followed a second order degradation rate.
- The ITP showed higher degradation rates for treating wastewater contaminated with higher initial concentration of phenol.
    - An initial degradation rate of 14.75 mg/L.hr can be achieved on treating wastewater contaminated with 50 mg/L of phenol as compared to 6.56 mg/L.hr on treating wastewater contaminated with 25 mg/L of phenol.
- The ITP was successfully operated in a continuous flow mode. After reaching steady state, phenol degradation exceeded 65%. Throughout the whole treatment duration the turbidity was insignificantly changed and Do levels remained constant around saturation level.
- Evaporation was encountered. Evaporation increased as the recirculating flow rate increased.
- Although the tray photoreactor did not achieve the highest throughput or the highest initial degradation rate, the tray photoreactor fulfil the very important requirement of photo-catalyst stability and resistance to abrasion for multiple treatment cycles.
- Epoxy TiO_2 sand composite is promising for application in wastewater treatment due to its photoactivity, resistance to abrasion, and cost-effectiveness. For the newly developed TiO_2

epoxy-sand composite, there are numerous opportunities for increasing efficiency and performance enhancement:

- Achieving better mixing and dispersion of the TiO_2 nanoparticles in the epoxy matrix. Ultrasonic mixing can be an option.
- Maximizing the surface area of the incorporated TiO_2 nanoparticles is also crucial. There is an active research on pore structure and design.
- Doping of incorporated TiO_2 nanoparticles with metals and non-metal dopants to increase the light absorption span and enhance the photocatalytic properties of the TiO_2.
- Optimizing the bed thickness to avoid using excess of TiO_2 that is not exposed while maintaining the bed integrity.
- Studying the mutual effect of TiO_2 particle sizes and sand particle sizes.
- Studies on long-term use of the photo-catalyst is required to assisst Epoxy resins resistance to long exposure to UV radiation.

7.2.4. Potential for Scale-up and Commercialization

- The ITP has an integrated storage which can accommodate for fluctuation in wastewater influent flow rate or disturbances in the treatment.
- The ITP has the merit of passive oxygenation. No temperature control is needed. The system complexity and operating costs associated with supplying air or oxidants additions, and cooling are totally eliminated in the ITP.
- The ITP is designed to use sunlight which decrease the treatment energy footprint. The ITP reactor can use artificial UV lighting as the application requires or during the non-sunny periods.
- Minimizing the chemical consumption and handling as well as minimizing energy requirement render the ITP optimum for sustainable wastewater treatment.
- The ITP does not include any transparent walls or pipes for radiation transmittance which may pose a limit on the reactor size, cause problems of filming, and are prone to breakage risks and UV- solarization.
- Since ITP uses fixed-bed catalyst, there is no cost associated with catalyst separation after treatment ends. For the proposed ITP configuration, there is no potential for clogging of pumps,

valves and fitting which will eventually lead to a lower maintenance cost and higher operation reliability.

- The only foreseen limitation for the ITP might be dealing with effluents containing suspended solids that might deposit on the photo-catalytic bed decreasing the treatment efficiency and requiring regeneration.
- After the development of the ITP based on modular basis design, future research on treatment of larger volumes of wastewater can be conducted through:
  - Use of multiple units, i.e. the use of several nozzles and trays with a common recirculating system.
  - Increasing the size of the nozzles and trays provided that proper light penetration is maintained.
- After the development of the ITP which is promising for scale-up and commercialization, treatment of difficult to treat wastewaters need to be tested.
  - To date chlorination is the most common disinfection method used for water disinfection. Viruses and protozoan ocysts and cysts are resistant to chlorine, they were found in reclaimed water effluents that have been disinfected by chlorination. The TiO_2 photocatalytic reactor is recommended for testing in difficult disinfection applications.

References

[1] UNEP/Grid-Arendal, "Vital water graphics: An overview of the state of the world's fresh and marine waters," UNEP, 2008, 2nd edition.

[2] Egyptian Ministry of Water Resources and Irrigation, "Water scarcity in Egypt: The urgent need for regional cooperation among the Nile basin countries," February 2014.

[3] CAPMAS, "Yearly statistical book, Issue 108," Egypt, September 2017.

[4] A. Angelakis, B. Durham, M. Marecos do Monte, M. Salgot, T. Wintgens and C. Thoeye , "Wastewater recycling and reuse in Eureau countries with emphasis on criteria used," EUREAU EU 1/2 Recycling and reuse working group EU1/2-07-WR-40(1), January 2007.

[5] A. Al-Jasser, "Saudi wastewater reuse standards for agricultural irrigation:Riyadh treatment plants effluent compliance," *Journal of King Saud University, Engineering Sciences*, vol. 23, pp. 1-8, 2011.

[6] Egyptian Environmental Affairs Ageny, "Egypt state of the environemnt report," Cairo, Egypt, 2011.

[7] EPA, "2012 Guidelines for water reuse," CDM Smith Inc, 2012.

[8] Egyptian code 501/2005 for reuse of treated wastewater in agriculture., Cairo: Housing and Building National Research Center, 2005.

[9] National Research Center, "Water reuse: potential for expanding the nation's water supply through reuse of municipal wastewater," The National Academies Press, Washigton D.C., 2012.

[10] L. Lishman, S. Smyth, K. Sarafin, S. Kleywegt, J. Toito, T. Peart, B. Lee, M. Servos, M. Beland and P. Seto, "Occurence and reductions of pharmaceuticals and personal care products and estrogens by municipal wastewater treatment plants in Ontario, Canada," *Science of the Total Environment*, vol. 367, pp. 544-558, 2006.

[11] C. Metcalfe, B. Koenig, D. Bennie, M. Servos, T. Ternes and R. Hirsch, "Occurrence of neutral and acidic drugs in the effluents of Canadian sewage treatment plants," *Environmental Toxicology and Chemistry*, vol. 22, no. 12, pp. 2872-2880, 2003.

[12] G. Boyd, H. Reemtsma, D. Grimm and S. Mitra, "Pharmaceuticals and personal care products (PPCPs) in surface and treated waters of Louisiana, USA and Ontario, Canada," *The Science of the Total Environment*, vol. 311, pp. 135-149, 2003.

[13] A. Ifelebuegu, "The fate and behaviour of selected endocrine disrupting chemicals in full scale wastewater and sludge treatment unit processes," *International Journal of Environmental Science and Technology.*, vol. 8, no. 2, pp. 245-254, 2011.

[14] B. Kasprzyk-Hordern, R. Dinsdale and A. Guwy, "The occurrence of pharmaceuticals, personal care products, endocrine disruptors and illicit drugs in surface water in South Wales, UK," *Water Research,* vol. 42, pp. 3498-3518, 2008.

[15] T. Ternes, "Occurence of drugs in German sewage treatment plants and rivers," *Water Research,* vol. 32, no. 11, pp. 3245-3260, 1998.

[16] M. Carballa, F. Omil, J. Lema, M. Llompart, C. Gracia-Jares, I. Rodriguez, M. Gomez and T. Ternes, "Behaviour of pharmaceuticals, cosmetics and hormones in a sewage treatment plant," *Water Research,* vol. 38, pp. 2918-2926, 2004.

[17] S. Castiglioni, R. Bagnati, R. Fanelli, F. Pomati, D. Calamari and E. Zuccato, "Removal of pharmaceuticals in sewage treatment plants in Italy," *Environmental Science and Technology,* vol. 40, pp. 357-363, 2006.

[18] O. Braga, G. Smythe, A. Schafer and A. Feitz, "Fate of steroid estrogens in Australian inland and coastal wastewater treatment plants," *Environmental Science and Technology,* vol. 39, pp. 3351-3358, 2005.

[19] F. Sodre, M. Locatelli and W. Jardim, "Occurrence of emerging contaminants in Brazillian drinking waters: Asewage-to-tap issue," *Water, Air, and Soil Pollution,* vol. 206, pp. 57-67, 2010.

[20] Y. Yoon, J. Ryu, J. Oh, B. Choi and S. Snyder, "Occurence of endocrine disrupting compounds, pharmaceuticals, and personal care products in the Han river (Seoul, South Korea)," *Science of the Total Environment,* vol. 408, pp. 636-643, 2010.

[21] N. Nakada, H. Shinohara, A. Murata, K. Kiri, S. Managaki, N. Sato and H. Takada, "Removal of selected pharmaceuticals and personal care products (PPCPs) and endocrine-disrupting chemicals (EDCs) during sand filteration and ozonation at a municipal sewage treatment plant," *Water Research,* vol. 41, pp. 4373-4382, 2007.

[22] B. Petrie, R. Barden and B. Kasprzyk-Horden, "A review on emerging contaminants in wastewaters and the environment: current knowledge, understudied areas and recommendations for future monitoring," *Water Research,* vol. 72, pp. 3-27, 2015.

[23] S. Lee and S. Park, "TiO2 photocatalyst for water treatment applications," *Journal of Industrial and Engineering Chemistry,* vol. 19, pp. 1761-1769, 2013.

[24] D. Miller, "Chemicals in the environment," in *Effects of pollutants at the ecosystem level*, Wiley & Sons Ltd, 1984, pp. 7-13.

[25] V. Likodimos, D. Dionysiou and P. Falaras, "Clean water: water detoxification using innovative photocatalysts," *Reviews in Environmental Science and Bio/Technology,* vol. 9, pp. 87-94, 2010.

[26] L. Dhanapal and A. Morse, "Effect of analgesics and their derivatives on antibiotic resistance of environmental microbes," *Water Science and Technology*, vol. 59, no. 9, pp. 1823-1829, 2009.

[27] C. Miege, J. Choubert, L. Ribeiro, M. Eusebe and M. Coquery, "Removal efficiency of pharmaceuticals and personal care products with varying wastewater treatment processes and operating conditions - conception of a database and first results," *Water Science and Technology,* vol. 57, no. 1, pp. 49-56, 2008.

[28] M. Klavarioti, D. Mantzavinos and D. Kassinos, "Removal of residual pharamceuticals from aqueous systems by advanced oxidation processes," *Environment International,* vol. 35, pp. 402-417, 2009.

[29] A. Deegan, B. Shaik, K. Nolan, K. Urell, M. Oelgemoller, J. Tobin and A. Morrissey, "Treatment options for wastewater effluents from pharmaceutical companies," *International Journal of Environmental Science & Technology,* vol. 8, no. 3, pp. 649-666, 2011.

[30] N. Miranda-Garcia, M. Maldonado, J. Coronado and S. Malato, "Degradation study of 15 emerging contaminants at low concentrationby immobilized TiO2 in a pilot plant," *Catalysis Today,* vol. 151, pp. 107-113, 2010.

[31] J. Blanco, S. Malato, P. Fernandez-Ibanez, D. Alarcon, W. Gernjak and M. Maldonado, "Review of feasilble solar energy applications to water processes," *Renewable and Sustainable Energy Reviews,* vol. 13, pp. 1437-1445, 2009.

[32] V. Snoeyink and D. Jenkins, in *Water Chemistry*, New York, John wiley & Sons, 1980, pp. 114-118.

[33] R. Munter, "Advanced oxidation processes - current status and prospects," *Proceedings of the Estonian Academy of Sciences. Chemistry,* vol. 50, no. 2, pp. 59-80, 2001.

[34] A. Dixit, A. Mungray and M. Chakraborty, "Photochemical oxidation of phenol and chlorophenol by UV/H2O2/TiO2 process: A kinetic study," *International Journal of Chemical Engineering and Applications,* vol. 1, no. 3, pp. 247-250, 2010.

[35] S. Malato, P. Fernandez-Ibanez, M. Maldonado, J. Blanco and W. Gernjak, "Decontamination and disinfection of water by solar photocatalysis: Recent overview and trends," *Catalysis Today,* vol. 147, pp. 1-59, 2009.

[36] D. Spasiano, R. Marotta, S. Malato and P. Fernandez-Ibanez, "Solar photocatalysis: Materials, reactors, some commercial and pre-industeralized applications. A comprehensive approach," *Applied Catalysis B: Environmental,* vol. 170, pp. 90-123, 2015.

[37] M. Chong, B. Jin, C. Chow and C. Saint, "Recent developments in photocatalytic water treatment technology: A review," *Water Research,* vol. 44, pp. 2997-3027, 2010.

[38] H. Choi, S. Al-Abed, D. Dionysios, E. Stathatos and P. Lianos, "TiO2-based advanced oxidation nanotechnologies for water purification and reuse," *Sustainability Science and Engineering,* vol. 2, pp. 229-254, 2010.

[39] S. Lee and A. Mills, "Detoxification of water by semiconductor photocatalysis," *Journal of Industrial and Engineering Chemistry,* vol. 10, no. 2, pp. 173-187, 2004.

[40] S. Kamble, S. Sawant and V. Pangarkar, "Novel Solar-based Photocatalytic Reactor for Degradation of Refractory Pollutants," *American Institute of Chemical Engineers Journal,* vol. 50, no. 7, pp. 1647-1650, 2004.

[41] INFORSE, "Solar Energy," [Online]. Available: www.inforse.org/europe/dieret/solar/solar.html. [Accessed 1 Dec 2017].

[42] J. Arana, J. Melian, J. Rodriguez, O. Diaz, A. Viera, J. Pena, P. Sosa and V. Jimenez, "TiO2-photocatalysis as a tertiary treatment of naturally treated wastewater," *Catalysis Today,* vol. 76, pp. 279-289, 2002.

[43] N. Al-Bastaki, "Performance of advanced methods for treatment of wastewater: UV/TiO2, RO and UF," *Chemical Engineering and Processing,* vol. 43, pp. 935-940, 2004.

[44] H. Dimitroula, V. Daskalaki, Z. Frontistis, D. Kondaides, P. Panagiotopoulou, N. Xekoukoulotakis and D. Mantzavinos, "Solar photocatlysis for the abatement of emerging micro-contaminants in wastewater: synthesis, characterization and testing of various TiO2 samples," *Applied Catalysis B: Environmental,* Vols. 117-118, pp. 283-291, 2012.

[45] M. Agullo-Barcelo, M. Polo-Lopez, F. Lucena, J. Jofre and P. Fernandez-Ibanez, "Solar advanced oxidation processes as disinfection tertiary treatments for real wastewater: implicatons for water reclamation," *Applied catalysis B: Environmental,* Vols. 136-137, pp. 341-350, 2013.

[46] R. Dominguez-Espindola, S. Silva-Martinez, M. Ortiz-Hernandez, J. Roman-Zubillaga and R. Guardian-Tapia, "Photocatlytic disinfection of municipal wastewater using TiO2 film

and Ag/TiO2 powder under UV and solar light irradiation," *Mexican journal of Scientific Research,* vol. 2, no. 2, pp. 60-68, 2013.

[47] S. Navalon, M. Alvaro, H. Garcia, D. Escrig and V. Costa, "Photocatalytic water disinfection of cryptosporidium parvum and Giardia lamlia using a fibrous ceramic TiO2 photocatalyst," *Water Science and Technology,* vol. 59, no. 4, pp. 639-645, 2009.

[48] J. Gamage and Z. Zhang, "Applications of photocatalytic disinfection," *International Journal of Photoenergy,* pp. Doi: 10.1155/2010/764870, 11 pages, 2010.

[49] P. Maness, S. Smolinski, D. Blake, Z. Huang, E. Wolfrum and W. Jacoby, "Bacericidal activity of photocatalytic TiO2 reaction: toward an understanding of its killing mechanism," *Applied and Environmetal Microbiology,* vol. 65, no. 9, pp. 4094-4098, 1999.

[50] M. Sokmen, S. Degerli and A. Aslan, "Photocatalytic disinfection of Giardia intestinals and acanthamoeba castellani cysts in water," *Experimental Parasitology,* vol. 119, pp. 44-48, 2008.

[51] J. Lee, M. Kang, S. Choung, K. Ogino, S. Miyata, M. Kim, J. Park and J. Kim, "The preparation of TiO2 nanometer photocatalyst film by a hydrothermal method and its sterilization performance for Giardia lamblia," *Water Research,* vol. 38, pp. 713-719, 2004.

[52] S. Ede, L. Hafner, P. Dunlop, J. Byrne and G. Will, "photocatalytic disinfection of bacterial pollutants using suspended and immobilized TiO2 powders," *Photochemistry and Photobiology,* vol. 88, pp. 728-735, 2012.

[53] C. Mccullagh, J. Robertson, D. Bahnemann and P. Robertson, "The application of TiO2 photocatalysis for disinfection of water contaminated with pathogenic micro-organisms: a review," *Research on Chemical Intermediates,* vol. 33, no. 3-5, pp. 359-375, 2007.

[54] M. Chong and B. Jin, "Photocatalytic treatment of high concentration carbamazepine in synthetic hospital wastewater," *Jouranl of Hazardous Materials,* Vols. 199-200, pp. 135-142, 2012.

[55] L. Rizzo, G. Ferro and C. Manaia, "Wastewater disinfection by solar heterogeeous photocatalysis: effect on tetracycline resistant/sensetive enterococcus strains," *Global Nest Journal,* vol. 16, no. 3, pp. 457-464, 2014.

[56] M. Y. Ghaly, T. S. Jamil, I. E. El-Seesy, E. R. Souaya and R. A. Nasr, "Treatment of highly polluted paper mill wastewater by solar photocatalytic oxidation with synthesized nano TiO2," *Chemical Engineering Journal,* vol. 168, p. 446–454, 2011.

[57] S. Kansal, M. Singh and D. Sud, "Effluent quality at kraft/soda agro-based paper mills and its treatment using a heterogeneous photocatalytic system," *Desalination,* vol. 228, p. 183–190, 2008.

[58] A. Amat, A. Arques , F. Lopez and M. Miranda, "Solar photo-catalysis to remove paper mill wastewater pollutants," *Solar Energy,* vol. 79, p. 393–401, 2005.

[59] A. Rodrigues , M. Boroski, N. Shimada, J. Garcia, J. Nozaki and N. Hioka, "Treatment of paper pulp and paper mill wastewater by coagulation-flocculation followed by heterogeneous photocatalysis," *Journal of Photochemistry and Photobiology A: Chemistry,* vol. 194, pp. 1-10, 2008.

[60] J. Banu, S. Anandan, S. Kaliappan and I. Yeom, "Treatment of dairy wastewater using anaerobic and solar photocatalytic methods," *Solar Energy,* vol. 82, pp. 812-819, 2008.

[61] P. Pekakis, N. Xekoukoulotakis and D. Mantzavinos, "Treatment of textile dyehouse wastewater by TiO2 photocatalysis," *Water Research,* vol. 40, pp. 1276-1286, 2006.

[62] M. Saquib, M. Abu Tariq, M. Faisal and M. Muneer, "Photocatalytic degradation of two selected dye derivatives in aqueous suspensions of titanium dioxide," *Desalination,* vol. 219, pp. 301-311, 2008.

[63] M. Luo, D. Bowden and P. Brimblecombe, "Removal of dyes from water using a TiO2 photocatalyst supported on black sand," *Water Air & Soil Pollution,* vol. 198, pp. 233-241, 2009.

[64] D. Oliveira, P. Batista, P. Muller Jr., V. Velani, M. Franca, D. Souza and A. Machado, "Evaluating the effectiveness of photocatalysts based on Titanium dioxide in the degradation of the dye Ponceau 4R," *Dyes and Pigments,* vol. 92, pp. 563-572, 2011.

[65] G. Zayani, L. Bousseimi, P. Pichat, F. Mhenni and A. Ghrabi, "Photocatalytic Degradation of four Textile Azo Dyes in Aqueous TiO2 Suspensions: Practical Outcomes and Revisited Pathways," *Journal of Advanced Oxidation Technology,* vol. 9, no. 1, pp. 65-78, 2006.

[66] J. Kasanen, J. Salstela, M. Suvanto and T. Pakkanen, "Photocatalytic degradation of methylene blue in water solution by multilayer TiO2 coating on HDPE," *Applied Surface Science,* vol. 258, pp. 1738-1743, 2011.

[67] M. Sokmen, I. Tatlidil, C. Breen, F. Clegg, C. Buruk, T. Sivlim and S. Akkan, "A new nano-TiO2 immobilized biodegradable polymer with self-cleaning properties," *Journal of Hazardous Materials,* vol. 187, pp. 199-205, 2011.

[68] A. Toor, A. Verma, C. Jotshi, P. Bajpai and V. Singh, "Photocatalytic degradation of direct yellow 12 dye using UV/TiO2 in a shallow pond slurry reactor," *Dyes and Pigments,* vol. 68, pp. 53-60, 2006.

[69] W. Gernjak, M.I. Maldonado, S. Malato, J. Caceres, T.Krutzler, A.Glaser and R.Bauer, "Pilot-plant treatment of olive mill wastewater (OMW) by solar TiO2 photocatalysis and solar photo-Fenton," *Solar Energy,* vol. 77, pp. 567-572, 2004.

[70] V. Nogueira, I. Lopes, T. Rocha-Santos, F. Goncalves, A. Duarte and R. Pereira, "Photocatalytic treatment of olive oil mill wastewater using TiO2 and Fe2O3 nanomaterials," *Water, Air, & Soil Pollution,* vol. 227, no. 3, article no 88, 2016.

[71] M. Anheden, D. Goswami and G. Svedberg, "Photocatalytic treatment of wastewater from 5-Flurouracil manufacturing," *Solar Energy Engineering,* vol. 118, pp. 2-8, 1996.

[72] V. Augugliaro, E. Gracia-Lopez, V. Loddo, S. Malato, I. Maldonado, G. Marci, R. Molinari and L. Palmisano, "Degradation of lincomycin in aqueous medium : coupling of solar photocatalysis and membrane separation," *Solar Energy,* vol. 79, pp. 402-408, 2005.

[73] V. Torbina, A. Vodyankin, I. Ivanchikova, O. Kholdeeva and O. Vodyankina, "Support pretreatment effect on the catalytic properties and reusability of silica-supported Titania catalysts in 2,3,6-Trimethylphenol oxidation with Hydrogen peroxide," *Kinetics and Catalysis,* vol. 56, no. 3, pp. 369 -374, 2015.

[74] M. Tasbihi, C. Ngah, N. Aziz, A. Mansor, A. Abdullah, L. Teong and A. Mohamed, "Lifetime and regeneration studies of various supported TiO2 photocatalysts for degradation of phenol under UV-C light in a batch reactor," *Industrial & Engineering Chemistry Research,* vol. 46, pp. 9006 - 9014, 2007.

[75] N. Zainudin, A. Abdullah and A. Mohamed, "Development of supported TiO2 photocatalyst based adsorbent for photocatalytic degradation of phenol," in *International conference on Environment*, 2008.

[76] M. Zulfakar, N. Hairul, H. Akmal and M. Abdul Rahman, "Photocatalytic degradation of phenol in a fluidized bed reactor utilizing immobilized TiO2 photocatalyst: characterization and process studies," *Journal of Applied Sciences,* vol. 11, no. 13, pp. 2320-2326, 2011.

[77] A. Haarstrick, O. Kut and E. Heinzle, "TiO2-assissted degradation of environmentally relevant organic compounds in wastewater using a novel fluidized bed photreactor," *Environment Science Technology,* vol. 30, pp. 817-824, 1996.

[78] T. Sivlim, S. Akkan, I. Altin, M. Koc and M. Sokmen, "TiO2 immobilized biodegradable polymer for photocatalytic removal of chlorophenol," *Water Air & Soil Pollution,* vol. 223, pp. 3955-3964, 2012.

[79] E. Seck, J. Dona-Rodriguez, C. Fernandez-Rodriguez, D. Portillo-Carrizo, M. Hernandez-Rodriguez, O. Gonzalez-Diaz and J. Perez-Pena, "Solar photocatalytic removal of hrebicides from real wastewater by using sol-gel synthesized nanocrystalline TiO2:

operational parameters optimization and toxicity studies," *Solar Energy,* vol. 87, pp. 150-157, 2013.

[80] M. Jimenez, M. Maldonado, E. Rodriguez, A. Hernandez-Ramirez, E. Saggioro, I. Carra and J. Perez, "Supported TiO2 solar photocatalysis at semi-pilot scale: Degradation of pesticides found in citrus processing industry wastewater, reactivity and influence of photogenerated species," *Journal of Chemical Technology & Biotechnology,* vol. 90, pp. 149-157, 2015.

[81] G. Echavia, F. Matzusawa and N. Negishi, "Photocatalytic degradation of organophosphate and phosphonoglycine pesticides using TiO2 immobilized on silica gel," *Chemosphere,* vol. 76, pp. 595-600, 2009.

[82] Y. Shavisi, S. Sharifnia, S. Hosseini and M. Khadivi, "Application of TiO2/perlite photocatalysis for degradation of ammonia in wastewater," *Journal of Industrial & Engineering Chemistry,* vol. 20, pp. 278-283, 2014.

[83] Y. Shavisi, S. Sharifnia, M. Zendehzaban, M. Mirghavami and S. Kakehazar, "Application of solar light for degradation of ammonia in petrochemical wastewater by a floating TiO2/LECA photocatalyst," *Journal of Industrial & Engineering Chemistry,* vol. 20, pp. 2806-2813, 2014.

[84] P. Singla, O. Pandey and K. Singh, "Study of photocatalytic degradation of environmentally harmful phthalate esters using Ni-doped TiO2 nanoparticles," *International Journal of Environmental Science & Technology,* vol. 13, pp. 849-856, 2016.

[85] B. Czech and M. Curie, "Advanced photooxidation of surfactants in wastewater," *Chemik,* vol. 66, no. 12, pp. 1314-1325, 2012.

[86] D. Alrousan, M. Polo-Lopez, P. Dunlop, P. Fernandez-Ibanez and J. Byrne, "Solar photocatalytic disinfection of water with immobilised titanium dioxide in re-circulating flow CPC reactors," *Applied Catalysis B: Environmental,* vol. 128, pp. 126-134, 2012.

[87] K. Nakano, E. Obuchi, S. Takagi, R. Yamamoto, T. Tanizaki, M. Taketomi, M. Eguchi, K. Ichida, M. Suzuki and A. Hashimoto, "Photocatlytic treatment of water containing dinitrophenol and city water over TiO2/SiO2," *Separation and Purification Technology,* vol. 34, pp. 67-72, 2004.

[88] M. Samarghandi, J. Nouri, A. Mesdaghinia, A. Mahvi, S. Nasseri and F. Vaezi, "Efficiency removal of phenol, lead and cadmium by means of UV/TiO2/H2O2 processes," *International Journal of Environmental Science and Technology,* vol. 4, no. 1, pp. 19-25, 2007.

[89] M. Motegh, J. Ommen, P. Appel and M. Kreutzer, "Scale-up study of a multiphase photocatalytic reactor - Degradation of Cyanide in water over TiO2," *Environmental Science and Technology,* vol. 48, pp. 1574-1581, 2014.

[90] S. Malato, J. Blanco, A. Vidal, P. Fernandez, J. Caceres, P. Trincado, J. Oliveira and M. Vincent, "New large solar photocatalytic plant: set-up and preliminary results," *Chemosphere,* vol. 47, pp. 235-240, 2002.

[91] A. Fostier, M. Pereira, S. Rath and J. Guimaraes, "Arsenic removal from water employing heterogeneous photocatalysis with TiO2 immobilized in PET bottles," *Chemosphere,* vol. 72, pp. 319-324, 2008.

[92] N. Deedar, A. Irfan and Q. Ishtiaq A., "Evaluation of the adsorption potential of titanium dioxide nanoparticles for arsenic removal," *Journal of Environmental Sciences,* vol. 21, pp. 402-408, 2009.

[93] Y. Abdel-Maksoud, E. Imam and A. Ramadan, "TiO2 Solar Photocatalytic Reactor Systems: Selection of Reactor Design for Scale-up and Commercialization—Analytical Review," *Catalysts,* vol. 6, no. 9, article no 138, 2016.

[94] A. Shan, T. Ghazi and S. Rashid, "Immobilization of titanium dioxide onto supporting materials in heterogeneous photocatalysis: A review," *Applied Catalysis A: General,* vol. 389, pp. 1-8, 2010.

[95] U. Gaya and A. Abdullah, "Heterogeneous photocatalytic degradation of organic contaminants over titanium dioxide: A review of fundamentals, progress and problems," *Journal of Photochemistry and Photobiology C: Photochemistry Reviews,* vol. 9, pp. 1-12, 2008.

[96] M. A. Lazar, S. Varghese and S. S.Nair, "Photocatalytic water treatment by Titanium dioxide: Recent updates,," *Catalysts,* vol. 2, pp. 572-601, 2012.

[97] S. Martinez, J. Morales-Mejia, P. Hernandez, L. Santiago and R. Almanza, "Solar photocatalytic oxidation of Triclosan with TiO2 immobilized on volcanic porous stones on a CPC pilot scale reactor," *Energy Procedia,* vol. 57, pp. 3014-3020, 2014.

[98] M. Behnajady, H. Eskandarloo, N. Modirshahla and M. Shokri, "Investigation of the effect of sol-gel synthesis variables on structural and photocatalytic properties of TiO2 nanoparticles," *Desalination,* vol. 278, pp. 10-17, 2011.

[99] M. Ahmadi, M. Ghasemi and H. Rafsanjani, "Study of differrent parameters in TiO2 nanoparticles formation," *Journal of Materials Science and Engineering,* vol. 5, pp. 87-93, 2011.

[100] V. Etacheri, C. Valentin, J. Schneider, D. Bahnemann and S. Pillai, "Visible-light activation of TiO2 photocatalysts: Advances in theory and experiments," *Journal of Photochemistry and Photobiology C: Photochemistry Reviews,* vol. 25, pp. 1-29, 2015.

[101] S. Rasalingam, R. Peng and R. Koodali, "Removal of hazardous pollutants from wastewaters: Applications of TiO2-SiO2 mixed oxide materials," *Journal of Nanomaterials,* vol. 2014, pp. Doi: 10.1155/2014/617405, 42 pages, 2014.

[102] D. Bahnemann, "Photocatalytic water treatment: solar energy applications," *Solar Energy,* vol. 77, pp. 445-459, 2004.

[103] C. Comninellis, A. Kapalka, S. Malato, S. Parsons, I. Poulios and D. Mantzavinos, "Perspective Advanced oxidation processes for water treatment: advances and trends for R&D," *Journal of Chemical Technology and Biotechnology,* vol. 83, pp. 769-776, 2008.

[104] D. Blake, "Bibliography of Work on the Heterogeneous Photocatalytic Removal of Hazardous Compounds from Water and Air, Update Number 4 to October 2001, NREL/TP-510-31319," National Renewable Energy Laboratory, Colorado, US, 2001.

[105] Y. Goswami, "Engineering of Solar Photocatalytic Detoxification and Disinfection Processes," *Advances in Solar Energy,* vol. 10, pp. 165-210, 1995.

[106] R. Braham and A. Harris, "Review of Major Design and Scale-up Considerations for Solar Photocatalytic Reactors," *Industrial & Enginering Chemistry Research,* vol. 48, pp. 8890-8905, 2009.

[107] O. Alfano, D. Bahnemann, A. Cassano, R. Dillert and R. Goslich, "Photocatalysis in water environments using artificial and solar light," *Catalysis Today,* vol. 58, pp. 199-230, 2000.

[108] A. Adesina, "Industrial exploitation of photocatalysis: progress, perspectives and prospects," *Catalysis Surveys from Asia,* vol. 8, no. 4, pp. 265-273, 2004.

[109] J. Blanco-Galvez, P. Fernandez-Ibanez and S. Malato-Rodriguez, "Solar photocatalytic detoxification and disinfection of water: recent overview," *Solar Energy Engineering,* vol. 129, pp. 4-15, 2007.

[110] J. Pacheco and C. Tyner, "Enhancement of processes for solar photocatalytic detoxification of water," *Solar Engineering 1990. Proceedings of the ASME Solar Energy Conference,* pp. 163-166, 1990.

[111] M. Mehos and C. Turchi, "Field testing solar photocatalytic detoxification on TCE-contaminated groundwater," *Environmental Progress,* vol. 12, no. 3, pp. 194-199, 1993.

[112] C. Minero, E. pelizzeti, S. Malato and J. Blanco, "Large solar plant photocatalytic water decontamination: degradation of pentachlorophenol," *Chemosphere,* vol. 26, no. 12, pp. 2013-2119, 1993.

[113] D. Goswami, J. Klausner, G. Mathur, A. Martin, K. Schanze, P. Wyness, C. Turchi and E. Marchand, "Solar photocatalytic treatment of groundwater at Tyndall AFB: field test results," in *proceedings of the 1993 American solar energy society annual conference*, washigton, D.C., 1993.

[114] L. Bousseimi, S. Geissen and H. Schroeder, "Textile wastewater treatment and reuse by solar catalysis: results from a pilot plant in Tunisia," *Water Science & Technology,* vol. 49, no. 4, pp. 331-337, 2004.

[115] R. Dillert, S. Vollmer, E. Gross, M. Schober and D. Bahnemann, "Solar-catalytic treatment of an industrial wastewater," *Zeitschrift fur Physikalische Chemie,* vol. 213, pp. 141-147, 1999.

[116] J. Blanco, S. Malato, P. Fernandez, A. Vidal, A. Morales, P. Trincado, J. Oliveira, C. Minero, M. Musci, C. Casalle, M. Brunotte, S. Tratzky, N. Dischinger, K. Funken, C. Sattler, M. Vincent, M. Collares-Pereira, J. Mendes and C. Rangel, "Compound parabolic concentrator technology development to commercial solar detoxification applications," *Solar Energy,* vol. 67, pp. 317 - 330, 1999.

[117] S. Mozia, P. Brozek, J. Przepiorski, B. Tryba and A. Morawski, "Immobilized TiO2 for phenol degradation in a pilot-scale photocatalytic reactor," *Journal of Nanomaterials,* vol. 2012, pp. Doi: 10.1155/2012/949764, 10 pages, 2012.

[118] A. Hendarsa, H. Hermansyah and Slamet, "A novel photobiodegradation technology for hydrocarbon wastewater treatment," *International journal of Engineering and Technology,* vol. 13, no. 1, p. 6 pages, 2013.

[119] C. Silva, W. Wang and J. Faria, "Photocatalytic and photochemical degradation of mono-, di- and tri-azo dyes in aqueous solution under UV irradiation," *Journal of Photochemistry & Photobiology,* vol. 181, no. 2-3, pp. 314-324, 2006.

[120] B. Serrano and H. De Lasa, "Photocatalytic Degradation of Water Organic Pollutants. Kinetic Modeling and Energy Efficiency," *Industrial & Engineering Chemistry Research,* vol. 36, no. 11, p. 4705–4711, 1997.

[121] J. Bolton, K. Bircher, W. Tumas and C. Tolman, "Figures-of-merit for the technical development and application of advanced oxidation technologies for both electric- and solar-driven systems," *Pure Applied Chemistry,* vol. 73, no. 4, pp. 627-637, 2001.

[122] E. Bandala and C. Estrada , "Comparison of Solar Collection Geometries for Application to Photocatalytic Degradation of Organic Contaminants," *Journal of Solar Energy Engineering,* vol. 129, no. 1, pp. 22-26, 2005.

[123] N. Rao, V. Chaturvedi and G. Puma, "Novel pebble bed photocatalytic reactor for solar treatment of textile wastewater," *Chemical Engineering Journal,* vol. 184, pp. 90-97, 2012.

[124] S. Mozia, "Photocatalytic membrane reactors (PMRs) in water and wastewater treatment. A review," *Separation and Purification Technology,* vol. 73, pp. 71-91, 2010.

[125] J. Torkarsky, V. Matejka, L. Neuwirthova, J. Vontorova, K. Kutlakova, J. Kukutschova and P. Capkova, "A low-cost photoactive composite quartz sand/TiO2," *Chemical Engineering Journal,* vol. 222, pp. 488-497, 2013.

[126] M. Prairie, J. Pacheco and L. Evans, "Solar Detoxification of water Containing Chlorinated Solvents and Heavy Metals Via TiO2 Photocatalysis," *Solar Engineering 1992. Proceedings of the ASME International Solar Energy Conference,* vol. 1, pp. 1-8, 1992.

[127] S. Malato, J. Blanco, A. Vidal and C. Richter, "Photocatalysis with solar energy at a pilot-plant scale:an overview," *Applied Catalysis B: Environmental,* vol. 37, pp. 1-15, 2002.

[128] H. de Lasa, B. Serrano and M. Salaices, Photocatalytic reaction engineering, Springer, New York, NY, USA, 2005 .

[129] D. Bahnemann, R. Dillert, J. Dzengel, R. Goslich, G. Sagawe, H. Schumacher and V. Benz, "Field Studies of Solar Water Detoxification Using Non Light Concentrating Reactors," *Journal of Advanced Oxidation Technologies,* vol. 4, pp. 11-19, 1999.

[130] D. Curco, S. Malato, J. Blanco, J. Gimenez and P. Marco, "Photocatalytic degradation of phenol : Comparison between pilot-plant-scale and laboratory results," *Solar Energy,* vol. 56, no. 5, pp. 387-400, 1996.

[131] M. Kositzi, I. Poulios, S. Malato, J. Caceres and A. Campos, "Solar photocatalytic treatment of synthetic municipal wastewater," *Water Research,* vol. 38, pp. 1147-1154, 2004.

[132] C. Navntoft, P. Araujo, M. Litter, M. Apella, D. Fernandez, M. Puchulu, M. Hidalgo and M. Blesa, "Field tests of the solar water detoxification SOLWATER reactor in Los Pereyra, Tucuman, Argentina," *Journal of Solar Energy Engineering,* vol. 129, pp. 127-134, 2007.

[133] N. Miranda-Garcia, S. Suarez, B. Sanchez, J. Coronado, S. Malato and M. Maldonado, "Photocatalytic degradation of emerging contaminants in municipal wastewater treatment plant effluents using immobilized TiO2 in a solar pilot plant," *Applied Catalysis B: Environmental,* vol. 103, pp. 294-301, 2011.

[134] J. Crittenden, Y. Zhang, D. Hand, D. Perram and E. Marchand, "Solar detoxification of fuel-contaminated groundwater using fixed-bed photocatalysts," *Water Environment Research,* vol. 68, no. 3, pp. 270-278, 1996.

[135] V. Oberg, D. Goswami and G. Svedberg, "On Photocatalytic Detoxification of Water Containing Volatile Organic Compounds," *Proceedings of the ASME International Solar Engineering Conference,* pp. 147-153, 1993.

[136] R. Vargas and O. Nunez, "Photocatalytic degradation of oil industry hydrocarbon models at alboratory and at pilot-plant scale," *Solar Energy,* vol. 84, pp. 345-351, 2010.

[137] P. Wyness, J. Klausner, D. Goswami and K. Schanze, "Performance of nonconcentrating solar photocatalytic oxidation reactors, Part II: Shallow pond configuration," *Journal of Solar Energy Engineering,* vol. 116, pp. 8-13, 1994.

[138] T. Kanki, S. Hamasaki, N. Sano, A. Toyoda and K. Hirano, "Water purification in a fluidized bed photocatalytic reactor using TiO2-coated ceramic particles," *Chemical Engineering Journal,* vol. 108, pp. 155-160, 2005.

[139] M. Keshmiri, M. Mohseni and T. Troczynski, "Development of novel TiO2 sol-gel-derived composite and its photocatalytic activities for trichloroethylene oxidation," *Applied Cataysis B: Envieonmental,* vol. 53, pp. 209-219, 2004.

[140] P. Wyness, J. Klausner, D. Goswami and K. Schanze, "Performance of nonconcentrating solar photocatalytic oxidation reactors, Part II: Shallow pond configuration," *Journal of Solar Energy Engineering,* vol. 116, pp. 8-13, 1994.

[141] M. Van Well, R. Dillert, D. Bahnemann, V. Benz and M. Mueller, "A novel nonconcentrating reactor for solar water detoxification," *Journal of Solar Energy Engineering,* vol. 119, no. 2, pp. 114-119, 1997.

[142] R. Dillert, A. Cassano, R. Goslich and D. Bahnemann, "Large scale studies in solar catalytic wastewater treatment," *Catalysis Today,* vol. 54, pp. 267-282, 1999.

[143] G. Plantard, T. Janin, V. Goetz and S. Brosillon, "Solar photocatalysis treatment of phytosanitary refuses : efficiency of industrial photocatalysts," *Applied Catalysis B: Environmental,* Vols. 115-116, pp. 38-44, 2012.

[144] P. Wyness, J. Klausner, D. Goswami and K. Schanze, "Performance of nonconcentrating solar photocatalytic oxidation reactors, Part I: flat-plate configuration," *Journal of Solar Energy Engineering,* vol. 116, pp. 2-7, 1994.

[145] G. Zayani, L. Bousselmi, F. Mhenni and A. Ghrabi, "Solar photocatalytic degradation of commercial textile azo dye : performance of pilot scale thin film fixed-bed reactor," *Desalination,* vol. 246, pp. 344-352, 2009.

[146] M. Bekbolet, M. Linder, D. Weichgrebe and D. Bahnemann, "Photocatalytic detoxification with the thin-film fixed-bed reactor (TFFBR) : Clean-up of highly polluted landfill effluents using a novel TiO2 photocatalyst," *Solar Energy,* vol. 56, no. 5, pp. 455-469, 1996.

[147] D. Bockelmann, D. Weichgrebe, R. Goslisch and D. Bahnemann, "Concentrating versus non-concentrating reactors for solar water detoxification," *Solar Energy Materials and Solar Cells,* vol. 38, pp. 441-451, 1995.

[148] A. Chan, C. Chan, J. Barford and J. Porter, "Solar photocatalytic thin film cascade reactor for treatment of benzoic acid cotaining wastewater," *Water Research,* vol. 37, pp. 1125-1135, 2003.

[149] A. Chan, J. Porter, J. Barford and C. Chan, "Photocatalytic thin film cascade reactor for treatment of organic compounds in wastewater," *Water Science and Technology,* vol. 44, no. 5, pp. 187-195, 2001.

[150] H. Thu, M. Kurkmaz, E. Puzenat, C. Guillard and J. Herrmann, "From the fundamentals of photocatalysis to its applications in environment protection and in solar purification of water in arid countries," *Research on Chemical Intermediates,* vol. 31, no. 4-6, pp. 449-461, 2005.

[151] G. Shama, C. Peppiatt and M. Biguzzi, "A Novel thin film photoreactor," *Journal of Chemical Technology & Biotechnology,* vol. 65, pp. 56-64, 1996.

[152] G. Puma, "Dimensionless analysis of photocatalytic reactors using suspended solid photocatalysts," *Chemical Engineering Research and Design,* vol. 83(A7), p. 820–826, 2005.

[153] G. Puma and P. Yue, "A novel fountain photocatalytic reactor: model development and experimental validation," *Chemical Engineering Science,* vol. 56, pp. 2733-2744, 2001.

[154] G. Puma and P. Yue, "A novel fountain photocatalytic reactor for water treatment and purification ; modeling and design," *Industrial & Engineering Chemistry Research,* vol. 40, pp. 5162-5169, 2001.

[155] H. Otalvaro-Martin, M. Mueses and F. Machuca-Martinez, "Boundary layer of photon absorption applied to heterogeneous photocatalytic solar flat plate reactor design," *International Journal of Photoenergy,* vol. 2014, pp. Doi: 10.1155/2014/930439, 8 pages, 2014.

[156] V. Vaiano, O. Sacco, D. Pisano, D. Sannino and P. Ciambelli, "From the design to the development of a continuous fixed bed photoreactor for photocatalytic degradation of organic pollutants in wastewater," *Chemical Engineering Science,* vol. 137, pp. 152-160, 2015.

[157] N. Rao and V. Chaturvedi, "Photoactivity of TiO2-coated pebbles," *Industrial & Engineering Chemistry Research,* vol. 46, pp. 4406 - 4414, 2007.

[158] R. Matthews, "Photooxidative degradation of coloured organics in water using supported catalysts TiO2 on Sand," *Water Research,* vol. 25, no. 10, pp. 1169-1176, 1991.

[159] D. Hanaor and C. Sorrell, "Sand supported mixed-phase TiO2 photocatalysts for water decontamination applications," *Advanced Engineering Materials,* vol. 16, no. 2, pp. 248-254, 2014.

[160] E. Remoundaki, R. Vidali, P. Kousi, A. Hatzikioseyian and M. Tsezos, "Photolytic and photocatalytic alterations of humic substances in UV (254nm) and solar concentric parabolic concentrator (CPC) reactors," *Desalination,* vol. 248, pp. 843-851, 2009.

[161] "ACTIFLO Brochure," Veolia Water Treatment Technologies, [Online]. Available: www.veoliawatertechnologies.com/actiflo. [Accessed 25 8 2017].

[162] WEF, Water Environemt Federation Manual of Practice No. FD-8 Clarifier Design, Mc-Graw Hill, 2005.

[163] V. Streeter and E. Wylie, Fluid Mechanics, McGraw-Hill , 1983.

[164] R. Droste, Theory and Practice of Water and wastewater Treatment, John Wiley & Sons, 1997.

[165] M. Vosper, D. Graham and P. Cloke, Principles and Applications of Radiological Physics, Elsevier Health Sciences, 2011.

[166] A. Taylor, Illumination fundamentals, Lighting Research Center, Rensselaer, 2000.

[167] "A guide to selecting lamps," Photonics media, [Online]. Available: www.photonics.com. [Accessed 30 August 2017].

[168] "Lamp emission Spectra," Photon Technology International, [Online]. Available: www.PTI-NJ.com. [Accessed 30 August 2017].

[169] "DC Arc lamps," Newport, [Online]. Available: https://www.newport.com/f/dc-arc-lamps. [Accessed 2017 August 2017].

[170] J. Waymouth, "Collision Phenomena in Electrical Discharge Lamps," in *Applied Atomic Collision Physics, Volume 5: Special Topics*, Academic Press, 2013, pp. 331-347.

[171] J. Kerr and V. Fioletov, "Surface ultraviolet radiation," *Atmosphere-Ocean,* vol. 46, no. 1, pp. 159-184, 2008.

[172] "Sylvania 20W 24in T12 Black Light Fluorescent Tube," [Online]. Available: http://www.bulbs.com/product/F20T12-350BL. [Accessed 31 August 2017].

[173] A. Kudish, V. Lyubansky, E. Evseev and A. Ianetz, "Inter-comparison of the solar UVB, UVA and global radiation clearness and UV indices for Beer Sheva and Neve Zohar (Dead Sea), Israel," *Energy,* vol. 30, pp. 1623-1641, 2005.

[174] EPA, "EPA Priority polluatants List," 1 7 2014. [Online]. Available: www.epa.gov. [Accessed September 2017].

[175] Z. Guo, R. Ma and G. Li, "Degradation of phenol by nanomaterial TiO2 in wastewater," *Chemical Engineering Journal,* vol. 119, pp. 55-59, 2006.

[176] P. Raja, M. Bensimon, A. Kulik, R. Foschia, D. Laub, P. Albers, R. Renganathan and J. Kiwi, "Dynamics and characterization of an innovative Raschig rings-TiO2 composite photocatalyst," *Journal of Molecular catalysis A: Chemical,* vol. 237, pp. 215-223, 2005.

[177] C. Su, B. Hong and C. Tseng, "Sol-gel preparation and photocatalysis of titanium dioxide," *Catalysis Today,* vol. 96, pp. 119-126, 2004.

[178] M. Borges, D. Garcia, T. Hernandez, J. Ruiz-Morales and P. Esparza, "Supported photocatalyst for removal of emerging contaminants from wastewater in a continuous packed-bed photoreactor configuration," *Catalysts,* vol. 5, pp. 77-87, 2015.

[179] P. Lei, F. Wang, X. Gao, Y. Ding, S. Zhang, J. Zhao and S. Liu, "Immobilization of TiO2 nanoparticles in polymeric substrates by chemical bonding for multi-cycle photodegradation of organic pollutants," *Journal of Hazardous Materials,* Vols. 227-228, pp. 185-194, 2012.

[180] H. Han and R. Bai, "Buoyant photocatalyst with greatly enhanced visible-light activity prepared through a low temperature hydrothermal method," *Industrial & Engineering Chemistry Research,* vol. 48, pp. 2891-2898, 2009.

[181] EPA, "Methods for Chemical Analysis of water and wastes, EPA/600/4-79/020," Office of Research and Development, Washington DC, March 1983.

[182] Hach, *Water Analysis Handbook, Phenols 4-Aminoantipyrine Test Method 8047, DOC316.53.01108,* 3/2014, Edition 8.

[183] F. Silva, M. Lansarin and C. Moro, "A comparison of slurry and immobilized TiO2 in the photocatalytic degradation of phenol," *Latin American Applied Research,* vol. 42, pp. 275-280, 2012.

[184] N. Barka, I. Bakas, S. Qourzal, A. Assabbane and Y. Ait-Ichou, "Degradation of phenol in water by Titanium Dioxide photocatalysis," *Oriental Journal of Chemistry,* vol. 29, no. 3, pp. 1055-1060, 2013.

[185] D. Montgomery, Design and analysis of experiments, Singapore: John wiley & Sons, 2013, eigth edition.

[186] E. Grabowska, J. Reszczynska and A. Zaleska, "Mechanism of phenol photodegradation in the presence of pure and modified-TiO2: A review," *Water Research,* vol. 46, pp. 5453-5471, 2012.

[187] F. Dakubo, J. Baygents and J. Farrell, "Hydrogen peroxide removal from chemical-mechanical planarization wastewater," *IEEE Transactions on Semiconductor Manufacturing,* vol. 25, no. 4, pp. 623-629, 2012.

[188] S. Borji, S. Nasseri, A. Mahvi, R. Nabizadeh and A. Javadi, "Invetigation of photocatalytic degradation of phenol by Fe(III)-doped TiO2 and TiO2 nanoparticles," *Journal of Environmental Health Science & Engineering,* vol. 12:101, p. 10 pages, 2014.

[189] R. Saratale, H. Noh, J. Song and D. Kim, "Influence of parameters on the photocatalytic degradation of phenolic contaminants in wastewater using TiO2/UV system," *Journal of Environmental Science and Health, Part A,* vol. 49, pp. 1542-1552, 2014.

[190] K. Naeem and O. Feng, "Parameters effect on heterogeneous photocatalysed degradation of phenol in aqueous dispersion of TiO2," *Journal of Environmental Sciences,* vol. 21, pp. 527-533, 2009.

[191] F. Shahrezaei, A. Akhbari and A. Rostami, "Photodegradation and removal of phenol and phenolic derivatives from petroleum refinery wastewater using nanoparticles of TiO2," *International Journal of Energy and Environment,* vol. 3, no. 2, pp. 267-274, 2012.

[192] N. Laoufi, D. Tassalit and F. Bentahar, "The degradation of phenol in water solution by TiO2 photocatalysis in a helical reactor," *Global Nest Journal,* vol. 10, no. 3, pp. 404-418, 2008.

[193] M. Alalm and A. Tawfik, "Solar photocatalytic degradation of phenol in aqueous solutions using titanium dioxide," *International Journal of Chemical, Molecular, Nuclear, Materials and Metallurgical Engineering,* vol. 8, no. 2, 2014.

[194] T. Zhang, X. Wang and X. Zhang, "Recent progress in TiO2-mediated solar photocatalysis for industrial wastewater treatment," *International Journal of Photoenergy,* vol. 2014, pp. Doi:10.1155/2014/607954, 12 pages, 2014.

[195] L. Lim, R. Lynch and S. In, "Comparison of simple and economical photocatalyst immobilisation procedures," *Applied Catalysis A: General,* vol. 365, pp. 214-221, 2009.

[196] G. Balasubramanian, D. Dionysiou, M. Suidan, V. Subramanian, I. Baudin and J.-M. Laine, "Titania powder modified sol-gel process for photocatalytic applications," *Journal of Materials Science,* vol. 38, pp. 823-831, 2003.

[197] Y. Chen and D. Dionysiou, "Sol-gel synthesis of nanostructured Tio2 films for water purification," in *Sol-gel Methods for Materials Processing,* Springer Science, 2008, pp. 67-75.

[198] Z. Qu, W. Huang, S. Zhou, H. Zheng, X. Liu, M. Cheng and X. Bao, "Enhancement of the catalytic performance of supported-metal catalysts by pretreatment of the support," *Journal of Catalysis,* vol. 234, pp. 33-36, 2005.

[199] K. Khuanmar, W. Wirojanagud, P. Kajitvichyanukul and S. Maensiri, "Photocatalysis of phenolic compounds with synthesized nanoparticles TiO2/Sn2," *Journal of Applied Sciences,* vol. 7, no. 14, pp. 1968-1972, 2007.

[200] Y. Bessekhouad, D. Robert and J. Weber, "Synthesis of photocatalytic TiO2 nanoparticles:optimization of the preparation conditions," *Journal of Photochemistry and Photobiology A: Chemistry,* vol. 157, pp. 47-53, 2003.

[201] F. Sayilkan, M. Asilturk, H. Sayilkan, Y. Onal, M. Akarsu and E. Arpac, "Characterization of TiO2 Synthesized in alcohol by a sol-gel process: the effects of annealing tempreture and acid catalyst," *Turkish Journal of Chemistry,* vol. 29, pp. 697-706, 2005.

[202] R. Spurr and H. Myers, "Quantitative analysis of anatase-rurle mixtures with an x-ray diffractrometer," *Analytical Chemistry,* vol. 29, no. 5, pp. 760-762, 1957.

[203] M. Thommes, K. Kaneko, A. Neimark, J. Olivier, F. Rodriguez-Reinoso, J. Rouquerol and K. Sing, "Phisiosorption of gases, with special reference to the evaluation of surface area and pore size distribution (IUPAC Technical report)," *Pure & Applied Chemistrty,* vol. 87, no. 9-10, pp. 1051-1069, 2015.

[204] M. Kurk and M. Jaroniec, "Gas adsorption characterization of ordered organic-inorganic nanocomposite materials," *Chemistry of Materials,* vol. 13, pp. 3169-3183, 2001.

[205] M. Choquette-Labbe, W. Shewa, J. Lalman and S. Shanmugam, "Photocatalytic degradation of phenol and phenol derivatives using a nano-TiO2 catalyst: Integrating

quantitative and qualitative factors using response surface methodology," *Water,* vol. 6, pp. 1785-1806, 2014.

[206] M. Hassan, H. Dylla, L. Mohammad and T. Rupnow, "Methods for the application of titanium dioxide coatings to concrete pavement," *International Journal of Pavement Research Technology,* vol. 5, no. 1, pp. 12-20, 2012.

[207] E. Boonen and A. Beeldens, "Recent photocatalytic applications for air purification in Belgium," *Coatings,* vol. 4, pp. 553-573, 2014.

[208] M. Delnavaz, B. Ayati, H. Ganjidoust and S. Sanjabi, "Application of concrete surfaces as novel substrate for immobilization of TiO2 nanopowder in photocatalytic treatment of phenolic water," *Journal of Environmental Health Science and Engineering,* pp. DOI: 10.1186/s40201-015-0214-y, 10 pages, 2015.

[209] I. Sopyan, N. Hafizah and P. Jamal, "Immobilization of TiO2 with cement : Photocatalytic degradation of phenol and its kinetic studies," *Indian Journal of Chemical Technology,* vol. 18, pp. 263-270, 2011.

[210] Y. Abdel-Maksoud, E. Imam and A. Ramadan, "Sand supported TiO2 photocatalyst inatrayphoto-reactor fortheremovalof emerging contaminants in wastewater," *Catalysis Today,* 2017.

[211] M. Popek and J. Szymanowski, "Abrasion resistance of concrete containing selected mineral powders," *Procedia Engineering,* vol. 153, pp. 617-622, 2016.

[212] M. Janus and K. Zajac, "Concretes with photocatalytic activity," in *High Performance Concrete Technology and Applications,* Intech, 2016, p. doi:10.5772/64779.

[213] A. Rashad, "A synopsis about the effect of nano-titanium dioxide on some properties of cementitious materials - a short guide for civil engineers," *Reviews on Advanced Materials Science,* vol. 40, pp. 72-88, 2015.

[214] B. Sun, A. Vorontsov and P. Smirniotis, "Role of platinum deposited on TiO2 in phenol photocatalytic oxidation," *Langmuir,* vol. 19, no. 8, pp. 3151-3156, 2003.

[215] M. Delnavaz, B. Ayati, H. Ganjidoust and S. Sanjabi, "Application of concrete surfaces as novel substrate for immobilization of TiO2 nanopowder in photocatalytic treatment of phenolic water," *Journal of Environmental Health Science and Engineering,* DOI: 10.1186/s40201-015-0214-y, 2015.

[216] M. Delnavaz, B. Ayati, H. Ganjidoust and S. Sanjabi, "Kinetics study of photocatalytic process for treatment of phenolic wastewater by TiO2 nanopowder immobilized on concrete surfaces," *Toxicological & Environmental Chemistry,* vol. 94, no. 6, pp. 1086-1098, 2012.

[217] C. Bianchi, E. Colombo, S. Gatto, M. Stucchi, G. Cerrato, S. Morandi and V. Capucci, "Photocatalytic degradation of dyes in water with micro-sized TiO2 as powder or coated on porcelain-gres tiles," *Journal of Photochemistry and Photobiology A: Chemistry,* vol. 280, pp. 27-31, 2014.

[218] C. Bianchi, M. Stucchi, C. Pirola, G. Cerrato, S. Morandi, B. Sacchi, S. Vitali, A. Di Michele and V. Capucci, "Micro-sized TiO2 catalyst in powder form and as a coating in porcelain gres tile for the photocatalytic degradation of phenol as model pollutant for water phase," *Advanced Materials Science,* vol. 2, no. 2, pp. 1-6, 2017.

[219] G. Kumara, F. Sultanbawa, V. Perera, I. Kottegoda and K. Tennakone, "Continuous flow photochemical reactor for solar decontamination of water using immobilized TiO2," *Solar Energy Materials & Solar Cells,* vol. 58, pp. 167-171, 1999.

[220] A. Nickheslat, M. Amin, H. Izanloo, A. Fatehizadeh and S. Mousavi, "Phenol photocatalytic degradation by advanced oxidation process under ultraviolet radiation using titanium dioxide," *Journal of Environmental and Public Health,* pp. Article ID 815310, 9 pages, 2013.

[221] M. Raslan and R. Abdel Wahab, "Water sector in Egypt: Current status and future prospective," in *Leading Trade Fair for Environmental Technologies (IFAt 2014)*, Munchen, Germany, 5-9 May, 2014.

[222] R. Abdel-Wahaab, "Wastewater reuse in Egypt: Opportunities and Challenges," in *Sustainable Water Technology*, Cairo, Egypt, 18-20 February, 2013.

Annexes

Annex I. Slurry Experimental Results

Operational parameters are summarized in the following tables

Slurry – Run 3

Phenol added: **150 mg** Total Volume: **7.4 L** Catalyst: **TiO_2 - P25 Powder**

Concentration: **20.3 mg/L** Light intensity: **92 W/m²** Catalyst loading: **0.34 g/L**

time	min	**T0**	**T60**	**T120**	**T180**	**T240**
T	°c	23.5	25.5	26	25.8	25.8
DO	mg/L	7.82	7.59	7.58	7.4	7.62
pH		8.07	8.04	8.09	8.08	8.26
Phenol	mg/L	20.3	18.6	17.5	16.7	15.9
Phenol reduction %			8	14	18	22
ΔT	°c		2	2.5	2.3	2.3

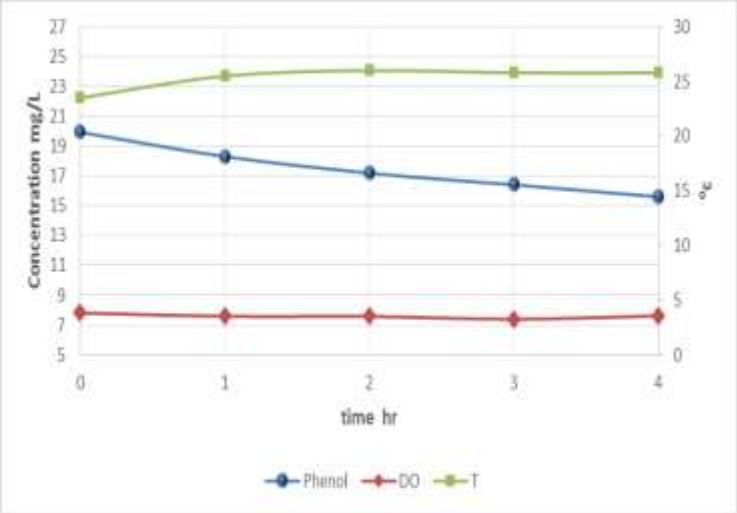

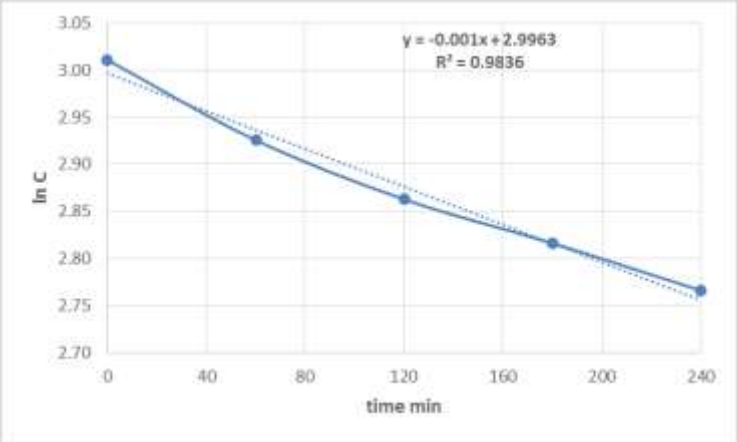

22 % Phenol reduction , K_{app} = 0.06 hr^{-1}

Maximum T rise during experiment = 2.5 °c

Slurry – Run 5

Phenol added: **150 mg** Flow rate: **19.1 L/min** Catalyst: **TiO_2 - P25 Powder**

Concentration: **20.5 mg/L** Light intensity: **89.8 W/m²** Catalyst loading: **1.4 g/L**

Total Volume: **7.3 L**

time	min	**T0**	**T60**	**T120**	**T180**	**T240**
T	°c	23.4	26.7	26.8	27.9	27.9
DO	mg/L	7.97	7.47	7.59	7.07	7.52
pH		7.75	8.52	8.6	8.61	8.62
Phenol	mg/L	20.5	17.1	15.5	13.1	11.9
Phenol reduction %			17	24	36	42
ΔT	°c		3.3	3.4	4.5	4.5

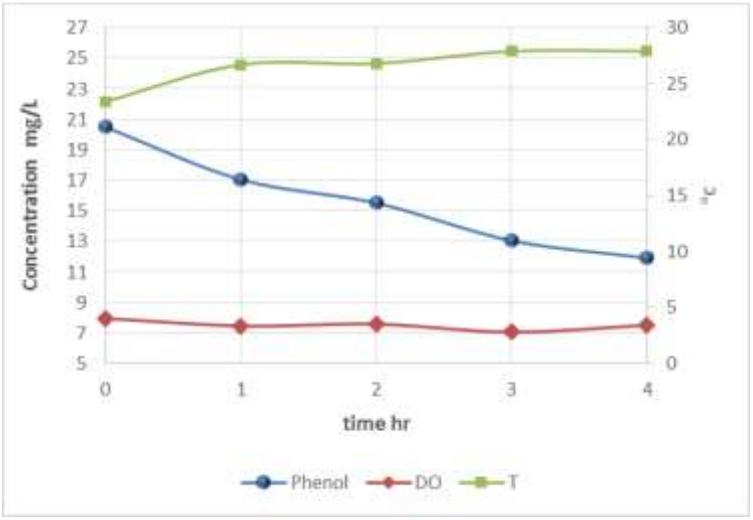

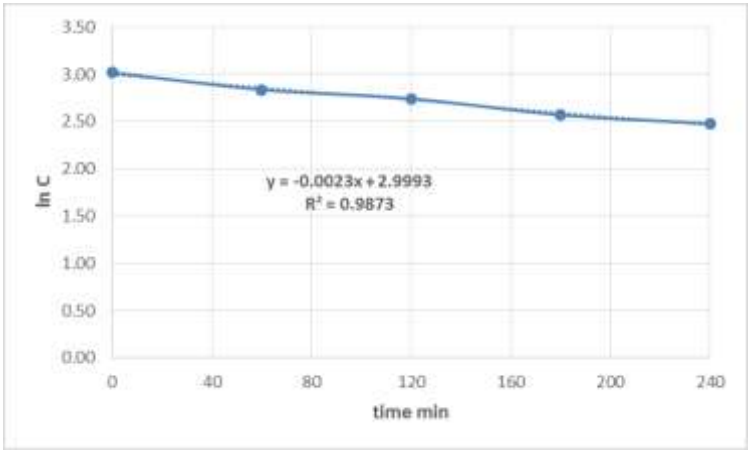

42 % Phenol reduction, K_{app} = 0.138 hr^{-1}

Maximum T rise during experiment = 4.5 °c

Slurry - Run 7

Phenol added : **150 mg** Flow rate: **18.7 L/min** Catalyst: **TiO_2 - P25**

Concentration: **19.9 mg/L** Light intensity: **62.2 W/m²** **slurry - used once**

Total Volume: **7.4 L** Catalyst loading: **0.7 g/L**

time	min	**T0**	**T60**	**T120**	**T180**	**T240**
T	°c	21.8	23.6	24.4	24.9	24.8
DO	mg/L	8.03	7.7	7.79	7.65	7.62
pH		8.02	8.34	8.16	8.16	8.18
Phenol	mg/L	20.2	18.7	17.4	16.5	15.3
Phenol reduction %			8	14	19	24
ΔT	°c		1.8	2.6	3.1	3

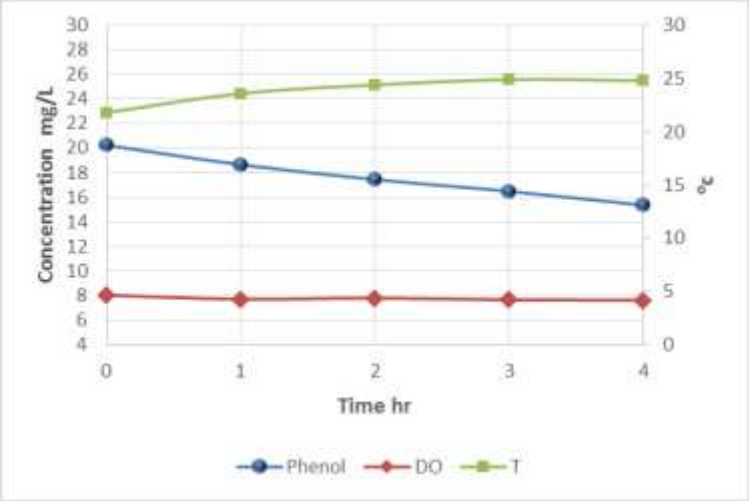

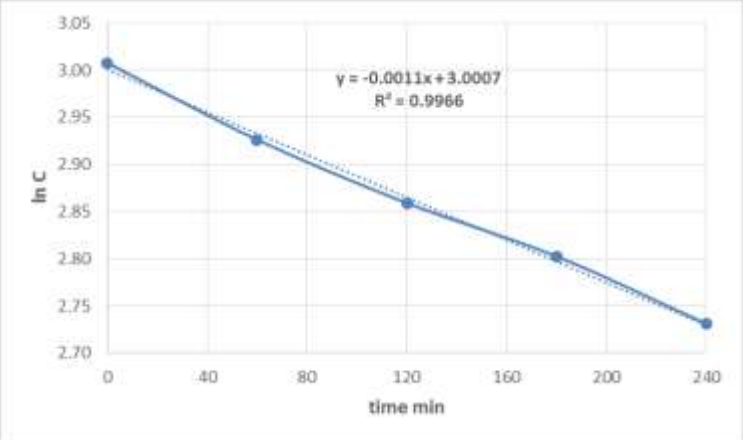

24 % Phenol reduction, K_{app} = 0.066 hr^{-1}

Maximum T rise during experiment = 3.1 °c

Slurry - Run 8

Phenol added: **140 mg** Flow rate: **19.2 L/min** Catalyst: **TiO_2 - P25 Powder**

Concentration: **20.1 mg/L** Light intensity: **61.4 W/m²** Catalyst loading: **3 g/L**

Total Volume: **7 L**

time	min	**T0**	**T60**	**T120**	**T180**	**T240**
T	°c	21.6	23.4	24	24.1	24.4
DO	mg/L	8.27	8.02	7.94	7.87	7.87
pH		7.92	7.71	7.99	8.1	8.17
Phenol	mg/L	20.1	15.8	12.8	10.4	8.9
Phenol reduction	%		21	36	48	56
ΔT	°c		1.8	2.4	2.5	2.8

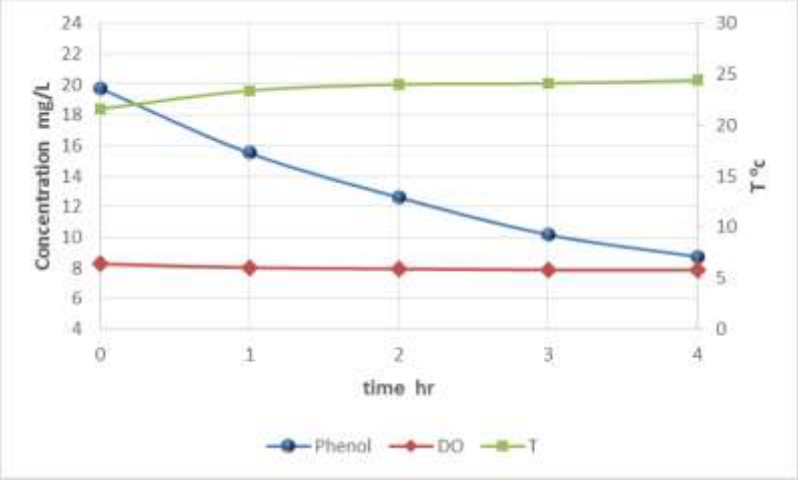

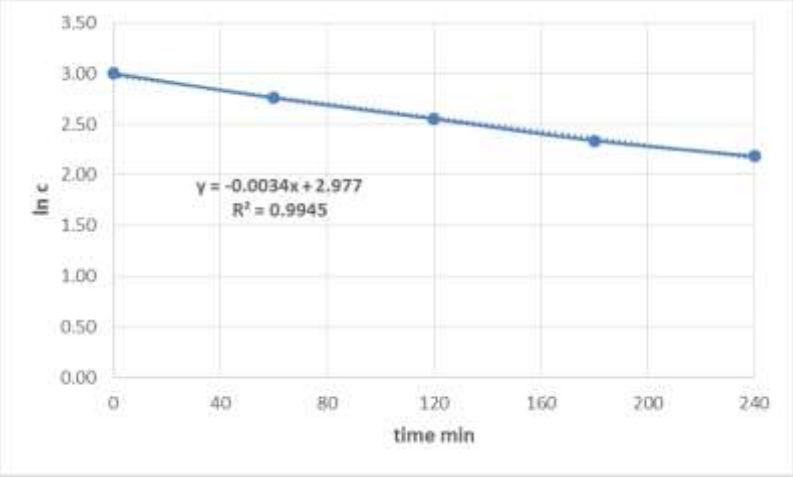

56 % Phenol reduction, K_{app} = 0.204 hr^{-1}

Maximum T rise during experiment = 2.8 °c

Slurry - Run 9

Phenol added: **140 mg** Flow rate: **18.9 L/min** Catalyst: **TiO_2 - P25**

Concentration: **19.8 mg/L** Light intensity: **90 W/m²** **slurry - used once**

Total Volume: **7.1 L** Catalyst loading: **3 g/L**

time	min	**T0**	**T60**	**T120**	**T180**	**T240**
T	°c	21.5	24.2	25.4	24.4	24.0
DO	mg/L	8.32	7.97	7.77	7.88	7.78
pH		8.10	8.02	8.06	8.07	8.07
Phenol	mg/L	19.8	16.2	14.0	11.4	10.1
Phenol reduction %			18	29	43	49
ΔT	°c		2.7	3.9	2.9	2.5

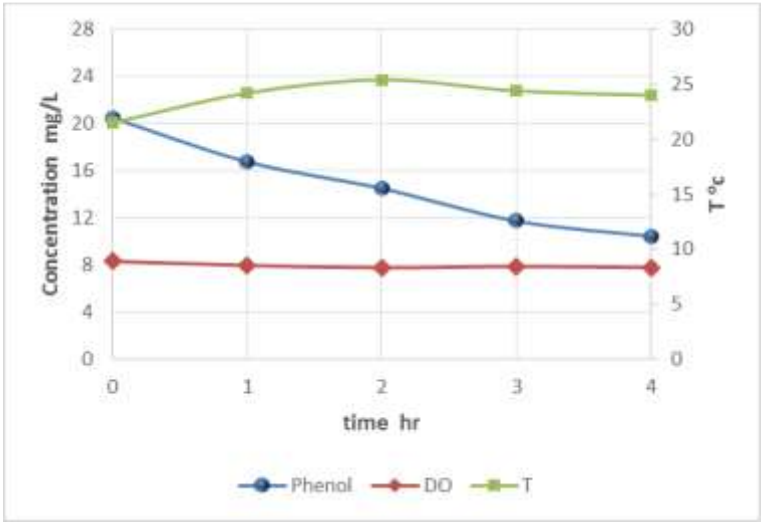

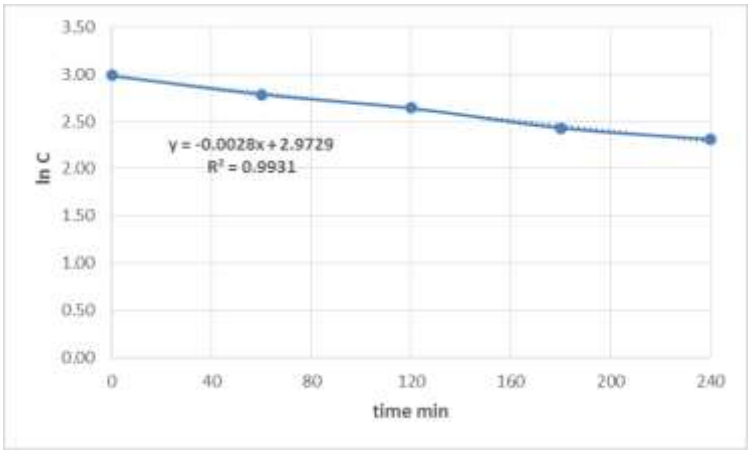

49 % Phenol reduction , K_{app} = 0.168 hr^{-1}

Maximum T rise during experiment = 3.9 °c

Slurry – Run 10

Phenol added: **40 mg** Flow rate: **18.8 L/min** Catalyst: **TiO_2 - P25**

Concentration: **12.8 mg/L** Light intensity: **60.2 W/m²** **slurry - used once**

Total Volume: **3.1 L** Catalyst loading: **2 g/L**

time	min	**T0**	**T30**	**T60**	**T90**	**T120**	**T150**	**T180**	**T210**	**T240**
T	°c	22.2	23.9	24.9	25.5	25.2	24.7	25.6	25	24.8
DO	mg/L	8.01	7.92	7.57	7.34	7.75	7.87	7.58	7.76	7.65
pH		8.45	8.05	8.05	8.08	8.09	8.11	8.13	8.21	8.18
Phenol	mg/L	12.8	11.6	10.0	9.2	8.1	7.5	7.3	6.4	5.9
Phenol reduction %			10	22	28	37	42	43	50	54
Δ T	°c		1.7	2.7	3.3	3	2.5	3.4	2.8	2.6

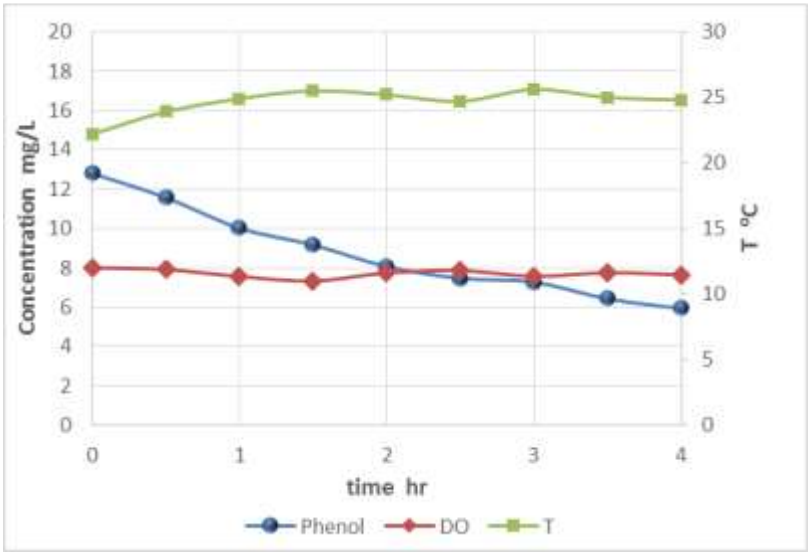

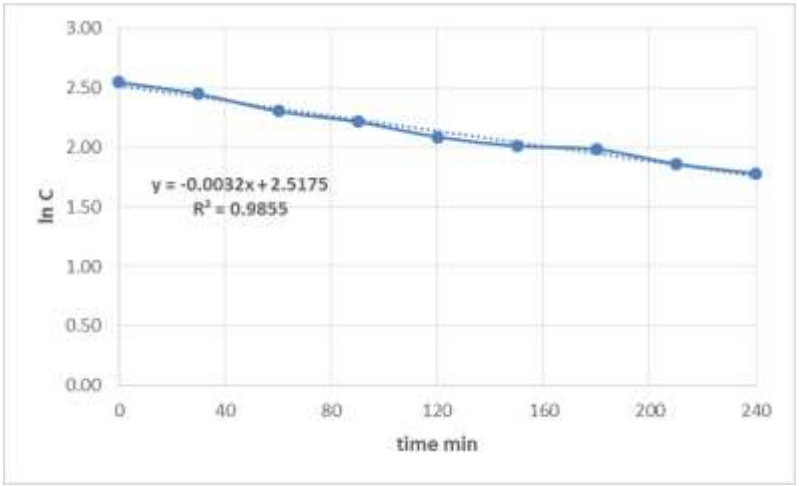

54 % Phenol reduction, K_{app} = 0.192 hr^{-1}

Maximum T rise during experiment = 3.4 °c

Slurry – Run 13

Phenol added: **75 mg** Flow rate: **18.6 L/min** Catalyst: **TiO_2 - P25**

Concentration: **24.7 mg/L** Light intensity: **61.1 W/m²** **slurry – used twice**

Total Volume: **3 L** Catalyst loading: **4.1 g/L**

time	min	**T0**	**T60**	**T120**	**T180**	**T240**
T	°c	20.7	23.6	25.1	24.5	25.4
DO	mg/L	9.28	8.93	8.61	8.87	8.65
pH		8.61	8.61	8.63	8.65	8.64
Phenol	mg/L	24.7	18.1	16.2	11.4	8.9
Phenol reduction %				27	34	54
ΔT	°c		2.9	4.4	3.8	4.7

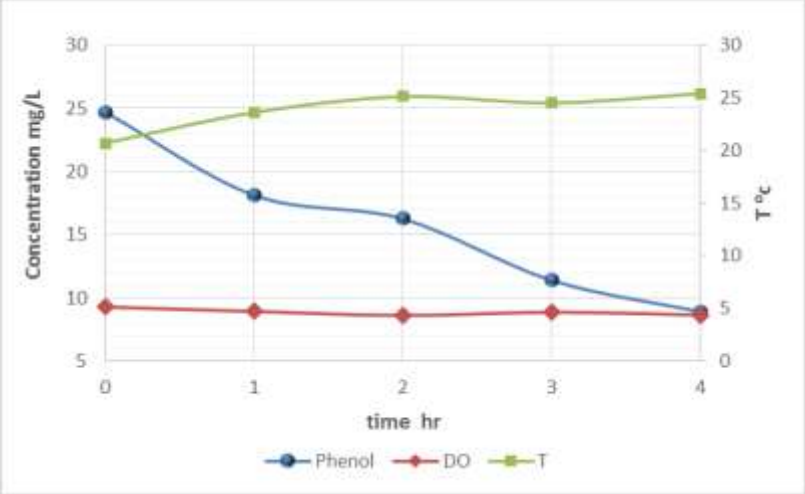

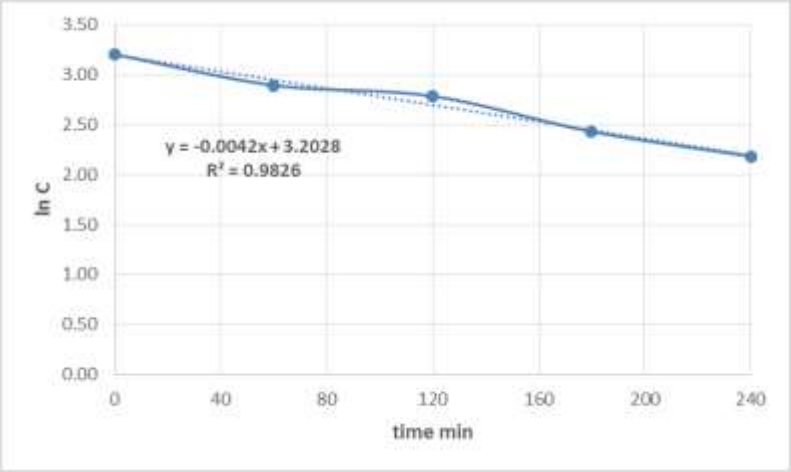

64 % Phenol reduction , K_{app} = 0.252 hr^{-1}

Maximum T rise = 4.7 °c

Slurry – Run 14

Phenol added: **75 mg** Flow rate: **18.6 L/min** Catalyst: **TiO_2 - P25**

Concentration: **25 mg/L** Light intensity: **61.7 W/m²** **slurry – used twice**

Total Volume: **3 L** Catalyst loading: **6 g/L**

time	min	**T0**	**T60**	**T120**	**T180**	**T240**
T	°c	20.2	22.3	22.1	22.5	22.3
DO	mg/L	9.4	9.11	9.18	9.1	9.18
pH		8.25	8.19	8.24	8.4	8.18
Phenol	mg/L	25.0	19.4	17.9	13.9	11.0
Phenol reduction %			22	28	45	56
ΔT	°c		2.1	1.9	2.3	2.1

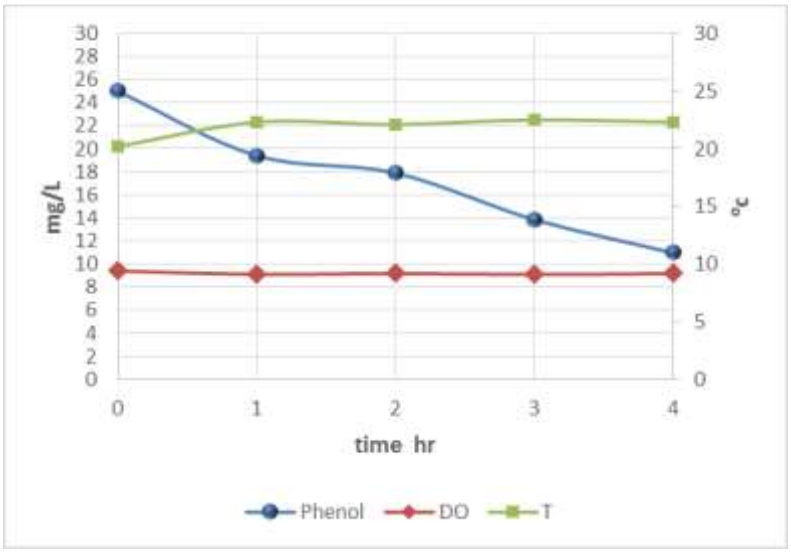

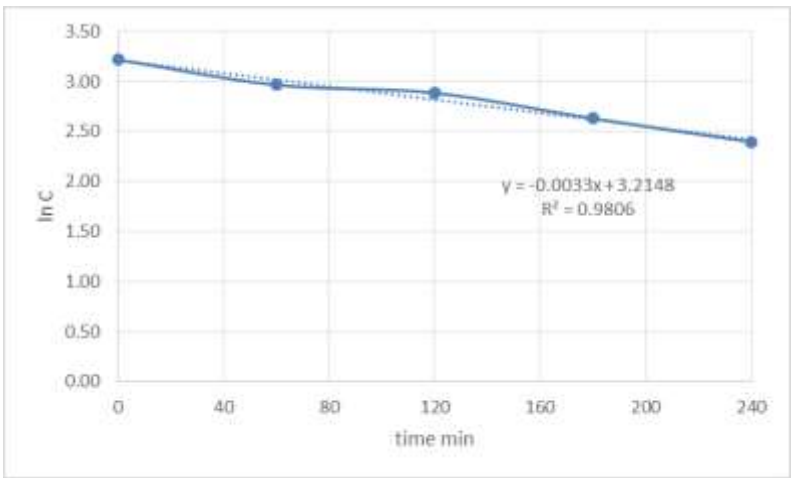

56 % Phenol reduction , K_{app} = 0.198 hr^{-1}

Maximum T rise = 2.3 °c

Slurry – Run 15

Phenol added: **75 mg** Flow rate: **18.4 L/min** Catalyst: **TiO_2 - P25**

Concentration: **24.8 mg/L** Light intensity: **60.2 W/m²** **slurry - used twice**

Total Volume: **3 L** Catalyst loading: **2 g/L**

time	min	**T0**	**T60**	**T120**	**T180**	**T240**
T	°c	21	23.3	23.7	23.4	23.2
DO	mg/L	9.41	9.07	9.01	9.14	9.16
pH		8.51	8.58	8.5	8.59	8.58
Phenol	mg/L	24.8	18.6	15.9	14.2	10.7
Phenol reduction %			25	36	43	57
ΔT	°c		2.3	2.7	2.4	2.2

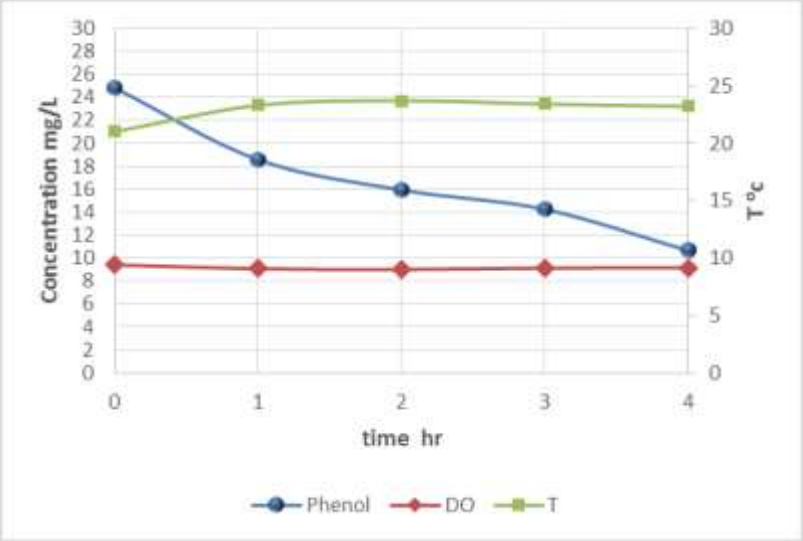

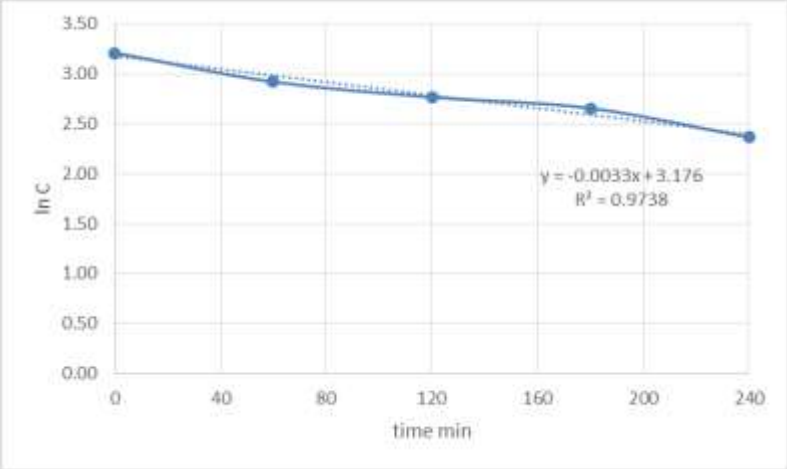

57 % Phenol reduction, K_{app} = 0.198 hr^{-1}

Maximum T rise = 2.7 °c

Slurry – Run 16

Phenol added: **140 mg** Flow rate: **19 L/min** Catalyst: **TiO_2 - P25**

Concentration: **19.8 mg/L** Light intensity: **Sun** **slurry - used 3 times**

Total Volume: **7.1 L** **43.1 W/m^2** Catalyst loading: **2 g/L**

time		**12:10**	**1:10**	**2:10**	**3:10**	**4:10**
	min	**T0**	**T60**	**T120**	**T180**	**T240**
T	°c	25.8	26.3	24.5	24.5	23.5
DO	mg/L	8.29	8.25	8.66	8.67	8.83
pH		8.37	8.63	8.65	8.65	8.66
Phenol	mg/L	19.8	16.3	13.0	10.7	8.7
Phenol reduction %			18	34	46	56
ΔT	°c		0.5	-1.3	-1.3	-2.3

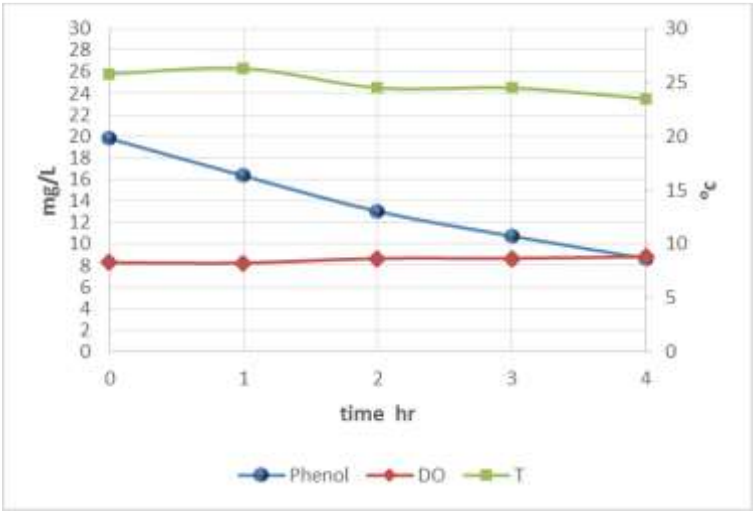

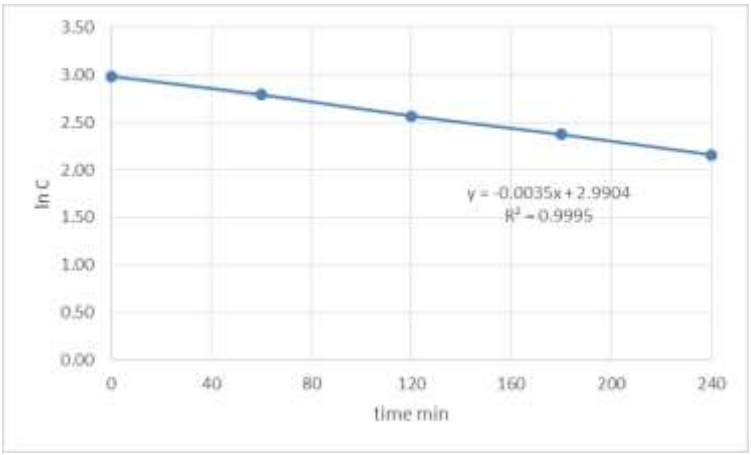

56% Phenol reduction, K_{app} = 0.21 hr^{-1}

Maximum T rise = 0.5 °c

Slurry – Run 17

Phenol added: **140 mg** Flow rate: **18.2 L/min** Catalyst: **TiO_2 - P25**

Concentration: **20 mg/L** Light intensity: **75.6 W/m²** Catalyst loading: **2 g/L**

Total Volume: **7.1 L**

time	min	**T0**	**T60**	**T120**	**T180**	**T240**
T	°c	23.4	26.4	25.8	26.3	26.8
DO	mg/L	8.91	8.34	8.72	8.57	8.54
pH		8.16	8.39	8.45	8.46	8.48
Phenol	mg/L	20.0	15.8	14.2	13.5	11.0
Phenol reduction %			20.91	29.11	32.26	45.09
ΔT	°c		3	2.4	2.9	3.4

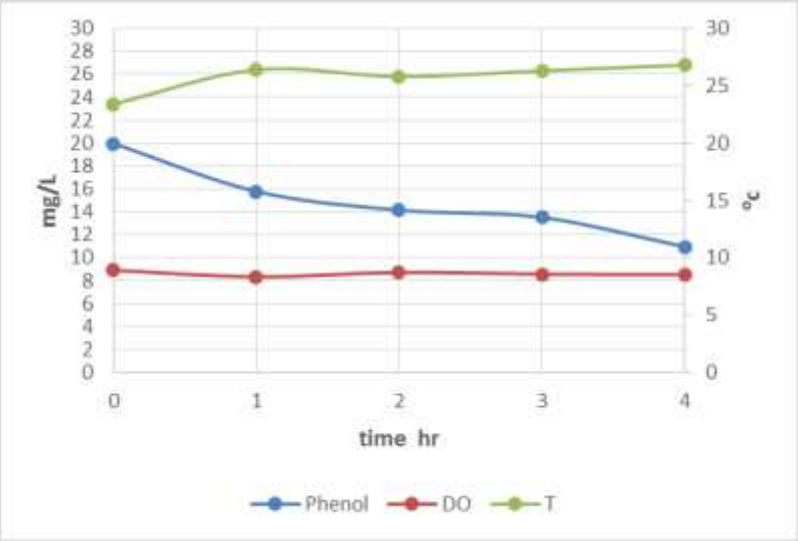

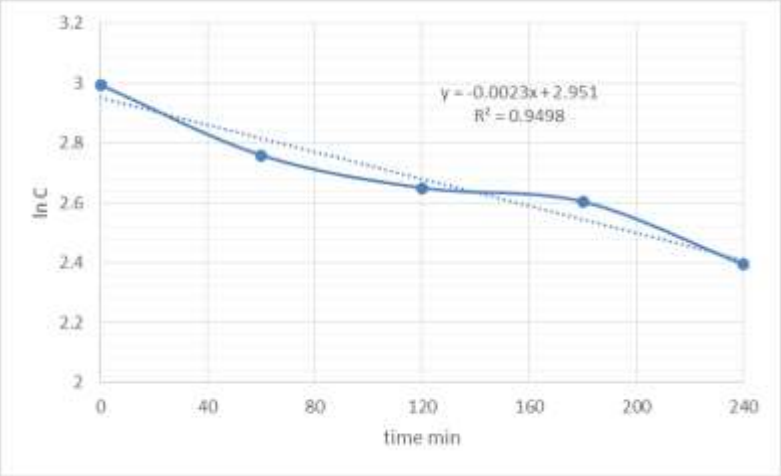

45 % Phenol reduction, K_{app} = 0.138 hr^{-1}

Maximum T rise = 3.4°c

Slurry – Run 18

Phenol added: **60 mg** Flow rate: **18.6 L/min** Catalyst: **TiO_2 - P25**

Concentration: **20.1 mg/L** Light intensity: **60.2 W/m²** **slurry – used twice**

Total Volume: **3 L** Catalyst loading: **1.9 g/L**

time	min	**T0**	**T60**	**T120**	**T180**	**T240**
T	°c	23.7	26	26.1	26.5	26.1
DO	mg/L	8.85	7.34	7.31	7.23	7.36
pH		8.47	8.55	8.58	8.6	8.62
Phenol	mg/L	20.1	14.7	12.9	9.6	8.7
Phenol reduction %			19	32	52	57
ΔT	°c		2.3	2.4	2.8	2.4

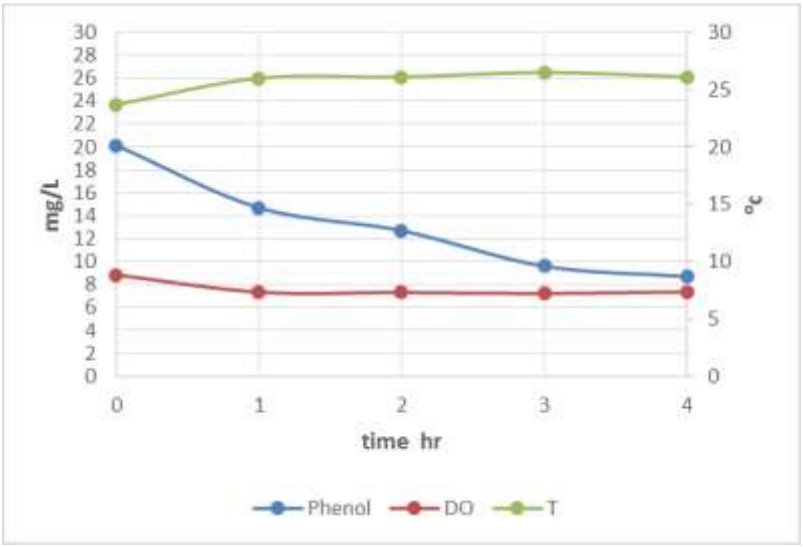

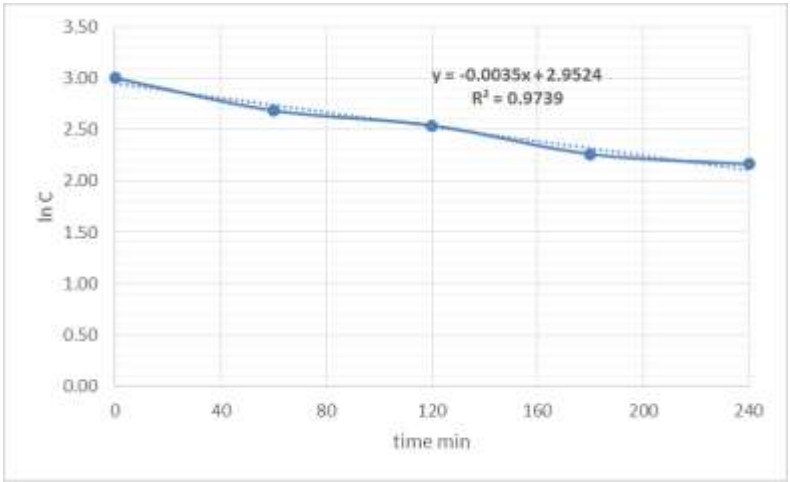

57 % Phenol reduction, K_{app} = 0.21 hr^{-1}

Maximum T rise = 2.8 °c

Slurry – Run 19

Phenol added: **362 mg** Flow rate: **20.2 L/min** Catalyst: **TiO_2 - P25**

Concentration: **20.1 mg/L** Light intensity: **59.9 W/m²** **slurry – used once**

Total Volume: **18 L** Catalyst loading: **2 g/L**

time	min	**T0**	**T60**	**T120**	**T180**	**T240**
T	°c	22.9	25.2	26.1	27.5	27.5
DO	mg/L	7.63	7.37	7.35	7.2	7.06
pH		8.20	8.36	8.45	8.44	8.5
Phenol	mg/L	20.09	15.03	17.83	16.51	14.52
Phenol reduction %				25.17	11.27	17.82
ΔT	°c		2.3	3.2	4.6	4.6

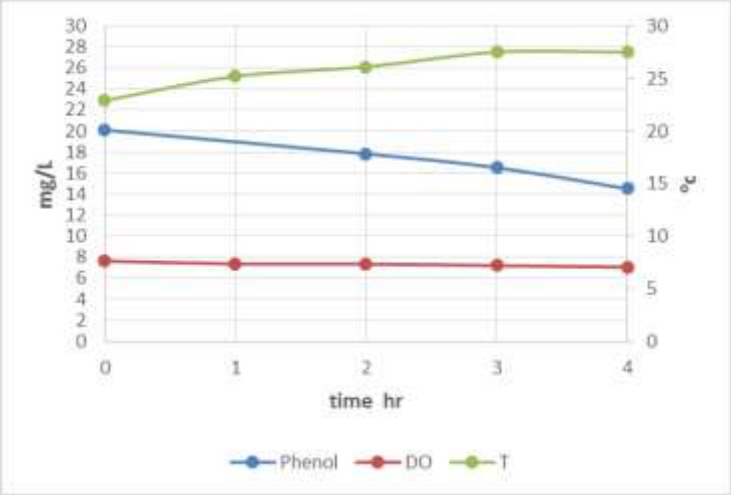

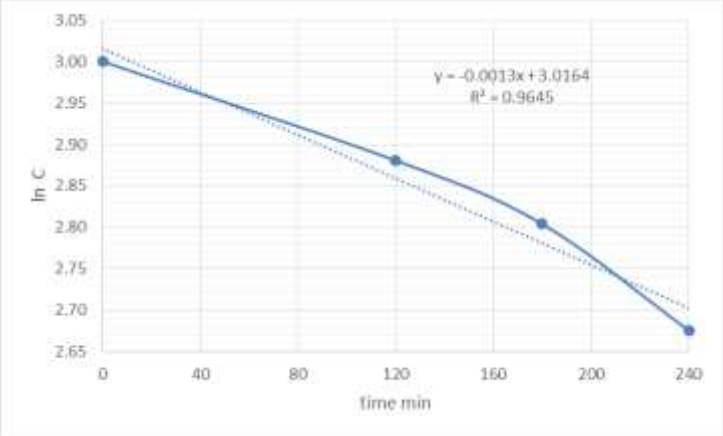

28 % Phenol reduction, K_{app} = 0.078 hr^{-1}

Maximum T rise = 4.6 °c

Slurry – Run 21

Phenol added: **140 mg** Flow rate: **20.3 L/min** Catalyst: **TiO_2 - P25**

Concentration: **19.3 mg/L** Light intensity: **60.2 W/m²** **slurry – used once**

Total Volume: **7.2 L** H_2O_2 : **50 mg/L** Catalyst loading: **2 g/L**

time	min	**T0**	**T60**	**T120**	**T180**	**T240**
T	°c	22.5	24.5	25.6	26	25.6
DO	mg/L	7.79	7.53	7.36	7.27	7.39
pH		7.84	7.97	8.03	8.11	8.19
Phenol	mg/L	19.3	14.2	13.1	11.1	6.4
Phenol reduction %			26.5	31.9	42.3	66.7
ΔT	°c		2	3.1	3.5	3.1

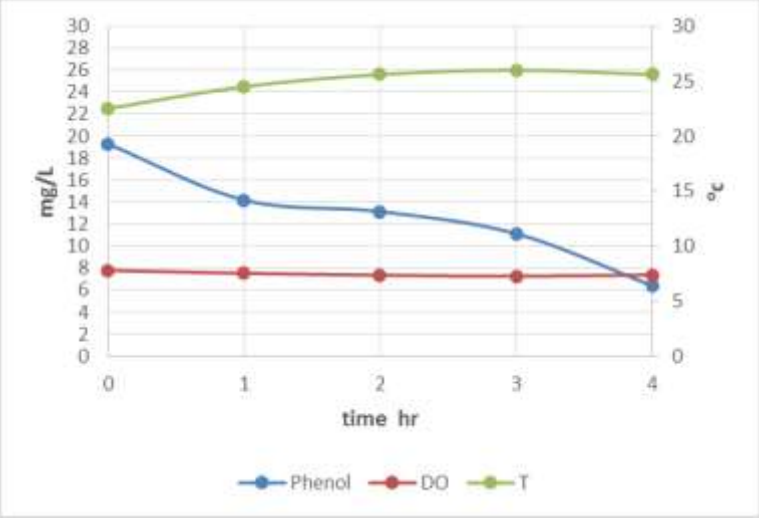

67 % Phenol reduction
Maximum T rise = 3.5 °c

Slurry – Run 22

Phenol added: **140 mg** Flow rate: **19.8 L/min** Catalyst: **TiO_2 - P25**

Concentration: **19.7 mg/L** Light intensity: **61.3 W/m^2** **slurry – used 4 times**

Total Volume: **7.1 L** H_2O_2 : **150 m g/L** Catalyst loading: **2 g/L**

time	min	**T0**	**T60**	**T120**	**T180**	**T240**
T	°c	22.8	24.2	25.6	25.1	25.1
DO	mg/L	7.65	7.68	7.3	7.5	7.44
pH		7.79	8.04	8.05	8.07	8.23
Phenol	mg/L	19.71	15.28	15.09	13.52	12.77
Phenol reduction %			22.44	23.40	31.38	35.18
ΔT	°c		1.4	2.8	2.3	2.3

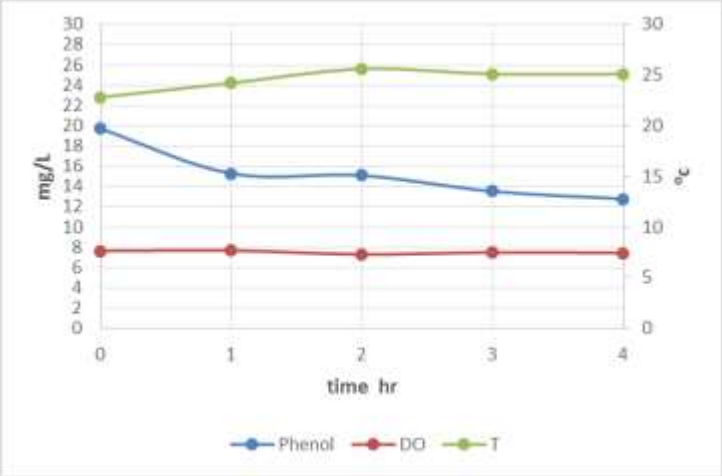

35 % Phenol reduction
Maximum T rise = 2.8 °c

Annex II. ANOVA Analysis: Catalyst Loading – Light Intensity

	Phenol Removed mg/L	
catalyst g/L	Light Intensity	
	60 W/m^2	90 W/m^2
0.35	16.7	15.9
0.7	15.3	15.1
1.4	14.6	11.9
2.9	8.9	10.1

Anova: Two-Factor Without Replication

SUMMARY	*Count*	*Sum*	*Average*	*Variance*
Row 1	2	32.60	16.30	0.33
Row 2	2	30.43	15.21	0.04
Row 3	2	26.53	13.26	3.60
Row 4	2	19.00	9.50	0.74
Column 1	4	55.55	13.89	11.85
Column 2	4	53.00	13.25	7.33

ANOVA

Source of Variation	*SS*	*df*	*MS*	*F*	*P-value*	*F crit*
Rows	53.66	3	17.89	13.78	0.03	9.28
Columns	0.81	1	0.81	0.63	0.49	10.13
Error	3.89	3	1.30			
Total	58.36	7				

Annex III. Tukey's Test: Catalyst Loading – Light Intensity

			Catalyst loading g/L	time hr 0	1	2	3	4
60 W/m^2	Run 2	1	0.35	19.9	18.1	17.4	17.1	16.7
	Run 7	2	0.7	20.2	18.7	17.4	16.5	15.3
	Run 6	3	1.4	20.1	18.2	17.7	15.5	14.6
	Run 8	4	3	20.1	15.8	12.8	10.4	8.9
90 W/m^2	Run 3	5	0.35	20.3	18.6	17.5	16.7	15.9
	Run 4	6	0.7	20.7	18.2	17.9	16.1	15.1
	Run 5	7	1.4	20.5	17.1	15.5	13.1	11.9
	Run 9	8	3	19.8	16.2	14.0	11.4	10.1

Anova: Two-Factor Without Replication

SUMMARY	*Count*	*Sum*	*Average*	*Variance*
Row 1	5	89.21	17.84	1.54
Row 2	5	88.18	17.64	3.60
Row 3	5	86.12	17.22	4.78
Row 4	5	67.95	13.59	20.04
Row 5	5	89.08	17.82	2.97
Row 6	5	88.06	17.61	4.74
Row 7	5	78.04	15.61	11.51
Row 8	5	71.57	14.31	15.16
Column 1	8	161.63	20.20	0.10
Column 2	8	140.92	17.62	1.24
Column 3	8	130.42	16.30	3.77
Column 4	8	116.68	14.58	6.89
Column 5	8	108.56	13.57	8.34

ANOVA

Source of Variation	*SS*	*df*	*MS*	*F*	*P-value*	*F crit*
Rows	103.04	7	14.72	10.48	2.12E-06	2.36
Columns	217.99	4	54.50	38.80	4.88E-11	2.71
Error	39.33	28	1.40			
Total	360.36	39				

$$T\alpha = q\alpha(a, f)\sqrt{MSE/n}$$

MS_E	1.40
n	5
a	8
N	40
α	0.05
f = a(n-1)	32
$q_{0.05}(8,32)$	4.6
Mse/n	0.280933
$T_{0.05}$	2.438144

$\bar{y}_{4.} - \bar{y}_{8.}$	-0.72441	the means of treatments are **not** different
$\bar{y}_{3.} - \bar{y}_{7.}$	1.614623	the means of treatments are **not** different
$\bar{y}_{2.} - \bar{y}_{6.}$	0.024158	the means of treatments are **not** different
$\bar{y}_{1.} - \bar{y}_{5.}$	0.02707	the means of treatments are **not** different

Annex IV. ANOVA Analysis : H_2O_2 Addition

	H_2O_2 mg/L	Time hr				
		0	1	2	3	4
Run 21	50	19.29	14.19	13.14	11.14	6.42
Run 22	150	19.71	15.28	15.09	13.52	12.77
Run 17	0	19.96	15.79	14.15	13.52	10.96

Anova: Two-Factor Without Replication

SUMMARY	*Count*	*Sum*	*Average*	*Variance*
Row 1	5	64.18	12.84	21.92
Row 2	5	76.38	15.28	7.25
Row 3	5	74.37	14.87	11.09
Column 1	3	58.96	19.65	0.11
Column 2	3	45.26	15.09	0.67
Column 3	3	42.39	14.13	0.95
Column 4	3	38.18	12.73	1.89
Column 5	3	30.15	10.05	10.72

ANOVA

Source of Variation	*SS*	*df*	*MS*	*F*	*P-value*	*F crit*
Rows	17.12	2	8.562	5.92	0.026	4.46
Columns	149.47	4	37.366	25.83	0.000	3.84
Error	11.57	8	1.447			
Total	178.16	14				

Annex V. Titanium Recovery Calculation

The XRF analysis for raw sand and coated sand are shown in Table 12.

Table 12: XRF analysis

Sample	*SiO2*	*Al2O*	*Fe2O3*	*CaO*	*MgO*	*SO3*	*K2O*	*Na2O*	*TiO2*	*Total*
S raw	*93.31*	*2.52*	*1.57*	*0.40*	*0.10*	0.05	*0.58*	*0.26*	*1.12*	99.91
SC 20%	*91.11*	*2.50*	*1.83*	*0.43*	*0.10*	0.04	*0.58*	*0.26*	*3.04*	99.89
SC 50%	*90.98*	*2.54*	*1.57*	*0.39*	*0.09*	0.05	*0.59*	*0.27*	*3.45*	99.93

The weight of TiO_2 thin film is given by Equation 45.

$$m_{TiO_2\ coat} = (x_{coated\ sand} - x_{raw\ sand})\, m_s \qquad \textit{Equation 45}$$

where $x_{coated\ sand}$ and $x_{raw\ sand}$ are the weight fractions of TiO_2 on the coated sand and the raw sand respectively, m_s is the weight of sand.

$Ti_{\ added}$ and $Ti_{\ recovered}$ are calculated from Equation 46 and Equation 47.

$$Ti_{\ added} = used\ TTIP * \frac{Ti_{atomic\ weight}}{TTIP_{molecular\ weight}} \qquad \textit{Equation 46}$$

$$Ti_{\ recovered} = TiO_2\ coat * \frac{Ti_{atomic\ weight}}{TiO_{2\ molecular\ weight}} \qquad \textit{Equation 47}$$

Table 13: Titanium recovery

	TiO_2 coat gm	Ti coat gm	TTIP %	TTIP gm	Ti added gm	% recovered on coat
SC 20%	0.384	0.230	20	4	0.673	34.2
SC 50%	0.466	0.279	50	10	1.682	16.6

Annex VI. Anatase Crystallite Size Calculation – Water Molar Ratio

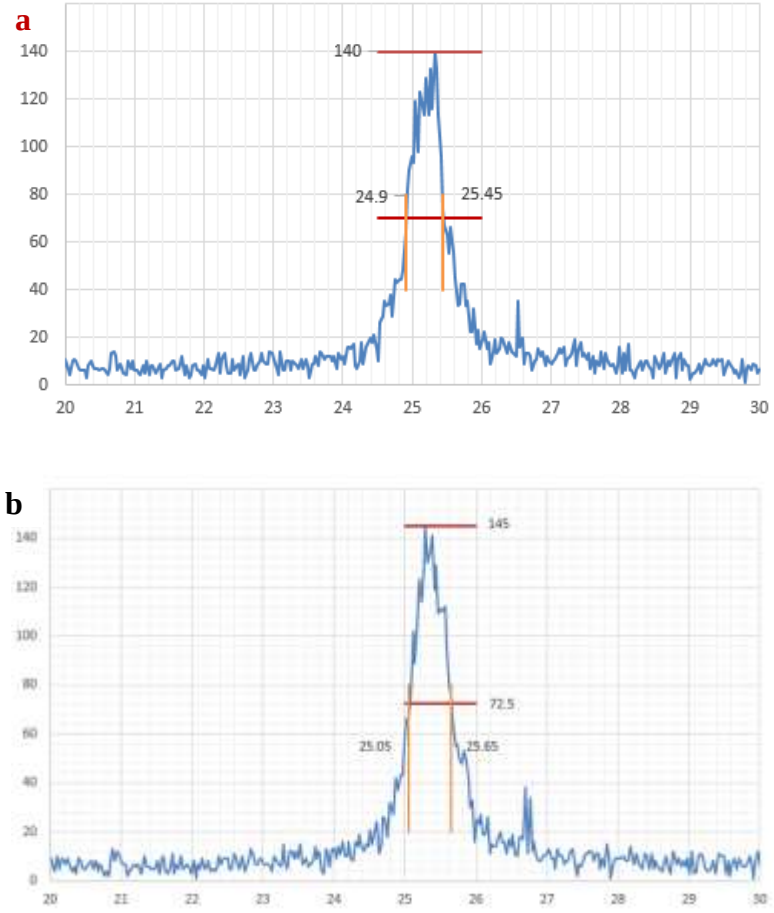

Figure 66: Anatase strong peak for water molar ratio a) 4 and b) 10

Table 14: Crystallite size for 4 and 10 water molar ratios

Hydrolysis ratio	k	λ nm	θ	B °	B radians	L nm
4	0.9	0.15418	25.281	0.55	0.0096	14.62
10	0.9	0.15418	25.281	0.6	0.0105	13.40

Annex VII. Anatase Crystallite Size Calculation – Aging

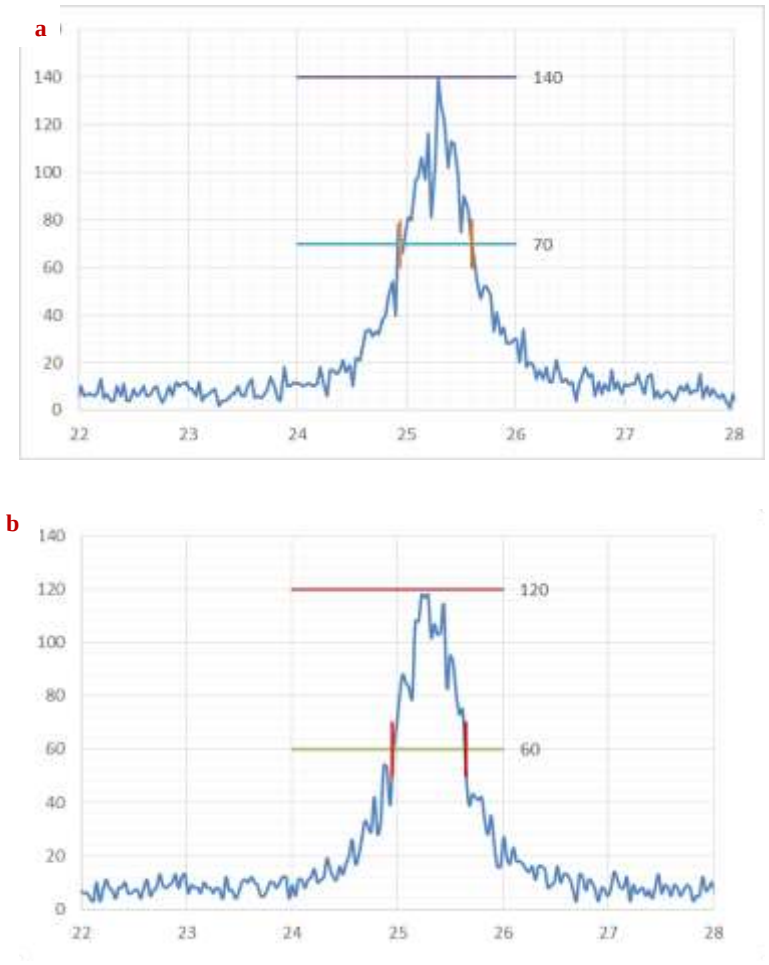

Figure 67: Anatase strong peak for a) aged and b) directly dried nanoparticles

Table 15: Crystallite size for aged and directly dried nanoparticles

Aging time	k	λ nm	θ	B °	B radians	L nm
24 hours	0.9	0.15418	25.281	0.65	0.0113	12.37
0	0.9	0.15418	25.281	0.7	0.0122	11.48

Annex IX. Supported Experimental Results

Operational parameters are summarized in the following tables

Supported – Run 3

Phenol added: **75 mg** Flow rate: **18 L/min** Catalyst: **TSC**

Concentration: **25.1 mg/L** Light intensity: **50.5 W/m²**

Total Volume: 3 **L**

time	min	**T0**	**T60**	**T120**	**T180**	**T240**
T	°c	23.9	25.5	25.6	25.5	25.5
DO	mg/L	7.92	7.95	7.96	8	8.1
pH		8.38	8.43	8.37	8.39	8.41
Phenol	mg/L	25.14	23.97	23.28	23.32	23.09
Phenol reduction %			4.65	7.39	7.24	8.13
Turbidity	FTU	25	69	80	125	174
ΔT	°c		1.6	1.7	1.6	1.6

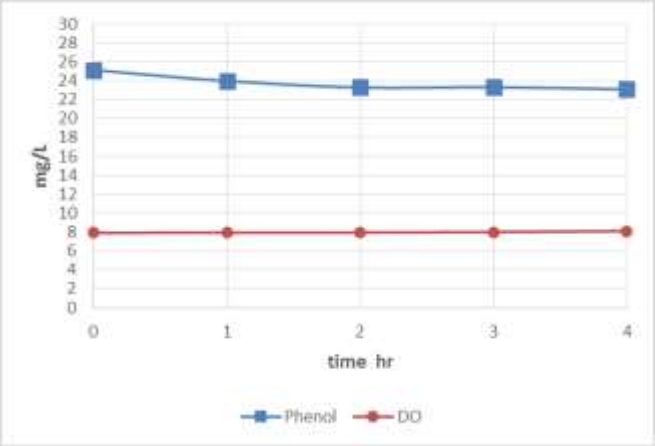

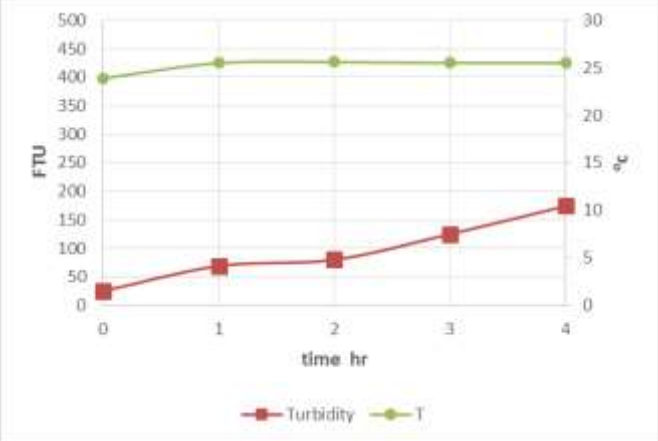

8 % Phenol reduction

Maximum T rise = 1.7 °c

Supported – Run 4

Phenol added: **75 mg** Flow rate: **18.5 L/min** Catalyst: **C- TSC**

Concentration: **24.9 mg/L** Light intensity: **51.6 W/m²**

Total Volume: **3 L**

time	min	**T0**	**T60**	**T120**	**T180**	**T240**
Phenol	mg/L	24.9	23.0	22.3	20.0	18.9
Phenol reduction %			8	10	19	24
Turbidity	FTU	34	105	302	440	461

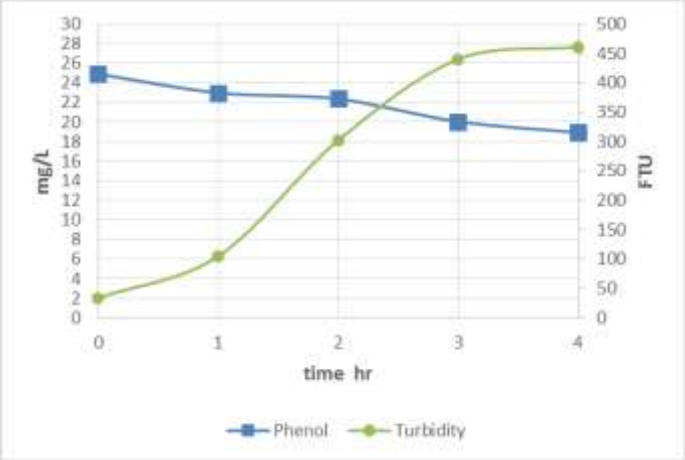

24% Phenol reduction

Supported – Run 5

Phenol added: **77 mg** Flow rate: **17.5 L/min** Catalyst: **E-TSC-10**

Concentration: **2 mg/L** Light intensity: **51 W/m²**

Total Volume: **3 L**

time	min	**T0**	**T60**	**T120**	**T180**	**T240**
Phenol	mg/L	25.2	21.3	18.3	17.6	16.8
Phenol reduction %			16	27	30	34
Turbidity	FTU	32	39	44	49	54

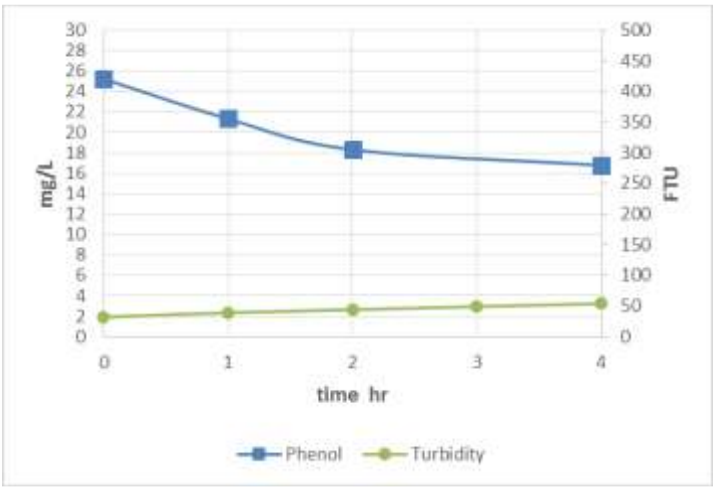

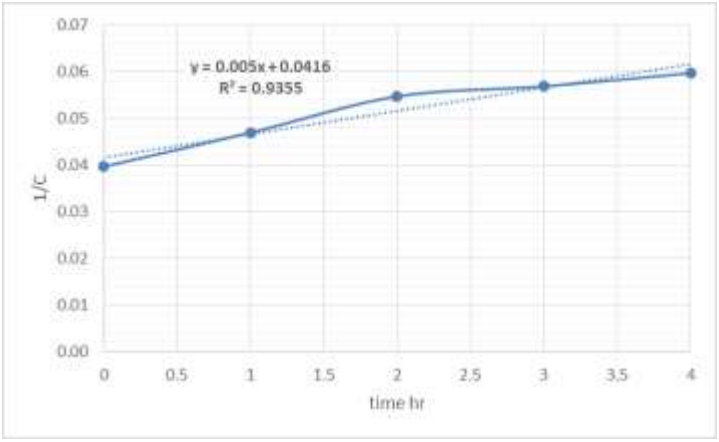

34 % Phenol reduction, K_{app} = 0.005 mgL^{-1} hr^{-1}

Supported – Run 8

Phenol added: **76 mg** Flow rate: **17.9 L/min** Catalyst: **E-TSC-5**

Concentration: **25.3 mg/L** Light intensity: **62.3 W/m²**

Total Volume: **3 L**

time	min	**T0**	**T60**	**T120**	**T180**	**T240**
T	°c	25.3	24.4	24.2	23.5	23.5
DO	mg/L	7.77	8.06	8.2	8.35	8.26
pH		8.34	8.33	8.27	8.28	8.3
Phenol	mg/L	25.3	18.3	16.7	15.2	13.6
Phenol reduction %			28	34	40	46
TOC	mg/L	19.73	19.72	19.21	18.18	17.15
TOC reduction %			0.06	2.67	7.85	13.08

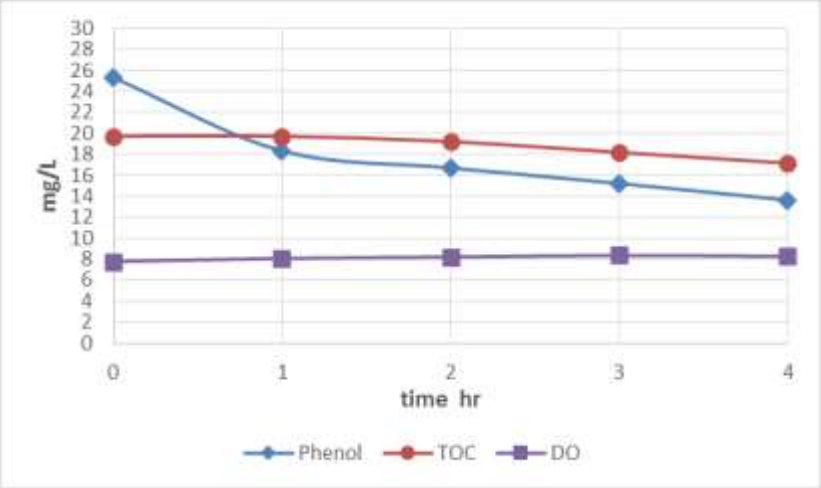

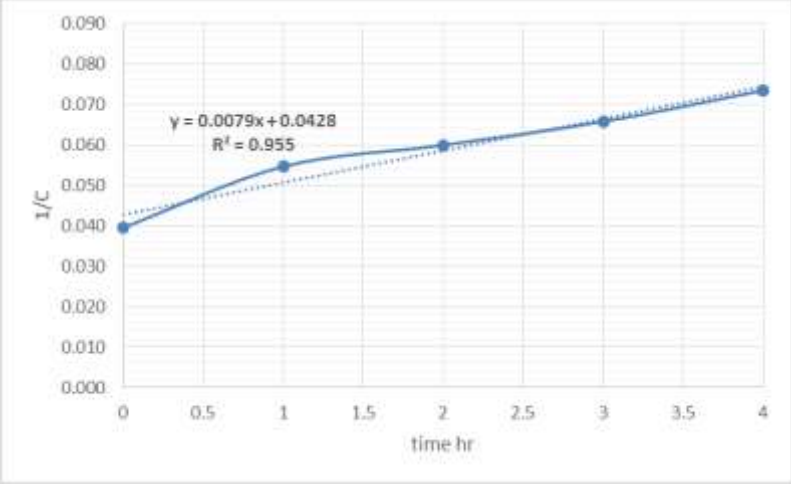

46 % Phenol reduction, K_{app} = 0.0079 mgL^{-1} hr^{-1}

Supported – Run 11

Phenol added: **75 mg** Flow rate: **25.5 L/min** Catalyst: **E-TSC-5**

Concentration: **24.8 mg/L** Light intensity: **59.5 W/m²**

Total Volume: **3 L**

time	min	**T0**	**T120**	**T240**	**T360**	**T450**
T	°c	24.8	24.4	24.5	25.9	26.4
DO	mg/L	8.52	8.7	8.85	8.45	8.49
Phenol	mg/L	24.7	19.3	13.8	12.6	8.5
Phenol reduction %			22	44	49	66
Turbidity	FTU	17.5	7.5	12	25.5	21.5

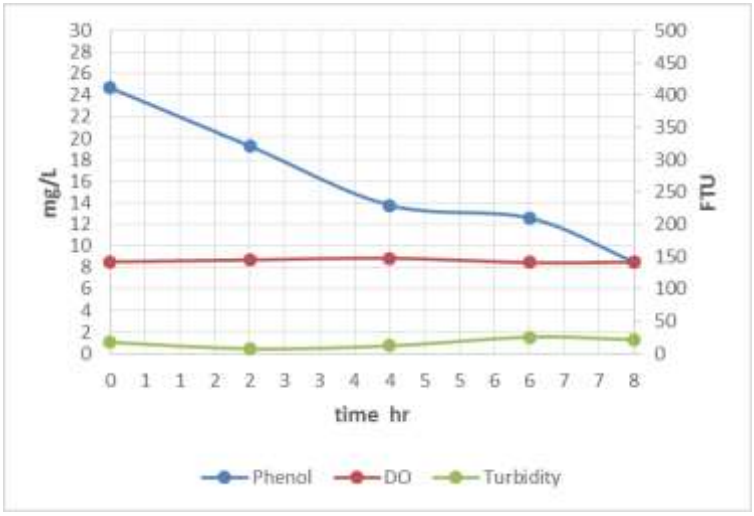

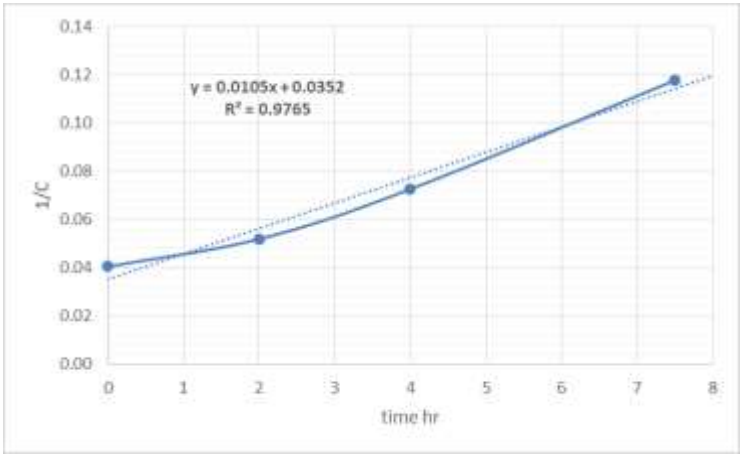

66 % Phenol reduction, K_{app} = 0.0105 mgL^{-1} hr^{-1}

Maximum T rise = 1.6 °c

Supported – Run 12

Concentration: **25 mg/L**

Total Volume: **3 L**

Flow rate: **20.7 L/min**

Light intensity: **60.5 W/m²**

Catalyst: **E-TSC-5**

Operation mode: **Continuous**

Influent/effluent flow rate: **500 mL/hr**

time	min	**T0**	**T120**	**T240**	**T360**	**T480**	**T600**
T	°c	25	23.2	22.7	23.4	23.1	24.1
DO	mg/L	8.45	8.51	8.5	8.49	8.59	8.5
pH							
Phenol	mg/L	25.2	12.9	12.5	11.5	11.8	10.4
Phenol reduction %		0	49	50	54	53	59
Turbidity	FTU	1	22	30	15	8	9

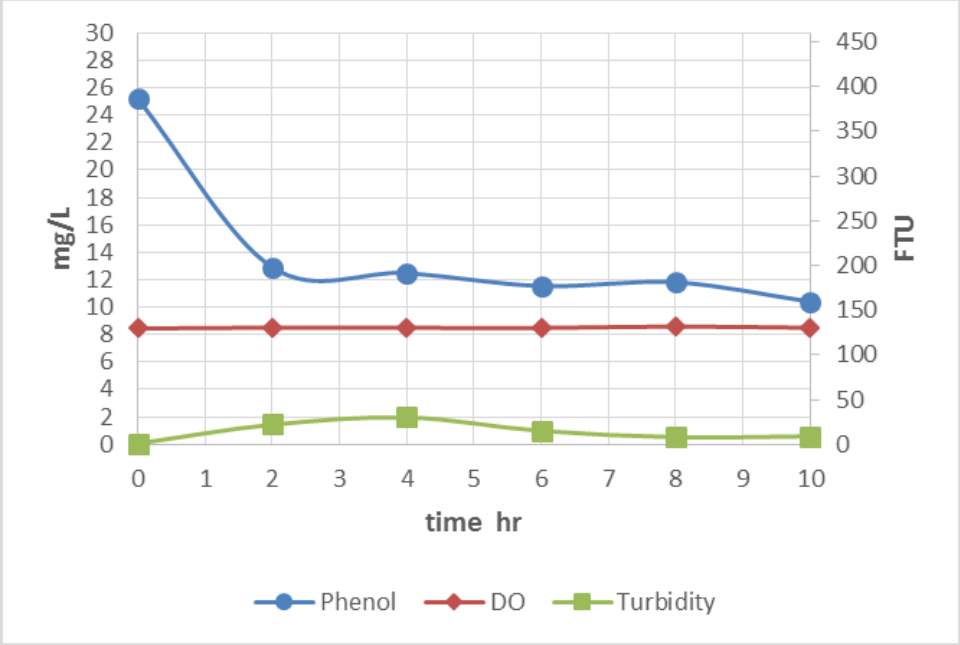

55 % Phenol reduction at steady state

Supported – Run 14

Concentration: **25 mg/L**

Total Volume: **3.4 L**

Flow rate: **23.6 L/min**

Light intensity: **43.3 W/m^2**

Catalyst: **E-TSC-5**

Operation mode: **Continuous**

Influent/effluent flow rate: **550 mL/hr**

time	min	**T0**	**T120**	**T240**	**T360**	**T480**	**T600**
T	°c	23.7	25.4	25.4	26.9	26.1	25.5
DO	mg/L	8.51	8.34	8.31	8.12	8.69	8.77
Phenol	mg/L	25.5	14.3	9.4	8.2	8.8	8.9
Phenol reduction %			44	63	68	65	65
TOC	mg/L	19.04	16.74	13.92	9.61	8.13	6.86
TOC reduction %			12.08	26.91	49.52	57.30	64.00
Theoretical TOC	mg/L	19.11	10.74	7.04	6.13	6.62	6.64

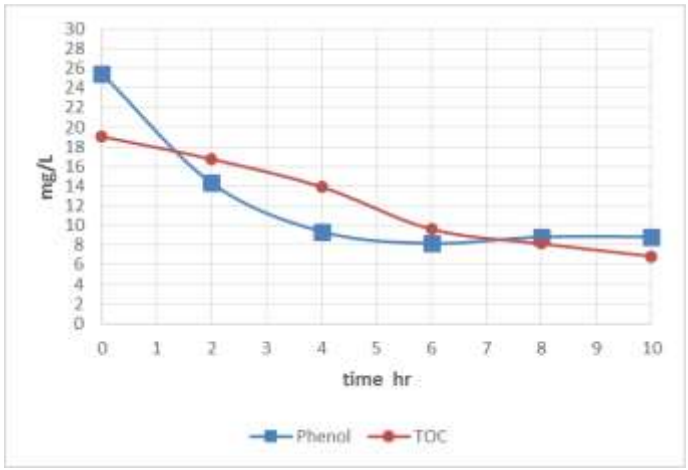

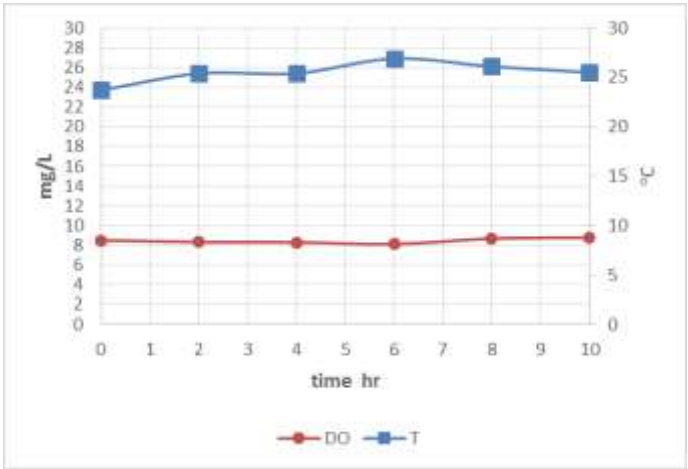

65 % Phenol reduction at steady state

Supported – Run 15

Phenol added: 1**70 mg** Flow rate: **23.2 L/min** Catalyst: **E-TSC-5**

Concentration: **49.5 mg/L** Light intensity: **45 W/m²**

Total Volume: **3.4 L**

time	min	**T0**	**T120**	**T240**	**T360**	**T480**
T	°c	21.6	22.6	22.7	22.7	22.2
DO	mg/L	8.94	8.8	8.9	9.14	9.3
Phenol	mg/L	49.55	31.80	23.62	18.56	14.73
Phenol reduction %			36	52	63	70
ΔT	°c		1.0	1.1	1.1	0.6

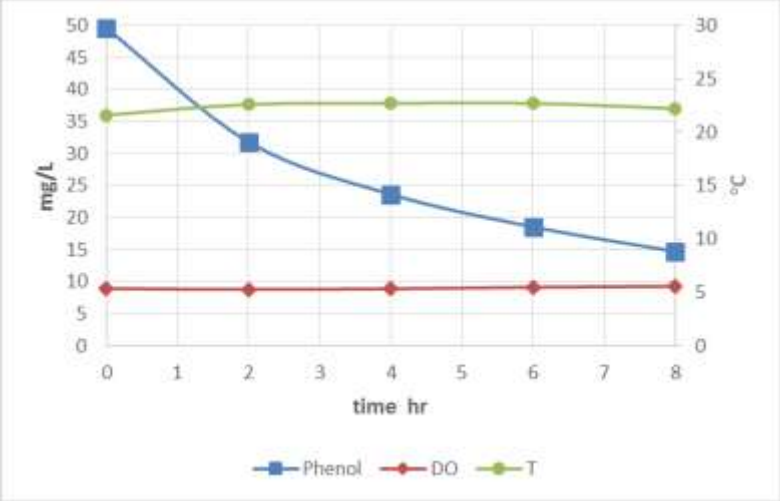

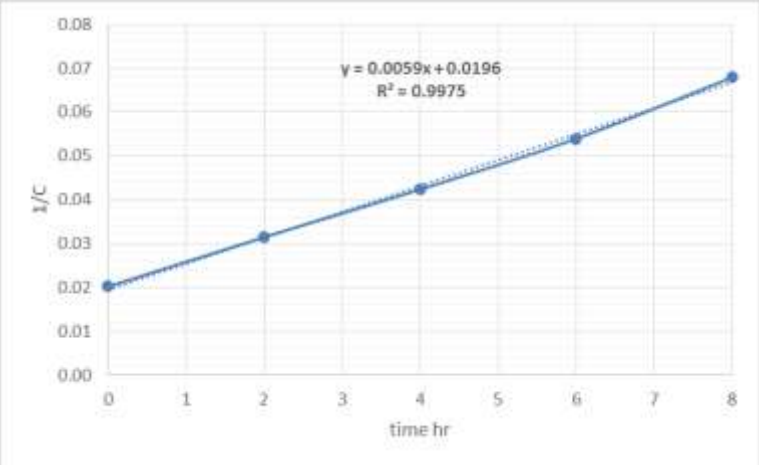

70 % Phenol reduction, K_{app} = 0.0059 mgL^{-1} hr^{-1}

Maximum T rise = 1.1 °c

ANOVA Analysis: Immobilization Techniques

	Time hr				
	0	1	2	3	4
C-TSC	24.89	22.98	22.35	20.04	18.92
E-TSC-10	25.22	21.31	18.29	17.61	16.77
TSC	25.14	23.97	23.28	23.32	23.09

Anova: Two-Factor Without Replication

SUMMARY	*Count*	*Sum*	*Average*	*Variance*
Row 1	5	109.17	21.83	5.66
Row 2	5	99.20	19.84	11.97
Row 3	5	118.79	23.76	0.70
Column 1	3	75.24	25.08	0.03
Column 2	3	68.25	22.75	1.81
Column 3	3	63.92	21.31	7.02
Column 4	3	60.96	20.32	8.20
Column 5	3	58.78	19.59	10.35

ANOVA

Source of Variation	*SS*	*df*	*MS*	*F*	*P-value*	*F crit*
Rows	38.40	2	19.199	9.354	0.008	4.459
Columns	56.92	4	14.230	6.933	0.010	3.838
Error	16.42	8	2.052			
Total	111.74	14				

Annex X. ANOVA Analysis: TiO_2 Loading on Epoxy Coating

	Time hr				
	0	1	2	3	4
E-TSC-2.5	25.00	22.65	20.09	19.20	17.80
E-TSC-5	25.32	18.32	16.70	15.22	13.63
E-TSC-10	25.22	21.31	18.29	17.61	16.77
E-TSC-20	25.08	24.25	23.00	21.98	21.12

Anova: Two-Factor Without Replication

SUMMARY	*Count*	*Sum*	*Average*	*Variance*
Row 1	5	104.73	20.95	8.25
Row 2	5	89.19	17.84	20.50
Row 3	5	99.20	19.84	11.97
Row 4	5	115.42	23.08	2.61
Column 1	4	100.62	25.15	0.02
Column 2	4	86.52	21.63	6.31
Column 3	4	78.08	19.52	7.29
Column 4	4	74.01	18.50	8.04
Column 5	4	69.31	17.33	9.52

ANOVA

Source of Variation	*SS*	*df*	*MS*	*F*	*P-value*	*F crit*
Rows	71.92	3	23.97	13.29	0.00040	3.49
Columns	151.70	4	37.93	21.02	0.00002	3.26
Error	21.65	12	1.80			
Total	245.27	19				

Annex XI. Phenol Theoretical Concentration Profiles

Theoretical concentration profile for the continuous mode operation calculated by Euler's method is shown in Table 16.

K	0.0105	$mgL^{-1}\ hr^{-1}$	Q_{in}	0.5	L/hr
C_{in}	25	mg/L	Q_o	0.5	L/hr
V	3	L/hr	$Q_{in}C_{in}/V$	4.17	

Table 16: Phenol theoretical concentration profile for continuous operation

t	C_t	Q_oC_t/V	KC_t	$(dC/dt)_t$	$C_{t+\Delta t}$
0	25.00	4.17	6.56	-6.56	18.44
1	18.44	3.07	3.57	-2.48	15.96
2	15.96	2.66	2.68	-1.17	14.79
3	14.79	2.47	2.30	-0.60	14.20
4	14.20	2.37	2.12	-0.32	13.88
5	13.88	2.31	2.02	-0.17	13.71
6	13.71	2.29	1.97	-0.09	13.62
7	13.62	2.27	1.95	-0.05	13.57
8	13.57	2.26	1.93	-0.03	13.54
9	13.54	2.26	1.93	-0.02	13.53
10	13.53	2.25	1.92	-0.01	13.52

Theoretical concentration profile for the batch mode operation calculated by the second order degradation rate model is shown in Table 17.

C_{in}	25	mg/L	K	0.0105	$mgL^{-1}\ hr^{-1}$

Table 17: Phenol theoretical concentration profile for batch operation

t	Kt	1/C	C
0	0.00	0.04	25.00
1	0.01	0.05	19.80
2	0.02	0.06	16.39
3	0.03	0.07	13.99
4	0.04	0.08	12.20
5	0.05	0.09	10.81
6	0.06	0.10	9.71
7	0.07	0.11	8.81
8	0.08	0.12	8.06
9	0.09	0.13	7.43
10	0.11	0.15	6.90

Annex XII. Photo-catalyst Multiple Use

E-STC-5 was used for the following consecutive runs as detailed in Table 18.

Table 18: E-TSC-5 multiple use

Experimental run	time hr	average flow rate L/min	Recirculated volume L
batch 2	4	23.5	94
long batch 1	8	23.2	185.6
long batch 2	7.5	25.5	191.25
continuous 1	10	20.7	207
continuous 2	10	23.6	236
continuous 3	10	22.8	228
average	**49.5**	**23.07**	**1141.85**